Discovery of Novel Lignin Oxidizing Enzymes from *Sphingobacterium* sp.T2

Goran Mahmood M. Rashid

A thesis submitted in partial fulfilment of the requirement for the degree of Doctor of Philosophy in Chemistry

Department of Chemistry

October 2015

Supervisor: Professor T.D.H Bugg

Contents

List of Figures

List of Tables

Abbreviations

AAO	The aryl alcohol oxidase
ABTS	2,2'-Azino-bis(3-ethylthiazoline-6- sulfonate)
Ala	Alanine
Arg	Arginine
Asn	Asparagine
Asp	Aspartate
BLAST	Basic local alignment search tool
CHMSDH	4-Carboxy-2-hydroxymuconate-6-semialdehydedehydrogenase
CMD	γ-carboxymuconolactone decarboxylase
CMLE	ß-Carboxymuconate lactonizing enzyme
Cys	Cysteine
°C	Degrees Celsius
Da	Dalton
DCP	2,4-dichlorophenol
5,5`-DDVn	5,5`-Dehydrodivanillin
DHP	Dehydrogenative polymer

DMSO	Dimethyl sulfoxide
DNA	Deoxyribonucleic acid
dNTPs	Deoxynucleotide triphosphates
DTT	Dithiothreitol
DyP	Dye-decolorizing peroxidases
E. coli	*Escherichia coli*
EDTA	Ethylenediaminetetraacetic acid
EIC	Extracted ion chromatogram
EI-MS	Electron impact mass spectra
ELH	Enolactone hydrolase
Enz	Enzyme
EPR	Electron paramagnetic resonance spectroscopy
ESI	Electrospray ionisation
Et_3N	Trimethylamine
ε	Extinction coefficient
FPLC	Fast protein liquid chromatograph
GC/MS	Gas chromatography/mass spectrometry
Glu	Glutamate

Asp	Aspartic acid
HBT	1-Hydroxybenzotriazole
HCl	Hydrochloric acid
His	Histidine
His_6	Hexa-histidine
HPLC	High-performance liquid chromatography
HRP	Horseradish peroxidase
4HOAL	4-hydroxy-4methyl-2oxoglutarate aldolase
ICP-OES	Inductively coupled plasma optical emission spectrometry
IL	Ionic liquid
IMAC	Immobilized metal affinity chromatography
INH	Isoniazid
IPTG	Isopropyl ß-D-1-thiogalactopyranoside
kb	Kilo base
k_{cat}	Turnover number
K_M	Michaelis constant
KO_2	Potassium superoxide
LB	Luria broth

LCCs	lignin-carbohydrate complexes
LC-MS	Liquid chromatography- mass spectrometry
Leu	Leucine
LiP	Lignin peroxidase
LRET	Long-range electron transfer
m/z	Mass to charge ratio
MALDI-MS	Matrix-assisted laser desorption/ionization- mass spectrometry
Mbp	Mega base pair
MCO	Multicopper oxidase
MeOH	Methanol
Met	Methionine
MnSOD	Manganese containing superoxide dismutase
TCA cycle.	Tricarboxylic acid cycle
Tyr	Tryptophan
Trp	Tyrosine
MnP	Manganese peroxidase
MOPS	3-(N-Morpholino)propanesulfonic acid
MSW	Municipal solid waste

Mv	Millivolt
MWL	Milled wood lignin
NAD	Nicotinamide adenine dinucleotide
NADH	Nicotinamide adenine dinucleotide
NBT	Nitro blue tetrazolium chloride
Ni-NTA	Ni-Nitrilotriacetic acid
OD	Optical density
4OMH	4-Oxalomesaconate hydratase
P. chrysosporium	*Phanerochaete chrysosporium*
P. fluorescens	*Pseudomonas fluorescens*
PCR	Polymerase chain reaction
PDB	Protein data bank
PDCL	2-Pyrone-4,6-dicarboxylate lactonase
Phe	Phenylalanine
PMSF	Phenylmethanesulfonylfluoride
Pro	Proline
3,4-PCD	Protocatechuate 3,4-dioxygenase
R. jostii RHA1	*Rhodococcus jostii* RHA1

RNA	Ribonucleic acid
ROS	Reactive oxygen species
RT	Rtention times
S. griseus	*Streptomyces griseus*
SCLAC	Small laccase
SDS	Sodium dodecyl sulfate
SDS-PAGE	Sodium dodecyl sulphate polyacrylamide gel electrophoresis
-$SiMe_3$	Trimethylsilyl
SOD	Superoxide dismutase
SpMnSOD	MnSOD from *Sphingobacterium* sp. T2
TBE	Tris-borate-EDTA
TEMED	Tetramethylethylenediamine
TEV	Tobacco Etch Virus
TH	ß-ketoadipyl-CoA thiolase
TR	ß-ketoadipate:succinyl-CoA transferase
Trp	Tryptophan
Tyr	Tyrosine
UV	Ultraviolet

UV-Vis	Ultraviolet-visible
Val	Valine
VP	Versatile peroxidases

Acknowledgments

I wish to express my deepest gratitude to the Kurdish Ministry of Higher Education for the 3.5 years grant which made this research possible, and my supervisor, Prof. Tim Bugg for a valuable opportunity that he gave me to do a Ph.D. in this field of research and all his support, encouragement and guidance throughout the course of my study.

Many thanks for all Bugg group members who have helped me throughout the project. Special recognition must go to Dr. Rahman Rahman Pour for his continuous support, Dr. Elizabith Hardiman for her help and during first year of my study, Dr. Peter Harrison, Dr. Paul Sainsbury, Fariza Joanna and Rebin for their friendship and helpful advices.

I would also like to offer my thanks to Anne Smith for keeping the chemical biology lab running, Dr Lijiang Song, Phill Aston and Rebecca for helping me with mass-spectrometry.

I am grateful to Prof. Vilmos Fulop and Dean Rea at School of Life Science, University of Warwick for crystallising SOD1 and solving its structure. Thanks to all my friends who always encourage me and they wish the best for me.

I would like to express my love and thank my mother, my sisters and my brothers for all their love and support. I am a privilege to thank my wife Hero for all her love, help, support and constant encouragement, She blessed me with a life of joy in the hours when the lab lights were off. Special thank for my lovely son, Shahan cheering me up by looking at him when things went wrong.

Declaration

This work represents original research; all experimental work has been conducted by the author in the Department of Chemistry at the University of Warwick unless otherwise acknowledged and has not been previously submitted for a degree at another institution.

Genomic DNA libraries used in Chapter 2 were prepared by Prof. Elizabith Wellington at School of Life Science, University of Warwick.

MChem project student Yangqingxue Liu has assisted in the structural characterisation of some metabolites presented in Chapter 4 and 5.

Work presented in Chapter 4 published in ACS Chem Biol.

Rashid, G. M. M., Taylor, C. R., Liu, Y., Zhang, X., Rea, D., Fülöp, V., & Bugg, T. D. H. (2015). Identification of Manganese Superoxide Dismutase from Sphingobacterium sp. T2 as a Novel Bacterial Enzyme for Lignin Oxidation. *ACS Chemical Biology*, *10*(10), 2286–2294. http://doi.org/10.1021/acschembio.5b00298

Goran Mahmood M Rashid Date

Abstract

Bacterial lignin-degrading strain *Sphingobacterium* sp. T2 is reported as most active strain among 12 isolates and proteomic analysis of extracellular fractions gave hits for two superoxide dismutase enzymes.

Two novel lignin-oxidising enzymes from *Sphingobacterium* sp. T2 were identified. Experimental and bioinformatic evidence revealed that these enzymes are extracellular superoxide dismutases, namely SOD1 and SOD2. Both enzyme genes have been cloned and overexpressed in *Escherichia coli*. The metal specificity of both enzymes was investigated using ICP-OES, UV-vis spectra and superoxide dismutation activity of different metal-containing enzyme preparations, the results indicate that both enzymes (SOD1 and SOD2) are manganese-containing SOD.

MnSOD1 and MnSOD2 from *Sphingobacterium* sp. T2 (SpMnSODs) exhibit time-dependent lignin-oxidising ability, they can depolymerise wheat straw organosolv lignin, modify Kraft lignin, and lignocellulose materials (pine and miscanthus). Analysis of reaction components of SpMnSOD enzymes with organosolv lignin by HPLC, LC/MS and GC/MS show that SOD1 and SOD2 generate 10 new products. These metabolites were identified by comparison of their retention times and mass fragmentation pattern produced by LC/MS and GC/MS with their authentic analogue. The mechanism of reaction and reactive species generated by SpMnSODs were elucidated from their identified reaction products. Results indicate that SpMnSOD enzymes produce highly reactive species (hydroxyl radical) and catalyse several types of reactions which include: C_{α}-C_{β} cleavage, arylC-C_{α} Cleavage, -OCH_3 group replacement with -OH group, hydroxylation of aromatic rings, Ipso-substitution

and decarboxylation. The X-ray crystal structure of MnSOD1 was determined to 1.35 Å resolution, showing that MnSOD1 has a typical homodimer with a Mn(II) ion in each active site ligated by three His, one Asp, and a water/hydroxide forming trigonal bipyramidal geometry.

The reaction of SpMnSOD enzymes with lignin model compounds confirms that these enzymes can catalyse C_α-C_β cleavage, arylC-C_α Cleavage, ipso-substitution, decarboxylation, demethoxylation, hydroxylation of aromatic rings and fragmentation of propenoic acid side chains which in turn are evidence of generation of highly oxidising species (hydroxyl radical).

1. Introduction

1.1. Lignocellulosic biomass

Lignocellulosic biomass is the most abundant carbon source on Earth. It is the principal structural component of all types of plants (woody and non-woody). Plant biomass consists of two carbohydrate polymers, cellulose and hemicellulose and an aromatic polymer, lignin (Figure 1.1). These three major components of lignocellulose are bound tightly together [1], [2], [3] .

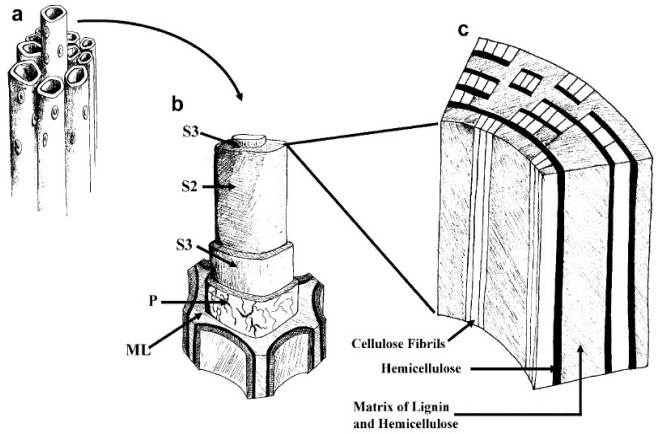

Figure 1.1. ***a-c.*** Configuration of wood tissues. (***a)*** Adjacent cells, (***b***) cell wall layers. S1, S2, S3 Secondary cell wall layers, P primary wall, ML middle lamella. (***c***) Distribution of lignin, hemicellulose and cellulose in the secondary wall. (Adapted from Pérez *et al*. [3])

In wood and groups of herbaceous plants, lignin is covalently linked to carbohydrates (Figure 1.2 and 1.3) forming lignin-carbohydrate complexes (LCCs). These covalent linkages can be via ester or ether linkages. In woody plants, the hydroxyl groups of sugar units are bound to the α- [4] and γ-carbons [5] of phenylpropane subunits in lignin, while in grass, p-coumaric acid and ferulic acid are linked via ester linkages to hemicellulose and lignin [4].

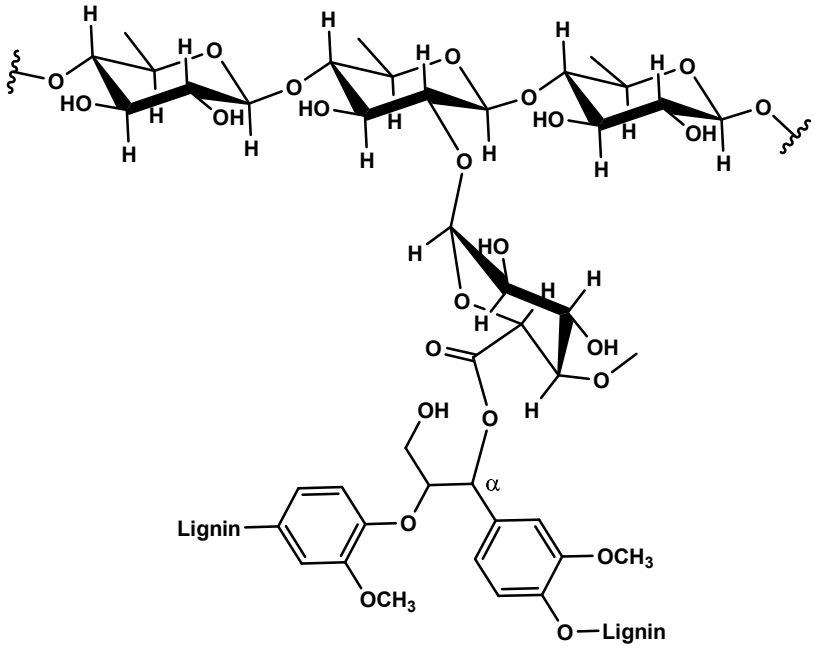

Figure 1.2. Ester linkage between lignin and glucuronoxylan in beech wood [6].

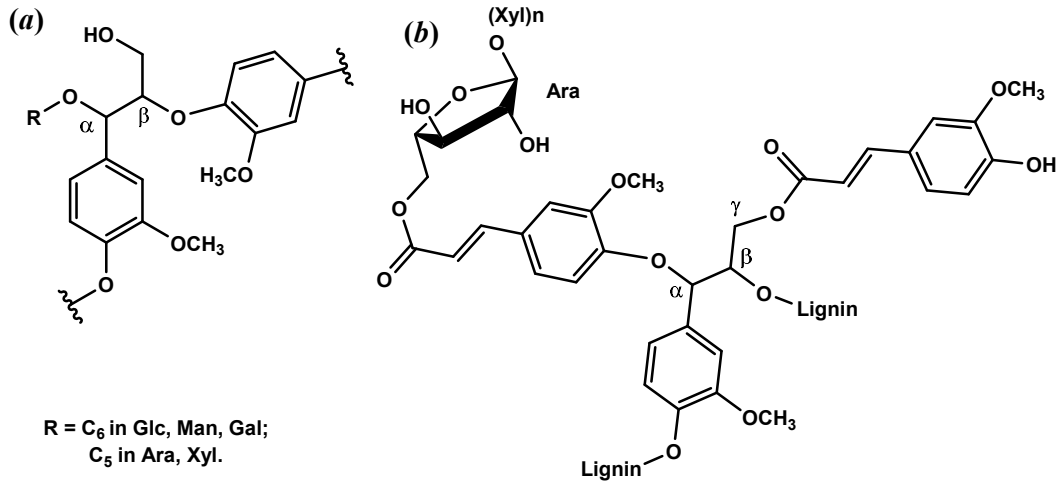

Figure 1.3. ***a***. Ether linkage from poplar wood between lignin and hemicellulose [5]. ***b***. Proposed ether linkage between ferulic acid and lignin and ester linkage between ferulic acid and hemicellulose in grass [4],[7].

As a renewable raw material for biofuel, mainly bio-ethanol, pulp and paper, chemicals and protein for food and feed using the microbial bioconversion process, lignocellulose feedstock has attracted considerable attention primarily as it is available in enormous quantities. Lignocellulosic biomass can be classified broadly

into four classes: woody feedstock, agricultural wastes, perennial grasses, and municipal solid waste (MSW). Wood feedstock can be softwoods or hardwoods. Agricultural wastes include corn stover, sorghum, sugarcane bagasse, rice straw, wheat straw, empty fruit bunch from oil palm and date palm, agave bagasse from the beverage industry. Perennial grasses consist of switchgrass, miscanthus, canary grass, erianthus, napier grass, giant reed, and alfalfa. MSW consists of biodegradable organic components of MSW composed of paper and cardboard, kitchen waste and garden waste. Most of these biomasses are produced as low-value by-products and not competitive with food supply [8].

1.2. Lignin

Lignin (Figure 1.4) is a complex three-dimensional disordered macromolecule consisting of various types of methoxylated phenylpropanoid units. In 1819, the term Lignin was introduced by de Candolle and came from the Latin word lignum, which means wood [9],[10].

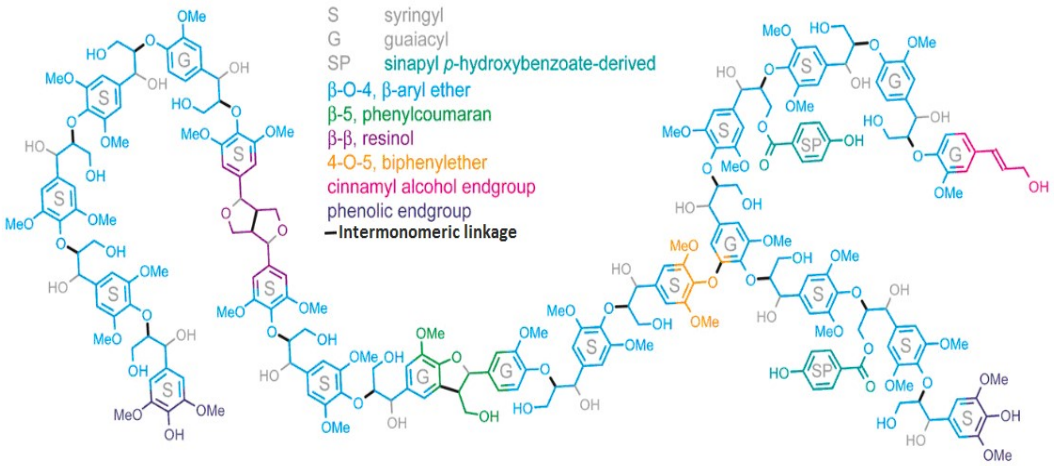

Figure 1.4. Representation of the structure of lignin from poplar, as predicted from NMR-based lignin. (Adapted from Vanholme *et al*. [11])

Lignin can be considered as polyphenolic material. Next to cellulose, lignin represents the second most abundant carbon source on earth. It can be found in woody plants but can also occur in non-woody plants such as grass [12]. As available oil reserves are in continual decline during the early 21st century, and there is concern about global warming [13], the importance of lignin as source of chemicals for society will increase in the future [14].

Lignin is biosynthesized from three monolignols (Figure 1.5): coumaryl alcohol, coniferyl alcohol and sinapyl alcohol, via free radical co-polymerisation of these precursor alcohols. The resulting polymer (lignin) is cross-linked, heterogeneous, optically inactive, and highly polydisperse [15].

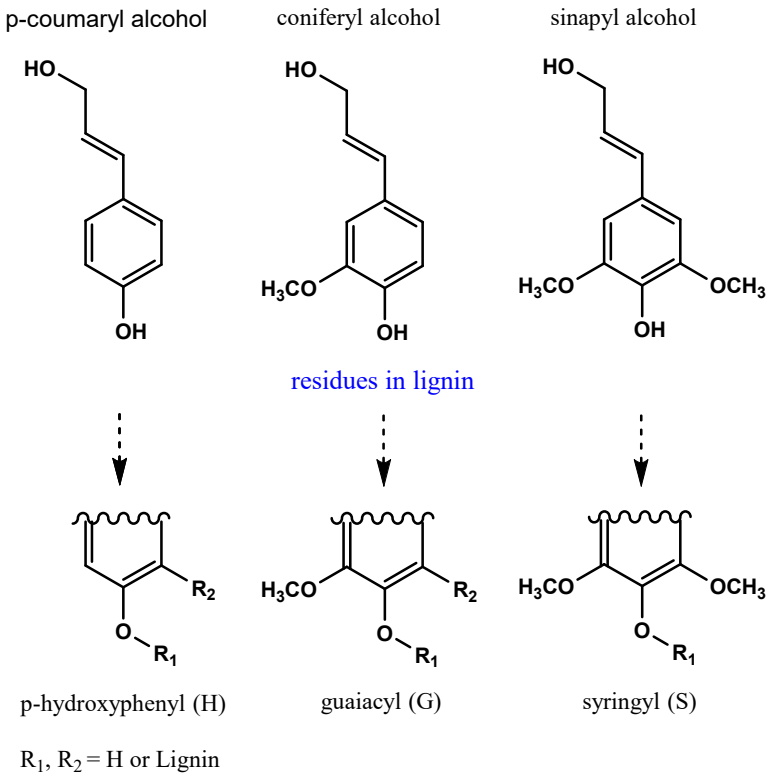

Figure 1.5. The structure of main monolignols and their residual structure in lignin.

The content of these monolignol derived units in hardwood, softwood, and annual crops are different. Coniferyl alcohol and sinapyl alcohol are the main phenylpropane units of the hardwood whereas softwoods contain significant amounts of p-coumaryl alcohol units in addition to the former monolignols. Commonly, in the lignin of both types of wood, the proportion of the coumaryl alcohol derived unit is usually very low, but it is more widespread in annual plants [16].

The amount and composition of lignin in plants vary widely from species to species, tree-to-tree, and even in different parts of the same tree. In woods the amount of lignin is in the range of 12% to 39%, softwoods contain a higher amount of lignin, next come hardwoods and grasses (Table 1.1). This range is determined according to Klason lignin analyses, which depend on removing the carbohydrates by acid-catalysed hydrolysis and solubilization of lignified material. The methoxyl content of lignin from hardwood is higher than softwood due to the presence of approximately equal amount of syringyl (S) and guaiacyl (G) units, while softwood contains roughly 90% of the total units are guaiacyl units. Studies on various extracted lignin have shown that the method of isolation significantly affects the actual structure and functional groups present in lignin [17],[8].

Lignin consists of a variety of linkages, and they are randomly connected by various aryl ethers (Figure 1.6). Although the ratio of these linkages differs depending on the type of wood, the majority of these linkages in lignin are ether linkages. The most frequent linkages in lignin are β-O-4, ß-5, 5-5, 4-O-5, ß-1, a-O-4 and β-β linkages. The β-O-4 linkage in hardwood lignin is about 1.5 times more abundant than in softwood lignin while the 5-5 and β-5 linkages are more abundant

in softwood lignin than in hardwoods. The most frequent linkage in lignin is β-O-4 [18],[19]. Table 1.2 shows the percentage of common linkages in lignin.

Table 1.1. The composition of structural components in assorted biomasses analysed extractives free [20].

Wood Species		Lignin (%)	Cellulose (%)	Hemicelluloses (%)
Softwoods	*Picea glauca*	27	41	31
	Pinus strobes	29	41	27
	Tsuga canadensis	33	41	23
	Norway spruce	28	46	25
	Loblolly pine	31	39	25
Hardwoods	*Eucalyptus globulus*	19	45	35
	Populus tremuloides	21	48	27
Agricultural residues	Corn stover	25	40	17
	Wheat straw	20	50	30
	Switchgrass	30	45	12

Table 1.2. The occurrence of inter-monomeric linkages in lignin from hard and soft wood, see Figure 1.6 for structures [16].

Type of bond	Substructure	%Softwood	%Hardwood
β-O-4	Phenylpropane β-aryl ether (*a*)	35-60	50-70
5-5’	Biphenyl (*b*)	10	5
β-β	Resinol (β-β-linked structure) (*d*)	2-3	3-4
β-1	1,2-diarylpropane (*e*)	1-2	1
β-O-4	Gylceryl aldehyde-2-aryl ether (*f*)	2	2
4-O-5	Diphenyl ether (*g*)	<4	7
β-5	Phenylcoumarane (*h*)	11-12	4-9

Lignin cannot be digested by animals and it forms a covalent bond with the other components in the cell, this also limits the accessibility of cellulose and hemicellulose to numerous microbial enzymes. Therefore, the digestibility of the overall plant feedstock is reduced, which is linked to the indigestibility of lignin. Nevertheless, some fungi and bacteria can degrade the polymer. Lignin degradation ability is crucial for the organism to remove the barrier that is required to reach cellulose, which is the nutrient source for them [21].

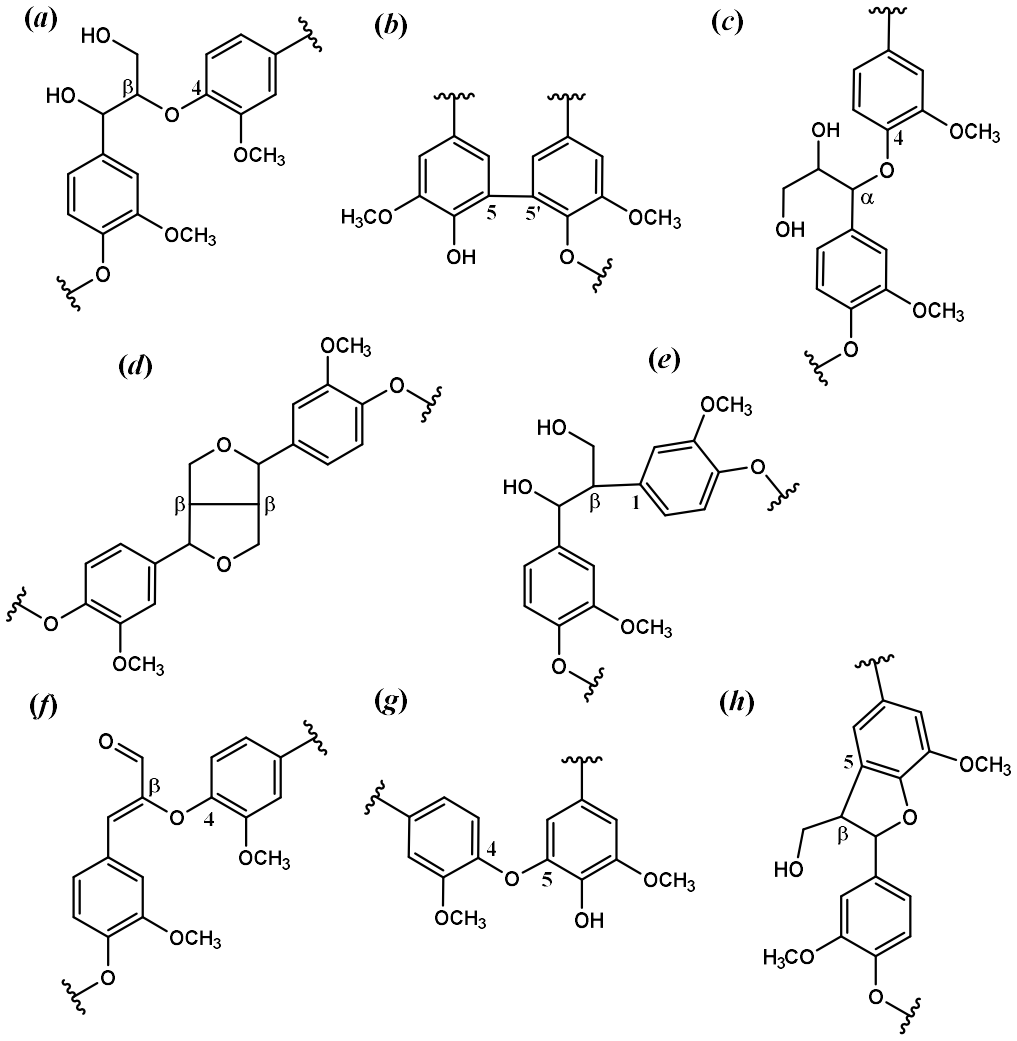

Figure 1.6. The common types of inter-monomeric bonds in lignin [13]. *a*. Phenylpropane β-aryl ether (β-O-4). *b.* Biphenyl (5-5'). *c.* Arylglycerol-α-aryl ether (α-O-4). *d.* Resinol (β-β (α-O-4)). *e* 1, 2-diarylpropane (β-1). *f.* Glyceryl aldehyde-2-aryl ether (β-O-4). *G.* Diphenyl ether (5-O-4). *h.* Phenylcoumarane (β-5)

1.3. Cellulose and hemicellulose

Cellulose and hemicellulose are carbohydrate polymers present in biomass. Plant matter contains about 35-48% cellulose and 22-30% hemicellulose [22]. The cellulose content in biomass varies among different plant sources, for example in cotton it is about 90% and in wood it is 40-50% [14].

Cellulose is fibrous, insoluble and a linear polymer of β-D-glucopyranose units (Figure 1.7). Glucose units are linked together via (β1→4) linkages, forming a crystalline polymer held together by a network of hydrogen bonds [23].

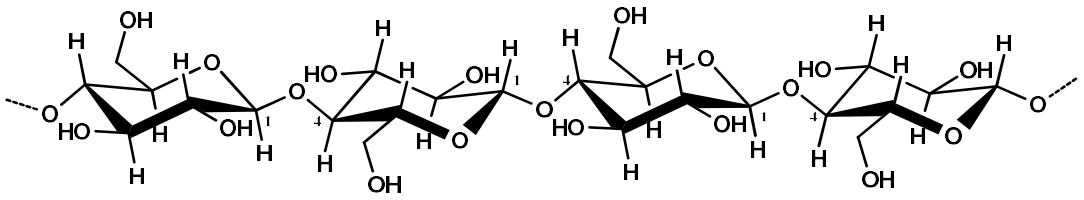

Figure 1.7. The structure of cellulose.

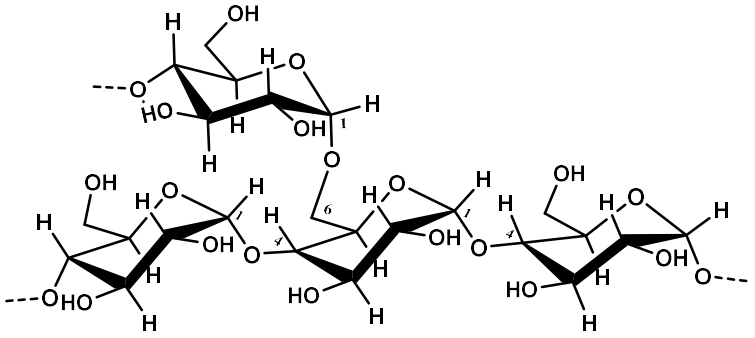

Figure 1.8. The structure of starch.

In contrast, starch is formed by glucose units linked by α (1→4), which also contains α (1→6) glycosidic linkage, and is therefore branched (Figure 1.8). Starch has a tendency to form a helical structure in solid state and solution [24].

Hemicellulose is also a major components of lignocellulose feedstock. It is a highly branched and substituted polysaccharide (Figure 1.9). Structurally, hemicellulose is diverse, and it is composed primarily of five-carbon sugars (D-xylose and L-arabinose), with a minor amount of six-carbon sugars (D-galactose and D-glucose). Hemicellulose is found connecting the cellulose and the lignin together [25].

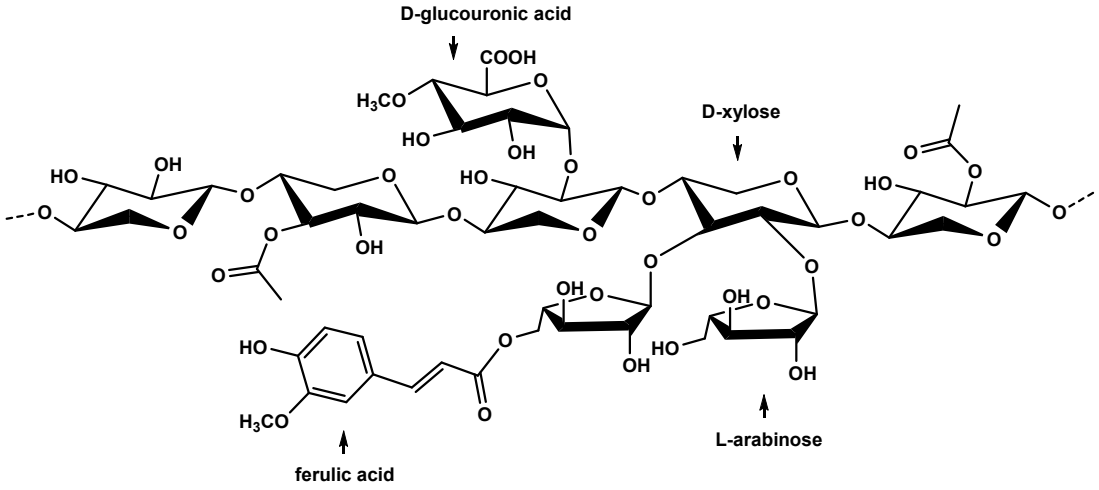

Figure 1.9. Hemicellulose structure.

1.4. Biofuel Production

Research into the production of liquid biofuels has increased significantly because of the dramatic rise in the price and the demand for fossil fuels in the last decade.

1.4.1. First generation of biofuel

There are three main and commercially available types of first generation biofuels. Figure 1.10 illustrates the main steps in bioethanol production. These include bioethanol, biodiesel and biogas (biomethane). There are established technologies for these kinds of biofuels, which lead to the production of large amounts worldwide. Biodiesel is produced from vegetable oil and residual fats and oils by a transesterification process (Figure 1.11). Biodiesel is an alternative for diesel, and it needs a slightly modified engine to serve as full substitute of diesel. Bio-ethanol is produced via fermentation of sugar from crops such as sugar cane or sugar beets, or starch from crops such as maize [26].

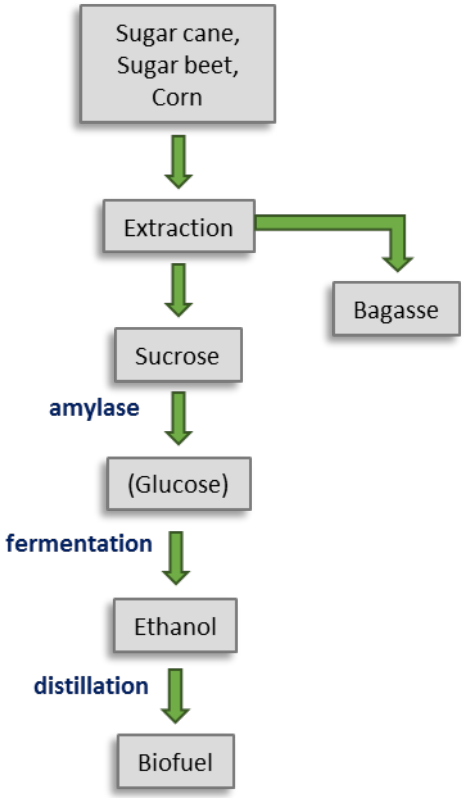

Figure 1.10. First generation bio-ethanol.

Bio-methane is produced from liquid manure by anaerobic bacteria. The main disadvantages of the first generation biofuels are the use of foods for the production of fuel, and it cannot be used as an absolute substitute for conventional fuel. This make it difficult to continue and led to researchers finding a new approach to making fuel from biomass which was not suitable for human consumption.

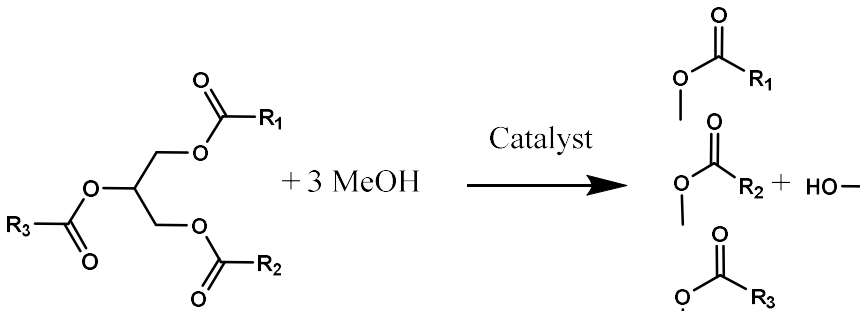

Figure 1.11. Chemistry of transesterification

1.4.2. Second generation biofuel

In second-generation biofuel production, non-food biomass is used or the non-food part of agricultural crops (e.g. wheat straw). This type of biofuel is more sustainable because the raw material (plant biomass) is renewable, cheap and available in large quantities. The second-generation biofuel is considered as carbon neutral or even negative in term of carbon dioxide emission. There are several technical barriers facing the production of fuel from lignocellulose. The most challenging obstacle is removing lignin from biomass, as it is linked covalently to polysaccharides in biomass and this limits their accessibility to hydrolyzing enzymes. Despite this, there are several thermochemical methods for pretreatment of lignocellulose for separation of lignin. Figure 1.12 is a schematic representation of second-generation biofuel production.

Another problem is the generation of hazardous material during the de-lignification process through thermo-chemical pretreatment, which inhibits carbohydrate digestive enzymes. Studies based on economic models with stylised representations of three biomass feedstocks (wheat straw, corn stover and warm season grass) for US second generation biofuel propose that generation of fuel from

lignocellulose material can compete with food crops or support food security. Biomass like wheat straw and corn stover are co-products of traditional food. Using these two types of biomass would result in a price increase of these residual materials and a greater allocation of land for the associated crops. While using dedicated biomass such as warm season grass would compete with the traditional food crops for land and would lead to rises in food prices [27].

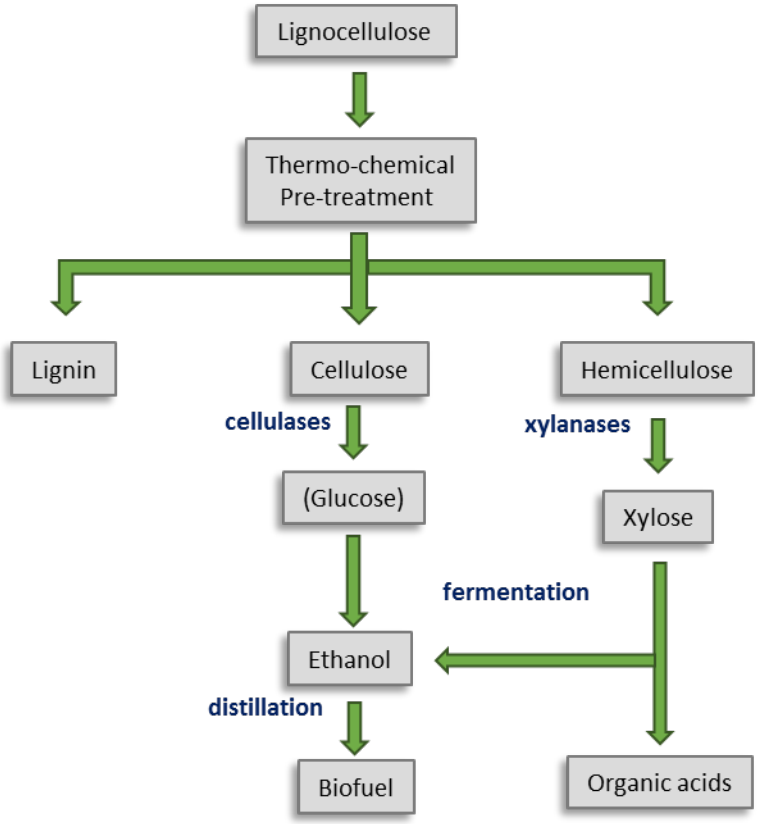

Figure 1.12. Production of fuel and valuable chemicals from lignocellulose biomass in second-generation bio-fuel production.

1.5. Isolation of lignin

Isolation of perfectly intact lignin is impossible [28], since, lignin is covalently bound to cellulose and hemicellulose in the lignocellulose structure. Thus, most isolated lignins are partially degraded or modified during the isolation process. Several methods have been used for isolation of lignin from biomass feedstock. These methods include physical, thermochemical and biological approaches. The majority of these methods are aimed at exposing cellulose and hemicellulose for the paper industry or second generation biofuel production while the remaining lignin is usually burned for energy after production [8]. In this section, some lignin isolation methods will be discussed.

1.5.1. Kraft lignin

In the paper industry, lignin is removed by a physicochemical method used to isolate individual cellulose fibres. This process is one of the most prevalent pre-treatment methods, known as Kraft pulping. The world production of lignin through the pulping process is over 30 million tons per year [9]. In the chemical pulping process, wood chips are cooked with an aqueous solution of sodium sulphide and sodium hydroxide at 170°C under high pressure [29]. Generally, lignin isolated by this method is heavily modified due to condensation reaction and cleavage of β-O-4 linkage which takes place during the Kraft pulping process. A proposed mechanism is shown in Figure 1.13, in which HS^- attacks at the α position, and then breaks the β-O-4 ether linkage.

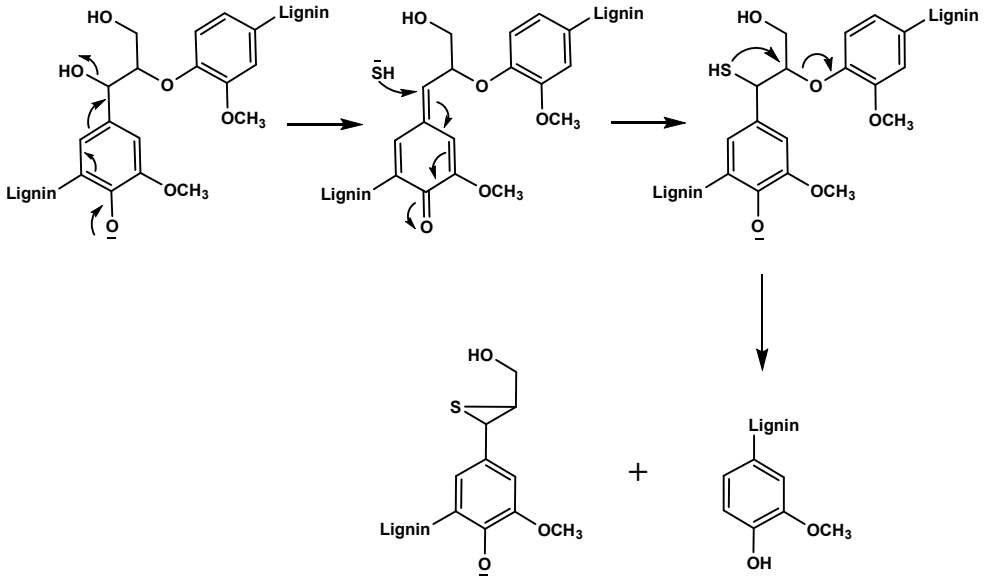

Figure 1.13. Lignin bond cleavage in Kraft pulping [16].

1.5.2. Organosolv lignin

Organosolv lignin pre-treatment is one of the most promising and environmentally friendly lignin preparation methods [30],[31]. Organosolv lignin can be prepared by treating biomass with organic or aqueous organic solvents at temperatures between 70 and 250°C [30],[32]. Sometimes catalyst such as acid or base is also added. In this process, lignin is efficiently removed from biomass with partial hydrolysis of its bonds, and most cellulose and hemicellulose are solubilised [33],[34]. In Figure 1.14, general steps in the preparation of organosolv lignin are explained [35].

The advantages of this technique include easy recovery of lignin by distillation and recycling of organic solvents [36], which decreases costs. In addition, removing organic solvents is essential for downstream fermentation processes, since the

solvents may inhibit hydrolytic enzyme [37]. The result of saccharification and fermentation suggest that the residual cellulose from organosolv pulp is free of fermentation inhibitors [38]. The sulphur-free organosolv lignin can be produced, and the isolated 90-100% of cellulosic material can be efficiently converted to glucose [39].

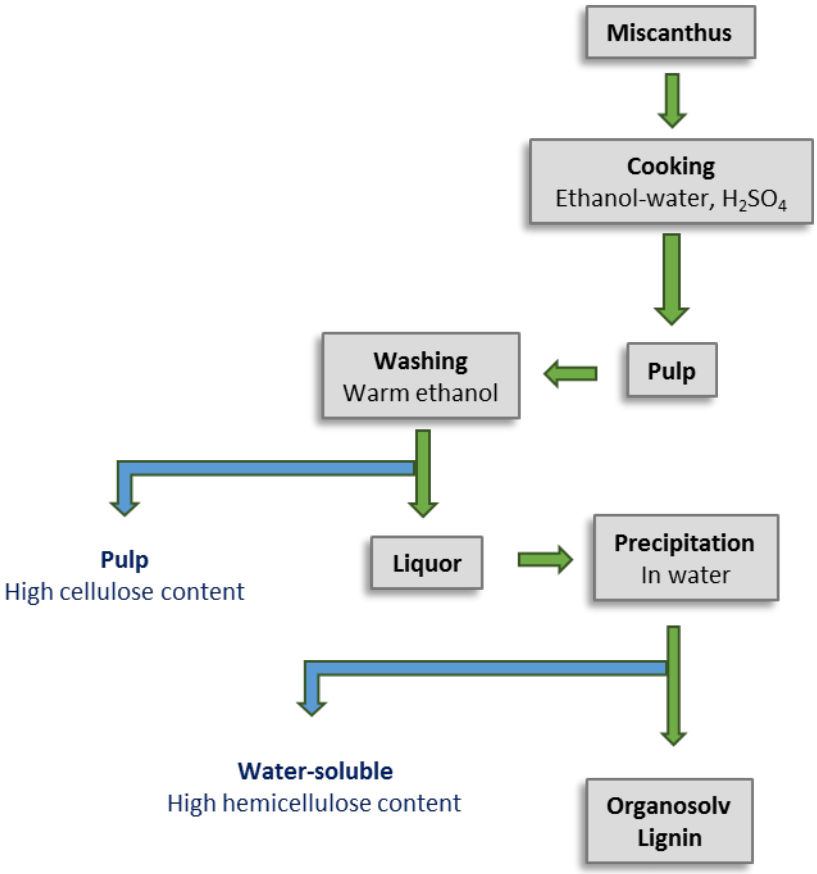

Figure 1.14. General steps in organosolv preparations

El Hage *et al.* described that the ethanol organosolv process can lead to efficient fractionation of lignocellulose material into two fractions including an aqueous fraction containing lignin and hemicellulose and the cellulose-rich residual material. In addition, the extracted lignin by this method can be degraded partially through breaking down of β-O-4 linkages and ester bonds (acetyl and coumaryl

residues) while the core of the lignin structure has not changed significantly [35]. In general, ethanol organosolv lignin contains a lower amount of residual carbohydrates (see Table 1.3). Among the solvent systems reported, a mixture of methyl isobutyl ketone, ethanol, and water (16/34/50 wt %) gave the highest yield of lignin (96.5-97.0%, based on percentage of lignin in feedstock) at optimal condition (120°C in 0.2 M H_2SO_4 and 160°C in 0.025 M H_2SO_4,). This fractionation system is thought to be the most suitable approach for biofuel and chemical production [40].

Table 1.3. Summary of reaction conditions for organosolv preparations, and the residual sugar percent in lignin.

Solvent system	catalyst	Sugar %	Time	Temperature	references
65-90% aqueous acetic acid (v/v)	0.1% HCl	1.8-2	4 hrs	85˚C	[31]
formic acid–acetic acid–H_2O (20/60/20, v/v/v)	0.1% HCl	4.3	4 hrs	85˚C	[31]
formic acid–acetic acid–H_2O (30/60/10, v/v/v)	0.1% HCl	2.8	4 hrs	85˚C	[31]
methanol–H_2O (60/40, v/v)	0.1% HCl	0.9	4 hrs	85˚C	[31]
ethanol–H_2O (60/40, v/v)	0.1% HCl	1	4 hrs	85˚C	[31]
DMSO	N/A	6.58	5 hrs	70˚C	[32]
70% aqueous ethanol	5% Et3N	3.35	5 hrs	70˚C	[32]

70% aqueous ethanol	0.5% NaOH	0.79	5 hrs	70˚C	[32]
40–60% aqueous ethanol (w/w)	H_2SO_4	0.25 -0.08	30–60 min	185–198˚C	[38]
65% aqueous ethanol	1.2% H_2SO_4	N/A	60 min	190˚C	[35]
Methyl isobutyl ketone, ethanol, and water (16/34/50 wt %)	0.2 and 0.025 M H_2SO_4	N/A	60 min	120 and 160˚C	[40]
88% aqueous formic acid	N/A	3.26	120 min	100.5˚C	[41]
95% aqueous ethanol	0.2 M HCl	0.04-0.05%	4 hrs	82-85˚C	[42]
95% aqueous acetone	0.2 M HCl	2.8%	4 hrs	~60˚C	[42]
95% aqueous dioxane.	0.2 M HCl	1.1%	4 hrs	~95˚C	[42]

1.5.3. Ionic liquid lignin

Ionic liquid (IL) pretreatment is a new and “green” approach for extraction of lignin and other plant biomass components. ILs are organic salts that can serve as a solvent for lignocellulosic biomass [43]. They comprise a pair of ions (cation/ anion), which melt at or below 100°C [44],[45]. Figure 1.15 is the structure of dialkylimidazolium ionic liquids. ILs can solubilise wood biomass and its components cellulose, hemicellulose and lignin [46].

The main advantage of ILs are that they are non-flammable, recyclable with low volatility, and have high thermal stability [45]. In addition, ILs can be designed with specific solvation properties depending on demand by selecting its cation and anion components [47],[48]. As a green designed solvent, ILs are attractive agents for lignocellulose pre-treatment [49].

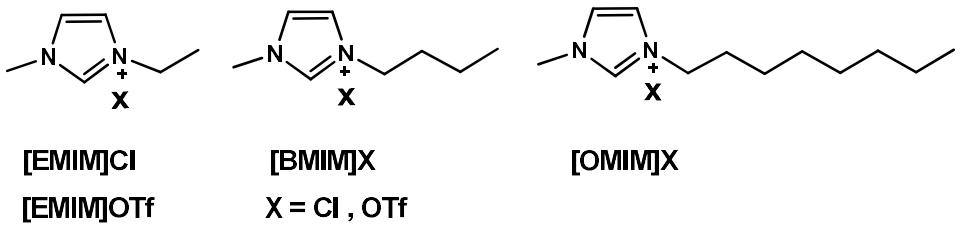

Figure 1.15. Dialkylimidazolium ionic liquids. These low- melting salts are promising solvents for lignin and, in the case of the chloride salts, lignocellulosic biomass [50].

Li *et al.* demonstrated that using (1-ethyl-3-methylimidazolium acetate ([C2MIM][OAc]) for lignification of switchgrass resulted in significant improvement in the rate of fermentation of cellulose by 16.7 fold, and a glucan yield of 96.0% obtained for 24 hrs [51]. Extraction of lignin from sugarcane waste through the use of a mixture of ionic liquids at elevated temperature (170-190°C) and atmospheric pressure gave a recovery of up to 93% lignin [49]. Lignin isolated through IL treatment has a partially modified structure [45]. Some research suggests that IL can break the ether and saturated alkyl groups in the presence of a catalyst (Brønsted acid) [18].

1.5.4. Milled wood-lignin

Milled wood lignin (MWL) is also called Bjorkman lignin, considered to be representative of the structure of native lignin [28]. Preparation of milled wood lignin involve a series of milling steps of biomass to increase solubility; then lignin is extracted into dioxane. This process is believed to protect the lignin structure from modification [52]. The main drawbacks of MWL preparation are that it is time-consuming, results in low yield, and can be contaminated with carbohydrate [53].

The technique encompasses a few steps. First, the lignocellulosic material is crushed to a size of 4 mm mesh with a Wiley mill, and lipid and wax are removed by treatment with 9:1 acetone: water. Second, the resulting material is ground with a rotary ball mill to a size of 0.1 mm mesh, then milled with a vibratory ball mill for 1 hour. Third, the product is stirred in 9:1 dioxane: water for one day, then the extracted material is separated. Fourth, an extraction with 1:1 dioxane: water is carried out and both extraction steps are repeated. Finally, the extracts are combined, and lignin recovered by rotary evaporation [54]. The whole process takes 1-2 weeks and gives a lignin recovery of typically < 2%.

1.6. Lignin biodegradation

Lignin is a recalcitrant, structural aromatic polymer that is formed commonly in response to injury and infection to protect plants from microorganisms [55],[56]. Despite this fact, there are some microorganisms that can degrade lignin such as fungi, bacteria [57] and yeast [56].

1.6.1. Fungal lignin degradation

Some fungi known as wood-decay fungi mainly from Ascomycetes, Deuteromycetes, or Basidiomycetes groups, have been found to degrade lignin. Lignin-degrading fungi can be classified into three categories: soft rot, brown rot, and white rot, depending on the constituent utilized and the colour characteristics of the decayed wood. These fungi can preferentially consume one or other cell wall component, causing the wood decay known as wood rot.

It has been found that Basidiomycetes fungal strains can degrade lignin. White rot fungi can degrade almost all wood components (cellulose, hemicellulose and lignin). The most efficient lignin-degrading fungi studied so far are *Phanerochaete chrysosporium, Trametes versicolor* and *Coriolus versicolor.*

Soft-rot fungi can only partially digest lignin while they can result in decomposition of cellulose and hemicellulose. This type of fungi typically grows on the surface of woods. The remnant of soft- decayed wood is spongy, wet, pitted, and brownish. Soft-rot fungi are less studied compared to other white and brown rot fungi.

Figure 1.16. Wood-rotting fungi (brown rot)

Brown-rot fungi degrade mainly cellulose and hemicellulose and leaving modified lignin as a dark brown residue, which can easily break down into powder.

Figure 1.17. White rot fungi.

White-rot fungi are the most studied wood-decay fungi. These fungi can degrade all three major biomass components efficiently, especially lignin. White-rot fungi typically belongs to the Basidiomycetes, which is a heterogeneous group of fungi. Different Basidiomycetes differ significantly in the relative rate at which they attack lignin and carbohydrate in biomass. The lignin-degrading enzymes produced by white-rot fungi will be discussed in section 1.7.

1.6.2. Lignin-degrading Yeast

Depolymerisation of relatively short lignin polymers (200-600 Dalton) to monomers and CO_2 by *Trichosporon fermentations* has been reported [56]. Some yeast species such as *Rhodotorula graminis*, *Geotrichum klebahnii*, *Rhodotorula mucilaginosa* can also degrade lignin monomers. *Rhodotorula spp.* strain can result in intense modification of lignin structure [58]. Yeast may have a major role in lignin degradation, but the size of lignin that can be degraded by yeast is limited. Perhaps,

yeast lacks an extracellular lignin-degradative system, which prevents them from effectively degrading polymeric lignin [56].

1.6.3. Bacterial degradation of lignin

Several studies have shown direct involvement of bacteria in lignin mineralisation. Also, there is growing evidence on bacterial lignin degradation. Bacterial lignin-degradation enzymology is less studied than that of wood rotting fungi such as white rot and brown rot fungi.

Some types of aromatic-degrading bacteria, mainly from the soil, can break down lignin. The bacterial lignin degrading strains are mostly found in Gram-positive Actinobacteria and the Gram-negative α-Proteobacteria classes.

Actinomycetes are usually found in association with wood decay. These bacteria are filamentous bacteria with some similarities to fungi and are the best-studied bacteria involved in lignin decomposition. The actinomycete *Nocardia autotropheia* can convert ^{14}C-labelled synthetic lignin to $^{14}CO_2$ [59]. *Norcadia* DSM 1069 can also result in decomposition of lignin and structural elements characteristic of lignin [60].

Rhodococcus jostii RHA1 (a polychlorinated biphenyl degrader) has been identified as a lignin degrader by using nitrated lignin assay. The assay involves chemically nitrated lignin, which gives an increase in absorbance at 430 nm upon depolymerization. The assay has been utilized for isolation of several bacterial lignin degrader strains (see Section 1.9. for more detail) [61]. Lignin degradation activities have been observed from extracellular fractions of the isolated strain. *Rhodococcus jostii* RHA1 results in decomposition of lignocellulose to small molecular weight

phenolic products (for example, ferulic acid and 5-carboxyvanillic acid) [62]. From the bioinformatic analysis of the genome of *R. jostii* RHA1 two types of Dyp peroxidases were identified (DypA and DypB) that were also found in other lignin degrading bacterial genomes. The latter has been identified as lignin peroxidase. Several experimental pieces of evidence confirm the involvement of *R. jostii* DypB in lignin degradation, whereas DypA most likely does not participating. These evidences include considerable impairment of lignin degradation ability of *dypB* deletion mutant of *R. jostii* , and kinetic results of recombinant DypB such as its activity in nitrated lignin UV/vis assay in the presence of hydrogen peroxide, kinetic behaviour with Kraft lignin samples, breaking down β-aryl ether model compound, and its effectiveness toward lignocellulose degradation. Consequently, the first bacterial lignin peroxidase has been cloned and overexpressed from *R. jostii* RHA1 [61].

Six lignin degrading bacterial strains from Actinobacteria family have been isolated from woodland soil using nitrated lignin spray assay on agar plates (see section 1.9. for more detail). Nitrated lignin UV-vis assay has been modified to adapt the method for use on agar plates [63]. The isolated lignin degraders included *Microbacterium phyllosphaerae, Microbacterium marinilacus, Microbacterium oxydans* and two *Micrococcus luteus* strains. The most active strain among Actinobacteria isolates was *Microbacterium phyllosphaerae* and one *Micrococcus luteus* when activity was tested using the nitrated lignin assay. In addition, all Actinobacteria isolates can grow on biphenyl and vanillic acid as a carbon source [63]. Figure 1.18 illustrates the screening method used for isolation.

The Streptomyces strains *Streptomyces viridosporus* T7A, and *Streptomyces setonii* can degrade softwood, hardwood and grass lignin [56]. However, they are more efficient in the degradation of grass lignin. *S. viridosporus* T7A produces an extracellular lignin peroxidase and this results in demethylation, ring cleavage and oxidation of the phenylpropanoid side chains in lignin [56]. An Actinomyces strain possessing lignin-decomposition ability has also been isolated from a tropical forest. The strain is only faintly related to the well-characterized *Streptomyces viridosporus* and *Rhodococcus spp* [64].

In the bacillus class, *Paenibacillus sp, Aneurinibacillus aneurinilyticus, Bacillus* sp. have been identified from pulp paper mill effluent sludge as efficient degraders of Kraft lignin [65].

Among Gram-negative bacteria, *Sphingobium* sp. SYK-6, formerly known as *Pseudomonas paucimobilis,* can break down various types of lignin-derived dimers and monomers such as β-aryl ether, biphenyl (dehydrodivanillic acid, DDVA), syringate and vanillate [66]. The catabolic pathways for degradation of these compounds are extensively studied. The detail about these pathways can be found in Section 1.8.

Three lignin-degrading Alphaproteobacteria were identified using nitrated lignin assay as a spray assay. Two of bacterial isolates were from Ochrobactrum species *Ochrobactrum pseudogrignonense* and *Ochrobactrum rhizosphaerae,* the third one was *Rhizobiales* [63]. Lignin metabolizing bacteria *Rhodomicrobium* in the family *Rhizobiales* have been detected by pyrosequencing analysis. It is also called purple non-sulphur bacterium. The Rhizobiales family can fix nitrogen and their ability to degrade lignin may be linked to their denitrification ability [64].

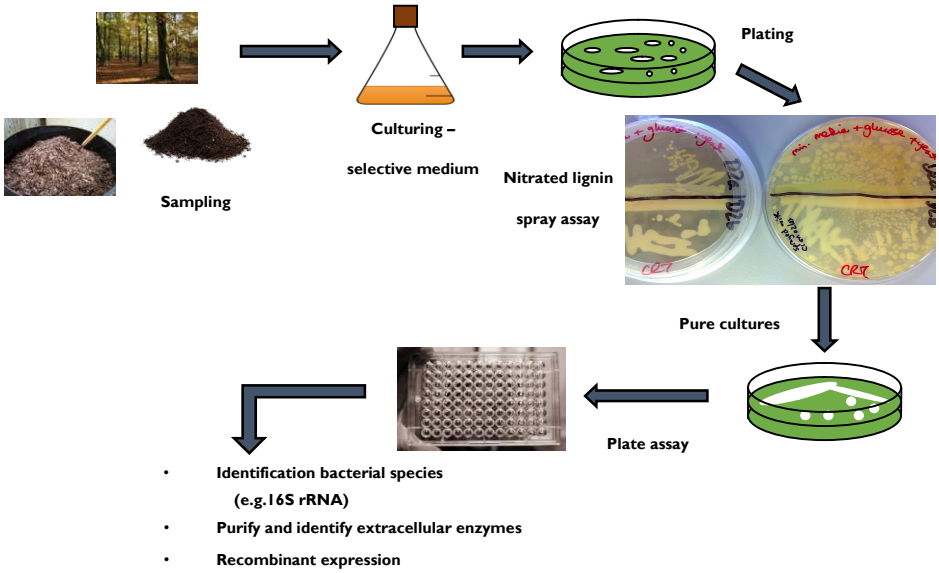

Figure 1.18. Steps in screening for novel bacterial lignin-degrading strains [63].

A lignin-decomposing Gammaproteobacteriaum has been isolated from tropical forest, which belongs to the family of the Enterobacteraceae, closely related to *Escherichia* spp. The latter has been observed as lignin degrader isolated from the gut of wood-boring beetles [64]. DeAngelis *et al.* isolated soil bacteria from rainforest *Enterobacter lignolyticus* SCF1 which can degrade lignin anaerobically. They sequenced the genome and identified two putative laccases, and a putative peroxidase using bioinformatics. The bacteria has a complete 4-hydroxyphenylacetate degradation pathway encoded in a single gene cluster [67].

A thermo-tolerant Bacteroidetes strain (*Sphingobacterium* sp. T2) has been isolated from compost using nitrated lignin assay for selection. The strain shows the highest ability for lignin depolymerization among 12 lignin degrading isolates [63]

(See Section 1.10 for more detail). Table 1.4 is a summary of the lignin-degrading bacteria so far isolated.

Table 1.4. Lignin-degrading bacterial strains reported in the literature and the compounds used for testing their degradation ability.

Family	*Strain*	Catabolic substrates	Reverences
Actinomyces	*Norcadia atotrophia*	synthetic lignin	[59]
	Norcadia DSM 1069	Lignin and lignin-related compounds	[60]
	Rhodococcus jostii RHA1	Nitrated lignin and β-aryl ether	[61]
	Rhodococcus spp	alkali lignin	[64]
	Rhodococcus erythropolis	Nitrated lignin	[63]
	Microbacterium phyllosphaerae	Nitrated lignin	[63]
	Microbacterium marinilacus	Nitrated lignin	[63]
	Microbacterium oxydans	Nitrated lignin	[63]
	Micrococcus luteus	Nitrated lignin	[63]
	Streptomyces viridosporus T7A	Lignin from wood and grass	[56]
	Leucobacter sp. SHC3	Kraft lignin	[68]
Bacillales	*Bacillus* sp	Kraft lignin	[69]
	Paenibacillus sp	Kraft lignin	[69]
	Aneurinibacillus aneurinilyticus	Kraft lignin	[69]
	Bacillus pumilus C6	Kraft lignin and β-aryl ether	[70]

	Bacillus atrophaeus B7	Kraft lignin and β-aryl ether	[70]
	Bacillus sp. Strains CS-1 and CS-2	Alkali lignin	[71]
	Bacillus sp. SHC1	Kraft lignin	[68]
Proteobacteria	*Sphingobium* sp. SYK-6	Lignin-derived mono- and bi-aryls	[66]
	Ochrobactrum pseudogrignonense	Nitrated lignin	[63]
	Ochrobactrum rhizosphaerae	Nitrated lignin	[63]
	Rhizobiales bacterium	Nitrated lignin	[63]
	Escherichia spp.	Alkali lignin	[64]
	Enterobacter lignolyticus SCF1	Alkali lignin	[67]
	Pseudomonas putida mt-2	Nitrated lignin	[62]
	Ochrobactrum sp. SHC2	Kraft lignin	[68]
Bacteroidetes	*Sphingobacterium* sp. T2	Lignin, biphenyl and vanillic acid.	[63]

1.7. Lignin-degrading enzymes

Lignin-degrading enzymes in white rot and brown rot fungi have been well studied during the last few decades. Three families of extracellular lignin-oxidising enzymes have been identified and characterised from fungi. These main enzyme families include lignin peroxidases, versatile peroxidase and laccases. There are two groups of peroxidases namely lignin peroxidases (LiPs) and manganese-dependent peroxidases (MnPs). However, the lignin degradation process is a complex catabolic process, which may need multiple enzymes. Enzymes such as glyoxal oxidase, aryl

alcohol oxidase (veratryl alcohol oxidase), pyranose 2-oxidase (glucose 1-oxidase), cellobiose/quinone oxidoreductase, and cellobiose dehydrogenase are believed to assist in lignin depolymerisation [8],[72].

1.7.1. Lignin peroxidases.

Lignin peroxidase is the first lignin oxidising enzyme identified in white rot fungi *Phanerochaete chrysosporium*. Structurally, LiPs are glycoproteins with a heme group in their active site (Figure 1.19). This enzyme catalyses hydrogen peroxide-dependent degradation of phenolic and non-phenolic compounds lignin model compounds (see Figure 1.21). Thus, they are considered to be the most powerful of the peroxidases [73]. They can oxidise a wide variety of organic compounds with high redox potentials (up to 1.4 V versus normal hydrogen electrode) in the presence of hydrogen peroxide [72].

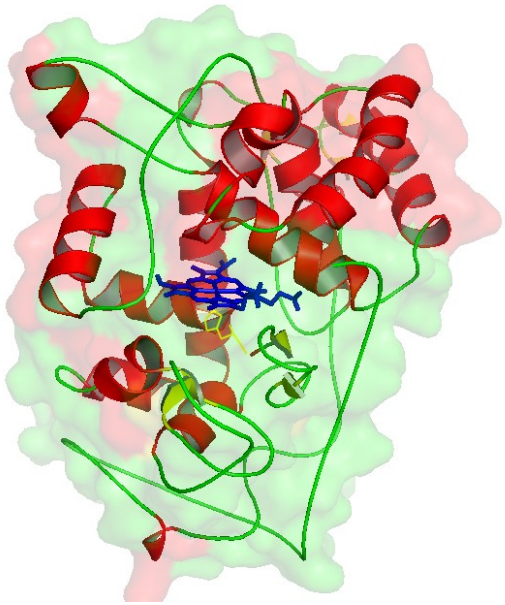

Figure 1.19. Lignin peroxidase structure (PDP entry 1B85).

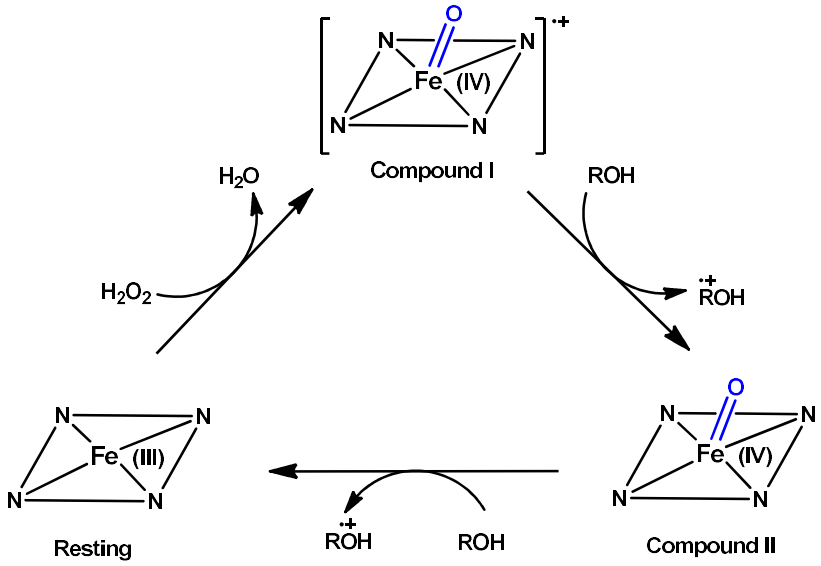

Figure 1.20. The catalytic cycle of lignin peroxidase**.** The cycle involves three steps: firstly, reaction of H_2O_2 with heme-ferric ion to produce oxyferryl iron radical cation [Fe (IV)=O•$^+$] which is known as compound I. This intermediate is formed as a result of cleavage of H_2O_2 at the O-O bond. Secondly, compound I is reduced by two consecutive 1e$^-$ with electron donor substrate. The first 1e$^-$ reduction results in the formation of compound II [Fe (IV)=O] and a radical cation of the substrate (ROH•$^+$). Finally, the reduction of compound II with the second electron returns the enzyme to resting state [Fe (III)] [72].

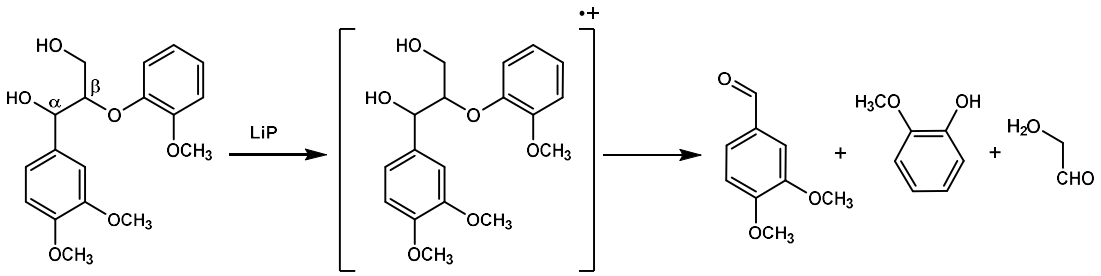

Figure 1.21. Cleavage of C_α-C_β bond of β-aryl ether non-phenolic lignin model compound by lignin peroxidase.

1.7.2. Manganese-dependent peroxidases.

MnPs are structurally related to LiPs and are glycoproteins with a heme group in their active sites, but their molecular weights are slightly higher [3]. MnPs can oxidise polymeric lignin, phenolic and non-phenolic lignin model compounds (Figure 1.22) via a diffusible redox mediator. This mediator is produced by MnPs through oxidation of Mn(II) to Mn(III), as a complex with a suitable organic acid chelator, for example malate or oxalate [74].

1.7.3. Versatile peroxidases.

Versatile peroxidases (VP) are a family of heme-containing peroxidase with high redox potential and broad substrate specificity. This group of the enzyme have the ability to oxidise both Mn(II) and lignin model compounds. Versatile peroxidases exhibit activity toward phenolic and non-phenolic substrates. The enzyme can oxidize high redox potential substrates, e.g. Reactive Black 5, veratryl alcohol, and methoxybenzenes without manganese [72],[75].

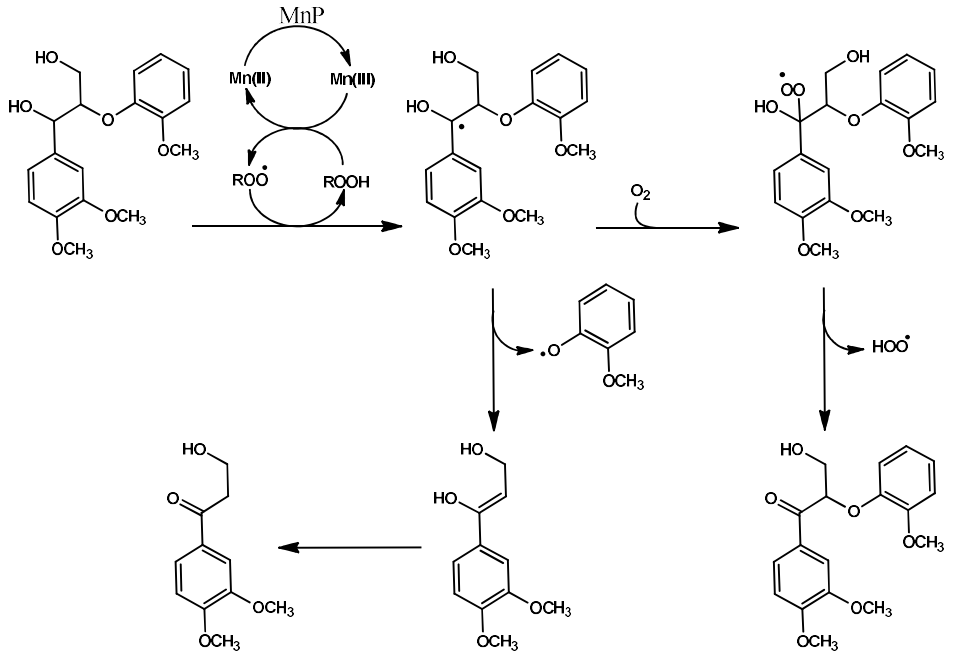

Figure 1.22. Oxidation of non-phenolic aryl ether (β-O-4) of a lignin model compound catalysed by Mn-dependent peroxidase [76],[72].

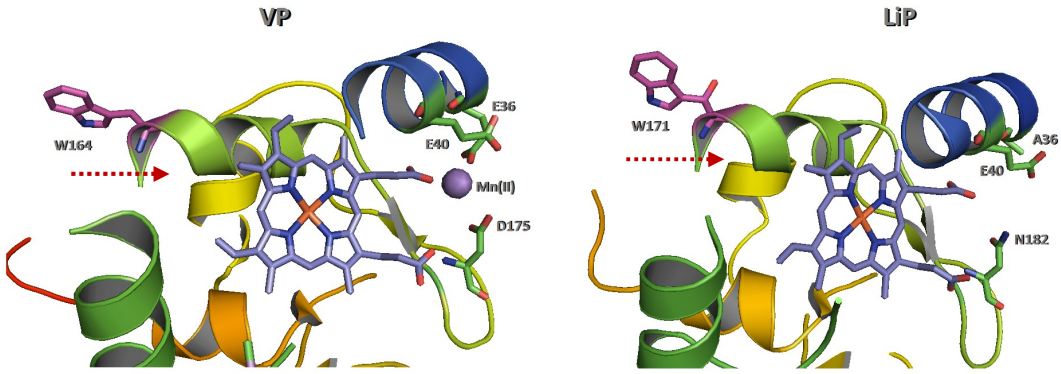

Figure 1.23. Heme-region of versatile peroxidase (VP) and lignin peroxidase (LiP). VP is similar to LiP having exposed catalytic tryptophan (W164 in VP and W171 in LiP) and long-range electron transfer (LRET) to heme (red arrow). This amino acid is responsible for the oxidation of high-redox-potential substrates. VP also has manganese binding site (Glu36, Glu40 and Asp175) similar to Mn-dependent peroxidase. From PDB entries 2BOQ and 1LLP [77].

1.7.4. Dye-decolourising enzymes.

Dye-decolourising peroxidases have been recently classified as a novel superfamily of heme-containing peroxidase enzymes. This superfamily of peroxidases is not related to plant or animal peroxidases, and DyP-type peroxidases are identified in bacteria, fungi and archaea [78]. This class of enzyme has two different type of catalytic activity: oxidation of organic compounds, and hydrolysis of wheat straw cellulose [79]. DyP-type peroxidases can decolourise a wide range of dyes [80], oxidize ß-carotene [81], and aromatic sulphides [82], as well as being involved in lignin degradation [78].

The first member of DyP-type peroxidases was discovered and purified in 1999 from fungus (*Geotrichum candidum*) [80]. Two DyP-type peroxidases have been purified from extracellular fractions of the basidiomycete *Marasmius scorodonius* (garlic mushroom). The enzymes were named as MsP1 and MsP2. The molecular weight of MsP1 and MsP2 were ~150 kDa and ~120 kDa respectively [81].

In bacterial strain *Rhodococcus jostii* RHA1, two Dyp peroxidase have been identified, DypA and DypB. Both enzymes show the ability to oxidize ABTS, pyrogallol, and Reactive Blue 4 in the presence of hydrogen peroxide. DypA and DypB are apparently possessing similar specificities for ABTS, with k_{cat}/K_M of 2.0×10^3 and 2.4×10^3 $M^{-1}S^{-1}$ respectively. Whereas, they utilise Reactive Blue 4 and pyrogallol in a different way, DypA possesses more specificity for Reactive Blue 4 (k_{cat}/K_M of 12800 $M^{-1}S^{-1}$) than pyrogallol (k_{cat}/K_M of 50 $M^{-1}S^{-1}$) and DypB exhibits more specificities for pyrogallol (k_{cat}/K_M of 600 $M^{-1}S^{-1}$) than Reactive Blue 4 (k_{cat}/K_M of 140 $M^{-1}S^{-1}$) [83]. Only DypB shows activity in the

nitrated lignin assay, and DypB also showed activity toward a variety of substrates including Kraft lignin, β-aryl ether lignin model compound (Figure 1.24) and Mn^{2+}. For crystal structure of DypB from *R. jostii* RHA1 and DyP-type peroxidase from *Thermobifida cellulosilytica* see Figure 1.25.

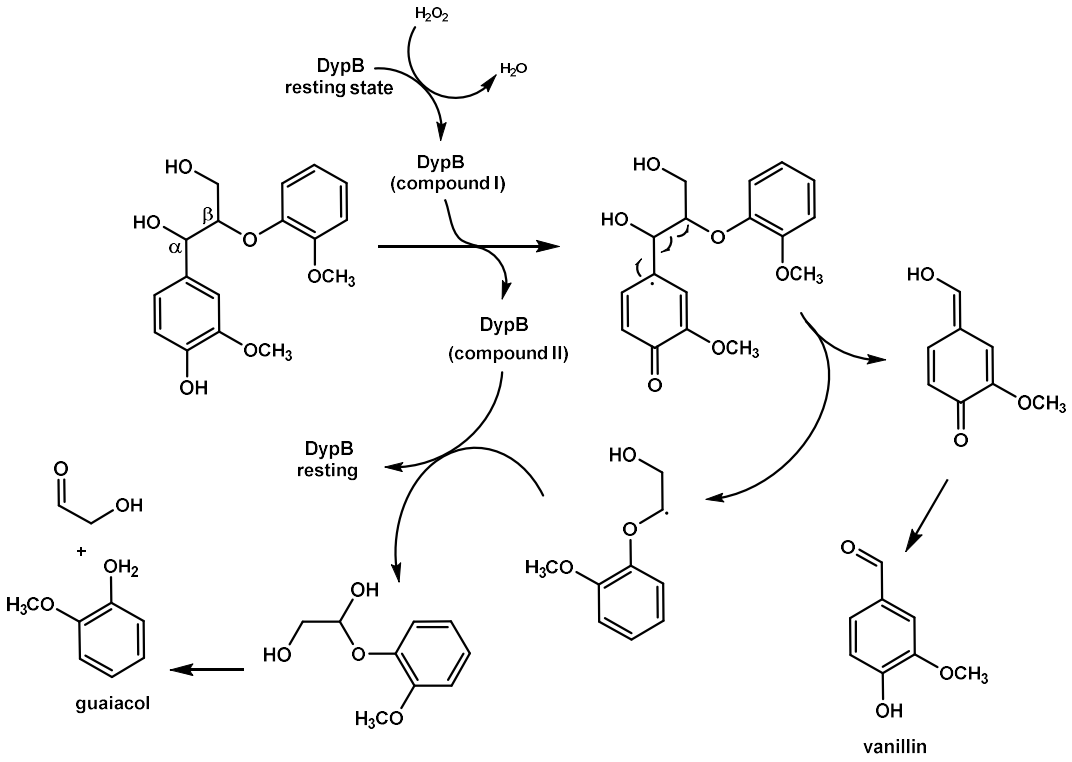

Figure 1.24. Breakdown of β-aryl ether lignin model compound by DypB from *Rhodococcus jostii* RHA1 [61].

Three genes related to the *dyp* family of peroxidase enzymes were identified in the genome of *Pseudomonas fluorescens* Pf-5 from bioinformatics searches using the BLAS algorithm [84]. Two of these enzymes (Dyp1B and Dyp2B) are belong to class B, and the other one is of class A (DypA) of dye decolourising peroxidases. Among of these three DyP enzymes only recombinant Dyp1B showed lignin degrading ability when tested with powdered wheat straw and Kraft lignin in presence of Mn^{2+}, and a comparable Mn^{2+} oxidation ability (k_{cat}/K_M of 3.3×10^1 $M^{-1}S^{-1}$) with DypB from *R. jostii* RHA1 [84]. From *Amycolatopsis* sp. 75iv2, a multi-

functional dye decolourising peroxidase has been characterized. This enzyme is classified as a type-C Dyp peroxidase with high peroxidase and Mn-oxidation ability [85].

The *R. jostii* RHA1 DypB has lower activity for oxidation of each of Mn^{2+} (k_{cat}/K_M of 2.5×10^1 $M^{-1}S^{-1}$) and ABTS [83] than *Amycolatopsis* sp. 75iv2 Dyp2 k_{cat}/K_M 1.2×10^5 $M^{-1}S^{-1}$ for Mn^{2+} and k_{cat}/K_M of 6.6×106 $M^{-1}S^{-1}$ for ABTS. The manganese oxidizing ability of *R. jostii* RHA1 Dyp-B has been improved 80 fold through substitution of Asn246 with alanine [86].

Stopped-flow UV-vis spectrophotometry shows that reaction of Dyp-B from *R. jostii* RHA1 with H_2O_2 forms a stable compound I-like intermediate with a λ_{max} of 397 nm. In addition, a compound II species was also detected at 417 nm using a β-aryl ether lignin model substrate [61]. For general catalytical cycle of DyP-type peroxidases see Figure 1.26.

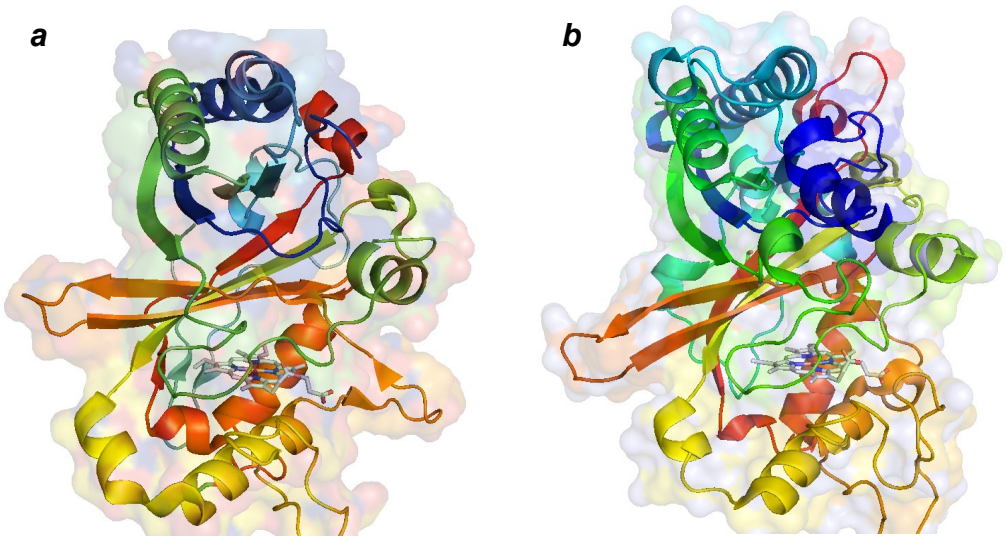

Figure 1.25. Structures of dye-decolorizing peroxidase ***a.*** DypB from *R. jostii* RHA1 (PDB: 3QNR) ***b.*** DyP-type peroxidase from *Thermobifida cellulosilytica* (PDB: 4GS1).

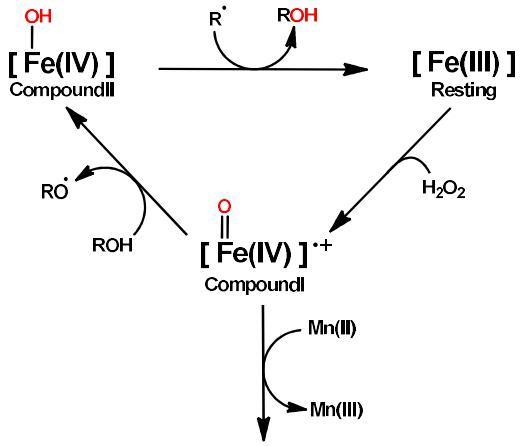

Figure 1.26. Catalytic cycle of dye-decolourising peroxidases Dyp-B [61].

1.7.5. Laccases.

Laccases are copper-dependent enzymes that catalyse the oxidation of phenolic compounds (Figure 1.27), methoxy-substituted phenols, diamines and a considerable range of other compounds [87] and they can also oxidise non-phenolic compounds in the presence of mediator molecules such as 2,2'-azinobis(3-ethylbenzothiazoline-6-sulfonic acid) (ABTS) and 1-hydroxybenzotriazole (HBT), see Figure 1.28.

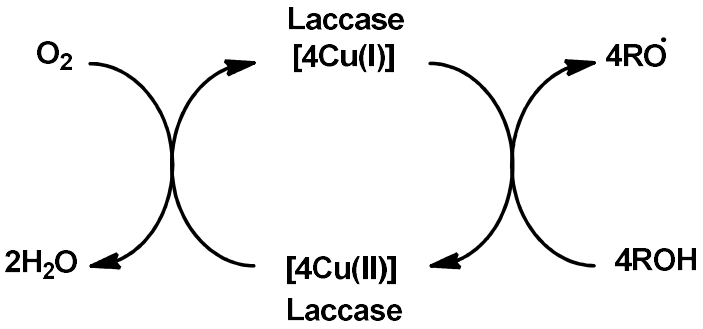

Figure 1.27. Laccase-catalysed redox cycles for substrate oxidation in the absence of mediator.

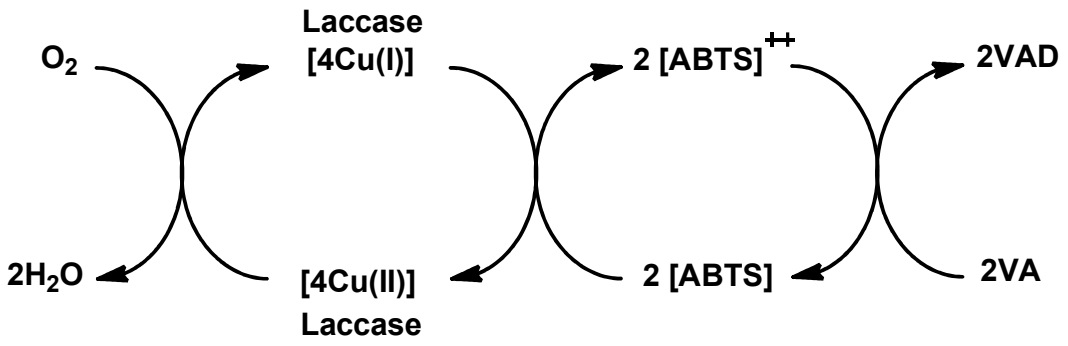

Figure 1.28. Laccase-catalysed the conversion of veratryl alcohol (VA) to veratryl aldehyde (VAD) in the presence of mediator (ABTS).

Laccases have been found in many organisms such as fungi, bacteria, insects and plants. Their physiological role is unclear because in plants they play a role in lignin biosynthesis while in fungi they are involved in the ligninolytic process [26]. Laccases are also known as blue multicopper oxidases containing four copper atoms with a highly conserved binding motif [88]. They can result in depolymerization and also polymerization of lignin because they form radicals by abstraction of one electron from phenolic or polyphenolic substrates [87]. For structure of laccases from two different organisms see Figure 1.29.

Laccases are of high biotechnological potential, since they exhibit a broad substrate specificity. Currently, only fungal laccases have been used in biotechnological applications, although bacterial laccases may have properties that make them more suitable for industrial application, such as thermostability, high tolerance to chlorine, broad pH range and efficient heterologous expression (Table 1.5) [71].

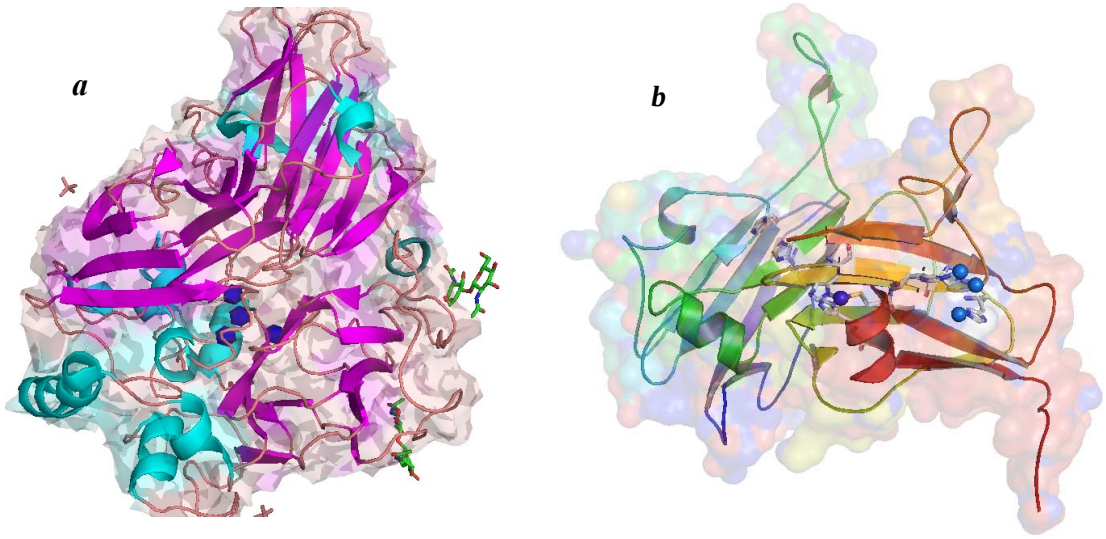

Figure 1.29 Crystal structure of two different laccases. ***a.*** laccase from white-rot fungi *Steccherinum ochraceum* (PDB, 3T6V)**.** ***b.*** Bacterial laccase (trinuclear cluster) from *Streptomyces coelicolor* which, has two domains (PDB, 3KW8).

Alexandre and Zhulin (2000) have identified several putative bacterial laccases (mainly in α-, γ- and ε-proteobacteria) using BLAST search, some of which have signal peptides for extracellular translocation [89]. Another study based on bioinformatics analysis shows that about 76% of 1,200 putative bacteria genes for laccase-like enzymes have signal peptides which may be responsible for export to the extracellular environment [90].

Laccase producing bacteria *Paenibacillus* sp. can depolymerise lignin and detoxify effluent from pulp and paper mills [91]. Chang *et al.* demonstrated that laccases from two *Bacillus* sp. strains (CS-1 and CS-2) isolated from forest soil can break down alkaline lignin [71]. Fang et al., (2012) found that laccase from aquatic bacteria identified through screening of marine metagenomic libraries exhibit high activity toward syringaldazine and decolourise azo dye without redox mediator [92]. Isolated soil bacterial strains (*Bacillus pumilus* C6 and *Bacillus atrophaeus* B7) from

rainforest with high laccase activities can degrade Kraft lignin and β-aryl ether lignin model compounds [70].

Actinomycetes produce laccases homologous to fungal laccases, but their sequences shorter than the latter, and therefore named as "small laccases". These small laccases described to have in vitro activity toward a wide spectrum of the substrate. *Streptomyces coelicolor* A3 genome encodes a gene for small laccase (SCLAC) which has sequence similarity to fungal laccases. *Streptomyces coelicolor* A3 SCLAC found to have a significant role in lignin depolymerization process. Gene replacement study (substitution of (SCLAC) with apramycin resistance cassette) shows a reduction of acid-perceptible polymeric lignin (APPL). The small laccases from other Streptomyces species, including *S. lividans* TK24, *Amycolatopsis* sp. 75iv2, and *S. griseus* NBRC 13350, reported to have ability in rearranging the nonphenolic β-O-4 lignin model compound in the presence of mediators and degradation of phenolic β-aryl ether (β-O-4) lignin model compound without any mediators [93].

Table 1.5. Properties of laccases from bacterial strains**.**

Bacterial strain	Proprieties
Bacillus subtilis	High thermostability The purified enzyme has a half-life of inactivation of 2 hrs at 80°C.
Thermus thermophilus	High thermostability High optimal reaction temperature (92°C) and a half-life of inactivation of > 14 hours at 80°C.
Bacillus halodurans	High stability toward chloride: simulation instead of inhibition by chloride
Streptomyces ipomoea	exhibits high thermal- and pH-stability

1.8. Aromatic degradation pathways for lignin degradation in bacteria.

Several Gram-positive and Gram-negative bacteria from different genera (examples: *pseudomonads*, *sphingomonads*, *Rhodococcus spp*. [26], *Ralstonia spp*., and *Burkholderia spp*. [94]) can degrade aromatic compounds. There are aromatic degradation cluster genes in the genome of these aromatic degraders. Some of these bacterial strains have pathways for breakdown of lignin- monomeric and -dimeric units [26],[95]. Most probably there is a link between the presence of aromatic degradation pathways and lignin depolymerisation ability in bacteria. Understanding of bacterial aromatic pathways is essential for adding value to lignin and production of renewable chemicals from lignin [95]. Catabolic pathways in *Sphingomonas paucimobilis* SYK-6 for degradation of lignin model compounds have been extensively studied [73].

1.8.1. Pathway for aryl ether degradation

Breakdown of aryl glycerol-β-aryl ether (see Figure 1.30) is the most important step in lignin decomposition [96], since, 50% of inter-monomeric linkages in lignin are of a β-O-4 type. In *S. paucimobilis* SYK-6, conversion of β-aryl ether model compound to its corresponding monomers is catalysed by two different enzymes. Initially, NAD-dependent dehydrogenase LigD oxidises the α-hydroxyl group of β-aryl ether to the corresponding ketone [96] and then, a novel glutathione-dependent β-etherase enzyme LigEFG breaks the ether linkage [26]. In contrast, in other bacteria only one enzyme such as dye decolourising peroxidase from *R. jostii* RHA1 is known to oxidise β-aryl ether to its consistent monomers [61].

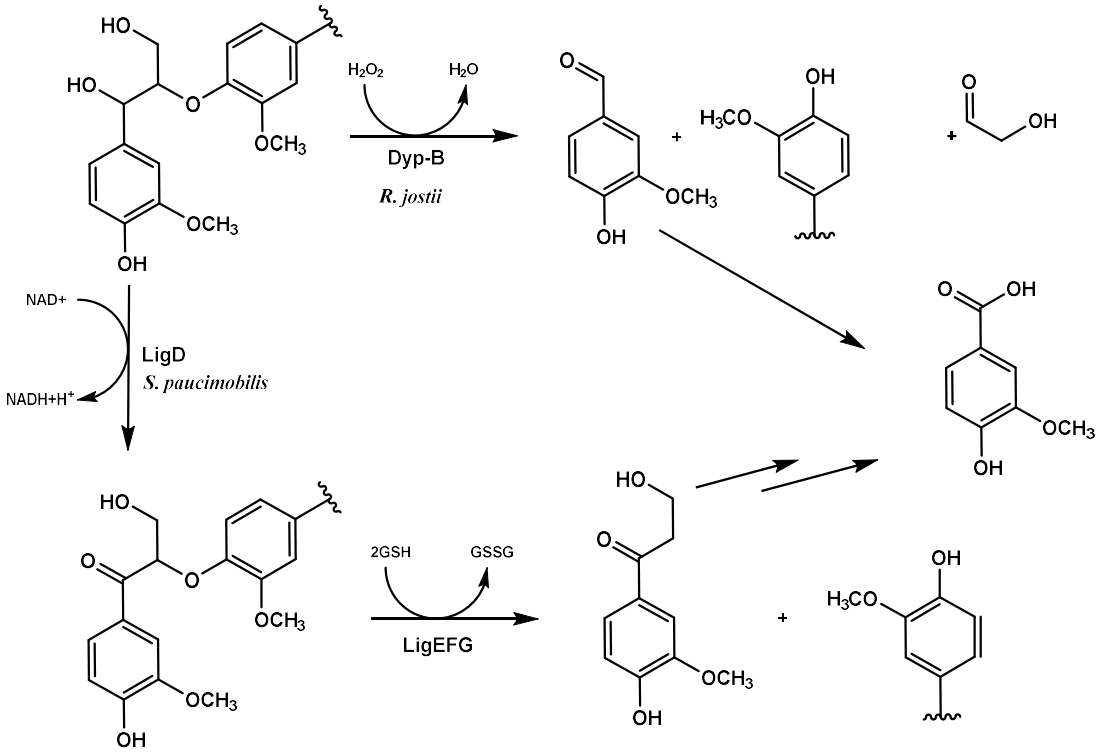

Figure 1.30. Pathway for a breakdown of β-O-4 aryl ether model compounds.

1.8.2. Pathway for biphenyl degradation

The biphenyl linkage is one of the main linkages in polymeric lignin; generally it can be found between guaiacyl subunits. Transformation of 5-5'-divanillic acid to 5-carboxyvanillic acid and 4-carboxy-2-hydroxypentadienoic acid is catalysed by four enzymes (Figure 1.31): demethylase (LigX), extradiol dioxygenase (LigZ) and C–C hydrolase (LigY). Firstly, demethylation of 5-5'-divanillic acid is performed by LigX. Secondly, the catecholic product of LigX undergoes oxidative meta-cleavage by LigZ. Thirdly, LigY converts the ring fission product to 5-carboxyvanillic acid and 4-carboxy-2-hydroxypentadienoic acid. Finally, 5-carboxyvanillic acid can be transformed to vanillic acid by a decarboxylase enzyme LigW [26].

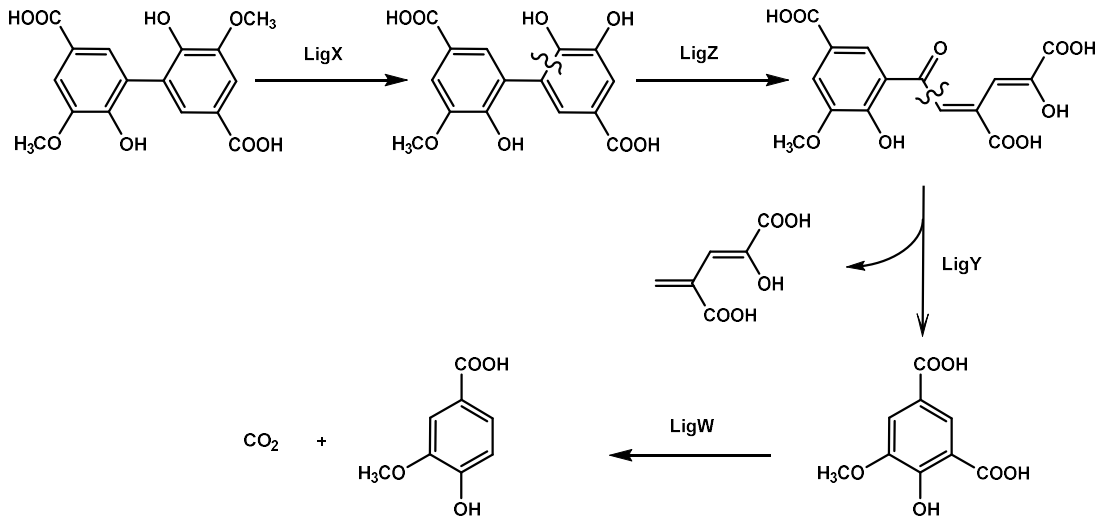

Figure 1.31. Dehydrodivanillic acid catabolic pathway.

1.8.3. Pathway for protocatechuic acid degradation

This pathway can be considered as a central pathway, since oxidation of most of the lignin related products and lignin model compounds such as β-aryl ether, 5, 5'-divanillic acid and ferulic acid, toluene and xylene result in production of precursor of protocatechuic acid (vanillin or vanillic acid) or related compounds. Protocatechuic acid can be generated from demethylation of vanillic acid [97]. In most bacteria, iron (III)-dependent protocatechuate 3,4-dioxygenase cleaves the ring of protocatechuic acid to give carboxy-cis,cis-muconic acid. Two pathways for catabolism of catechol are exist: meta-cleavage (extradiol) pathway involves cleavage between the two phenolic hydroxyl groups, and ortho-cleavage (intradiol) pathway involves cleavage adjacent to the phenolic hydroxy groups (Figure 1.32) [73],[97],[98].

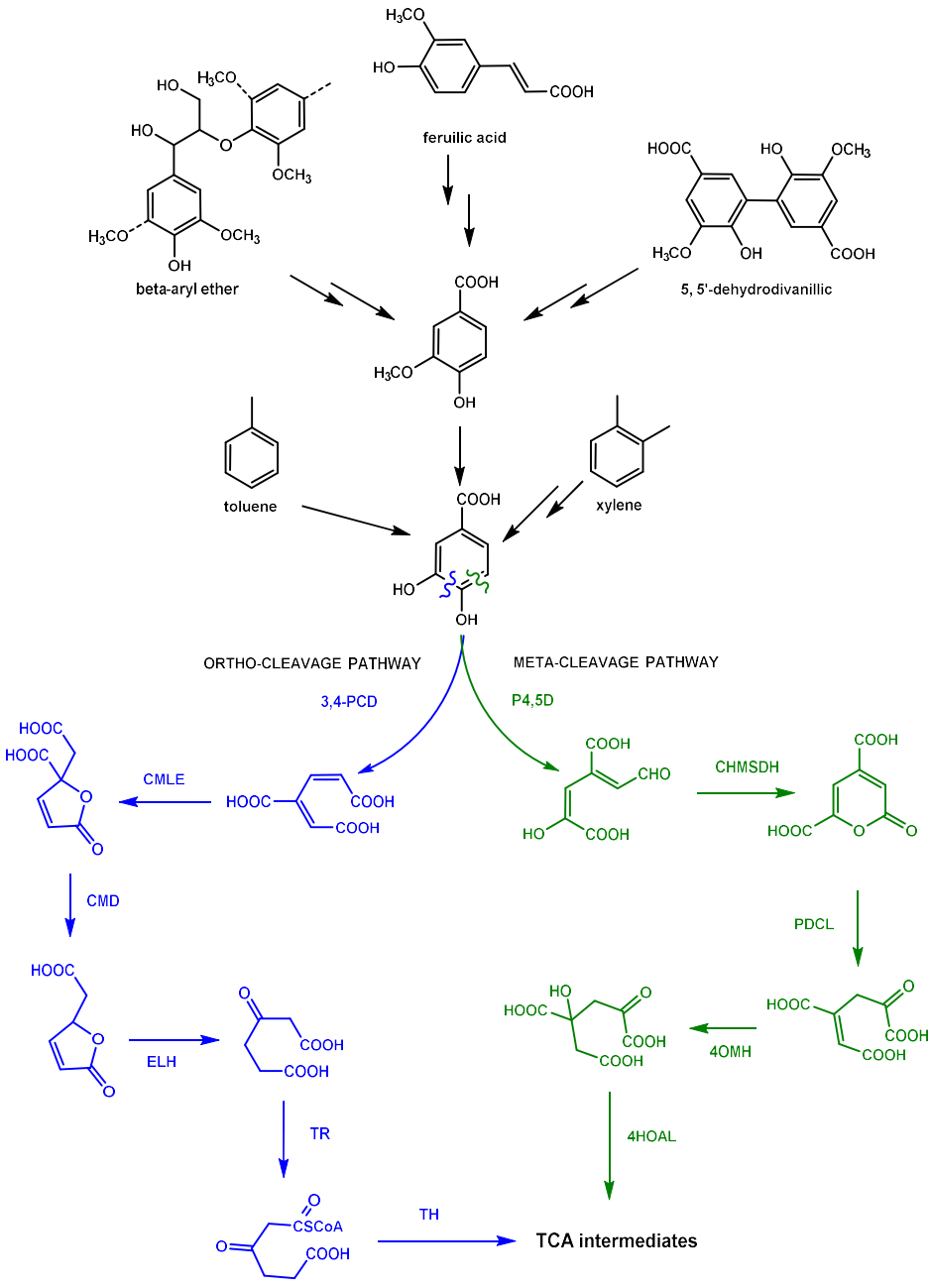

Figure 1.32. Pathway for degradation of protocatechuic acid and its derivatives. Enzymes involved in ortho-cleavage (intradiol) pathway are: protocatechuate 3,4-dioxygenase (3,4-PCD); ß-carboxymuconate lactonizing enzyme (CMLE); γ-carboxymuconolactone decarboxylase (CMD); enolactone hydrolase (ELH); ß-ketoadipate:succinyl-CoA transferase (TR); ß-ketoadipyl-CoA thiolase (TH). Enzymes for meta-cleavage (extradiol) pathway are: protocatechuate 4,5-dioxygenase (P4,5O); 4-carboxy-2-hydroxymuconate-6-semialdehydedehydrogenase (CHMSDH); 2-pyrone-4,6-dicarboxylate lactonase (PDCL); 4-oxalomesaconate hydratase (4OMH); 4-hydroxy-4methyl-2oxoglutarate aldolase (4HOAL).

In *S. paucimobilis* SYK-6, there is only extradiol cleave reaction which is catalysed by protocatechuate 4,5-dioxygenase enzyme LigAB. This enzyme is a crucial catalyst in the catabolism of syringate and vanillate. The extradiol pathway results in the production of pyruvate and oxaloacetate and then leads to the TCA cycle (Tricarboxylic acid cycle) to further oxidation [26]. While the intradiol pathway starts with cleavage of protocatechuate acid by protocatechuate 3,4-dioxygenase, leading to the production of β-ketoadipate. This product is then subsequently converted to 3-oxoadipate, which in turn is transformed to succinate and acetylCoA [26],[98]. These products then enter the TCA cycle. Proteomic analysis and gene sequencing show the presence of intradiol cleavage pathway in aromatic degrader strain *Rhodococcus* sp.TFB [99].

1.9. Methods for monitoring lignin biodegradation.

Investigation of microbial lignin breakdown is hampered by the absence of a convenient assay. There are several ways in the literature, which have been used in isolation of lignin-degrading organism and/or purification and evaluation of ligninases. However, each of the methods has certain disadvantages.

The earliest method for monitoring of lignin biodegradation included the use of ^{14}C-labelled lignin as a substrate and quantitation of released $^{14}CO_2$ [56],[62],[100] or other ^{14}C-fragment [56]. The ^{14}C-lignins were prepared by feeding labelled lignin precursors such as ^{14}C-phenylalanine or ^{14}C-cinnamic acid to growing plants then isolating ^{14}C-labelled lignin. Alternatively, ^{14}C-labelled synthetic lignin (Dehydrogenative polymer, DHP) was made from ^{14}C-coniferyl alcohol or other monolignols using horseradish peroxidase (HRP) as a catalyst [56]. This approach is

rather a time-consuming method, and it cannot be used for screening a large number of samples, nor is it convenient to use for determination of ligninase activities or enzyme kinetic parameters.

Monomeric and dimeric lignin model compounds are widely used for assessment of lignin degradation ability. Model compounds β-O-4 and biphenyl are examples of dimeric model compounds utilized in the determination of mechanism of lignin breakdown process. Phenolic and non-phenolic β-O-4 are particularly the most frequent dimeric model compounds used. However, there is no colorimetric method to monitor their breakdown.

The aryl alcohol oxidase (AAO) activity of lignin peroxidases from different organism was determined using veratryl alcohol as a substrate. This substrate can only be oxidised by high redox potential enzymes [72],[75]. The product of this reaction is a veratryl aldehyde, which can be followed by measuring absorbance increase at 310nm. The drawback of veratryl alcohol assay is spectral interference, as most lignins derived compounds have an absorbance at 310 nm (Figure 1.33).

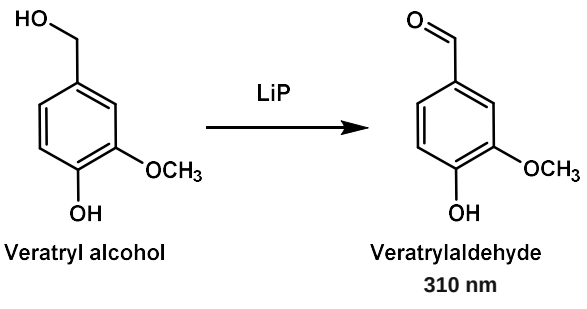

Figure 1.33. Veratryl alcohol assay

Guaiacol can be oxidized by laccases to produce a brown coloured product (Figure 1.34), which is a tetramer of guaiacol and has an absorption maximum at 456

nm [101]. This assay is quick and convenient for a large number of samples, and can be performed on agar plates. Fungi with lignin degradation ability show brown zone around themselves. However, guaiacol oxidation activity does not necessary correlate to lignin degrading activity.

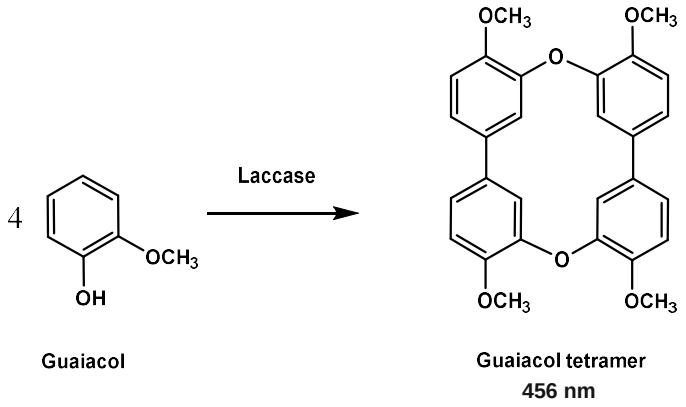

Figure 1.34. Guaiacol assay.

Syringaldazine (4,4'-[azinobis(methanylylidene)]bis (2,6-dimethoxyphenol)) is an azo dye derivative of lignin model compound which can be used as an indicator of laccases and peroxidase. It has been considered as an excellent and specific substrate for rapid detection of laccases [102]. Syringaldazine is oxidised to syringaldazine quinone by laccases in the presence of dioxygen or peroxidases in the presence of hydrogen peroxide. The formation product can be monitored at 530 nm (Figure 1.35).

Numerous synthetic dyes have been utilized for isolation of lignin depolymerising fungi and bacteria in both liquid cultures and on solid agar plates. In addition, these dyes have been also used in the evaluation of lignin breakdown ability of ligninases. Structurally, synthetic textile dyes are quite different from lignin, but decolourisation of these dyes in some cases correlates with lignin depolymerisation [56]. Synthetic dyes have a stable chemical structure, are not broken down by

conventional chemical and physical methods, and have resistance toward microbial attack [103]. These dyes can provide a rapid colourimetric assay. These properties make dyes a good candidate for use in the assessment of lignin degradation ability.

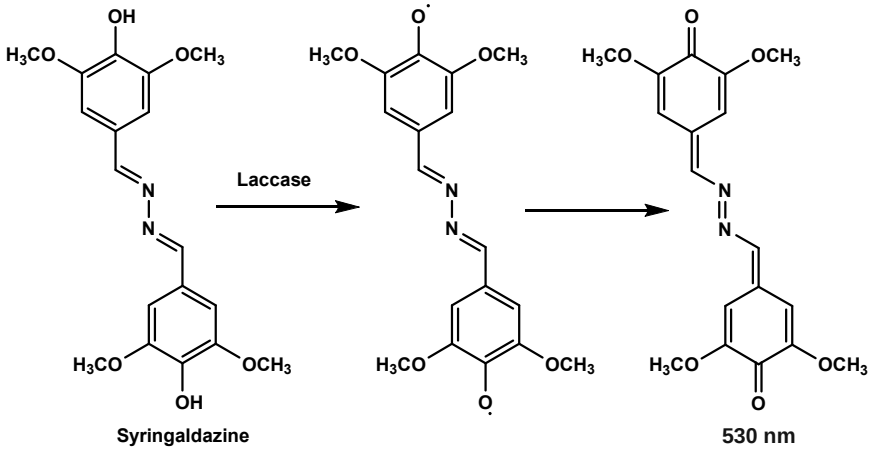

Figure 1.35. Oxidation of syringaldazine.

ABTS, azure B, Remazol Brilliant Blue R (Reactive Blue 19) and Remazol Black B (Reactive Black 5) are the most commonly used dyes. ABTS is a general redox substrate giving rapid spectroscopic assay (see Figure 1.36). It can be used to detect laccases in the presence of dioxygen and peroxidase in the presence of hydrogen peroxide. ABTS has been used widely as a redox mediator for laccases.

Azure B is a heterocyclic dye used as a substrate for lignin peroxidase and manganese-dependent peroxidase from fungi. There is a positive correlation between decolourisation of azure B and lignin peroxidase activity [104]. Azure B assay is considered as one of the standard assays for lignin peroxidases but not for laccases [105]. In comparison study between azure B assay and veratryl alcohol assay, azure B assay appeared more reliable because the change in absorbance can be monitored at 651 nm, which results in exclusion of interfering compounds with strong

absorbance at 310 nm. In addition, azure B assay can be amended to different media while veratryl assay is detected only in mineral salts broth [106].

Reactive Black 5 and Reactive Blue 19 are recalcitrant azo dyes and can only be oxidised by enzymes with high redox potential such as versatile peroxidase [75]. The transformation of Reactive Blue 19 can be monitored at 592 nm [103], and Reactive Black 5 at 598 nm [75].

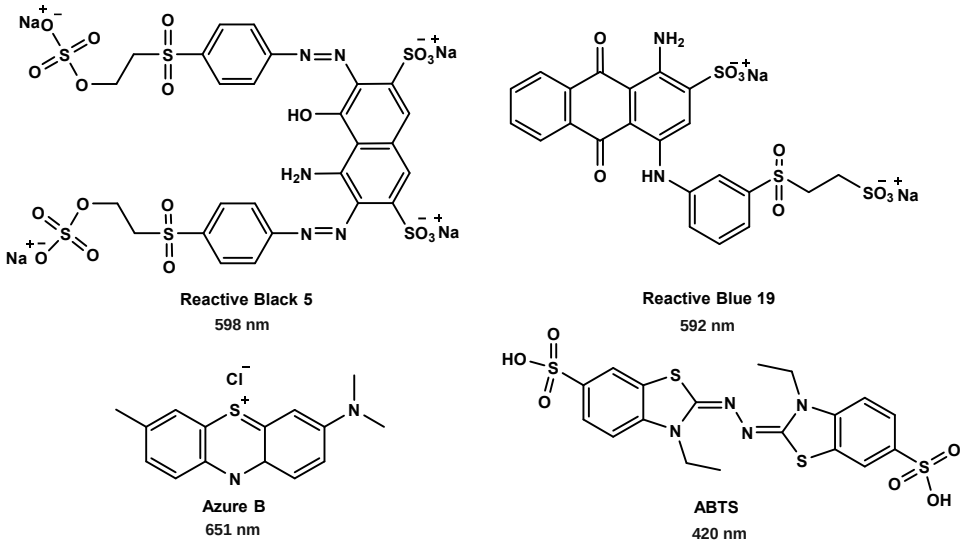

Figure 1.36. Structures of the most commonly used dyes in the assessment of lignin oxidation ability.

The latest methods for detection and measuring lignin degrading activity are two spectrophotometric methods that were developed by Mark Ahmad at the University of Warwick. The first method involves fluorescently derivatised lignin (Figure 1.37) and the second assay involves chemically nitrated lignin (Figure 1.38). These assays allow continuous monitoring of the lignin degradation process. Both, fluorescence and nitrated lignin UV-visible assays could be applied for the identification of novel ligninolytic enzymes of plant lignocellulose.

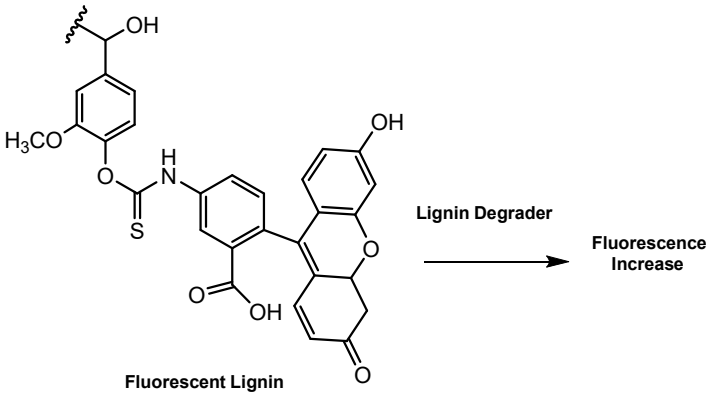

Figure 1.37. Fluorescence assay using fluorescently labelled lignin [62].

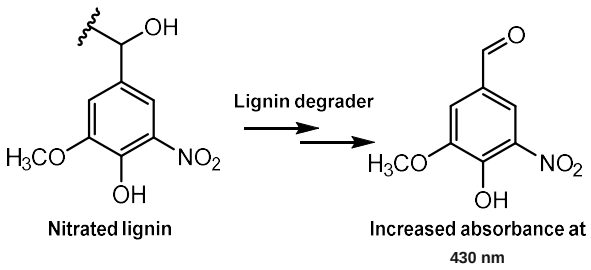

Figure 1.38. Nitrated lignin UV–vis assay [62]**.**

Nitrated lignin and fluorescently derivatised lignin assays can be used for the purification of lignin breakdown enzymes and kinetic studies as well. Furthermore, the nitrated lignin assay can be performed on agar plates. The nitrated lignin can be sprayed onto grown micro-organisms; the micro-organisms with lignin-decomposing ability will develop a yellow colouration around their colonies after overnight incubation at 30°C. This form of nitrated lignin assay is known as spray assay [62],[63].

1.10. Discovery of *Sphingobacterium* sp.T2 as a lignin degrading bacteria.

Lignin-depolymerising bacteria are most likely to be found in places where lignin is being broken down. Identification of such bacterial strains from the environment can be performed through screening of soil in forestry locations and gut of insects [107], which can digest wood. Whereas geothermal environments such as hot springs, compost piles and fermentations of lignocellulosic material are possible places where thermotolerant bacteria can be found [100].

Therefore, composted wheat straw has been screened for isolation of bacteria with lignin degradation ability. Samples from composted wheat straw were enriched at 45ºC for 21 days in M9 salts containing 2% wheat straw, and then aliquots were plated on agar plates with the same composition. After growth, the enrichment culture was diluted to give single colonies on agar plates. The plates were sprayed with nitrated lignin. Three thermophile bacterial strains have been identified by analysis of their 16S rRNA gene sequences (*Rhizobiales* sp., *Sphingobacterium* sp.T2 and *Thermobifida fusca*). In addition, nine lignin degrading mesophilic bacteria have been also isolated from soil using the same approach but at 30ºC instead of 45ºC. To assess the lignin-degradation ability among all isolated bacteria nitrated-lignin UV-vis assay have been carried out. The results show that *Sphingobacterium* sp.T2 is 10-fold more active than the rest of bacterial lignin degrader isolates (Table 1.6) [100]. However, sequencing of the genomic DNA of *Sphingobacteria* sp. T2 by the group of Prof. L Eltis (UBC) revealed no putative *dyp* peroxidase or laccase genes.

Table 1.6. Comparison of lignin degradation ability of bacterial lignin degrading Isolate using nitrated lignin UV-vis assay.

Strain	Identification from 16S rRNA sequencing	Bacterial family	Activity in nitrated lignin assay (mAU)	
			+ H_2O_2	-H_2O_2
A1.1	*Microbacterium phyllosphaerae*	Actinobacteria	1.9	2.7
A1.2	*Microbacterium marinilacus*	Actinobacteria	1.7	0.6
A2.1	*Microbacterium marinilacus*	Actinobacteria	0.9	1.4
A4.3	*Ochrobactrum pseudogrignonense*	α-Proteobacteria	1.2	4.7
A5.1	*Rhodococcus erythropolis*	Nocardioform	1.6	1.9
A5.2	*Microbacterium oxydans*	Actinobacteria	1.1	5.4
B5.3	*Micrococcus luteus*	Actinobacteria	1.9	1.1
C4.1	*Ochrobactrum rhizosphaerae*	α-Proteobacteria	2.0	1.9
E1.1	*Micrococcus luteus*	Actinobacteria	0.9	1.1
T1	*Rhizobiales sp.*	α-Proteobacteria	0.2	2.0
T2	*Sphingobacterium sp.*	Bacteroides	9.0	30

For finding the identity of ligninase enzyme produced by the isolated bacterial lignin-degrader strain, proteomic analysis was then performed. The enzyme capable of degradation of lignin is most likely extracellular. Therefore, cultures of *Sphingobacterium sp.*T2 were pelleted by centrifugation, and the extracellular protein fraction was separated using ammonium sulphate precipitation (70% (w/v) saturation). The fraction was then purified partially for lignin-degrading enzyme activity, using three chromatographic methods (anion exchange, hydrophobic interaction and gel filtration chromatography). The enzyme samples have been concentrated after each chromatographic method. Lignin-degradation activity was monitored using nitrated lignin UV-vis assay, and also oxidation of ABTS monitored as well. A number of active fractions were detected (Figure 1.39). The molecular weight and the number of protein bands in each active fraction were assessed via SDS-PAGE (Figure 1.40).

The fractions showing multiple proteins bands on SDS-PAGE at low protein concentration were submitted for tryptic digestion of the gel bands and proteomic analysis using MALDI-MS. The proteins were identified by comparing observed molecular fragments from tryptic digest with protein databases. The analysis resulted in the identification of a range of several enzymes and some receptors including enolase, aldehyde dehydrogenase, and two slightly different superoxide dismutases and phosphoenolpyruvate carboxykinase (Table 1.7). Among identified enzyme, the two superoxide dismutases are of particular interest, since these enzymes interconvert peroxide and superoxide with dioxygen. This may link to an observation that *Sphingobacterium sp.*T2 displayed higher lignin breakdown activity without hydrogen peroxide (in the presence of dioxygen). However, the involvement of superoxide dismutase in lignin decomposition had not previously been reported.

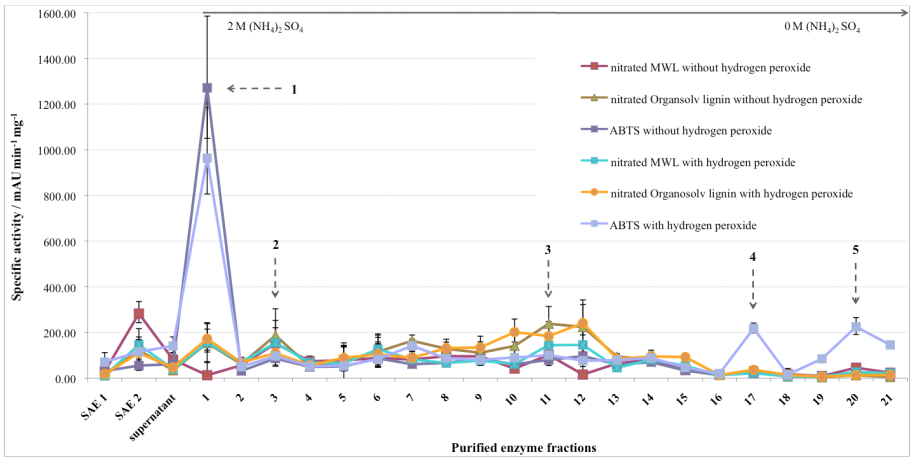

Figure 1.39. Active fractions from partial purification of *Sphingobacterium* sp. T2 supernatant, via phenyl Sepharose hydrophobic interaction chromatography [100].

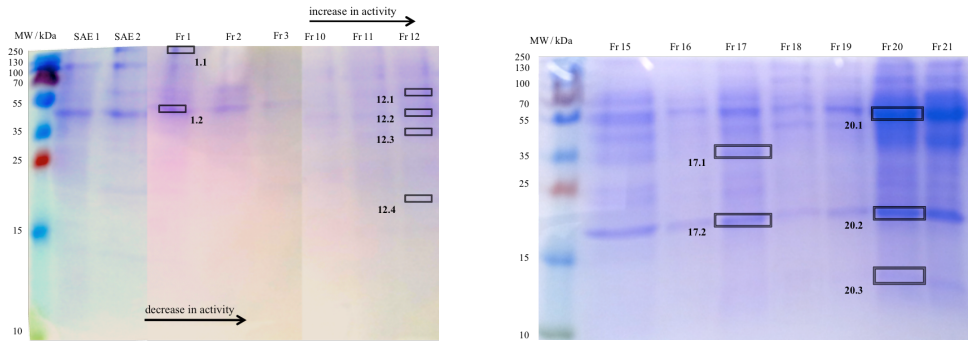

Figure 1.40. SDS-PAGE gels of active fractions indicated above, showing samples used for proteomic analysis. Fractions 20.2 and 12.4 respectively yielded proteomic data for superoxide dismutases SOD1 and SOD2 [100].

Table 1.7. Database matches for proteomic data from extracellular fractions of *Sphingobacterium* sp. T2 [100].

Protein name	Parent strain	Accession code	Sequence identity
Outer membrane proteins:			
OmpA/MotB family protein	Sphingobacterium spiritivorum ATCC 33300	ZP_03966060.1	374/472 (79%)
TonB-dependent receptor plug	Leadbetterella byssophila DSM 17132	YP_003999361.1	298/521 (57%)
TonB outer membrane protein	Sphingobacterium spiritivorum ATCC 33300	ZP_03967958.1	609/1096 (56%)
TonB outer membrane protein	Sphingobacterium spiritivorum ATCC 33300	ZP_03966383.1	558/1083 (52%)
Enzymes:			
Superoxide dismutase (Mn)	Sphingobacterium spiritivorum ATCC 33861	ZP_07080073.1	173/203 (85%)
Superoxide dismutase (Mn)	Chryseobacterium gleum ATCC 35910	ZP_07084820.1	163/224 (73%)
Aldehyde dehydrogenase	Sphingobacterium spiritivorum ATCC 33861	ZP_07080700.1	306/345 (89%)
Glucosamine-6-phosphate deaminase	Sphingobacterium spiritovorum ATCC 33861	ZP_07080477.1	129/174 (74%)
C56 family peptidase	Sphingobacterium spiritivorum ATCC 33300	ZP_03968079.1	177/192 (92%)
M20/M25/M40 family peptidase	Sphingobacterium spiritivorum ATCC 33861	ZP_07079812.1	400/456 (88%)
Proteins:			
Peroxiredoxin	Sphingobacterium spiritivorum ATCC 33300	ZP_03969338.1	181/208 (87%)
Thioredoxin family protein	Sphingobacterium spiritivorum ATCC 33861	ZP_07080480.1	108/209 (52%)
Chaperonin GroEL	Sphingobacterium spiritivorum ATCC 33861	ZP_07080256.1	365/383 (95%)
Translation factor EF-Tu	Pedobacter sp. BAL39	ZP_01885032.1	357/394 (91%)

Another potential gene was identified from bioinformatics analysis, which codes for peroxidase enzyme (catalase-peroxidase KatG). *Sphingobacterium* sp. T2 KatG has sequence similarity with a peroxidase from *Amycolatopsis* sp. 75iv2. The latter enzyme was reported to show ability in the degradation of lignin model compound [108]. Therefore, the decision was made to investigate the ability of the *Sphingobacterium* sp. T2 KatG in breakdown of lignin and lignin model compounds.

1.11. Aims of this study

This project aims to discover novel bacterial lignin-degrading enzymes. Bacterial lignin breakdown enzymes are not explored very well compared to those of fungal ligninolytic enzymes. In addition, bacteria are more tolerant than fungi towards environmental restrictions, they grow more rapidly than fungi and they have ample metabolic flexibility against aromatic substrates. Thus, bacteria seem to be promising for the screening of novel ligninolytic enzymes.

- Development of a method for screening DNA libraries of *Microbacterium phyllosphaerae* and *Sphingobacterium* sp. T2.

Several attempts have been made to purify lignin degrading enzymes from extracellular fractions of *M. phyllosphaerae* and *Sphingobacterium* sp.T2, but this has proved very difficult due to very low extracellular protein concentration. Therefore, we wish to develop a method for screening ligninolytic enzymes from these lignin degraders. Prof. E. Wellington (Life Sci., Univ. of Warwick) has prepared plasmid DNA libraries of *M. phyllosphaerae* and *Sphingobacterium* sp., which have been transformed into *E. coli*. Therefore, we will test several methods including the nitrated lignin assay to detect novel ligninolytic enzymes from DNA libraries of bacterial lignin degraders transformed into *E. coli* cells.

- Identification of lignin-degrading genes.

The screening of genomic DNA libraries of *M. phyllosphaerae* and *Sphingobacterium* sp. T2 will allow to identify novel enzymes. On the other hand, recently the *Sphingobacterium* sp.T2 genome has been sequenced, this enabled us to

identify two types of genes, which possibly are lignin-degrading genes. One of these genes encodes catalase-peroxidase and the other is a superoxide dismutase. There are two superoxide dismutase (*sod*) genes in *Sphingobacterium* sp.T2 genome, namely *sod1* and *sod2*. Catalase peroxidase *katG* is homologous to a peroxidase from *Amycolatopsis* sp. 75iv; the latter can degrade β-O-4 lignin model compound [108]. On the other hand, proteomic analysis of extracellular protein fractions shows hits for superoxide dismutases [100]. Therefore, specific aims of this project are as follows:

- If lignin-degrading enzymes found through screening of the genomic libraries of *M. phyllosphaerae* and *Sphingobacterium* sp. T2 their genes will be sub-cloned into a suitable vector.
- Cloning of *Sphingobacterium* sp.T2 *katG*, *sod1* and *sod2* genes into suitable vectors.
- The enzymes will be overexpressed in *E. coli* and purified.

- Characterisation of lignin-degrading enzymes.

- Assessment of their activity with a range of lignin substrates, lignocellulose, lignin model compounds and synthetic dyes will be investigated by enzyme kinetics and HPLC-based assay.
- Their cofactor requirement will be determined. Spectroscopic and kinetic characterization of the purified lignin-degrading enzymes will be performed.
- Metal cofactors of the enzymes will be characterised if it is found that they are metalloproteins.
- The breakdown product(s) will be identified, using LC/MS and GC/MS.

2. Development of a method for screening genomic DNA libraries for Novel Bacterial lignin-degrading enzymes.

2.1. Introduction

Lignin is an amorphous, heterogeneous, three-dimensional polymer formed mainly in the plant cell wall. It can be found in woody plants but can also occur in non-woody plants such as grasses [12]. It is the second most abundant carbon source on earth. The annual production of lignin through biosynthesis is estimated to be 2×10^{10} tonnes. As available oil reserves are in continuous decline during the early 21st century lignin will be an important renewable source of chemicals for our future society [109]. Lignin, which composes about 24% of lignocellulose biomass, is considered as a waste product and its energy content is not well exploited. Therefore, it is crucial to screen for novel lignin-degrading enzymes, in order to extract chemicals and increase the value of this natural polymer.

Twelve bacterial lignin-degrader strains have been isolated previously at the University of Warwick from woodland soil and composted wheat straw from solid-state fermentation [63]. These isolates include nine mesophilic and three thermophile bacterial strains. The mesophilic strains were four *Microbacterium* isolates, two *Micrococcus* isolates, *Rhodococcus erythropolis* (all Actinobacteria) and two *Ochrobactrum* isolates (Alphaproteobacteria). Three thermotolerant isolates were *Thermobifida fusca* and two isolates related to uncharacterized species of *Rhizobiales* and *Sphingobacterium* (Bacteroidetes). The *Sphingobacterium* strain has been

identified as the most active strain, showing ten-fold higher lignin degradation activity than the other isolates [63].

Attempts were made by previous Ph.D. student Charles Taylor to purify lignin-degrading enzymes from extracellular fractions of *Microbacterium phyllosphaerae* and *Sphingobacterium sp*., but this proved very challenging due to very low extracellular protein concentration. Therefore, a new approach is needed for screening lignin depolymerising enzymes from these lignin degraders. Consequently, the group of Prof. E. Wellington (Life Sci., Univ. of Warwick) has prepared plasmid DNA libraries of *M. phyllosphaerae* and *Sphingobacterium* sp., which have been transformed into *E. coli*. Therefore, our aim was to develop methods to detect novel lignin-degrading enzymes from DNA libraries of bacterial lignin degraders transformed into *E. coli* cells.

Often, screening for enzyme activity is performed via monitoring changes in the optical absorption or fluorescence. A number of screens can be operated via direct visualisation or by digital image analysis of observed colour change in agar plates. In contrast, the majority of screens involve growing single colonies in multi-well microtitre plates until stationary phase in suitable culture media, and protein is overexpressed using an inducer. For the detection of intracellular enzymes, a cell lysis step is essential to liberate the cellular contents. Ultimately, the enzyme activity will be measured with a plate reader spectrophotometer [110].

Numerous substrates have been used for the isolation of lignin-degrading microorganisms and /or screening of ligninolytic enzymes. Kraft lignin, milled wood lignin, lignocellulose [63], and synthetic lignin have been used to isolate some fungi

and bacteria with ligninolytic potential. Radioactively labelled lignin has been also used for isolation of lignin degraders [111]. Monitoring ^{14}C-labelled lignin is a quantitative method. However, the assay requires a long time, and it requires the preparation of radioactively labelled lignin [62].

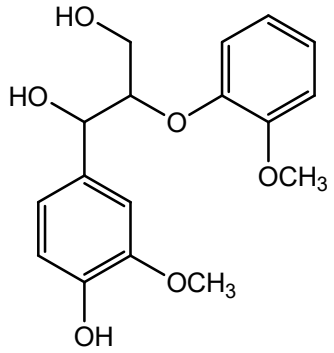

Figure 2.1. An example of β-O-4 model compound

The earliest method for detection and measuring LiP activity was made via oxidation of a β–aryl ether (β-O-4) model compound [112] (Figure 2.1). The β-O-4 linkage is the most prevalent linkage in lignin polymer, and it comprises more than 50% of linkages [15]. In another approach, researchers tested the growth of the micro-organisms on media containing lignin model compounds as sole carbon source that may correlate with their lignin-degrading ability. This method has been adopted by several researchers [113],[114].

Lignin mimicking dyes have also been used for isolation and detection of lignin degraders. These dyes are either used as a sole carbon source for growth studies or as indicators of the ability of a micro-organism to decolourise them, which may correlate with the lignin-decomposing ability [105]. The dyes employed in lignin degrader studies include Methylene Blue, Malachite Green, Congo red, Remozal Brilliant Blue R and Azure B [115] (see Figure 1.36 for structures of the most commonly used dyes). It has been proposed that poly-R can be used as a

standard method for determination of LiP activity [105]. In another study, Azure B has been employed in quantitative measurements of LiP activity. In addition, the Azure B assay is more accurate than the veratryl alcohol assay that is considered to be the standard assay for routine quantitation of LiP activity [106],[112].

Several phenolic and non-phenolic aromatic compounds have been utilised in ligninase and lignin degrader studies. Some of these substrates are lignin-derived compounds such as guaiacol (see Figure 1.34 for guaiacol assay), syringaldehyde, acetosyringone, and veratryl alcohol [116]. Guaiacol and syringaldazine (a dimer of syringaldehyde) have been used separately for measuring microbial laccase activities (see Figure 1.35 for syringaldazine assay) [117]. Recently, guaiacol has been used in screening of a metagenomic library from mangrove soil [118]. Syringaldazine has been proposed to be a more convenient substrate for the determination of laccase activity since syringaldazine can differentiate between laccases and other phenol oxidases produced by fungi [119].

In contrast, veratryl alcohol is widely employed in measuring LiP activities. It can also be utilised for quantitative measurement of laccase activity with the addition of a mediator such as ABTS (Figure 2.2) [76],[120]. However, the veratryl alcohol assay has some drawbacks such as measuring absorbance at 310nm, which causes absorption interference from phenolic and other aromatic compounds. The other substrates employed in ligninolytic studies are synthetic compounds. Examples of these substrates are (DCP) with 4-aminoantipyrine (Figure 2.2) and ABTS. The latter can be used for detection and quantitative measurement of both LiP and laccase activities as well. Moreover, the potential oxidation of ABTS is not pH-dependent within the range 2–11 [117]. Hence, these make ABTS more suitable for screening

different organisms. Finally, care should be taken in using both ABTS and 2,4-dichlorophenol for measuring enzyme activity because they have some background, non-enzymatic reactivity.

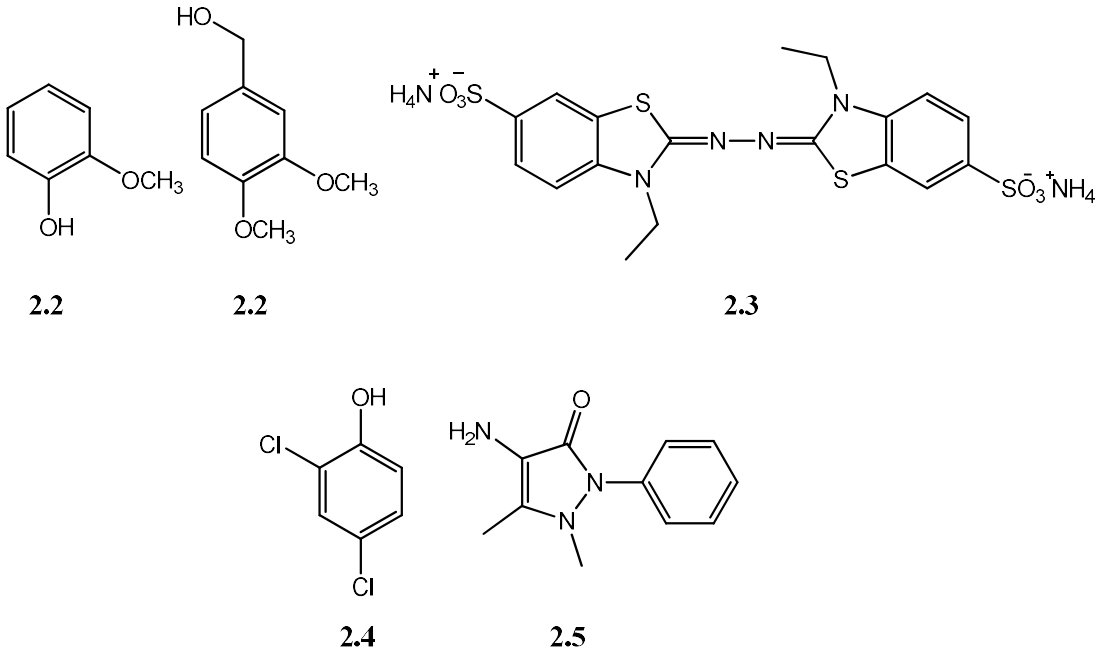

Figure 2.2. Chemical structures of guaiacol **2.1,** veratryl alcohol **2.2,** ABTS **2.3,** 2,4-diclorophenol **2.4** and 4-aminoantipyrine **2.5.**

The newest approaches for monitoring lignin breakdown are nitrated-lignin and fluorescent derived lignin UV-vis methods (see Figure 1.37 and 1.38). The nitrated-lignin spray method is particularly useful because it allows selection of a putative lignin degrader on agar plates among several organism [121]. For more detail, please see Chapter One (Section 1.9).

These assays have been used to compare the activity of known lignin and aromatic degraders. As a consequence, the known aromatic degraders have been shown to act as lignin degraders, including *Rhodococcus jostii* RHA1 and

Pseudomonas putida [121]. Bioinformatics analysis of the genome of *Rhodococcus jostii RHA1* revealed the presence of a Dyp-type peroxidase while spectrophotometric analysis indicated that DypB can break down lignin [61].

2.2. Examining of the feasibility of Nitrated lignin spray test as a screening method.

Previously identified positive and negative bacterial lignin-degrading strains were used to validate the spray test for screening of lignin-degrading enzymes. The positive strains that were examined *M. phyllosphaerae*, *M. luteus*, *R. erythropolis*, and *Sphingobacterium sp.*T2 while the negative strains were *E. coli*, *Leuconostoc mesenteroides*. Four different types of nitrated substrates were employed in several experimental trials. The nitrated substrates used were nitrated milled wood lignin (MWL), nitrated-Alkaline lignin, nitrated-organosolv lignin and nitrated-β-aryl ether. The nitrated substrates were sprayed onto strains after plating on LB agar and incubation overnight. The sprayed agar plates were re-incubated at 30 or 45ºC (for *Sphingobacterium sp.* T2) for up to two days. Other researchers in the group had seen small differences in colour between lignin degraders and non-degraders under this condition. However, no significant differences were observed in yellow coloration between individual strains sprayed with nitrated substrates and the same strain sprayed with water (distilled and autoclaved) which were grown and incubated under the same conditions. The experiments were repeated on minimal media agar plates containing 2% (w/v) glucose as a carbon source, because LB agar plate is yellow in colour and small differences in the thickness of plates make the comparison more difficult. The same set of known lignin degraders were sprayed with nitrated substrates (as described above) or water after 48 hours of incubation at 30 or 45 ºC

(for *Sphingobacterium sp. T*2). Again, no observable differences in yellow colouration were noticed between plates for the same strain sprayed with nitrated substrates or sprayed with water (distilled and autoclaved) that were grown and incubated at the same condition.

2.3. The viability of UV-vis nitrated lignin assay as a screening method.

The same set of nitrated substrates and bacterial lignin-degrading strains were used (as described in the nitrated spray test) to check suitability of the nitrated lignin spectrophotometric assay for screening of *M. phyllosphaerae* and *Sphingobacterium sp.*T2 DNA libraries. Culture supernatant from the stationary phase of bacterial samples was used in the assay. The effect of H_2O_2 at 2 mM final concentration was also examined. Treatment of nitrated substrates with culture supernatants of strains as mentioned above shows that only *Sphingobacterium* sp.T2 supernatant gave some increase in absorbance, especially without H_2O_2. The rise in absorbance at 430nm over 20 minutes was 19.9, 13.5, 7.4 and 1.4 mAU for nitrated- β-aryl ether, alkaline lignin and organosolv lignin without H_2O_2 and for nitrated- organosolv lignin with H_2O_2 respectively (Figure 2.3). While the absorbance changes over 20 minutes for all the other strains (data not shown) and *Sphingobacterium* sp. supernatant with remaining nitrated substrates was lower than 1.4 mAU (Figure 2.4).

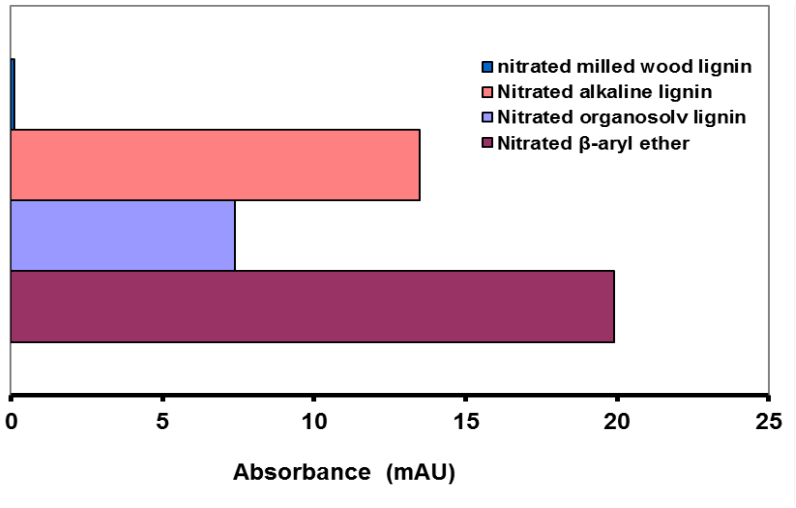

Figure 2.3. Change in absorbance at 430 nm over 0-20 min for *Sphingobacterium* Sp.T2 without H_2O_2.

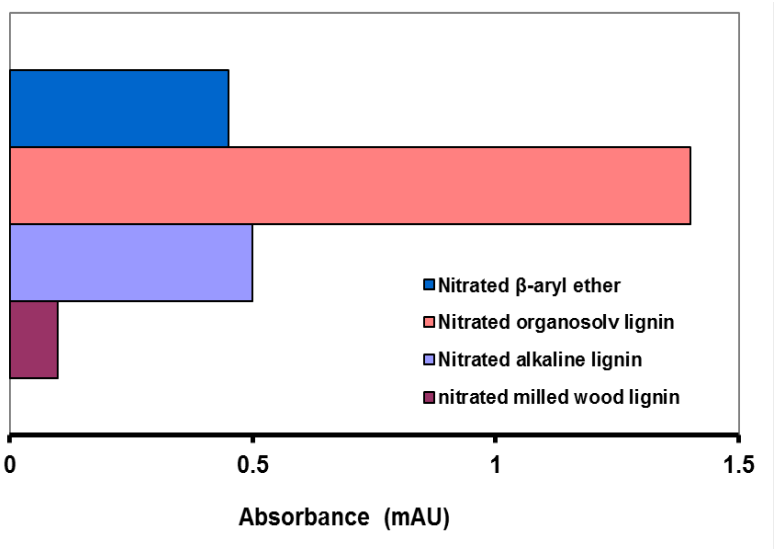

Figure 2.4. Change in absorbance at 430 nm over 0-20 min for *Sphingobacterium* sp. T2 with H_2O_2.

Due to the small signal generated in the nitrated lignin spectrophotometric assay attempts were made to optimise the assay. Previous researchers in the group had seen activity using either 750 mM Tris buffer pH 7.4 or 150 mM Tris buffer pH 7.4. Therefore, different ionic strengths were examined from 100 to 1000 mM of the same buffer. Some increase in absorbance was observed for *Sphingobacterium sp.*T2 at 300 and 200 mM buffer concentrations, which are comparable to the increase

have seen at 750 mM pervioulY [62], but *R. erythropolis* shows an increase at 500 mM of the same buffer only (Figure 2.5 and 2.6). This may suggest that 750 mM buffer solution is not suitable for the nitrated lignin assay. Although, the absorbance change was still too small to be used for screening of ligninolytic enzymes. Finally, the discovery of novel enzymes may need a range of substrates.

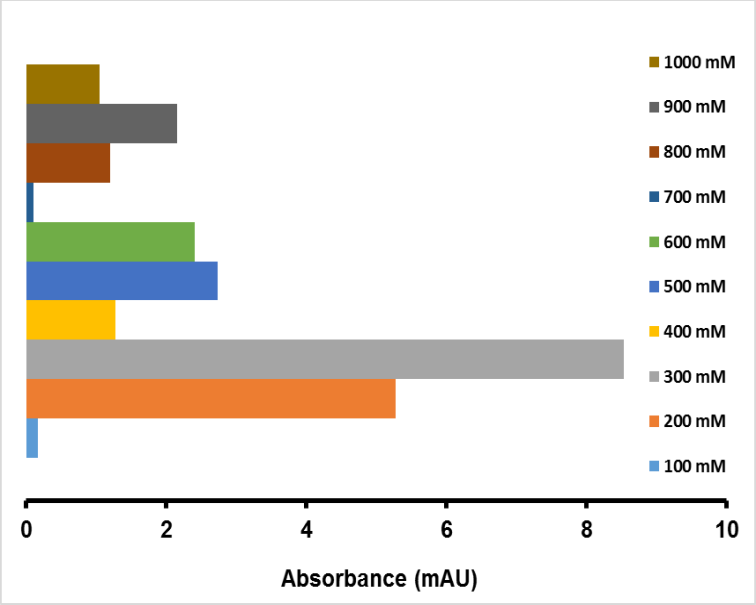

Figure 2.5. Effect of different ionic strength (100 to 1000 mM Tris buffer pH 7.4) on enzyme activity of *Sphingobacterium* sp. T2 supernatant with nitrated alkaline lignin and two mM H_2O_2. The absorbance was measured at 430 nm.

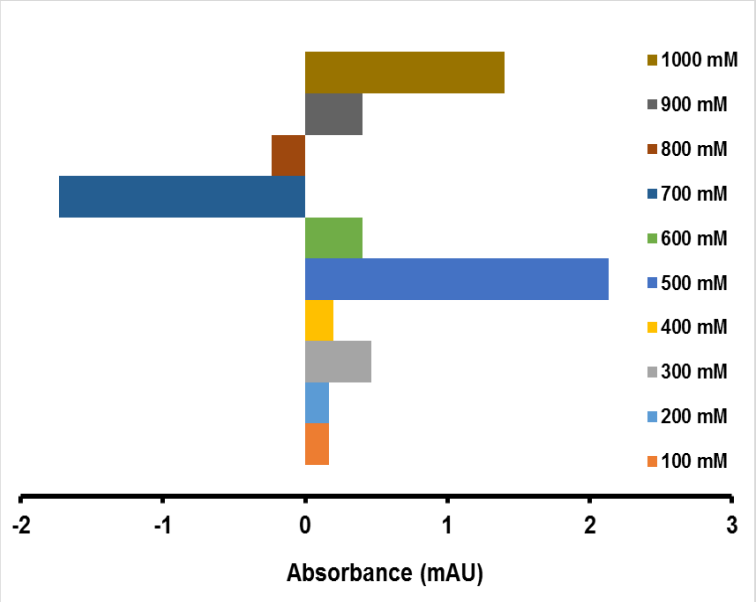

Figure 2.6. Effect of different ionic strength (100 to 1000 mM Tris buffer pH 7.4) on enzyme activity of *R. erythropolis* supernatant with nitrated MWL and two mM H_2O_2 measured at 430 nm.

2.4. Testing a number of substrates with *E. coli* containing *dypB* and *mco* constructs on agar plates.

Dye-decolourising peroxidase (DypB) from *Rhodococcus jostii* RHA1 has been identified as a bacterial ligninase enzyme [61]. It has been demonstrated that it can oxidise a β-aryl ether lignin model compound, and can attack Kraft lignin or wheat straw lignocellulose in the presence of Mn^{2+}. Dyp1B enzyme from *Pseudomonas fluorescens* has also been identified as a lignin-degrader enzyme [84]. Bacterial lignin degrader *Rhodococcus jostii* RHA1 also has a gene encoding a multi-copper oxidase (*mco*) enzyme that is a homolog of a laccase enzyme. Therefore, *E. coli* strains containing *dypB* or *mco* from *Rhodococcus jostii* RHA1 and the empty vector (pET200) as a control were used to examine known lignin-

degrading enzyme substrates to find a screening method. Several substrates have been tested in four different ways as following:-

1. The addition of the substrates into media before plating.
2. Spraying of the substrates after growth.
3. The addition of the substrates to wells on agar plates (produced by cutting agar).
4. The addition of secondary agar layer containing substrates onto grown *E. coli* plates.

2.4.1. The addition of the substrates into medium before plating.

In this method, substrates to be examined and 0.5 mM Isopropyl β-D-1-thiogalactopyranoside (IPTG) were added to the LB agar medium, and then, *E coli* strains were plated. After a 24 hrs incubation at 37ºC, no colour change was observed for all substrates that were employed at different concentration (for more detail see experimental section). The plates were left for more than ten days for autolysis of the bacterial cells and releasing expected enzyme. The results were negative after ten days. The experiments were repeated in the presence or absence of H_2O_2 and IPTG but the results were also negative for all substrates (ABTS, DCP, Guaiacol and Remozal BBR) which were used at different concentration (see experimental section). Except for phenol red the colour change was observable after 24 hrs of incubation in the absence of H_2O_2 for all *E coli* strains (*dypB*, *mco* and control). This colour change most probably did not correlate to ligninolytic enzymes because its control strain also gave a colour change.

2.4.2. Spraying the substrates after growth.

The addition of the substrates and IPTG at the same time to agar media before plating *E. coli* strains shows a negative impact on the growth of the *E coli* strains. Therefore, the spraying technique has been examined. Colonies were allowed to grow on minimal media containing 1 mM $CuSO_4$ (to induce laccases) for 24 hours at 37ºC then sprayed with 0.5 mM IPTG and re-incubated overnight prior to spraying with substrates (Table 2.1). The plates were checked for colour change after 30 min, 1 hour, one day of incubation at 30ºC and ten days at room temperature. The plates did not show any observable change in colour for all substrates used. The test was repeated, and the effect of different concentrations of H_2O_2 examined with and without cell lysis reagent celLytic^{TM} B was examined. The plates did not display any observable colour change for all substrates used during ten days except for DCP (5-50 mM) with 4-aminoantipyrine in the presence of H_2O_2 (1-5 mM) after 24 hours (Table 2.1). This colour change can not be correlated to enzyme activity because the change in colour was in areas that did not have any colonies and the areas around and under colonies was colourless. In addition, when the experiment repeated several times, control plates (*E. coli* with empty vector) also showed the same extent of colour change. Therefore, this colour change most probably comes from a non-enzymatic reaction.

Table 2.1. Observed colour change for different substrates sprayed on *E. coli* containing *dypB* and *mco* constructs on agar plates. The strains were induced for protein expression by 0.5 mM IPTG.

Substrates	Colour change ± celLytic™ B reagent & ± H_2O_2		
	DypB	MCO	Control
ABTS (20 and 40 mM)	ND	ND	ND
DCP (50 mM)	pink*	pink*	pink*
Guaiacol (10, 20, & 50 mM)	ND	ND	ND
Nitrated Alkaline lignin (4 mg/mL)	ND	ND	ND

ND: not detectable. ±: with and without H_2O_2 or celLytic™ B reagent. See an experimental section for more detail. * The colour change was observed in the presence of H_2O_2 at all concentration used without celLytic reagent after 24 hrs.

2.4.3. Well test (Addition of the substrates to wells on agar plates).

Spraying plated bacterial colonies with reagents can disturb colonies and combines them. In addition, spraying more than one reagent is difficult. Hence, another technique has been tested. The method includes cutting a well in the agar plates before streaking the bacterial samples on it. The wells allow the addition of several reagents to agar plates. In this method, *E. coli* strains were grown for 24 hours then induced overnight at 37ºC by the addition of IPTG to wells on agar plates. The induced colonies were tested by adding substrates (ABTS, DCP, Guaiacol and Remozal BB R) to the wells. The agar medium was supplemented with 0.001% (w/v) $FeSO_4$, 0.001% (w/v) $CuSO_4$, and 0.001% (w/v) $MnSO_4$), urea and yeast extract to support protein expression. Each well on the plates was used for testing the effect of cell lysis reagents (CelLytic ™ B 10X, (Sigma-Aldrich), BugBuster Protein Extraction Reagent and B-PER Protein Extraction Reagents

(Thermo)) at two different concentrations (concentrated reagent and C2: diluted reagent 1:2 with sterile water) with and without H_2O_2. None of the tested substrates showed an observable colour change after 30 min, 1 hour, one day of incubation at 30°C and ten days at room temperature (Table 2.2).

Table 2.2. Observed colour change for different substrates added to wells on agar plates of *E. coli* strains containing *dypB* and *mco* constructs on agar plates. The strains were induced for protein expression by IPTG.

Substrates ± Cell lysis reagents (50 µL)* & ± H_2O_2	**Colour change of agar plates of *E. coli* constructs**		
	DypB	**MCO**	**Control**
ABTS (40 mM)	ND	ND	ND
DCP* (5 mM)	pink**	pink**	pink**
Guaiacol (10 mM)	ND	ND	ND
Remozal B B R** (0.04 %) (w/v)	ND	ND	ND

ND: not detectable; ±: with and without H_2O_2 or cell lysis reagents. * Three types of cell lysis reagents were used at two different concentrations. See experimental section for more detail.* *the colour change was observed in the presence of H_2O_2 at all concentration used without Cell Lysis Reagent after 24 h

2.4.4. The addition of the secondary agar layer containing substrates onto grown *E. coli* plates.

The well test technique failed to give a positive result, and it seems that the reagents do not disperse evenly and rapidly. To solve these problems a top agar method has been examined in which the strains to be tested were streaked on growing medium (the same medium used in well test) then the analysis medium was added after 24 hour incubation. The analysing agar medium consisted of the substrate to be

tested (Table 2.3), antibiotic, and 0.5 mM IPTG. After the addition of the analysis medium, the plates were re-incubated at 30ºC overnight. Subsequently, the plates did not display a visible colour change with any of the substrates employed even after ten days at room temperature.

Table 2.3. Observed colour change for different substrates added to top agar layer with IPTG onto grown *E. coli* strains containing *dypB* and *mco* constructs on primary agar plates.

Substrates	Colour change		
	DypB	MCO	Control
ABTS (40 mM)	ND	ND	ND
Guaiacol (50 mM)	ND	ND	ND
Azure B (0.001 & 0.002%)	ND	ND	ND
Phenol red (0.001%)	ND	ND	ND

ND: not detectable.

In conclusion, several methods using whole *E. coli* cells containing *dypB* and *mco* constructs for screening of ligninases with a range of substrates (ABTS, Guaiacol, DCP with 4-aminoantipyrine, Azure B, Phenol red, Tanin, nitrated lignin and Remozal BBR) gave a negative result after induction with IPTG. This suggests that most of these substrates were not taken up by the *E. coli* cells or the colour change was not detectable by the naked eye. Furthermore, three types of cell lysis reagents (CelLytic™ B 10X (Sigma-Aldrich), BugBuster™ Protein Extraction Reagent (Novagen) and B-PER Protein Extraction Reagents (Thermo)) were examined at 2 different concentrations (concentrated reagent or diluted 1:2). Therefore, these lysis reagents may not be able to lyse the *E. coli* cells, or the colour changes are not enough to be detected visually.

2.5. Testing *E. coli* containing *dypB* and mco constructs in liquid culture with ABTS assay after cell lysis

Colour change on agar plates for different substrates and methods were not observed. In addition, the cell lysis reagents used did not seem to be able to lyse the *E. coli* cells. Therefore, the lysis ability of the CelLytic™ B was investigated via ABTS assay. At first, CelLytic™ B was diluted 10-fold and used to lyse the cells after induction by 0.5 mM IPTG for protein expression. Consequently, the cell lysate was tested with ABTS assay after removing cell debris. No detectable colour change was observed visually after 60 minutes. Then, the experiment was repeated, and lysozyme (1 mg/mL) or sonication was used along with the CelLytic™ B (10-fold diluted). The observable green colour was developed after 30 min in both cases. Thus, this suggests that CelLytic™ B was not able to lyse *E. coli* BL21 cells without lysozyme or sonication. In addition, it may also explain why all substrates gave negative results with *E. coli* containing recombinant *dypB* or *mco* when examined on the agar plate.

Since CelLytic™ B is expensive, we looked for cheaper alternatives. Buffer solution with detergent (Tween-20) and lysozyme were used for lysing the *E. coli* cells before spectrophotometric assay. First, the strains were inoculated in LB liquid medium overnight and induced with IPTG (0.5 mM). Second, the induced cells were lysed using the lysis reagent (phosphate buffer with 0.25 % (v/v) Tween-20 and 1 mg/mL lysozyme). Finally, the enzyme activities were examined using a UV-vis plate reader with ABTS as a substrate. A significant difference in absorbance was observed between *E. coli* strains containing *dypB* and the control in the presence of 2

mM H_2O_2. In contrast, the *E. coli* strain containing the *mco* construct shows lower absorbance difference than that of *dypB* when compared with the control without H_2O_2 (Figure 2.7). Moreover, the absorbance of both *dypB* and *mco* constructs was approximately 2-fold higher than that of their corresponding control.

On the basis of this method a screening method has been adapted (Figure 2.8) which included growing single bacterial colonies in sterile 96-well plates overnight then diluting the culture medium 1:20 with fresh medium (800 µL) and transferring it into 96-deep well plates (2 mL capacity). After 3.30 hrs (the OD_{600} were between 0.6-0.7), the cells were induced overnight at 15ºC then the cells were harvested by centrifugation (1600 ×g for 10 min).

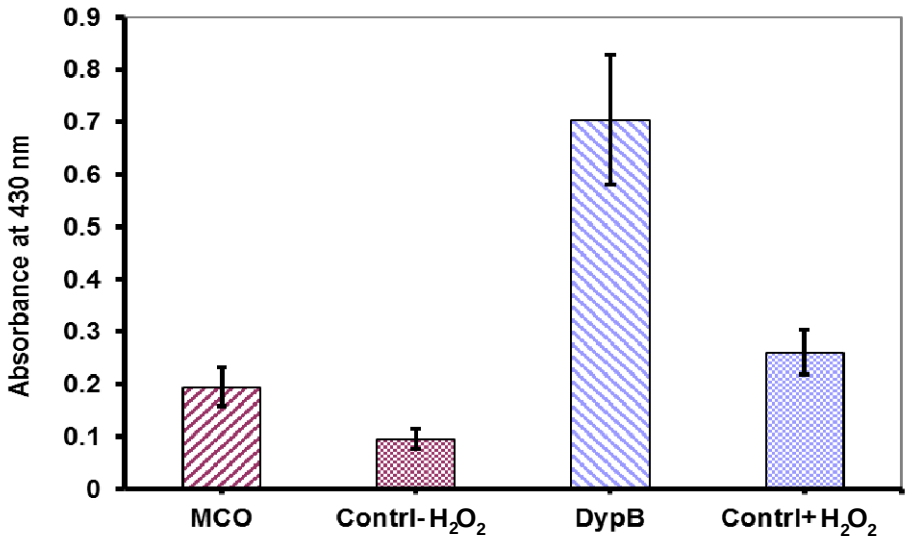

Figure 2.7. Enzyme activity of intracellular solution of *E. coli* strains containing *dypB* and *mco* constructs and *E coli* containing empty vector (pET200) measured by ABTS assay at 430 nm. The *dypB* and control were tested in the presence of 2 mM H_2O_2 while *mco* with another control were tested without H_2O_2.

The cells were lysed with lysis reagent, and the cell debris were removed by centrifugation (1600 xg for 15 min). Finally, the extracted enzymes were assayed spectrophotometrically using the ABTS assay.

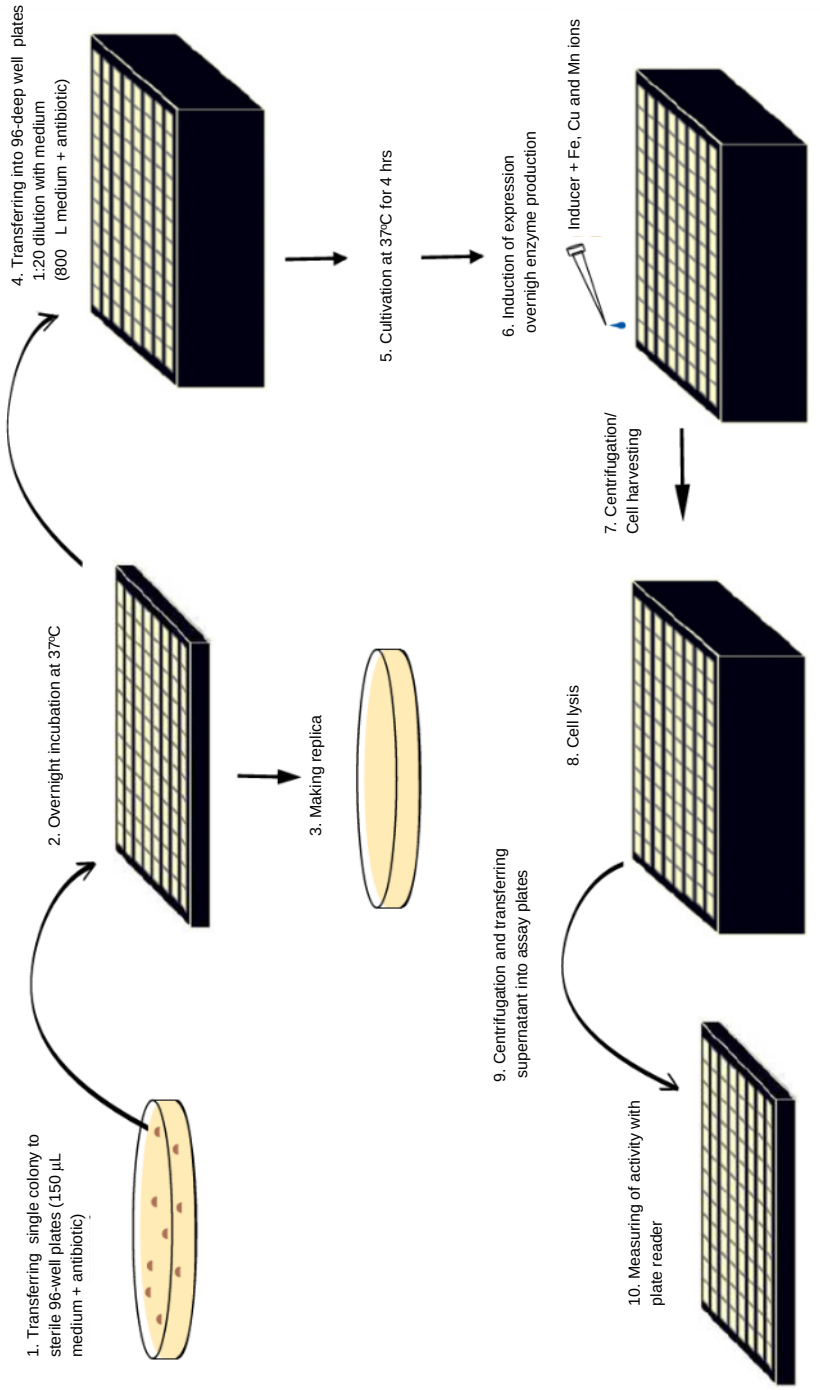

Figure 2.8. A functional screening method for genomic libraries

2.6. Pilot screening experiment using a mixture of *E. coli* strains containing *dypB* and control (1:10) in 96- well plate with ABTS assay.

Before applying the adapted screening method on DNA libraries of *M. phylosphaerae* and *Sphingobacterium sp.* T2, a pilot experiment was conducted to prove its validation. Therefore, *E. coli* strains containing *dypB* and control were mixed in the ratio of 1:10 then plated on LB agar plates containing kanamycin (30 µg/mL). Subsequently, the adapted screening method has been applied. Figure 2.9 shows the result when hypothetical libraries that were grown in 96-deep wells plates (2 mL capacity) and induced by IPTG (0.5 mM). The intracellular solution was tested with the ABTS assay in the presence of 2 mM H_2O_2 after lysis of the cells with cell lysis reagent (as described in previous Section 2.5), and cell debris were removed. Significant differences can be seen between 6 of these hypothetical libraries (D1, F9, C1, G1, E8 and H9) and the rest of libraries. This indicates that the adapted screening method may be suitable for functional screening of genomic libraries for ligninolytic enzymes using the ABTS assay.

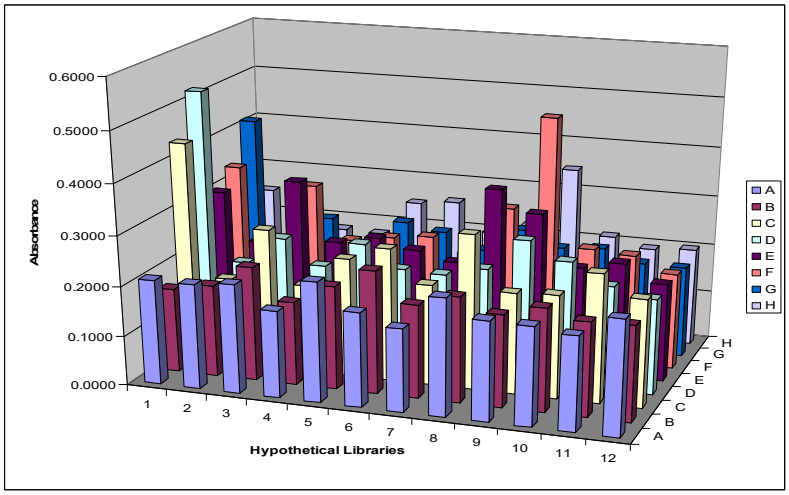

Figure 2.9. Pilot screening experiment. Enzyme activity measured by the ABTS assay (430 nm) in presence 2 mM H_2O_2 of intracellular solution of mixture (1:10) of *E. coli* strains containing *dypB* construct and *E coli* control (containing empty vector (pET200)), mimicking genomic DNA libraries.

2.7. Screening of *M. phylosphaerae* and *Sphingobacterium sp.* DNA libraries.

We were provided with plasmid and fosmid genomic DNA libraries of *Sphingobacterium sp.*T2. The estimated average insert size of *Sphingobacterium* sp. T2 plasmid libraries were 4.75 kb while the estimated average inserts size of the same strain fosmid libraries was 35 kb. In addition, the assumed genome size of *Sphingobacterium* sp. T2 is about 3.2 Mb. About 1200 colonies from the plasmid libraries have been screened. However, only 33% of cloned plasmids had an insert. We were also provided with plasmid DNA libraries of *M. phyllosphaerae,* but most of the clones contained no insert, hence were not suitable for screening. The problem of the fosmid vector was absence of inducible promoter for protein expression. This decrease the chance of observing enzyme activity. Therefore, screening of *Sphingobacterium* sp. T2 plasmid libraries only was performed.

The whole *Sphingobacterium* sp. T2 plasmid libraries were diluted 10-fold and divided between 190 wells (2× 96-well plates, namely plate 1 and 2) and one well per each plate was left as a control. After the induction with arabinose (50 mM) [122] and lysing cells with lysis reagent (as described in Section 2.5), and the cell lysates were tested with ABTS with and without H_2O_2 after removing cell debris. The differences between the absorbance of libraries and their corresponding control were not significant in either case (with and without H_2O_2) see Figure 2.10, 2.11, 2.12 & 2.13. These preliminary results suggest that there is no potential laccase or lignin peroxidase in *Sphingobacterium* sp. T2 genome. However, several wells in plate 2 (Figure 2.11) showed activity greater than the control only detected without H_2O_2. Therefore, the plasmid of these active colonies were extracted and sent for sequencing, but the results revealed that there was no insert in the plasmids.

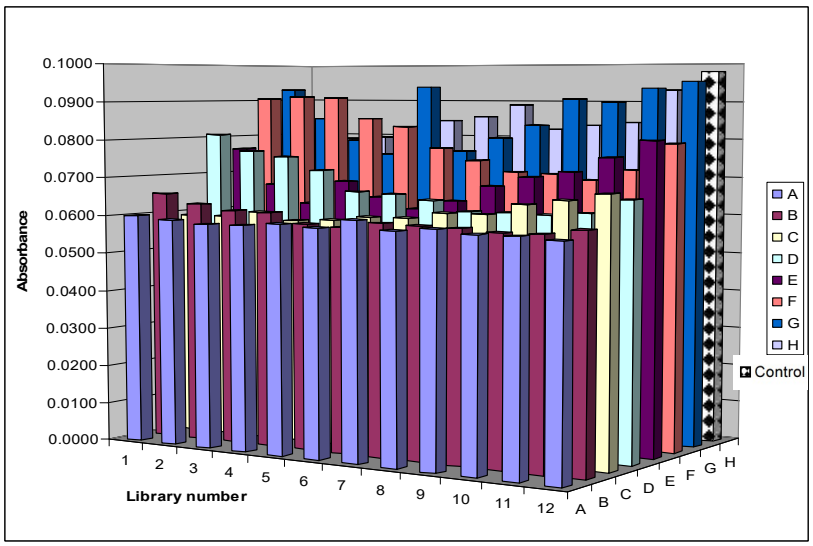

Figure 2.10. Enzyme activities of *Sphingobacterium* sp. *T2* T2 plasmid libraries measured using ABTS assay for plate no 2 without H2O2

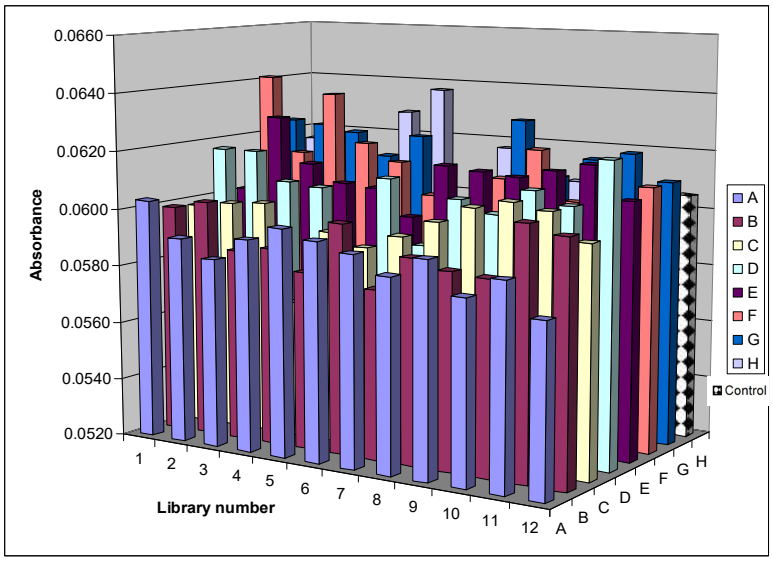

Figure 2.11. Enzyme activities of *Sphingobacterium* sp. T2 plasmid libraries measured using ABTS assay for plate no 2 without H_2O_2.

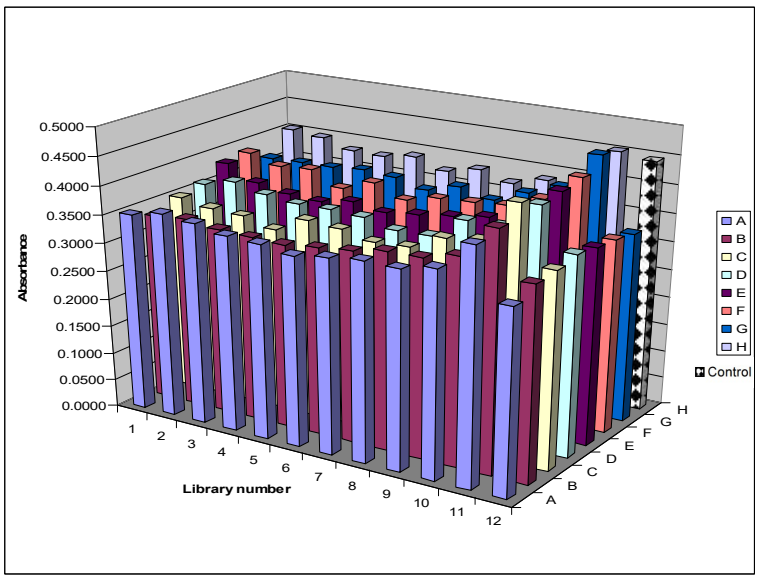

Figure 2.12. Enzyme activities of *Sphingobacterium* sp. T2 plasmid libraries measured using ABTS assay for plate no 1 with H_2O_2.

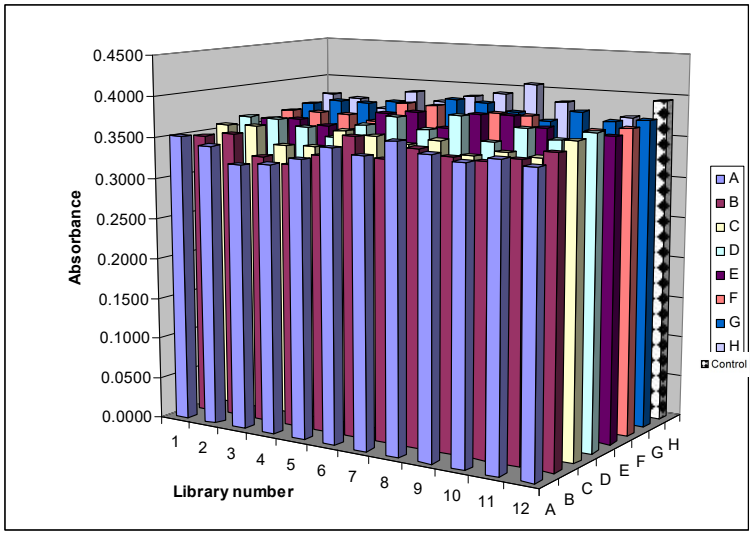

Figure 2.13. Enzyme activities of *Sphingobacterium* sp. *T2* plasmid libraries measured using ABTS assay for plate no. 1 with H_2O_2.

2.8. Conclusion

A range of substrates were tested for developing a colourimetric screening method on agar plates for detection of ligninase activity but this was unsuccessful, however, several different methodologies were examined. This may be the substrates cannot be taken up by *E. coli.* There is a possibility of dispersion of substrate or product on the agar plate and not giving enough colourization to be visible. On the other hand, *E. coli* strain having *dypB* and *mco* constructs were tested in liquid culture, and both constructs showed a significant absorbance change using ABTS as substrate. This assay was adapted to the screening method in 96 well microtiter plates successfully.

A pilot screening experiment for hypothetical libraries shows that the functional screening method is valid, but no peroxidase or laccase enzymes were detected by screening of genomic DNA libraries of *Sphingobacterium* sp.T2. At this point in the project, the expression and purification of three targeted enzymes

identified from proteomic analysis and bioinformatics analysis of *Sphingobacterium* sp.T2 was undertaken.

3. Biochemical Characterization of Catalase Peroxidase KatG from *Sphingobacterium* sp. T2.

3.1. Introduction

Sphingobacterium sp.T2 has been isolated and identified as a highly active bacterial lignin-degrading strain among twelve isolates at Warwick University in 2012 [63]. Its genome has been sequenced recently and has been examined for possible ligninase enzyme(s). Surprisingly, no known lignin-degrading genes (for example dyp-peroxidase, laccase and lignin peroxidase) can be detected in its genome. This may indicate that there are different enzyme(s) responsible for its high lignin-degrading ability. Two possible lignin-degrading genes have been identified from the genome sequence and proteomic data for this organism: catalase-peroxidase KatG and Mn superoxide dismutase. Recently it has been reported that an extracellular heme-dependent enzyme from *Amycolatopsis* sp.72vi2 can degrade lignin model compounds, which shows sequence similarities with catalase-peroxidase KatG [108].

Catalase-peroxidases (KatGs) are bifunctional heme-containing enzymes. KatGs exhibit both catalytic (reaction 1) and peroxidatic (reaction 2) activities and belong to the "Class I" family of peroxidases [123]. KatG activates isoniazid (INH) which has been in continual use as an antibiotic to treat tuberculosis infection since the early 1950s [124]. They also possess additional catalytic activities such as cytochrome P450-like oxygenase, Mn^{2+} dependent peroxidase and peroxynitritase activities [125].

$$H_2O_2 \xrightarrow{\text{Catalase}} H_2O + O_2 \quad (1)$$

$$H_2O_2 + 2HA \xrightarrow{\text{Peroxidase}} 2H_2O + 2A \quad (2)$$

KatG from several bacterial species such as *Burkholderia pseudomallei*, *Escherichia coli*, and *Mycobacterium tuberculosis* have been reported to exhibit NADH oxidizing ability with a pH optimum at 8.75. This oxidation requires molecular oxygen and produces NAD^+, and either H_2O_2 or superoxide radical, depending on pH (reactions 3 and 4). The oxidation of NADH by KatG does not require hydrogen peroxide, and is not inhibited by superoxide dismutase or catalase enzymes. KatG catalysed NADH oxidation is clearly different from the NADH peroxidase- oxidase reaction of horseradish peroxidase [126].

$$NADH + O_2 + H^+ \longrightarrow NAD^+ + H_2O_2 \quad \text{(at pH 8)} \quad (3)$$

$$NADH + 2O_2 \longrightarrow NAD^+ + O_2^{\bullet -} + H^+ \quad \text{(at pH 8.5)} \quad (4)$$

Another catalytic activity of KatG is an oxygen- and H_2O_2-independent hydrolysis of INH. The rate of radical generation from an NADH, INH mixture is 2-3 fold higher than the combined rates of separate NADH and INH reactions (Figure 3.1). The primary product of the coupled reaction is isonicotinoyl-NAD and its formation is activated by manganese in the presence of KatG [126].

KatG exhibits a significant sequence homology to eukaryotic peroxidases, plant ascorbate peroxidases [123],[125], but not to mono-functional catalase [123]. It also has extensive sequence similarity with cytochrome c peroxidase in both the N-terminal and C-terminal domains, but it has only one heme binding site per

polypeptide (Figure 3.2) [123],[127]. This agrees with a low absorbance ratio for the soret region near 407 nm compared to the absorbance at 280 nm. In turn, it has led to an incorrect assumption that these multimeric enzymes contain only half the heme per binding site [127].

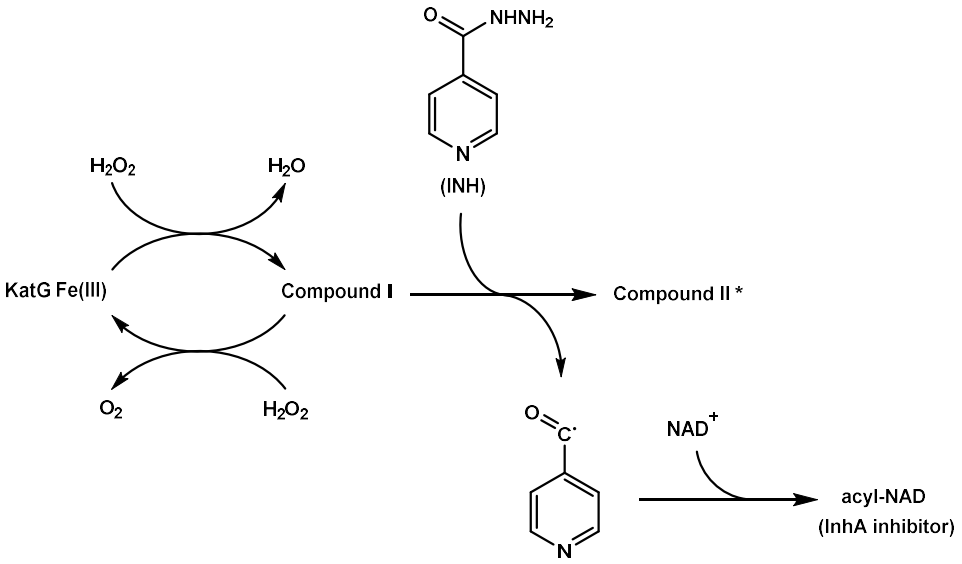

Figure 3.1. Proposed mechanism of hydrogen peroxide-dependent activation of isoniazid (INH) by catalase-peroxidase KatG [128].

Crystal structures of KatG enzymes from four different bacterial species have been reported, and it was found that all enzymes possess a similar peroxidase core structure. All four enzymes exhibit unique structural features, which are specific for catalases and not evident in peroxidases. The covalent cross-linking of the side chains of Met255, Tyr107 and Trp11 (numbering in *Mycobacterium tuberculosis* KatG) near the heme cofactor (Figure 3.3) is one of the most impressive of these features. In addition to these three residues, Asp141 is required for catalase activity but not peroxidase activity, and Arg426, which reversibly associates with Tyr238 to form a molecular switch modulating catalase activity, and is also essential for activity [129].

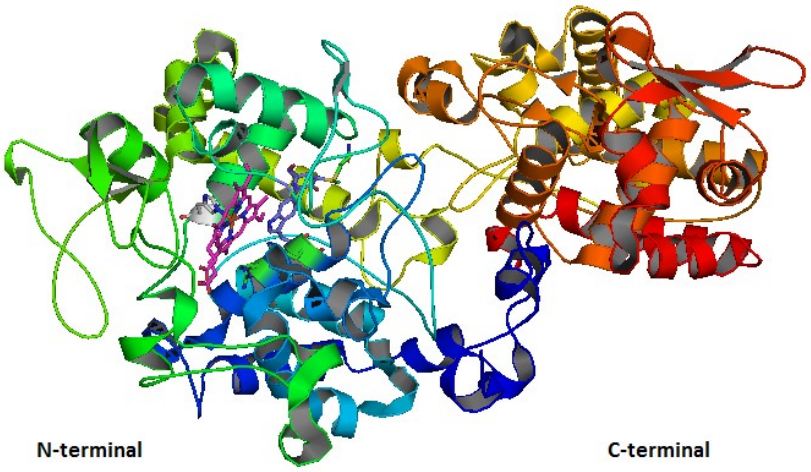

Figure 3.2. Structure of KatG from *M. tuberculosis* showing N-terminal domain, which has heme-binding site, and C-terminal domain. File (2CCA) downloaded from the Protein Data Bank and displayed using the PyMOL program**.**

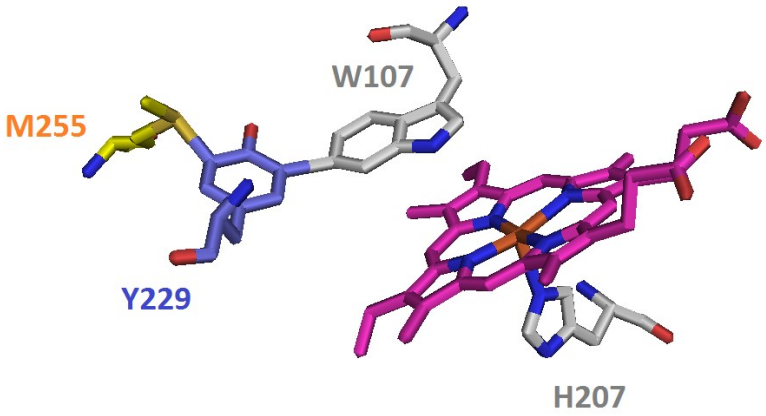

Figure 3.3. Active site of KatG depicting the Met- Tyr-Trp cross-link and its proximity to the heme cofactor. Coordinates were obtained from the Protein Data Bank (2CCA) and displayed using the PyMOL program.

KatG is found in many organisms (in plants [125], fungi, bacteria and archaebacteria) [125],[129], some of them are especially sensitive to the pro-drug isoniazid. They exist as monomers [125], dimers and tetramers. They have subunits of about 80 kDa, that is twice the polypeptide chain length of plant peroxidases. Each subunit contains two domains of 40 kDa, it is assumed to have arisen by a gene

duplication event. Only the N-terminal domain has a heme binding site while the C-terminal domain has not [123],[127],[129].

Study of catalase-peroxidase or KatGs from seven different organisms revealed that all enzymes show high sensitivity to azide and cyanide with IC_{50} values of 0.2–20 μM and 50–170 μM, respectively, and exhibit similar pH optima for peroxidase (4.25-5) and catalase reactions (5.75). The seven enzymes also showed similar turnover rates for activation of isoniazid as an anti-tubercular drug. Only the NADH oxidising activity was widely varied from 10^{-4} to 10^{-2} s^{-1} [129].

Catalase peroxidase KatG from 32 different species (Gram-negative bacteria, Gram-positive bacteria, fungi, and archaea) were compared with KatG from *Sphingobacterium* sp.T2 (Sphingo-KatG). The organisms include:- *Acremonium chrysogenum* ATCC 11550, *Cyphellophora europaea* CBS 101466, *Mycosphaerella pini* (strain NZE10 / CBS 128990), *Phaeosphaeria nodorum* (SN15 / ATCC MYA-4574 / FGSC 10173), *Pseudozyma brasiliensis* (GHG001), *Thielavia heterothallica* (ATCC 42464 / BCRC 31852 / DSM 1799), *Verticillium longisporum*, *Haloarcula marismortui* (ATCC 43049 / DSM 3752 / JCM 8966 / VKM B-1809), *Halobacterium salinarum* (ATCC 700922 / JCM 11081 / NRC-1), *Methanosarcina acetivorans* (ATCC 35395 / DSM 2834 / JCM 12185 / C2A), *Natronomonas pharaonis* (ATCC 35678 / DSM 2160), *Haloferax mediterranei* (ATCC 33500 / DSM 1411 / JCM 8866 / NBRC 14739 / NCIMB 2177 / R-4), *Halalkalicoccus jeotgali* (DSM 18796 / CECT 7217 / JCM 14584 / KCTC 4019 / B3), *Salinarchaeum* sp. Harcht-Bsk1, *Thermoplasmatales archaeon* Gpl, *Rhodococcus jostii* (RHA1), *Rhodococcus ruber*, *Rhodococcus* sp. JVH1, *Clostridium botulinum* (Eklund 17B / Type B), *Clostridium celatum* DSM 1785, *Corynebacterium glycinophilum* AJ 3170,

Corynebacterium terpenotabidum Y-11, *Clostridium botulinum* (Eklund 17B / Type B), *Burkholderia pseudomallei* (K96243), *Escherichia coli* (K12), *Synechocystis sp*. (PCC 6803 / Kazusa), *Mycobacterium smegmatis* (ATCC 700084 / mc(2)155), *Mycobacterium tuberculosis*, *Enterobacter* sp. (638), *Pseudomonas syringae* pv. syringae (B728a), *Rhodobacter capsulatus* and *Streptomyces griseus* subsp. griseus (JCM 4626 / NBRC 13350). These amino acid sequences for KatG were downloaded from the UniProt [130] website and were aligned with CLC Main workbench 6.5 software. The number of amino acids in these KatG sequences are between 763-576, the majority ~700 amino acids.

Alignment of amino acids sequences of KatG from the 32 organisms mentioned above shows highly conserved amino acid sequence in their N-terminal domain. Particularly, the amino acids that, bind to the heme group (H271), making covalent adduct (W84-Y230-M256), distal arginine (R96) and distal histidine (H85) (These numbers refers to KatG from *Sphingobacterium* sp.T2) (Figure 3.4). The KatG of these species show high similarity in their C-terminal sequence as well (see appendices).

To establish the degree of evolutionary links among the various KatGs the most likely phylogenetic tree was computed using the programs CLC Main Workbench 6.5 software. For this analysis, protein sequences of catalase-peroxidase were selected from 33 organisms including seven Gram-positive bacteria, ten Gram-negative bacteria, eight archaea and seven fungi. *Sphingobacterium* sp. T2 KatG is clustered with two Gram-negative bacteria (*Escherichia coli* and *Enterobacter* sp., see Figure 3.5).

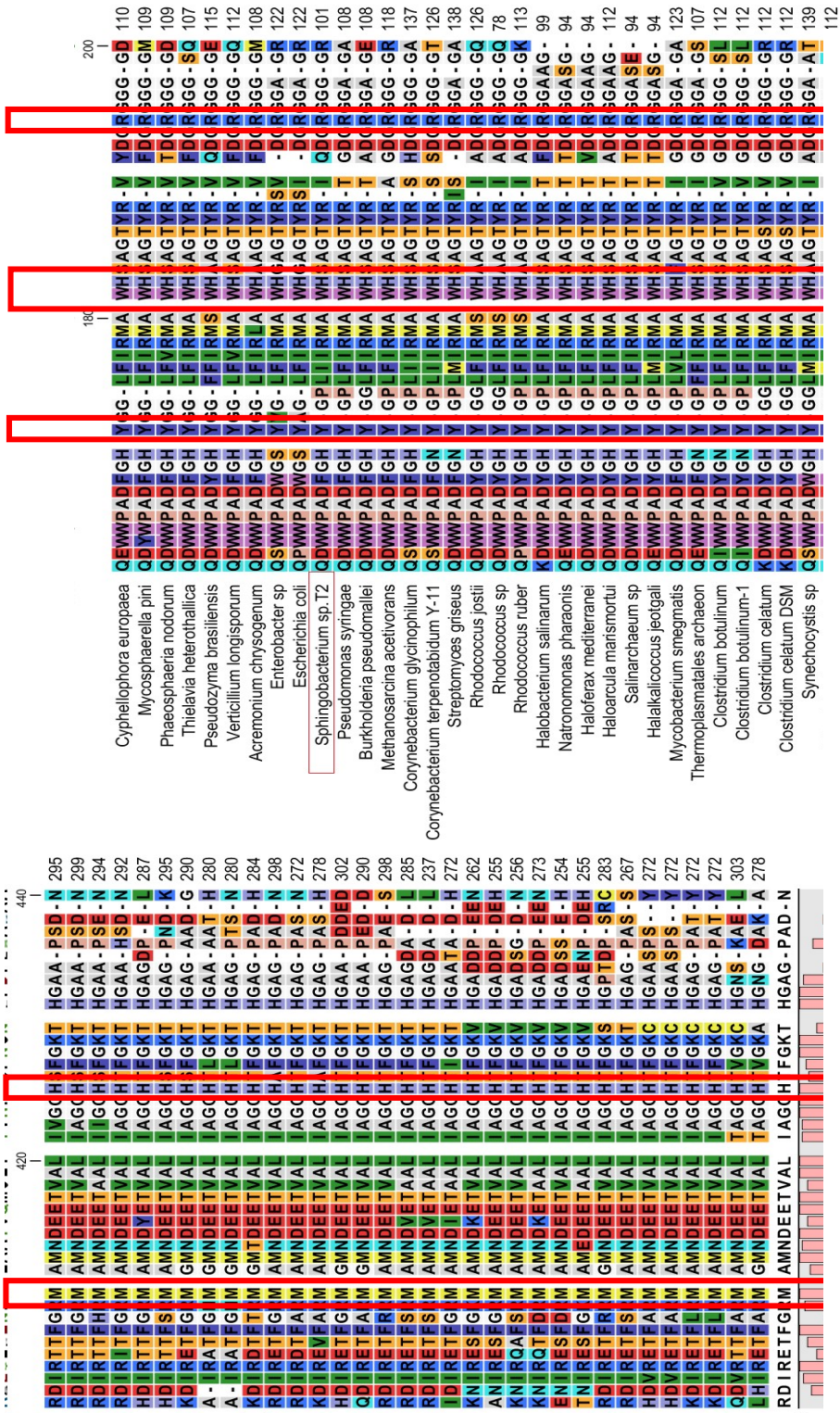

Figure 3.4. Alignment of KatG amino acid sequence from 32 different species with *Sphingobacterium* sp. T2. The species are bacteria (Gram-positive and Gram-negative), fungi and archaea. In these KatG sequences high similarity can be observed. In addition, amino acids that bind to heme group (H271), making covalent adduct (W84-Y230-M256), distal arginine (R96) and distal histidine (H85) are conserved (numbering in *Sphingobacterium* sp. T2. KatG), which are boxed. For more detail see appendices.

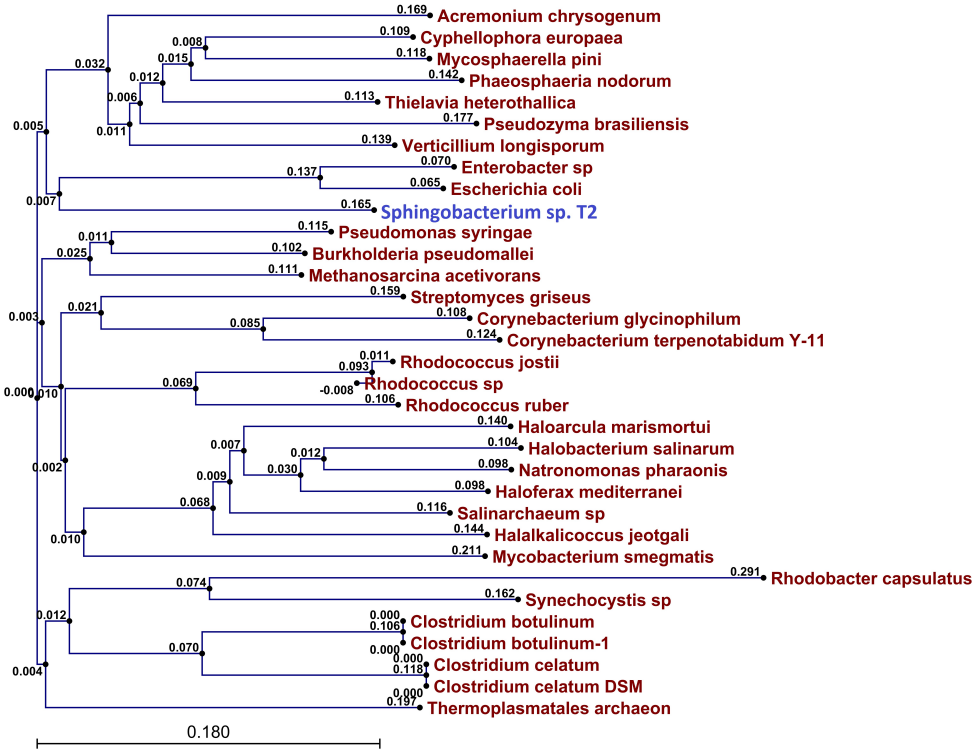

Figure 3.5. Phylogenetic relationships of KatGs from 33 organisms using CLC Main workbench 6.5 software.

Catalase peroxidase from different bacterial species has shown amazing catalytical activities. These activities include degradation of lignin model compounds, Mn^{2+} dependent peroxidase, NADH-oxidizing ability and P450-like oxygenase activities [125]. In addition, it shows sequence similarity with eukaryotic peroxidase and plant peroxidases. All of these properties of the KatG make it an excellent candidate for investigation on lignin degradation ability, especially from strains such as *Sphingobacterium* sp. T2 that has been identified as the most active lignin degrader strain among 12 soil bacterial isolates. In addition, the strain does not have any lignin peroxidase or Mn-dependent peroxidase or Dye de-colourizing peroxidase (DypB). Therefore, we decided to clone, express and characterise the *Sphingobacterium* sp. T2 KatG.

3.2. Overexpressing, purification, and characterization of Sphingobacterium sp. T2 Catalase peroxidase (KatG)

Catalase peroxidase *katG* gene from *Sphingobacterium* sp. T2 was amplified by PCR and cloned into pET-200 (Figure 3.6.*a*). The cloned gene was transformed into *E. coli* BL21 and over-expressed as a N-terminal His_6 fusion protein, and then purified using immobilized metal affinity chromatography (IMAC) resin (Figure 3.6.*b*).

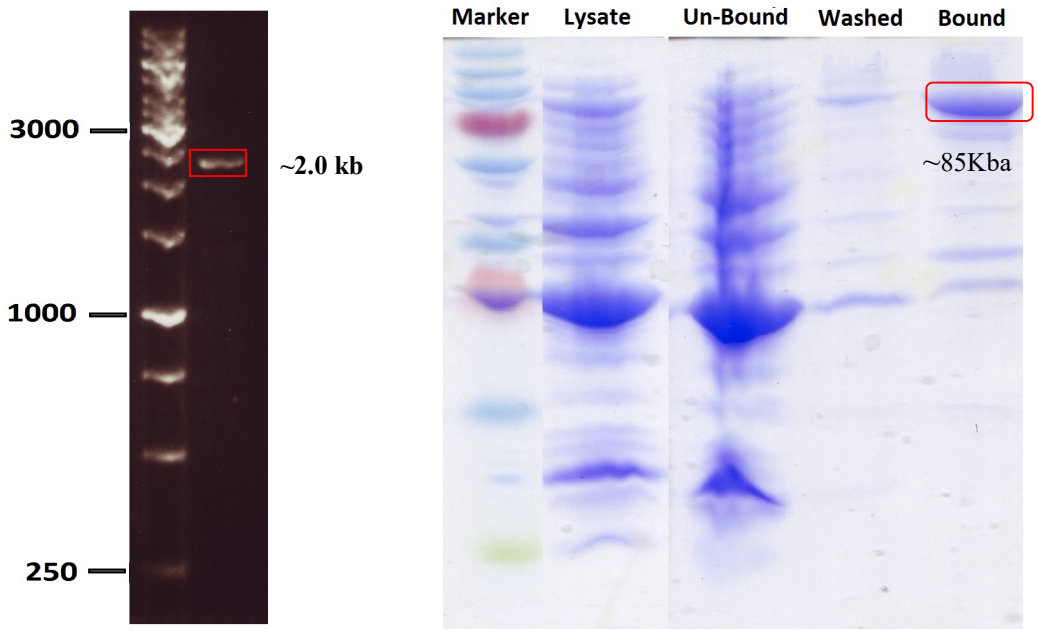

Figure 3.6. Analysis of KatG gene and enzyme, (*a)* agarose gel separation for amplified KatG gene (2226 bp). (*b)* SDS-PAGE electrophoresis analysis of purified KatG by IMAC column.

For further purification of the enzyme, gel-filtration chromatography on Superdex-200 has been used (Figure 3.7.). The total amount of purified KatG was 35.2 mg from 2 L of *E. coli* culture containing *katG* construct, and the purity number (Reinheitzahl value or R_Z) was 0.733 after reconstitution with the heme. The catalase-peroxidase KatG enzymes are characterised by low R_Z values because their

polypeptide chain is twice that of other peroxidases, and it contains only one heme binding site per polypeptide sequence at their N-terminal domain [127].

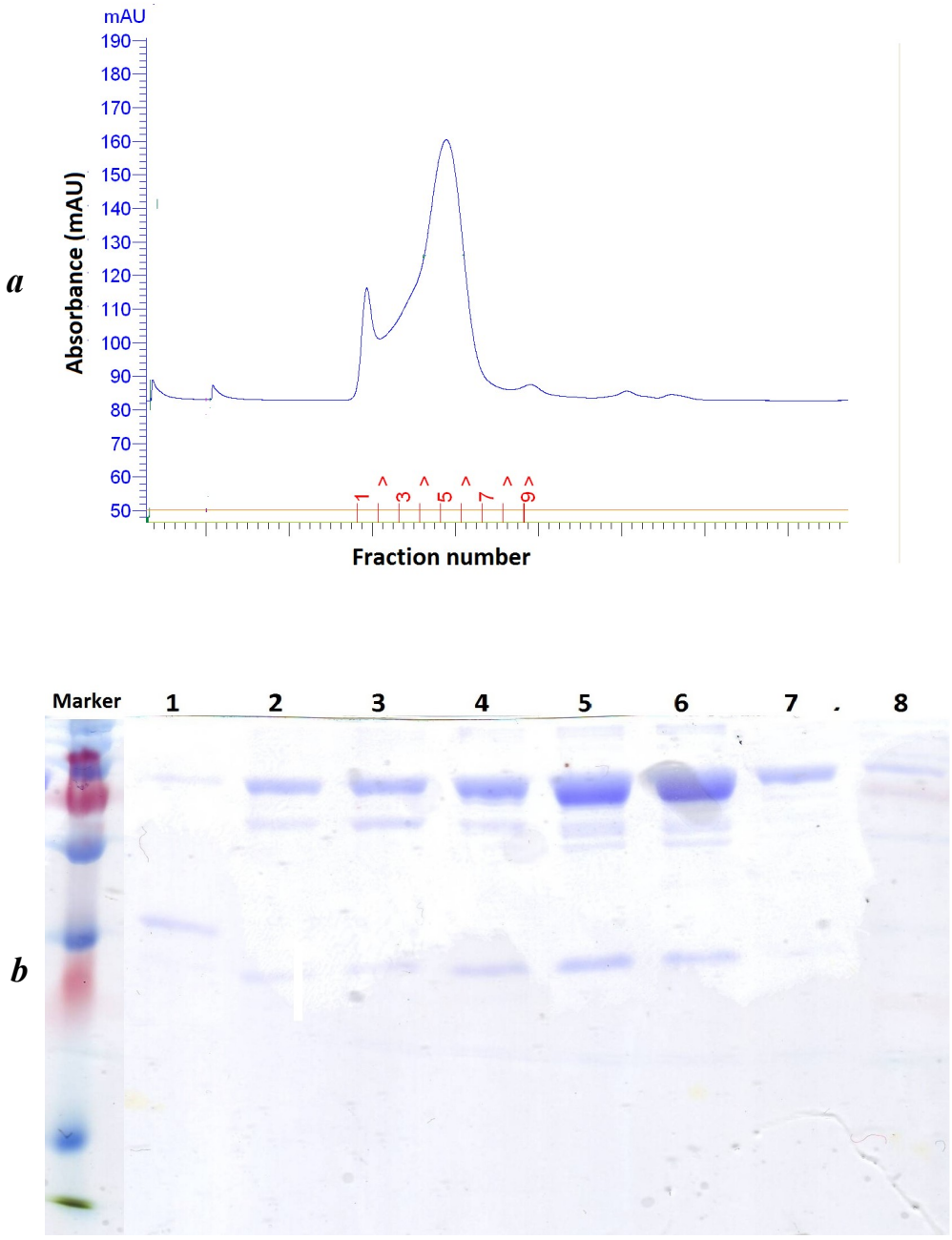

Figure 3.7. (*a*) Gel filtration chromatoGram of KatG on Superdex-G200. (*b*) Analysis of fractions from gel filtration with SDS-polyacrylamide gel.

The UV-vis absorption spectrum shows that KatG has a Soret band at 405 nm and two additional peaks at 503 and 637 nm (Figure 3.8) which match with spectra

of KatG(Y229F) [uv-vis spectra, Soret 406, 504,and 638nm] from *Mycobacterium tuberculosis* [125]. This indicates that the Met-Tyr-Trp cross link is not formed. The Met-Tyr-Trp adduct is essential for catalase activity of the KatGs but not its peroxidase activity which forms in an autocatalytic process that is solely dependent upon compound I [(Por*)FeIV=O, oxoferryl porphyrin π-cation radical] [125].

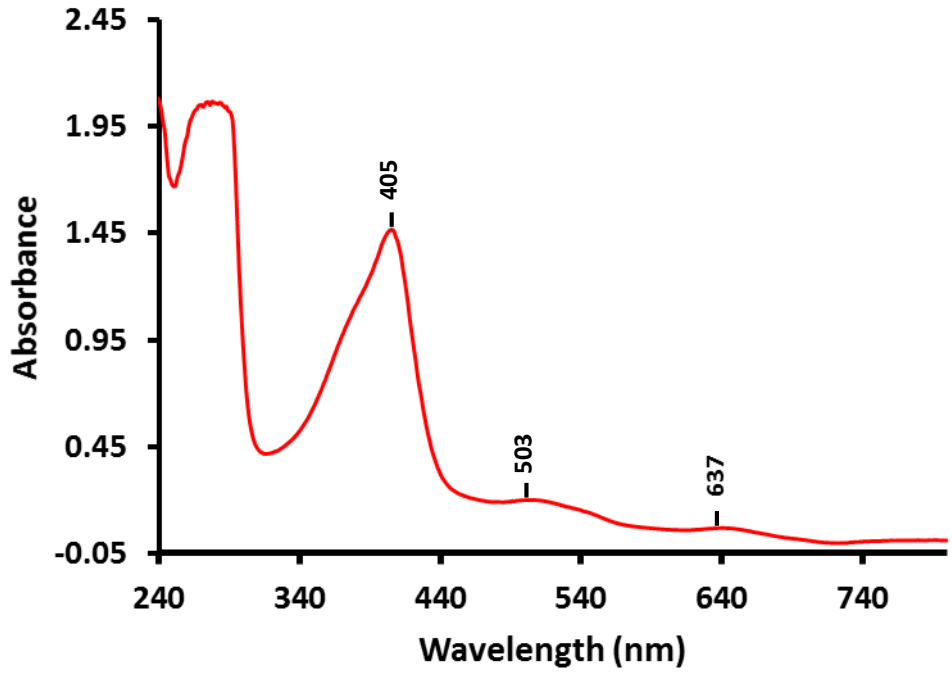

Figure 3.8. UV-Vis spectrum of 25 µM of purified KatG in 50 mM phosphate buffer pH 7.5)

The pH profile indicates that KatG has pH optimum at 5.0 for peroxidase activity using ABTS as a substrate (Figure 3.9) which is compatible with pH optima (4.25-5) of other KatGs from seven different bacterial species [129].

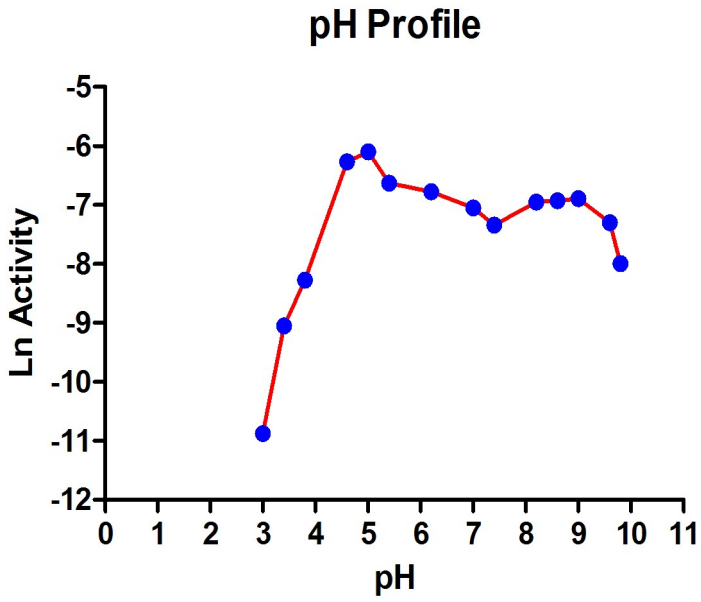

Figure 3.9. The pH-rate profile for oxidation of ABTS. the buffer system were 50 mM glycine-HCl buffer (pH 2.2-2.8), acetate (pH 3-6), phosphate (pH 6-7.8), Tris-HCl (pH 8-9) and glycine-NaOH buffer (pH 9-10.4).

3.3. Peroxidase activity

The chromogenic substrate ABTS is a classical substrate for testing peroxidase activity. However, this substrate does not show whether the enzyme can degrade lignin or not. Lignin peroxidase activity can be examined by using lignin model compounds, DCP, veratryl alcohol, guaiacol. Mn-dependent peroxidase activity can be tested by examining Mn-oxidation ability of the enzyme. ABTS and guaiacol were first used as electron donors to examining the peroxidase activity of KatG from *Sphingobacterium* sp. T2. The apparent kinetic parameters for the ABTS oxidation were (v_{max} 0.0061 µmol min^{-1} mg $protein^{-1}$, K_m 5.3 µM and k_{cat}, 0.057 s^{-1}) and guaiacol (v_{max} 0.0050 µmol min^{-1} mg $protein^{-1}$, K_m 2.1 mM and k_{cat} , 0.047 s^{-1}) in the presence of 4 mM hydrogen peroxide (Figure 3.10 and Figure 3.11).

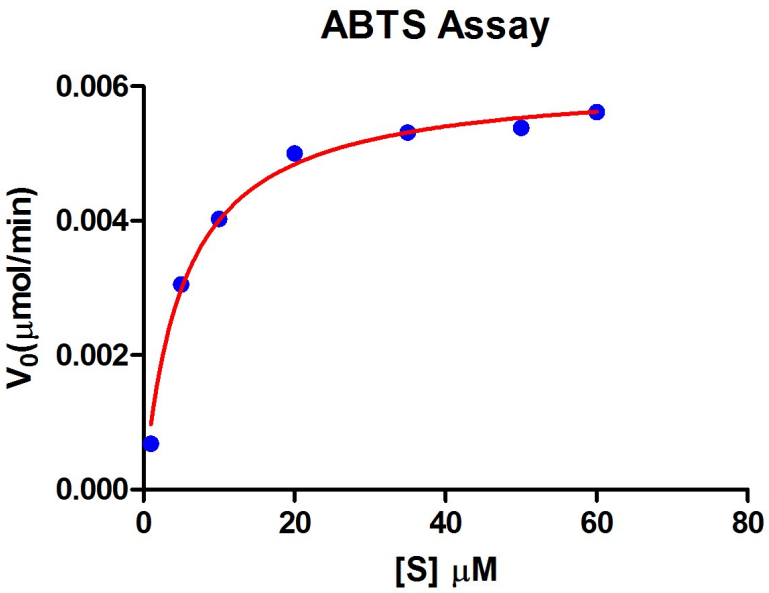

Figure 3.10. KatG enzyme activity using ABTS as substrate.

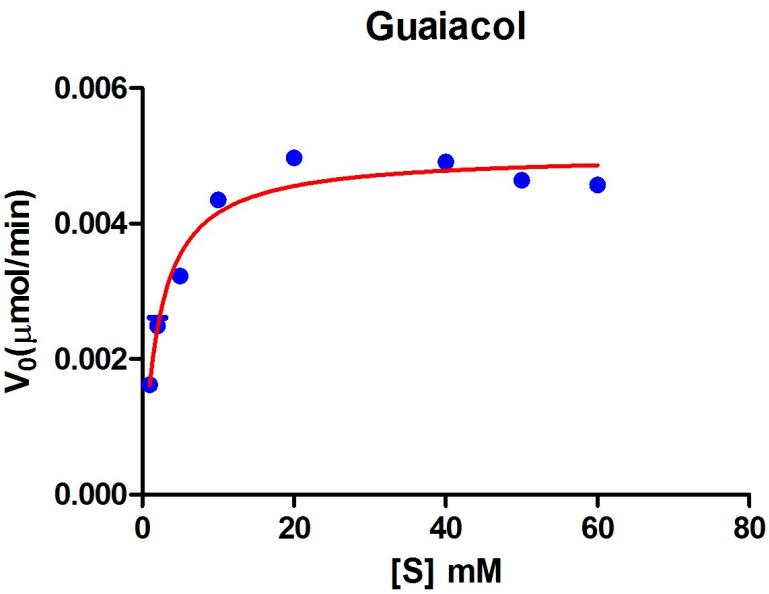

Figure 3.11. KatG enzyme activity using Guaiacol as substrate

The K_m value for ABTS is comparable with the K_m for KatG from *Burkholderia pseudomallei* (5.5 µM) and *Synechocystis sp* (7.0 µM) for the same

substrate but they are the lowest values (7-300 μM) for ABTS-K_m out of KatG from different species [129]. Moreover, the k_{cat} for ABTS of Sphingo-KatG is very low compared to KatG enzymes from *Burkholderia pseudomallei* (0.29 s^{-1}) and *Synechocystis sp* (13 s^{-1} μM) and is 400 times lower than k_{cat} for KatG from *E. coli*. These kinetic parameters for *Sphingobacterium* sp. T2 -KatG using ABTS as an electron donor may indicate that the enzyme is not efficient for binding and turnover of ABTS as a substrate.

The K_m value for guaiacol indicates that Sphingo-KatG has a higher affinity to guaiacol than K_m value (0.05 mM) for horseradish-peroxidase (HRP), however the k_{cat} value for Sphingo-KatG is not promising and not comparable with HRP, which is 4600 s^{-1} [131].

Oxidation of DCP, Mn^{2+} and NADH by KatG were also tested. The specific activity of DCP oxidation was 4 μM $mg^{-1}min^{-1}$, this enzyme activity is about 15 fold lower than a specific activity (59.8 μM $mg^{-1}min^{-1}$) of lignin peroxidase from *Phanerochaete chrysosporium* [132]. KatG from *Sphingobacterium* sp. T2 showed no activity for oxidation of Mn^{2+} or NADH.

3.4. Dye decolourising activity

A wide spectrum of lignin-mimicking dyes have been tested for isolation of the lignin degraders and detection of the ligninase activities. These are dyes either used as a sole carbon source for growth studies, or as indicators of the ability of micro-organism to decolourise them, which may correlate with lignin decomposing ability [105]. The dyes employed in lignin degrader studies include Methylene Blue,

Malachite Green, Congo red, Remozal Brilliant Blue R and Azure B [115]. Azure B has been employed in quantitative measurements of LiP activity. In addition, the Azure B assay is more accurate than the veratryl alcohol assay that is considered to be the standard assay for routine quantitation of LiP activity [106], [112].

Twelve different dyes (Table 3.1) have been used to examine the dye-decolourising activity of KatG. Most of these dyes have been used for detection of lignin-degrading enzymes widely. KatG causes 20.4, 3.2 and 0.8 %, decolourization of Bromophenol Blue, Bromothymol Blue (Figure 3.12). and Reactive Black 5 (Figure 1.36). Therefore, Sphingo-KatG has very low dye decolourizing activity, and is not comparable with Dye-decolourizing peroxidase (for example the turnover number of DyP-like enzyme from fungus *Auricularia auricula-judae* is 11.9 s^{-1} using Reactive Black 5 as substrate) [133] or lignin peroxidase.

Table 3.1. Dyes used for testing dye-decolourising activity of KatG. The amount of purified Sphingo-KatG used varied between (100-200 nM) with 4 mM H_2O_2. For more detail about assay condition, please see experimental section.

No.	Dyes	% of decolourization	No.	Dyes	% of decolourization
1	Azure B	ND	7	BBR250	ND
2	RBBR	ND	8	Bromothymol Blue	3.2
3	Bromophenol Blue	20.4	9	Methyl Orange	ND
4	Malachite Green	ND	10	Methylene Blue	ND
5	Congo Red	ND	11	Phenol Bed	ND
6	Orange G	ND	12	Reactive Black 5	0.8

ND: not detactable.

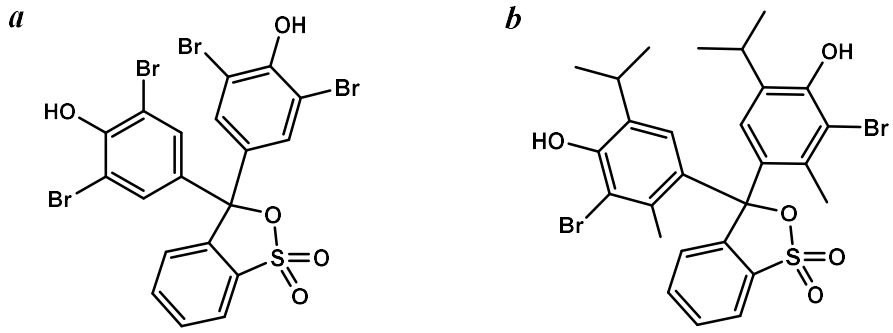

Figure 3.12. Structures of lignin mimicking-dyes which can be decolourised by KatG from *Sphingobacterium sp.* T2. (*a)* Bromophenol Blue. (*b*) Bromothymol Blue.

3.5. Degradation lignocellulose and lignin model compounds

Purified KatG was incubated with wheat straw lignocellulose (1 mg/mL) with and without Mn^{2+} (1 mM) and H_2O_2 (4 mM) at pH 5.5 in succinate buffer for 48 hrs, and the reaction mixture was analysed by reverse phase HPLC at different time intervals (1, 2, 4, 24, and 48 hrs). The experiment was repeated, and H_2O_2 was replaced by a mixture of glucose oxidase (0.5 µg/mL) and glucose (12 mM) to produce H_2O_2. No change was detected in the HPLC chromatogram. These results may indicate that KatG cannot degrade the lignocellulose under conditions described. Kraft lignin and organosolv lignin were also examined in the same manner, but again no change was observed in the HPLC chromatogram. These results may show that KatG from *Sphingobactrium* sp. T2 cannot degrade polymeric lignin and lignocellulose biomass. A similar enzyme from *Amycolatopsis* sp.72vi2 has been reported as a degrader of an aryl ether lignin model compound [108], but not polymeric lignin. Therefore, three different lignin-model compounds were examined

for further investigation of the ability of the KatG of *Sphingobactrium* sp. T2 in oxidation of lignin related compounds.

Di-substituted and trisubstituted -aryl ether model compounds were tested. These two aryl ether compounds have -O-4 linkages that represent about 50% of linkages in lignin polymer. The di-substituted aryl ether is called G-type (containing guaiacyl functional group (***a***)) while the trisubstituted one is called S-type (containing Syringyl functional group (***b***)). In addition, a bi-phenyl model compound (***c***) was also examined to test the ability of the enzyme in breaking 5-5' linkage in the model compound that represents about 10% of linkages in the lignin. 5 mM of each compound ***a***, ***b*** and ***c***, (Figure 3.13) were tested separately in succinate buffer pH 5.5 containing KatG and H_2O_2 with and without Mn^{2+}. No observable changes in HPLC trace were detected when analysed after 1, 2, 3, 4, 24, 48 hrs. These results may illustrate that KatG from *Sphingobactrium* sp. T2 cannot degrade lignin, lignocellulose, and lignin model compounds.

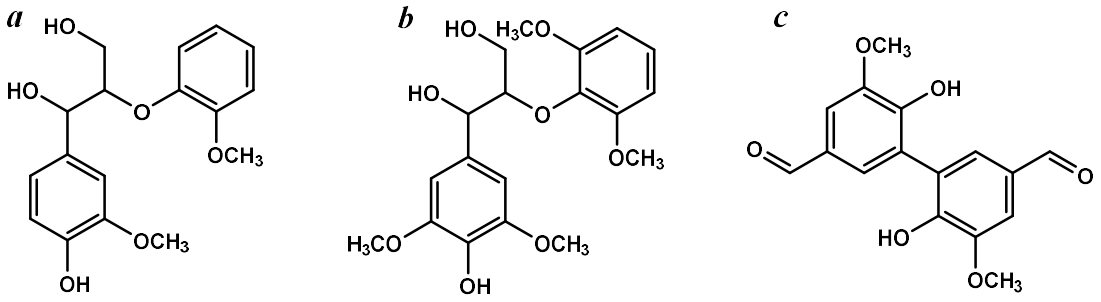

Figure 3.13. Lignin model compounds examined with KatG. ***a***: Guaiacylglycerol-beta-guaiacyl ether, ***b***: 2-(2, 6-dimethoxyphenol)-1-(4-hydroxy-3,5-dimethoxyphenyl)-1, 3-propanediol and ***c***: 3, 3'-dicarboxaldehyde, 6,6'-dihydroxy-5-5'-dimethoxy-1, 1'-biphenyl.

3.6. Conclusion

Heme containing peroxidase enzyme catalase-peroxidase KatG from thermophilic and highly active lignin-degrader strain (*Sphingobacterium* sp. T2) was examined for oxidative depolymerisation of lignin. The *Sphingobacterium* sp. T2 KatG shows weak oxidation of guaiacol, DCP and ABTS. Surprisingly, it cannot oxidize Mn^{2+} and NADH as other KatG homologues do. The enzyme also cannot degrade any of two β-aryl ether lignin model compound (compound ***a***, ***b*** and ***c***, Figure 3.13) as homologous enzyme from *Amycolatopsis* sp.72vi2 can. Therefore, a decision has been made to investigate two superoxide dismutases of *Sphingobacterium* sp. T2.

4. Identification and Characterisation of Two Lignin Degrading Extracellular Mn-Superoxide Dismutase Enzymes from *Sphingobacterium* sp. T2.

4.1. Introduction

As described in Chapter One (Section 1.10) two superoxide dismutase enzymes, were detected by proteomic analysis of a purified extracellular protein fraction of *Sphingobacterium* sp. T2, a highly active lignin-degrader. There are two genes encoding manganese superoxide dismutases in its genome, named *sod1* and *sod2.* The *sod1* is located adjacent to an ECF sigma factor and anti-sigma factor regulatory genes, while *sod2* is located within a cluster of 14 genes containing two *araC* regulatory genes and three ABC transporter component genes (see Appendices).

4.2. Superoxide dismutase

Superoxide dismutases (SODs) are metalloproteins which catalyse the disproportionation of superoxide anion to hydrogen peroxide and oxygen. They have an important role in the protection of cellular components from oxidative damage by the superoxide anion. The overall breakdown of the superoxide anion is accomplished by Fe-SOD, Mn-SOD, Ni-SOD and Cu/Zn-SODs in two steps [134][135][136]:-

$$M^{oxidized}\text{-SOD} + \dot{O}_2^- \longrightarrow M^{reduced}\text{-SOD} + O_2$$

$$M^{reduced}\text{-SOD} + \dot{O}_2^- + 2H^+ \longrightarrow M^{oxidized}\text{-SOD} + H_2O_2$$

where $M^{oxidized}$ –SOD and $M^{reduced}$ –SOD represent the Cu^{2+} /Zn^{2+} and Cu^{+} /Zn^{2+}, Fe^{3+} and Fe^{2+}, Mn^{3+} and Mn^{2+}, Ni^{3+} and Ni^{2+} states of the Cu/Zn-SOD, Fe-SOD, Mn-SOD and Ni-SODs, respectively.

4.3. Types of superoxide dismutase

Superoxide dismutases (SODs) can be classified into three classes according metal ion content; Cu/Zn-SODs, Mn-SOD or Fe-SODs and Ni-SODs. Cu/Zn-SODs contain both Cu and Zn ions in their active sites. Mn- and Fe-SODs contain Fe or Mn in their active sites. Mn-SOD or Fe-SODs can be further subdivided into three classes: enzymes that are active with Mn and Fe or either of the two metal ions in their active site [137]. The mechanisms and redox regulation of active sites of Mn-SOD and Fe-SODs appear to incorporate crucial differences [138]. However, their active sites, structure, and amino acid sequence are quite similar to each other. H_2O_2 inhibits the Fe and the Cu/Zn, but not the Mn-containing superoxide dismutase. Ni–SODs are entirely different from well-known Cu/ Zn-, Fe-SOD and Mn-SODs [137].

4.3.1. Cu/Zn-SODs

Cu/Zn-SOD (erythrocuprein) was the first SOD to be identified. The oxidized form of Cu/Zn-SOD has a Cu^{2+} ion coordinated in a distorted square pyramid by four histidines, one of which is also a ligand for a distorted tetrahedral Zn^{2+} ion and a solvent molecule, while Zn^{2+} is coordinated by three additional ligands two histidines and an aspartic acid [138]. The structure of Cu/Zn-SOD and its catalytic cycle are

shown in Figures 4.1 and 4.2, respectively. Nearly all cells in eukaryotes contain Cu/Zn-SOD [139]. In yeast such as *Saccharomyces cerevisiae* and mammals, Cu/Zn-SOD is found mainly in the cytosol with a lower fraction in the mitochondrial intermembrane space. Also, it has been detected in nuclei, lysosomes, peroxisomes using immunocytochemical methods. Several bacteria also have been reported to contain Cu/Zn-SODs and have been demonstrated to be embedded in the periplasm. In prokaryotes, Cu/Zn-SOD is important for their survival especially in late stationary phase and their growth ability in aerobic environments [140]. Most of the reported Cu/Zn-SODs are from Gram-negative bacteria including *E. coli,* and they are localised in the periplasm, found only in Gram-negative bacteria [141].

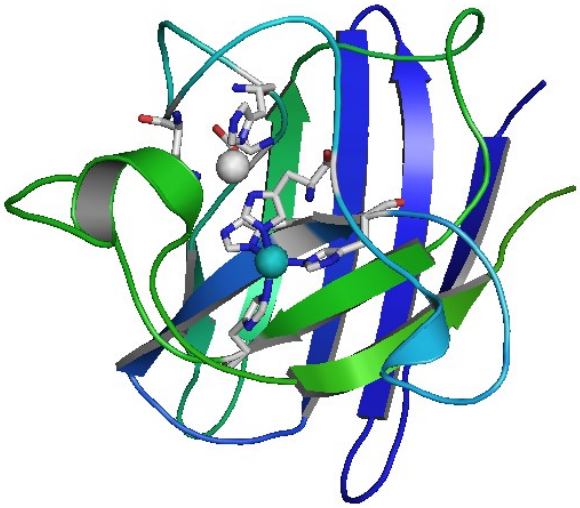

Figure 4.1. Crystal structure of Cu/Zn superoxide dismutase from bovine erythrocyte with copper (cyan) and zinc (gray) ions in the active site [142], generated by PyMOL, PDB entry [1SXC].

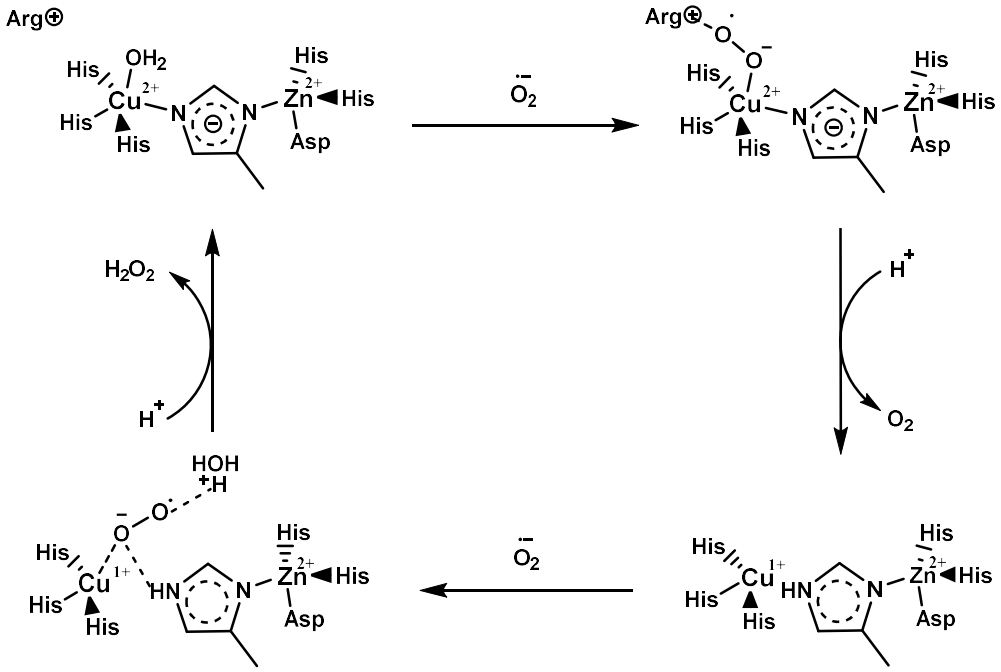

Figure 4.2. The catalytic cycle of Cu/Zn superoxide dismutase. Superoxide radical anion displaces the axial water and binds to Cu^{2+} centre for electron transfer. This binding is stabilised by a positively charged arginine residue. Reduction of Cu(II) leads to the release of dioxygen and protonation of imidazolate group (His61) loses its binding to Cu(I). The second superoxide radical coordinates with Cu(I). Hydrogen peroxide is formed by electron transfer from inner-sphere and is protonated. Additional protonation results in the release of hydrogen peroxide, and a water molecule coordinates with Cu(II) again, reforming the imidazolate bridge [143],[144].

4.3.2. Fe-SODs and Mn-SODs

FeSODs are found mainly in prokaryotes while Mn-SODs are occurring in both prokaryotic and eukaryotic cells, in a high frequency [139]. The Mn-SOD and Fe-SOD family was first discovered by Fridovich in 1970 and 1973, respectively [140]. The catalytic mechanism of Fe-SOD and Mn-SODS are similar to that of Cu/ZnSODs (see Figure 4.3 for more detail). Inside the active side of each subunit is a single manganese or iron center bound to three histidines, one aspartate (Figure 4.4) and water molecule or hydroxide anion in a trigonal bipyramidal geometry [139],[140]. Therefore, their active site is completely unrelated to Cu/ZnSODs [138].

The Fe-SOD and Mn-SOD enzymes share a well-conserved protein fold and significant sequence similarity across different phyla of archaea, eubacteria and eukaryotes. They encompass a dimer or tetramer of about 21 kDa subunits. Usually, both metal forms are expressed in the same cells. The dimeric forms are expressed by bacteria, but tetrameric forms are found in a limited number of prokaryotes, such as hyperthermophiles. Generally, in eukaryotes only tetrameric Mn-SODs are found [140].

The location of Fe-SOD and Mn-SOD in cyanobacteria and photosynthetic bacteria is different. Mn-SOD is embedded in the plasma and thylakoid membranes while Fe-SOD is localised in the cytosol. In photosynthetic organisms, the expression profile of Fe-SOD and Mn-SOD show differences as well. Expression of Mn-SOD is strongly regulated and inducible by stress conditions. In contrast, expression of Fe-SOD has been revealed to be regulated developmentally and by light and is changed by environmental stimuli. It has been reported that FeSOD is important for protection of photosynthetic organisms from damage as a consequence of chilling, sulphur dioxide stress, drought, Cu toxicity, and superoxide radicals produced by the electron transport chain [137].

In the cyanobacterium *Anabaena sp.* strain PCC7120, two SOD enzymes (FeSOD and MnSOD) have been isolated and purified: the FeSOD enzyme is cytosolic while MnSOD is localised in the thylakoid membrane. MnSOD has a leader peptide and a membrane attachment motif in the N-terminal sequence. In addition, it has been reported that the leader peptide is essential for its activity and membrane localization. The *Anabaena* sp. strain PCC 7120 genome contains no Cu/ZnSODs [145].

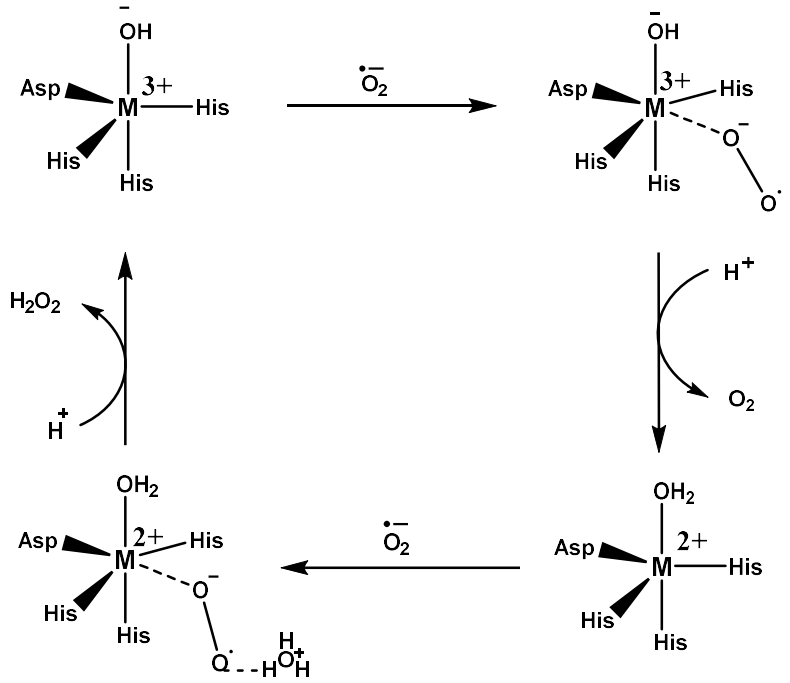

Figure 4.3. The catalytic cycle of Mn-SOD and Fe-SOD, M represent Fe and Mn ions [146].

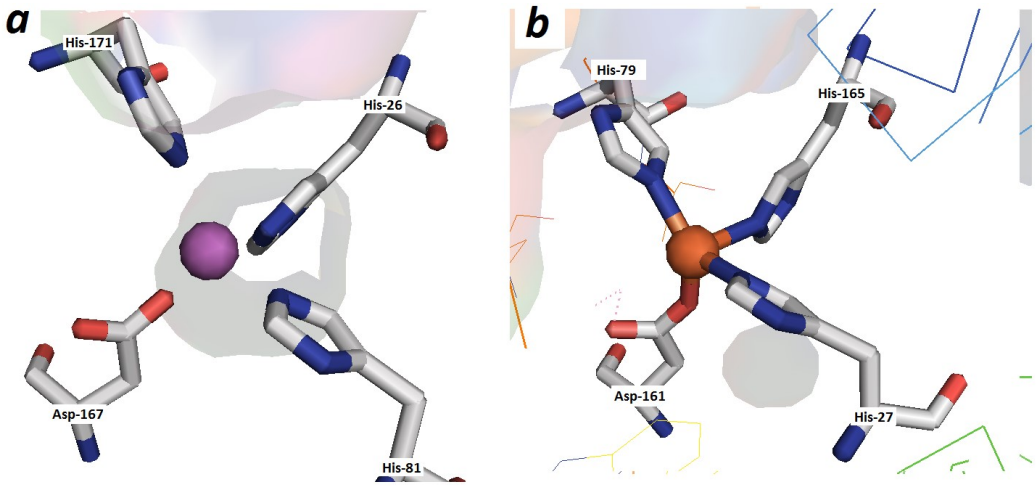

Figure 4.4. The active site of superoxide dismutase (*a)* in MnSOD from *E. coli* (PDB code: 1EN5) and (*b*) in FeSOD from *Thermosynechococcus elongatus* (PDB code: 1MY6). PyMol was used for display.

Studies indicate that FeSOD enzymes from *E coli* and *Pseudomonas ovalis* can be inactivated by H_2O_2. Cu/ZnSODs can also be inactivated by H_2O_2 but MnSODs are not. The inactivation of FeSOD from *E. coli* by H_2O_2 has been correlated with loss of tryptophan and some loss of iron, but not histidine or another amino acid as detected in FeSOD from *Pseudomonas ovalis*. The proposed mechanism of Cu/Zn SOD inactivation is through a reduction of Cu(II) to Cu(I) by H_2O_2, followed by a Fenton-like reaction between Cu(I) and H_2O_2. The strong oxidant (Cu(II)-O) is probably generated at the Cu site by the latter reaction, and then this oxidant attacks an adjacent histidine, leading to the loss of one histidine residue per subunit during inactivation [147].

4.3.3. NiSODs

Ni-dependent SODs are completely unrelated to the well-known Cu/ZnSOD, FeSOD, and MnSODs. It has been shown that *Cyanobacteria* [139] and several *Streptomyces* species produce nickel containing SODs. The active site of NiSODs contain one Ni per monomer [138].

4.4. SOD in lignin-degrading fungi

Study of oxidative stress in the lignin-producing culture of *Phanerochaete chrysosporium* shows the involvement of ROS in the induction of lignin peroxidase gene expression [11]. Considerable increase in the specific activity of MnSOD, catalase, glutathione reductase, and glutathione peroxidase and the consumption of glutathione have been observed during lignin breakdown, and a significant increase in intracellular hydrogen peroxide and oxidative damage to macromolecules has been

observed. Studies indicated that reactive oxygen species can induce LiP gene expression in Mn^{2+}-deficient cultures while addition of each of •OH scavenger and Mn^{2+} to cultures resulted in reduction in LiP gene expression [148],[149].

It has been shown that superoxide is produced during oxidation of veratryl alcohol by lignin peroxidase. The produced superoxide can react with LiP to produce compound III, which is an inactive form of LiP. It has been demonstrated that SOD can enhance veratryl alcohol oxidation by LiP while the addition of KO_2 can inhibit veratryl alcohol oxidation [150].

4.5. MnSODs and degradation of rubber

Although the function of extracellular SODs is not certain, they are apparently significant for certain environments, such as the involvement of SODs of pathogenic microorganism in resistance against the immune defence. An increase in SOD activity has been seen during exposure of diatom *Skeletonema costatum* to 2,4-dichlorophenol, and the lignin degrader *Phanerochaete chrysosporium* expresses SOD during exposure to dibenzo-*p*-dioxin [151].

Extracellular MnSOD enzymes from both *Gordonia westfalica* Kb1 and *Gordonia polyisoprenivorans* have been demonstrated to have a possible involvement in degradation of poly (*cis*-1,4-isoprene). They have been found in a gene cluster required for growth on poly (*cis*-1,4-isoprene), and both strains contain only one MnSOD. It has been reported that both strains show a significant reduction in growth on poly (*cis*-1,4-isoprene) when their MnSOD genes are knocked out, as

well as when a small amounts of SOD inhibitor (NaN_3) is added to their growth culture separately [151].

4.6. Assays for determination of SOD activity.

Most assay methods for determination of SOD activity are indirect and based on inhibition of a chemical reaction since the superoxide anion radical cannot be easily detected by conventional analytical tools. In addition, the unavailability of the substrate (superoxide radical anion) in pure and stable form makes testing the activity of superoxide dismutase complicated. Hence whenever turnover of superoxide radical is required, it has to be produced within the assay system. Therefore, SOD assays consist of two major components: a superoxide generator and a superoxide indicator (detector). As the enzyme (superoxide dismutase) transforms superoxide radical to hydrogen peroxide and molecular oxygen, SOD can compete with the indicator and hence the enzyme activity can be determined (Figure 4.5) [152],[153],[154].

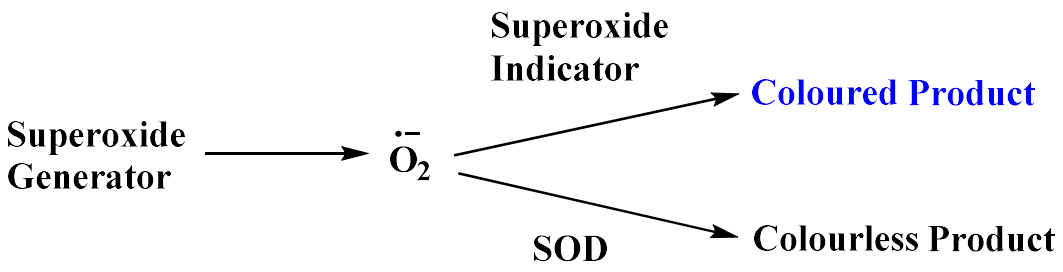

Figure 4.5. Superoxide dismutase assay components: a generator to produce superoxide radical anion and an indicator to detect superoxide radical and produce a coloured product. Superoxide dismutase competes with the indicator and decreases the production of the coloured product, and then from the percentage of inhibition the SOD activity can be calculated.

Indicators such as cytochrome c and nitroblue tetrazolium (NBT) [155] are used to detect and quantify the superoxide anion radical. NBT can scavenge superoxide radical anion and convert NBT to formazan which can be monitored at 550 nm (Figure 4.6). The oldest and most specific superoxide indicator is cytochrome c while nitroblue tetrazolium is more sensitive but less specific [153].

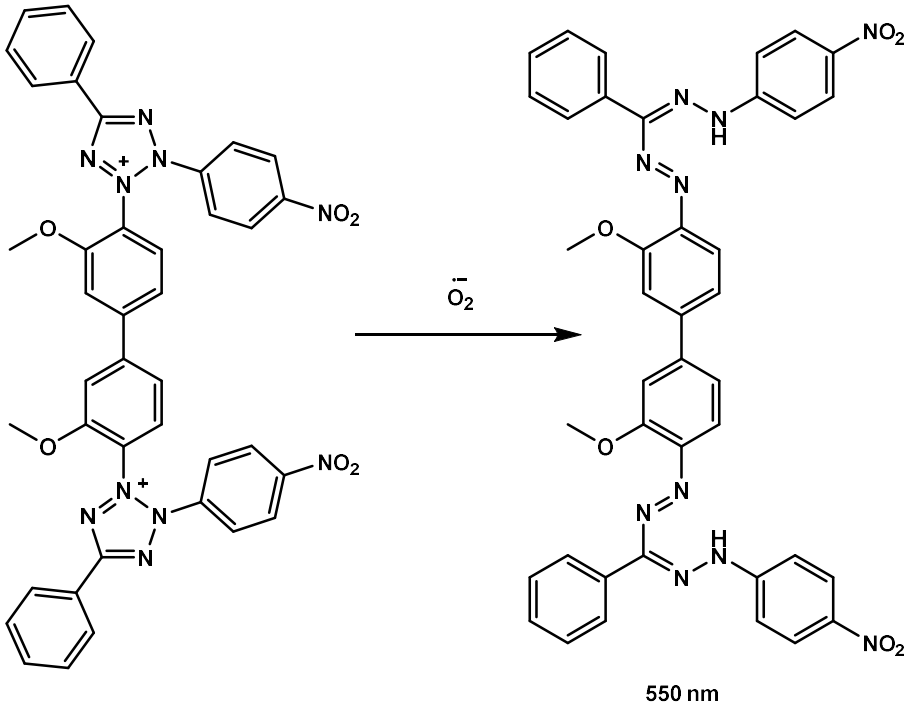

Figure 4.6. Reduction of Nitroblue tetrazolium (NBT^{2+}) with superoxide radical anion and formation of formazan.

Several methods are available for generation of the substrate (superoxide radical) for SOD enzyme assays. In oxygenated aqueous medium it has been produced by a) pulsed radiolysis, by exposure to γ-rays for a particular time; b) by flash photolysis; c) by a flow system involving irradiation with a beam of electrons; d) by enzyme (xanthine oxidase) in the presence of its substrate (xanthine) [152]; and e) by autoxidation of pyrogallol in basic media [156]. In non-aqueous solution,

superoxide radical has been generated by electrolytic reduction of dioxygen in an aprotic solvent such as diethylformamide [152] and by dissolving potassium superoxide in dimethylsulfoxide [157].

4.6.1. Ferricytochrome c reduction method

In 1969, McCord and Fridovich identified the SOD function and described the assay method, the assay was based on the ability of superoxide radical to reduce ferricytochrome c. The superoxide anion radical is generated enzymatically via xanthine/xanthine oxidase system, which results in an absorption increase at 550 nm. Superoxide dismutase inhibits ferricytochrome c reduction due to the disproportionation of the reaction partner (Figure 4.7). The enzyme activity can be calculated from the percentage of superoxide radical inhibition. One unit of SOD activity is defined as the amount of enzyme required to generate 50% inhibition of the rate of ferricytochrome c reduction [152],[153],[154].

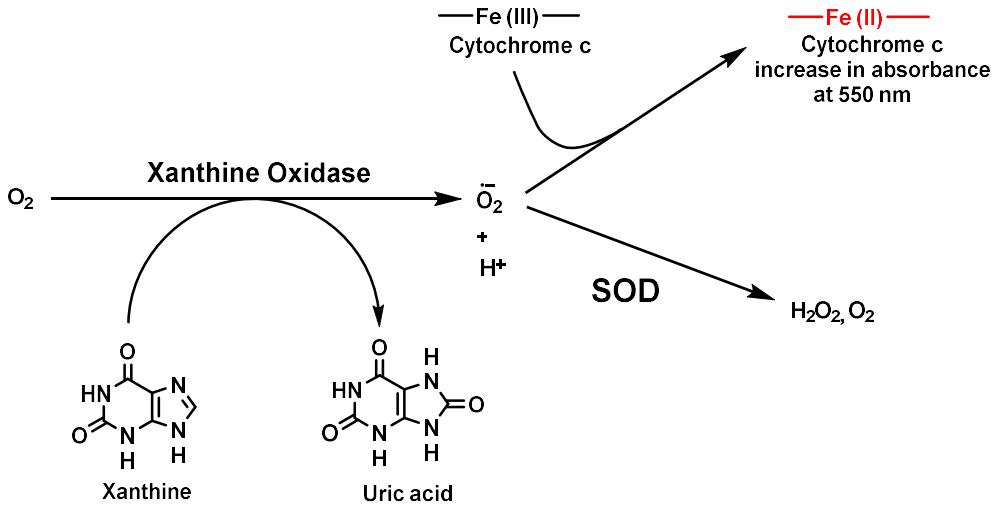

Figure 4.7. Ferricytochrome assay. The substrate (superoxide radical) is generated enzymatically by xanthine/xanthine oxidase system; then cytochrome c competes with SOD to react with superoxide radical anion.

4.6.2. Pyrogallol autoxidation assay

Pyrogallol undergoes autoxidation in basic medium. It has been found that superoxide radical anion is involved in the autoxidation of pyrogallol. The assay is based on the ability of SOD to inhibit pyrogallol autoxidation. The rate of reaction can be monitored at 420 nm [156] or 325 nm for oxidized pyrogallol products [158]. The SOD enzyme activity can be measured by the amount of enzyme needed to generate 50% inhibition of pyrogallol autoxidation [156].

4.7. Overexpressing *Sphingobacterium* Superoxide dismutase

The genomic DNA sequence of *Sphingobacterium* sp. T2 (deposited as DDBJ/EMBL/GenBank accession JXAC00000000) contains two genes encoding manganese superoxide dismutases, named as *SOD1*(684 bp) and *SOD2* (543 bp) (see Appendices for sequences), matching the proteomic amino acid sequences obtained by previous Ph.D. student Charles Taylor. These genes encoding for proteins that showed sequence similarity to the SODA family of superoxide dismutases, with SOD1 and SOD2 showing 49% and 47% sequence identity to *E. coli* SODA respectively, and 73% sequence identity to each other.

4.7.1. Cloning, expressing and purification of SOD1 in *E. coli*

Sphingobacterium sp. T2 strain was obtained from stored glycerol stock collections of our group (isolated from compost by Charles Taylor). The strains were grown overnight in Luria-Bertani broth. The genomic DNA was extracted from a total of 1 mL culture using Wizard® Genomic DNA Purification Kit from Promega. Two primers (forward and reverse) were designed for amplification of *SOD1* gene

using TOPO cloning method, in which a CACC overhang was added to forward primer at the 5' end. The forward primer was $_{5'}$CAC CATG ATG AAG ATG AAT ATT TTT AAG ACT G$_{3'}$ and reverse primer was $_{5'}$TTA TTT TTT CAA GGC TTT CTC ATA TCG$_{3'}$. The *SOD1* gene was amplified by PCR using Platinum Pfx-DNA polymerase from Invitrogen, following the manufacturer's instructions. The amplified gene with 684 bp was separated and analysed by agarose gel (see Figure 4.8).

The amplified gene was cloned into expression vector pET151 using the Champion™ pET 151 Directional TOPO®. The plasmid was transformed into *E. coli* TOP10 competent cells (Invitrogen). The transformants were analysed by PCR and restriction digest. The extracted plasmids were sent for sequencing to confirm sequence and ligation accuracy. The sequencing result showed that the recombined gene has the correct orientation in the vector, and no mutation has been observed. The plasmid was transformed into BL21 *E. coli* (Invitrogen) competent cells, for protein expression.

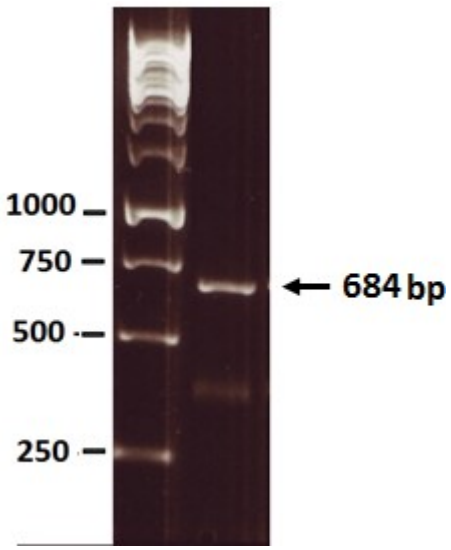

Figure 4.8. Agarose gel analysis of PCR amplified *SOD1* genes from *Sphingobacterium* sp. T2

The transformed *SOD1* gene was overexpressed by growing the *E. coli* BL21 with *SOD1* construct in 1 litre Luria-Bertani broth for 3 hours at 37ºC in the presence of 100 mg/mL ampicillin, then the cells were induced by adding 0.5-1 mM IPTG at 20 ºC shaken overnight and 1 mM $MnCl_2$ was also added. The cells were harvested using a centrifuge at 5000 rpm and disrupted by constant system cell disrupter, followed by centrifugation at 11000 rpm for 34 minutes. The supernatant was filtered through a syringe filter (Millipore). The clean supernatant was incubated with pre-equilibrated Ni-NTA resin (2 mL) with washing buffer for 1 hr and washed with the same buffer. The bound proteins were eluted with elution buffer (for more detail, please see experimental section) and collected. The analysis of protein fractions by SDS-PAGE gel electrophoresis indicated that there was no corresponding protein band for SOD1 expected at 30.5 kDa (Figure 4.9), this may be due to the formation of inclusion bodies or that the His_6 fusion tag is not exposed to bind to the immobilised ion affinity chromatography (IMAC) resin.

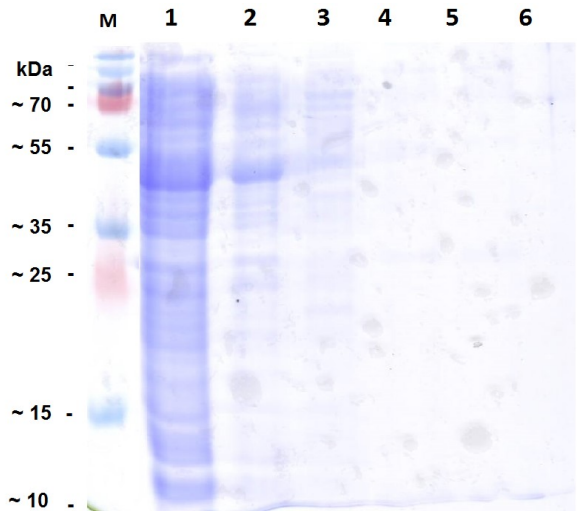

Figure 4.9. Analysis of protein preparations by SDS-PAGE electrophoresis, : SOD1 enzyme fractions from IMAC column under native condition; lane 1: unbound fraction, 2 wash fraction with 10 mM imidazole in 20 mM Tris; 3, 4, 5 and 6: eluted with 150, 175, 200, 250, and 300 mM imidazole in 20 mM Tris with 0.05 M NaCl pH 8 (No band is found).

The structure of SOD1 was generated using a web-based environment for protein structure homology modelling [159],[160] and it shows that the N-terminal sequence is exposed (Figure 4.10). Therefore, the protein may produce inclusion bodies, or it may have a signal peptide for translocating it to the periplasmic membrane.

4.7.2. Solubilisation of recombinant SOD1

Efforts were made to prevent the formation of inclusion bodies by SOD1. The inducing temperature was kept low (15ºC) 1% of sucrose added to the induced culture, and different concentrations of IPTG (0.2, 0.4, 0.5 and 0.6 mM) were used and 0.5 mM Mn^{2+} was added to culture to support correct folding of the enzyme. Then, two different buffers have been used to extract the enzyme from cell lysates. The buffers employed were Tris.Cl pH 8.0 with 10 mM imidazole, with and without Triton X100 (1%) (Figure 4.11.*a*).

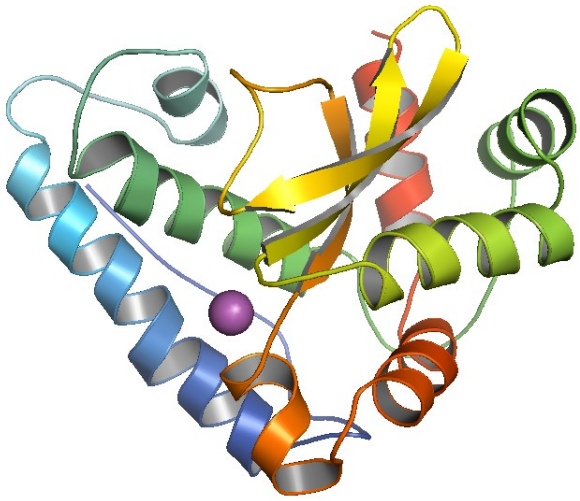

Figure 4.10. Structure of SOD1 generated by homology modelling [159],[160], it shows that N-terminal sequence is quite exposed (light blue).

The cell lysate of induced (0.5 mM IPTG and 0.5 mM $MnSO_4$) SOD1 construct was treated with 6 M guanidine hydrochloride in Tris.Cl (pH 8.0) containing 20 mM 2-mercaptoethanol and loaded onto the IMAC resin. In this case, the enzyme band on SDS gel can be observed (Figure 4.11.*b*). The result shows that the SOD1 is partially solubilized by Triton X100, but total solubilization can be achieved with 6 M guanidine hydrochloride.

4.7.3. Prediction of signal peptide

The SOD1 protein sequence was analysed by web-based software (signal peptide prediction program, SignalP 4.0) [161]. The result revealed that the enzyme has a leader sequence which is 24 amino acids in length. The leader sequence is (MMKMNIFKTALVATALFATQTTFA) (Figure 4.12). Therefore, we decided to re-clone *SOD1* without the leader sequence.

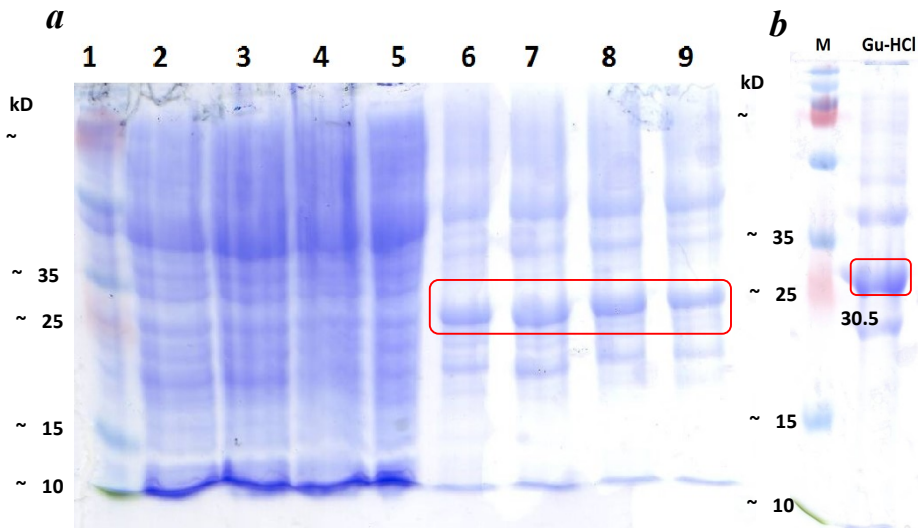

Figure 4.11. SDS-PAGE analysis of over-expressed SOD1 lysates, ***a***: *E. coli* cells containing SOD1 construct induced with 0.2, 0.4, 0.5 and 0.6 mM IPTG (1% sucrose and 0.5 mM Mn^{2+} was also present in induced cultures) lane 2 and 6, 3 and 7, 4 and 8 and 5 and 9 respectively. The protein fractions were extracted with two types of buffer: 10 mM imidazole, 20 mM Tris in HCl, 0.5 M NaCl pH 8, lane 2, 3, 4 and 5, and the same buffer containing 1% Triton X100. ***b***: cell lysate from *E. coli* containing SOD1 induced with 0.5 mM IPTG and the protein fraction was extracted with 20 mM 2-mercaptoethanol, 50 mM Tris.Cl, 6 M guanidinium hydrochloride pH 8.0.

4.7.4. Cloning, expressing and purification of mature SOD1 in *E. coli*

Since the SOD1 has a signal peptide for translocation to the periplasmic membrane, removing the signal peptide may be one of the best choices to prevent the formation of inclusion body, and to overexpress and purify recombinant enzyme in native condition. For this purpose, two new primers have been designed to amplify only the mature gene. The designed primers are $_{5'}$CACCCAATTTAAACAGACCC$_{3'}$ as a forward primer and reverse primer $_{5'}$TTATTTTTCAAGGCTTTCTCA TATCG$_{3'}$. The forward primer has CACC overhang at the 5' end. The mature *SOD1* gene was amplified and cloned into the pET151 vector using Champion™ pET Directional TOPO® Expression Kit (Invitrogen). The cloned vector was transformed into TOP10 *E. coli* competent cells (Invitrogen). The correct construct was found after analysis of transformants by PCR and DNA sequencing. The sequencing result revealed that the plasmid has a mature *SOD1* gene with the right orientation in the vector and without any mutation.

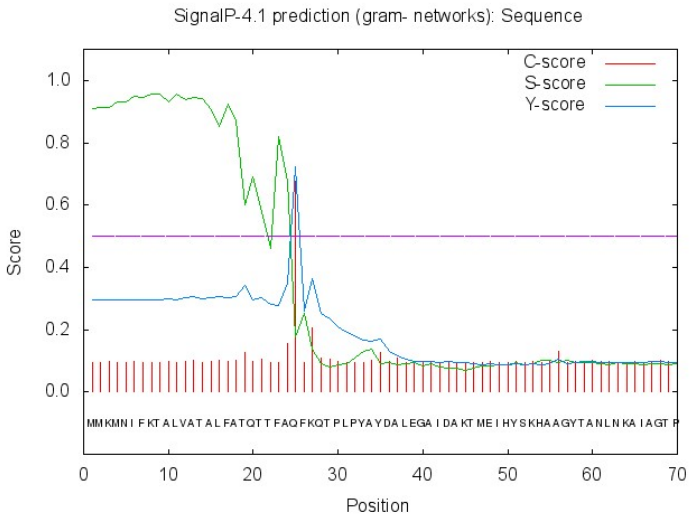

Figure 4.12. Predicted structure and leader peptide of the SOD1 prediction of leader peptide generated by SignalP4.1 [161].

The plasmid with mature *SOD1* was transformed into competent BL21 *E. coli* cells. Overexpression and purification were carried out in the same condition as described previously in Section 4.6.1. The collected fractions from IMAC purification was analysed by SDS-PAGE gel electrophoresis and the result shows a broad protein band for the SOD1 enzyme (Figure 4.13), this indicates that removing signal peptide significantly improves the solubility of SOD1. Therefore, the SOD1 enzyme fraction (eluted from IMAC) was concentrated 2 to 3-fold using a 10 kDa Amicon centricon device, then the protein preparation solution was subjected to buffer exchange through a PD-10 column into 20 mM MOPS 80 mM NaCl buffer pH 7.0. The fusion tag (His_6 tag) of a fraction of purified SOD1 was removed using TEV protease (Figure 4.13). The concentration of enzyme was estimated by Bradford assay. The enzyme was frozen in liquid nitrogen and stored at -80ºC or stored in -20 ºC with 50% glycerol. The yield of mature SOD1 was 28 mg per liter of bacterial culture.

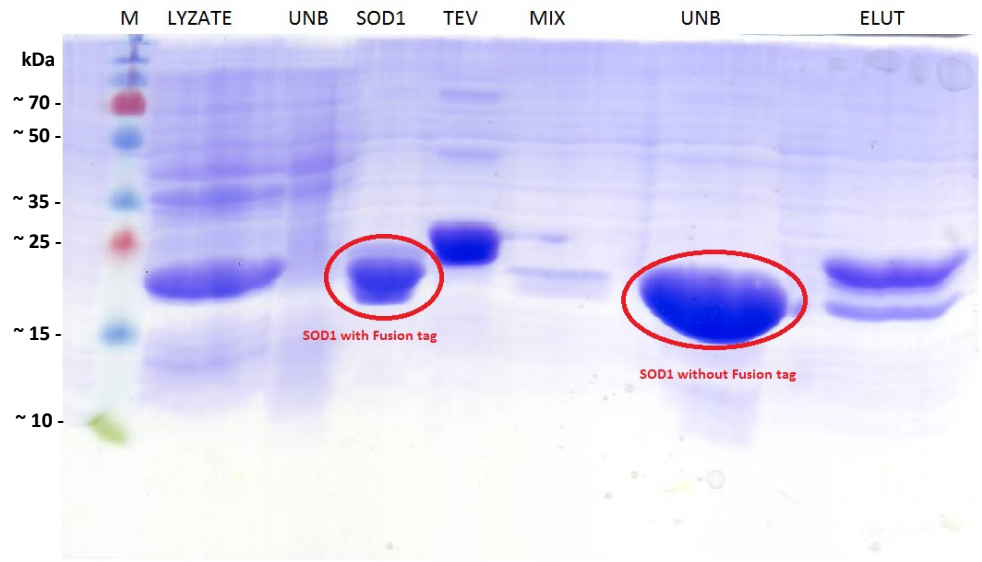

Figure 4.13. Analysis of SOD1 preparations by SDS-page electrophoresis before and after removing a His_6 tag with TEV-protease.

4.7.5. Cloning, expressing and purification of SOD2 in *E. coli*

The *SOD2* gene was amplified using two designed primers for conventional cloning. The primers used are forward $_{5'}$GAT CTA CAT ATG ATG GAA ATC CAT CAC G$_{3'}$ and reverse primer $_{5'}$ACT ATC GGA TCC TTA TTT TTT AGC AGC TGC$_{3'}$. The forward primer contains NdeI restriction site while the reverse primer includes BamHI enzyme cleavage site. Both primers have six extra random bases for endonuclease enzyme cleavage at the 5' end. The *SOD2* gene was amplified and digested with FastDigest NdeI and BamHI enzymes (Thermo Scientific^{TM}) using manufacturer's protocols. The vector (pET28a^{+}) was also digested with the same enzymes. The digested vector and PCR product were separated by agarose gel electrophoresis and purified (Figure 4.14). The ligation reaction was carried out using T4-DNA-ligase (Thermo Scientific^{TM}) following manufacturer's recommendations. The recombined vector was transformed into *E. coli* TOP10 competent cells (Invitrogen). The transformants were analysed, and a positive clone was found. The plasmid that can be amplified by PCR was sent for sequencing to confirm its orientation and sequence. The construct without any mutation was selected and transformed into BL21 competent cells for overexpression.

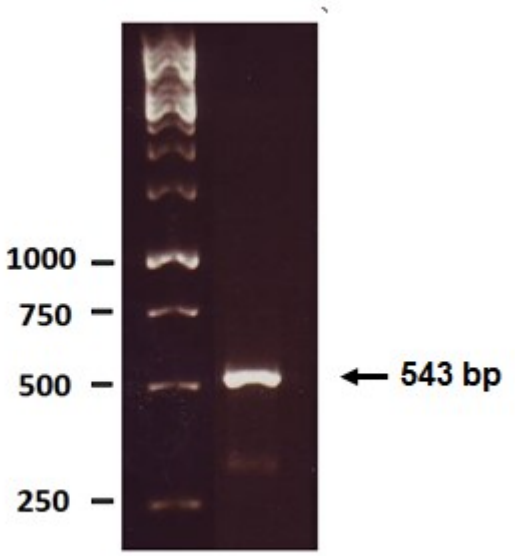

Figure 4.14. Agarose gel electrophoresis of SOD2**.**

The SOD2 was overproduced (using pET28a$^+$ vector with *SOD2* construct) and purified using IMAC resin under native conditions (Figure 4.15) in a similar manner as described in Section 4.7.1. The enzyme preparation was quantified using a Bradford assay. The yield of SOD2 was 39 mg from 2 liters of bacterial culture. The SOD2 buffer was exchanged by PD-10 gel filtration column, to 50 mM potassium phosphate buffer pH 7.8, then flash frozen and stored at -80ºC.

The *SOD2* was re-cloned into the expression vector pET151. Two new primers (forward $_{5'}$CAC CATG GAA ATC CAT CAC GAT CGT C$_{3'}$ and reverse $_{5'}$TTA TTT TTT AGC AGC TGC ATA GTT AG$_{3'}$) were designed. The vector pET28a$^+$ with *SOD2* construct was used as a template. The cloned *SOD2* gene on pET151 was first transformed into competent TOP10 *E. coli* cells and the accuracy of sequence and orientation of the gene confirmed, and then retransformed into BL21 competent *E. coli* cells.

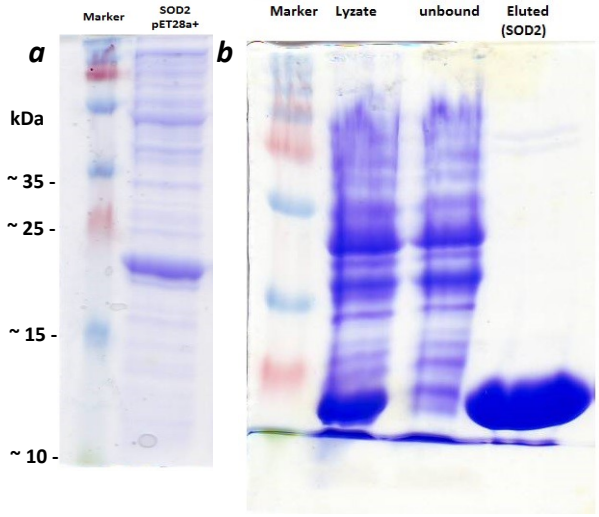

Figure 4.15. SDS-PAGE analysis of purified SOD2: ***a***.cell lysate of *E. coli* construct containing SOD2 (on pET28a^{+}) extracted with buffer containing 10 mM imidazole, 20 mM Tris in HCl, 0.5 M NaCl pH 8. ***b.*** purified SOD2 by IMAC, overexpressed using *SOD2* construct on pET151 vector*)*.

SOD2 was overexpressed and purified using IMAC resin (using pET151 vector with *SOD2* construct, Figure 4.16). The His_6 fusion tag was removed by TEV-protease, and the enzyme was concentrated, flash-frozen with liquid nitrogen and stored at -80ºC in 50 mM potassium phosphate buffer pH 7.8.

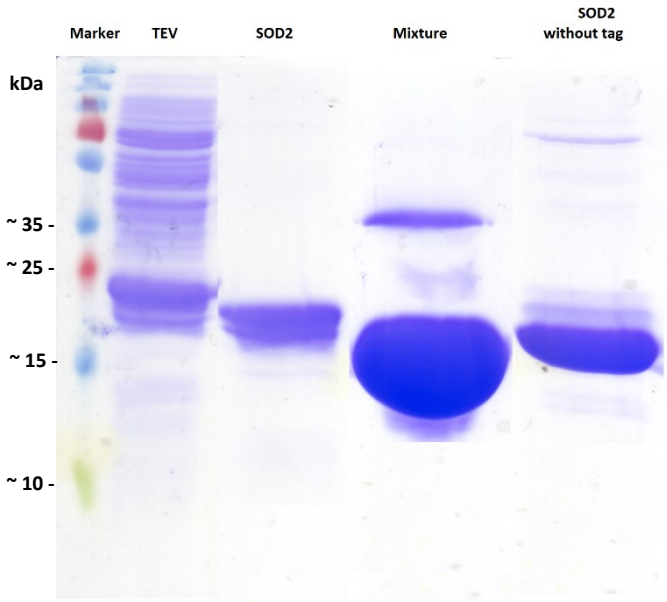

Figure 4.16. Analysis of SOD2 preparations by SDS-page electrophoresis before and after removing 6His tag with TEV-protease.

4.8. Characterization of SpSOD enzymes

4.8.1. SpSOD enzyme activity

Superoxide dismutation activity was measured using two methods, pyrogallol method (inhibition of pyrogallol autoxidation by SOD [156]) and ferricytochrome c method (inhibition of cytochrome c reduction by SOD [154]). The former was performed in 50 mM Tris-HCl buffer pH 8.0 and 50 mM potassium phosphate buffer in the presence of 0.1 mM ethylenediaminetetraacetic acid (EDTA). In the ferricytochrome c assay, the superoxide radical was generated using xanthine/ xanthine oxidase. The activity of SpSODs was calculated from 50% inhibition, which was achieved by changing the amount of enzyme in the assay mixture. Using the pyrogallol assay, the specific activities of SOD1 and SOD2 were 402 units/mg; and 124 units/mg repectively, and via inhibition of cytochrome c reduction, the specific activities were: SOD1 3090 units/mg; SOD2 860 units/mg.

4.8.2. Determination of metal ion contents of SpSOD enzymes using ICP-OES

Purified SOD1 and SOD2 (300 µL of 1 mg/mL of each to 5 mL) in 3% nitric acid were analysed by ICP-OES. A series of standard solutions of each of sulphur, iron, manganese, copper and zinc were also analysed with the same machine under the same conditions. The protein concentration was estimated based on sulphur content, the molecular weights and sulphur stoichiometry of SOD enzymes were taken from their amino acid sequences, using these values and observed concentration of sulphur by ICP-OES the concentration of protein was calculated.

The metal stoichiometry was then determined using protein concentration and metal concentrations estimated from a calibration curve of corresponding metal ions.

The results of ICP-OES show that both enzymes (SOD1 and SOD2) contain less than one equivalent of metal ions (Table 4.1). This may be due to the speed of overexpression. As the overproduction takes place very fast, it may be that the bacteria do not have enough time to reconstitute all the SOD enzyme produced with its metal ions. Both enzymes are mostly apo-proteins, 28% of SOD1 enzyme and 19% of SOD2 constituted with metal ions. The majority of metal in SOD1 is Mn (91%) with 7.4% Fe and 1.16% Cu ions, suggesting that SOD1 is a manganese-containing enzyme (Figure 4.17). SOD2 was found to contain a high concentration of Zn (54.6%) a low concentration of Cu (4.1%), and somewhat higher Mn (22.6%) content than Fe (18.4%) (Figure 4.18). The ICP-OES results for SOD2 are not very convincing because the Mn and Fe content is rather similar.

Table 4.1. Number of metal ion per molecule of protein.

Enzyme	Zn^{2+}	Cu^{2+}	Fe^{2+}	Mn^{2+}
SOD1	0	0.003	0.02	0.26
SOD2	0.1	0.009	0.04	0.05

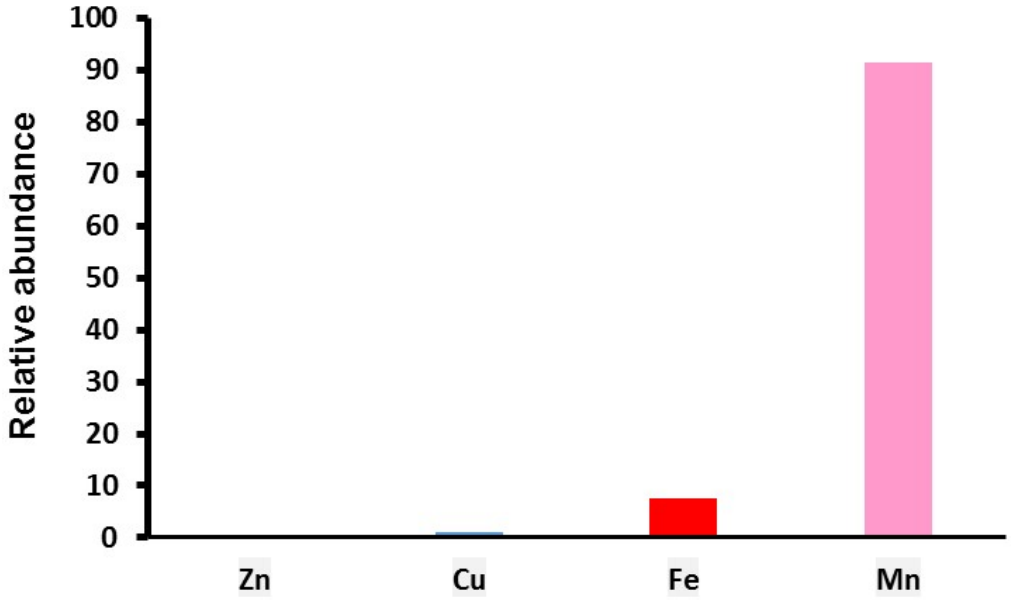

Figure 4. 17. Percentage of metal ions in SOD1 measured by ICP-OES**.**

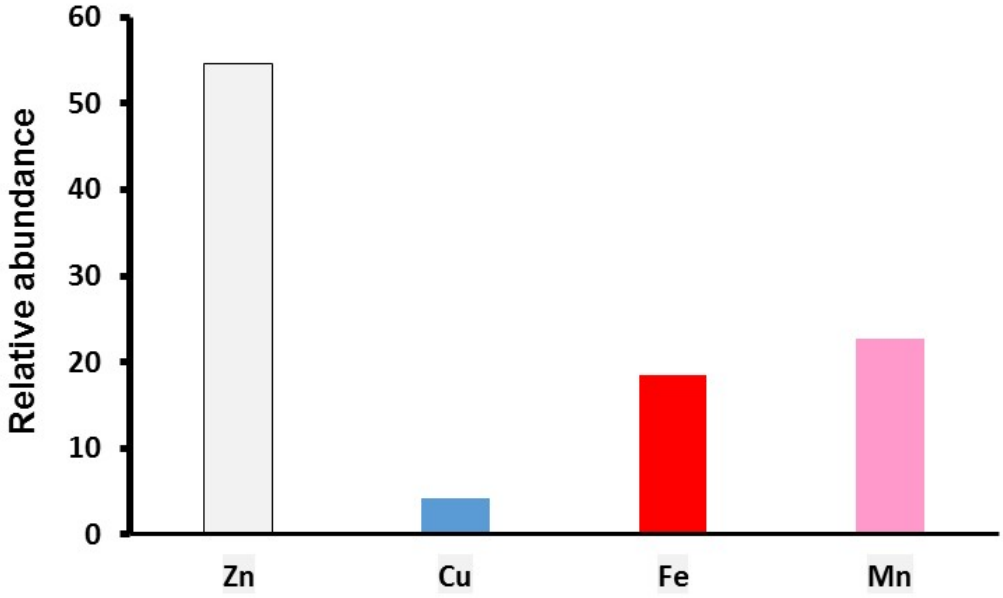

Figure 4.18. Percentage of metal ions in SOD2 measured by ICP-OES**.**

4.8.3. Metal ion removal and reconstitution

The removal and reconstitution of metal ions with desired purified enzymes were carried out by sequential dialysis with different buffers [162]. The Apoprotein was prepared with 10 mM EDTA and 8 M urea in 50 mM acetate buffer then gradually the buffer was changed to phosphate buffer pH 7.0 containing 8 M urea without EDTA. The reconstitution was carried out in 50 mM acetate buffer (pH 3.8) containing 8 M urea and 10 mM of metal ions (Fe^{2+} or Mn^{2+}), then gradually the concentration of urea was decreased and the pH increased to 7.0 (phosphate buffer containing 0.5 mM EDTA) with dialysis (for more detail, please see experimental section).

The activity of reconstituted SOD1 and SOD2 with Fe^{2+} and Mn^{2+} were determined using pyrogallol autoxidation method. The result shows that Mn-reconstituted SOD1 is more active than Fe-reconstituted SOD1. Mn-reconstituted SOD2 also appeared to be more active than Fe-reconstituted SOD2 using the same method for determination of enzyme activity (Figures 4.19 and 4.20). In addition, SOD1 was found to be more stable after the reconstitution process (denaturing with 8 M urea and re-folding with gradually decreasing urea to zero concentration) than SOD2, whereas activity was 27-fold higher than that of an untreated enzyme. This experiment gave further evidence that SOD1 appears to be a Mn-dependent enzyme. For SOD2, because the difference between the activities of Mn-reconstituted SOD2 and Fe-reconstituted SOD2 were not large, further experiments were needed to confirm the metal dependence for activity.

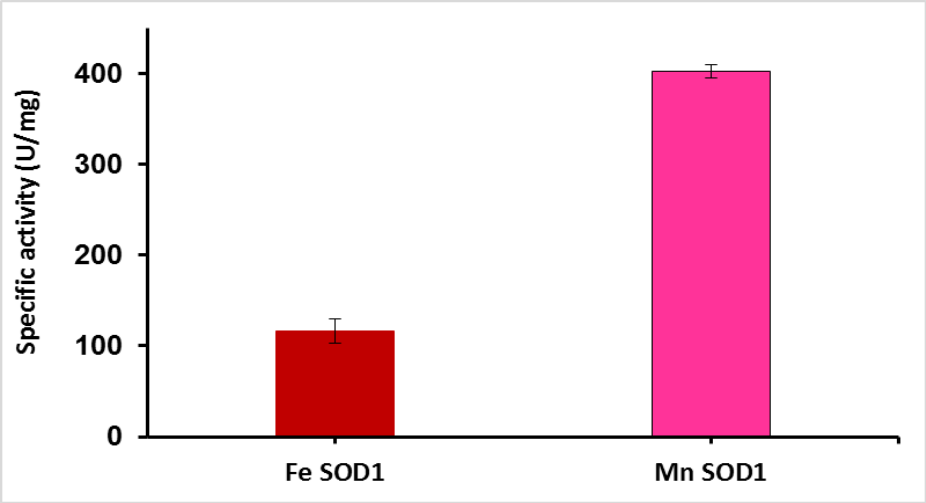

Figure 4.19. The activity of reconstituted SOD1 with Fe^{2+} and Mn^{2+} ions. For detail, please see experimental section.

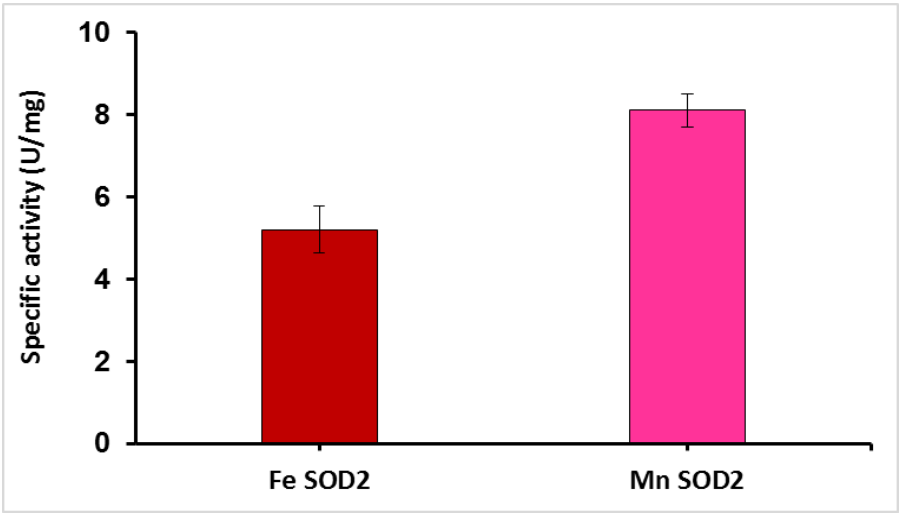

Figure 4.20. The activity of reconstituted SOD2 with Fe^{2+} and Mn^{2+} ions. For detail, please see experimental section.

4.8.4. Titration of SOD2 with different metal ions

In order to confirm the SOD2 metal ion dependency for activity, SOD2 apoenzyme was prepared by overproduction in M9 salts without supplement with any metal ions. The purified apoprotein was incubated overnight at room temperature

with Fe^{2+}, Cu^{2+} and Mn^{2+} at four different enzyme/ metal ion ratios (4:1, 2:1, 1:1 and 1:2) separately. The enzyme activity was determined with pyrogallol substrate.

SOD2 shows a significant increase in enzyme activity with increasing Mn concentration only with optimum activity requiring 1-2 molar equivalents of manganese ion (Figure 4.21). The other metal ions (Fe^{2+} and Cu^{2+}) do not show an effect or slightly negative impact on SOD2 enzyme activity especially at 1:1 molar ratio or higher. This experiment suggests that SOD2 is also a manganese-dependent enzyme.

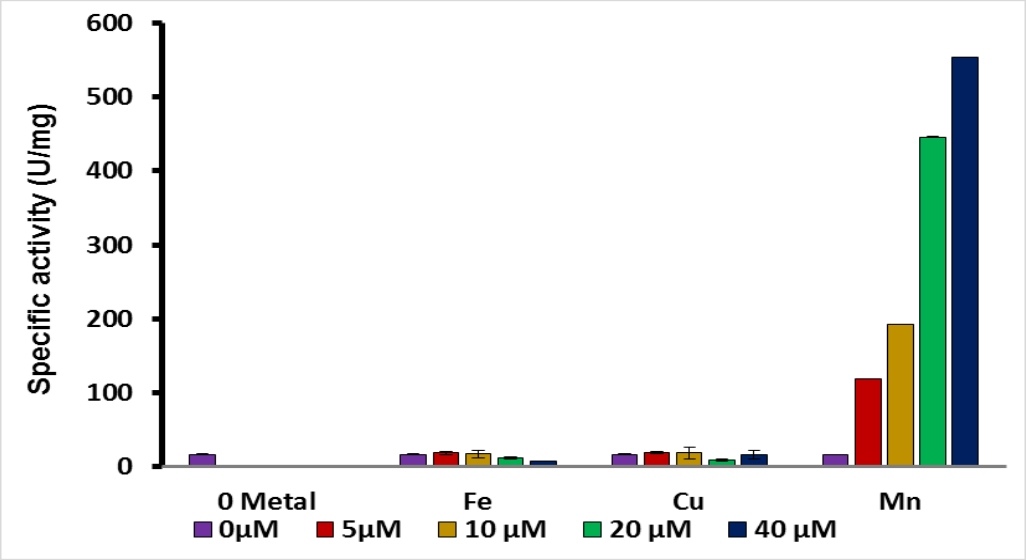

Figure 4.21. Metal ion dependency of SOD2 for superoxide dismutation activity (measured by pyrogallol method).

4.8.5. UV-vis spectra

Manganese-containing SODs are reported to have a specific absorption band at 480 nm and FeSODs at 350 nm. Purified SOD1 and SOD2 were scanned from 200 to 800 nm to determine their absorption properties (Figures 4.22 and 4.23). 1.8 mg/mL of 68 µM of SOD1 did not show any specific peak in the range 360-600 nm but 18

mg/mL of SOD1 was a pale pink colour, and gave an absorption peak at 465 nm (ε = 470 $M^{-1}cm^{-1}$) in 50 mM potassium phosphate buffer pH 7.8, comparable to reported λ_{max} values of 480 nm for the human [163] and *Anabaena* [145] MnSOD enzymes. This weak absorption peak of SOD1 suggests that most of the enzyme was not constituted with its cofactor (Mn^{2+}) and matches with ICP-OES results for the enzyme. 0.16 mg/mL (7.8 μM) SOD2 in 50 mM potassium phosphate buffer pH 7.8 displays two absorbance peaks at 411 nm (ε = 6410 $M^{-1}cm^{-1}$) and 503 nm (ε = 3840 $M^{-1}cm^{-1}$).

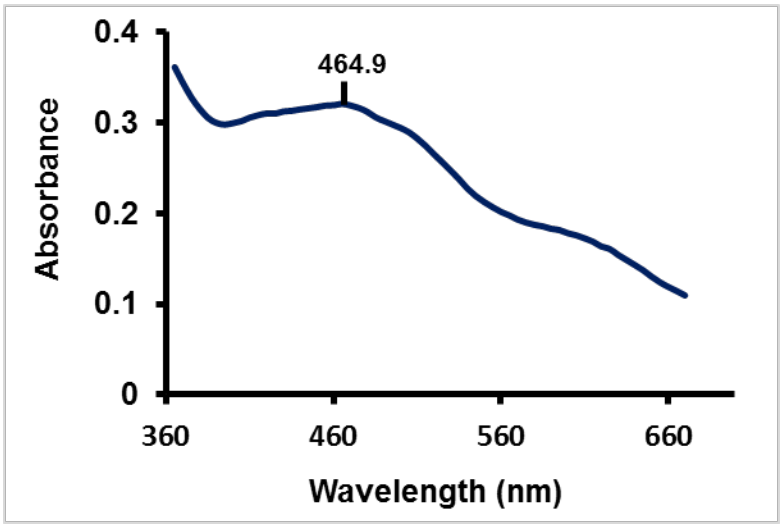

Figure 4.22. UV-vis spectrum of recombinant SOD1 (18 mg/mL) in 50 mM potassium phosphate buffer pH 7.8.

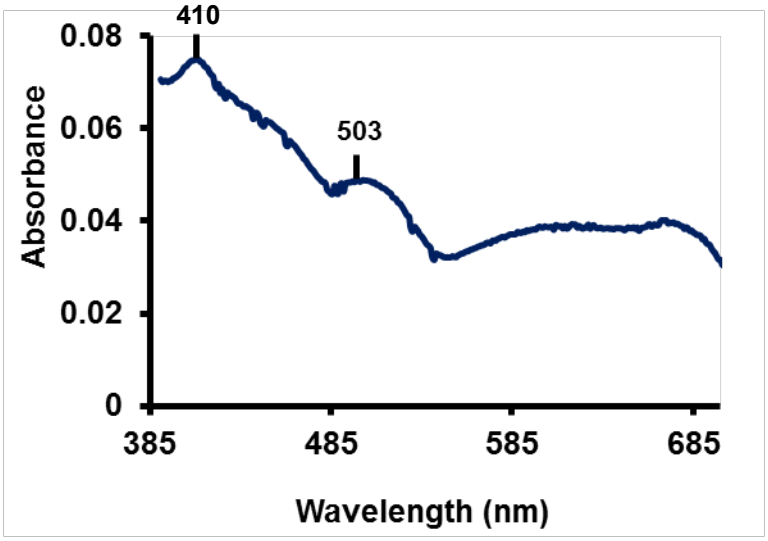

Figure 4.23. UV-vis spectrum of recombinant SOD2 (0.16 mg/mL) in 50 mM potassium phosphate buffer pH 7.8.

4.9. Lignin degradation ability of SODs

The lignin degradation ability of SphMnSOD enzymes was examined using organosolv lignin, Kraft lignin and lignocellulose (pine and miscanthus). Organosolv lignin is a high purity type of lignin which has gained much interest from researchers and industries [164]. Kraft lignin is the most abundant type of industrial lignin, its annual production is over 30 million tons, but it can be most difficult lignin to break down, as condensation of lignin takes place during Kraft pulping process [165]. The experiments (for investigating lignin degradation ability of SpMnSOD) were conducted in the potassium phosphate buffer pH 7.8 in the presence of 0.1 mM EDTA, which is the optimum condition for dismutation activity of SOD enzymes [152],[153],[154]. However, lignin degradation ability is quite different. Metal chelator EDTA is usually used as an additive in biological assays to prevent the effect of trace metal ions [153] which may catalyse Fenton reaction or Haber-Weiss

reaction, it also used to encourage these reactions [166]. In the Fenton reaction $^{\bullet}OH$ is generated from H_2O_2 by one-electron reduction catalysed by Fe(II) or other reduced transition metals (Figure 4.24). In the Haber-Weiss reaction, first Fe(III) is reduced to Fe(II) by superoxide radical anion, then $^{\bullet}OH$ is generated from H_2O_2 in the same manner to that in the Fenton reaction [167]. The SOD substrate (superoxide radical anion) was generated chemically using potassium superoxide in dimethyl sulfoxide (DMSO). A saturated solution of KO_2 in DMSO is assumed to be 5 mM superoxide radical anion [168]. This solution is stable in a dry aprotic solvent for up to 4 hours at room temperature, and months at -20°C, while in aqueous solutions decomposition of superoxide takes place rapidly [153].

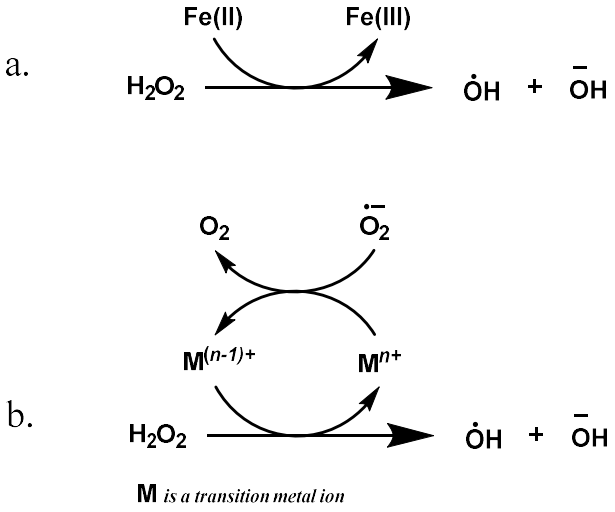

Figure 4.24. Generation of the hydroxyl radical, a) Fenton reaction. b) Haber-Weiss reaction [168].

4.9.1 Depolymerisation of organosolv lignin.

Purified SpMnSOD1 or SpMnSOD2 (0.18-0.2 mg/ml) was incubated with 5 mg of organosolv lignin in 50 mM potassium phosphate buffer pH 7.8 containing 0.1 mM EDTA, to which was added a solution of KO_2 in dry DMSO (final

concentration 1.25 mM) to start the reaction. A control experiment was also conducted in which SOD solution was replaced with buffer. Aliquots of 500 µL of reaction mixture were taken after 30, 60, 180 and 300 min, to which was added 50 µL of CCl_3COOH (1 g/mL). Finally, the solution was centrifuged at 13000 rpm for 10 min.

4.9.1.1. Analysis of reaction components by HPLC

High-performance liquid chromatography (HPLC) with a variable wavelength detector and a reverse phase column was used for analysis of samples from each time points. The separation was monitored at 310 nm. A visible colour change from yellow to orange over 60 min and a change in the solubility of the lignin was observed, becoming noticeably more water soluble (see Figure 4.25 ***a***). Comparison of HPLC results of organosolv lignin treated with SpMnSOD in the presence of superoxide and its reaction with superoxide only, revealed a number of new peaks, together with an envelope of products in the range 16-20 min after 1 hour of incubation. The intensities of peaks are time dependent, a significant increase in intensity was observed after 5 hours of SpMnSOD treatment as shown in Figure 4.25 ***b***.

In order to identify the degradation products of organosolv treatment with SpMnSOD, the HPLC was calibrated using 0.5 mM of each of lignin model compounds: vanillin, vanillic acid, ferulic acid, p-hydroxybenzaldehyde and 5-carboxyvanillic acid. Comparison of retention times (RT) of new peaks from incubation of organosolv lignin with retention times of authentic lignin model compounds reveals that peak 1 (RT= 6-8 min) most probably corresponded to 2-

methoxyhydroquinone, peak 2 (RT=11-12 min) possibly to vanillic acid, peak 3 (RT=13 min) probably to p-hydroxybenzaldehyde, peak 4 (RT=16-20) probably was vanillin, and finally peak 5 (20.13 min) which eluted with 100% MeOH may contain several compounds such as dimers and/or higher molecular weight entities with low polarity. This analysis indicates that SpMnSOD enzymes can decompose organosolv lignin and generate multiple low molecular weight products. Although the HPLC analysis gave some ideas of the new products generated by the SpMnSOD enzymes, further investigation was needed to identify the reaction products with confidence.

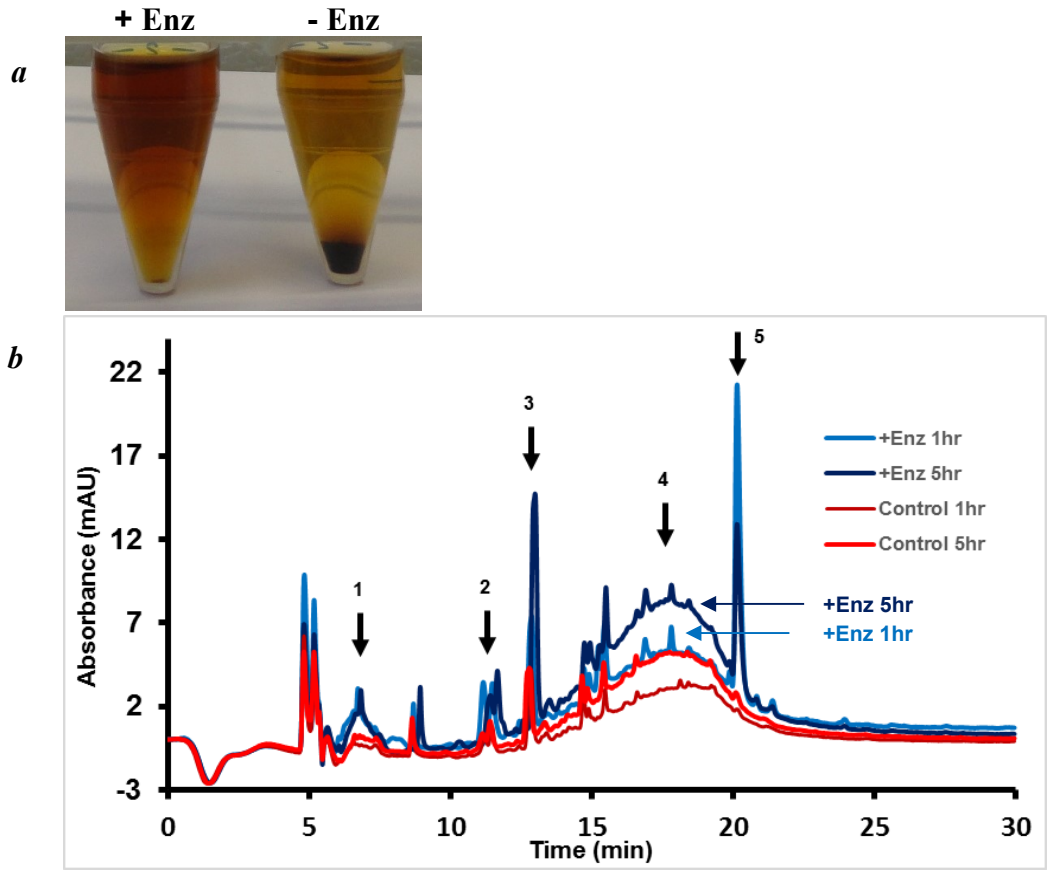

Figure 4.25. Reaction of Organosolv lignin with SpMnSOD1 (8 µM), in 50 mM potassium phosphate buffer pH 7.8 containing 0.1 mM EDTA and in presence of 1.25 mM KO_2. *a*. Change in visual appearance upon addition of SpMnSOD1 and KO_2 to a solution of wheat straw Organosolv lignin (on left), compared with the control reaction with no enzyme (on right). *b*. Reaction products from reaction of SpMnSOD1 with Organosolv lignin, observed by HPLC analysis.

4.9.1.2. Identification of organosolv degradation product using LC/MS and GC/MS.

Samples (4 mL) from reaction of each enzyme (SOD1 and SOD2) with organosolv lignin and a control reaction after 5 hrs of incubation were acidified with 1 mL HCl (1 M), extracted into ethyl acetate and dried in *vacuo*, then the residues were reconstituted with either 400 µL MeOH/water 1:1 for LC/MS analysis or 400 µL dry chloroform for GC/MS analysis.

4.9.1.2.1. LC/MS analysis of SpMnSOD treated organosolv

The reaction components were analysed by LC/MS in positive mode and monitored at 310 and 270 nm (see experimental section for details), and compared with authentic compounds vanillin (**4.1**), vanillic acid (**4.2**), ferulic acid (**4.3**), 5-carboxyvanillic acid (**4.4**), protocatechuic acid (**4.5**), guaiacol (**4.6**), catechol (**4.7**), pyrogallol (**4.8**), 2-methoxyhydroquinone (**4.9**), 2-methoxyquinone (**4.10**), p-hydroxybenzaldehyde (**4.11**), p-hydroxybenzoic acid (**4.12**), salicylic acid (**4.13**), acetovanillone (**4.14**) and 4-(1-hydroxyethyl) guaiacol(**4.15**), see Figure 4.26 for structures), which were also analysed under the same conditions.

The LC/MS result shows that the extracted ion chromatogram (EIC) has an envelope for *m/z* of 139 at retention time (RT) of 25.2 min which correspond to positively charged ion (MH^+) of 2-methoxyquinone **4.10**. Peaks were also observed for *m/z* 207 (RT= 26.8 min), 219 (RT= 29 min) and 229 (RT=18.7 min), which may correspond to MH^+ of compound **4.16,** MH^+ of **4.17,** and sodium adduct MNa^+ of compound **4.18** respectively. These peaks were observed in SpMnSOD1 reactions, but not in control.

In SpMnSOD2 reaction, more products were observed which did not appear in control. It can be seen within the EIC for *m/z* 169 and 191 (RT 32.4 min, corresponding to MH^+ and MNa^+ of vanillic acid **4.2**), 185 and 207 (RT 27 min, corresponding to MH^+ and MNa^+ of compound **4.16**), 155 (RT 23.6 min, corresponding to MH^+ of protocatechuic acid **4.5**), 139 (RT 26 min, corresponding to MH^+ of 2-methoxyquinone **4.10**), 197 (RT 29.8 min, may corresponding to MH^+ of compound **4.17**), 125 (RT 40 min, corresponds to MH^+ of guaiacol **4.6**), 229 (RT 19 min, may correspond to MH^+ of compound **4.18**), see Figure 4.27 for structures.

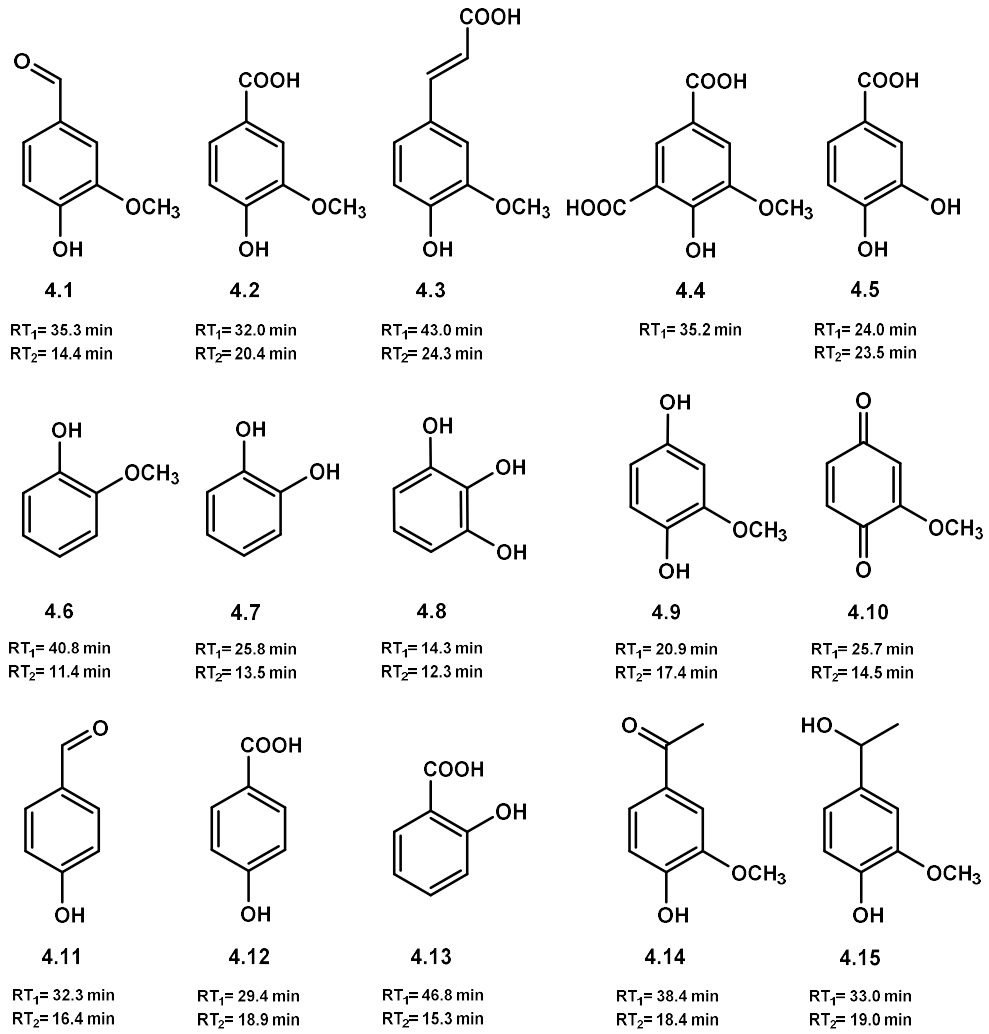

Figure 4.26. The structure of monomeric lignin model compounds and their retention time (RT) (retention time on LC/MS (RT_1) and GC/MS (RT_2)) used for identification of SpMnSOD reaction components.

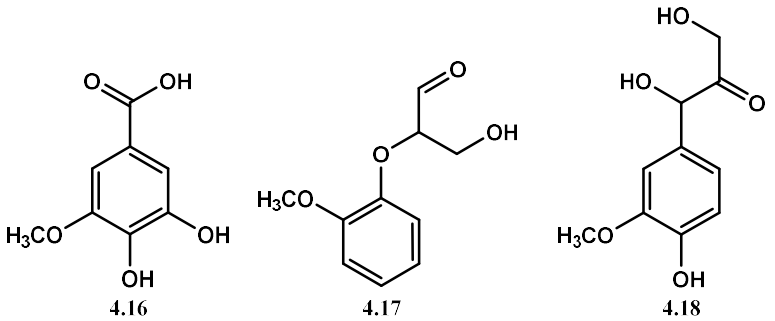

Figure 4.27. Proposed structures of some metabolites detected by LC/MS, 5-hydroxy vanillic acid **4.16**, 3-hydroxy-2-(2-methoxyphenoxy)propanal **4.17**, 1,3-dihydroxy-1-(4-hydroxy-3-methoxyphenyl)propan-2-one **4.18**.

4.9.1.2.2. GC/MS analysis of SpMnSOD treated organosolv.

The reaction products extracted into chloroform were divided into two fractions, one of the fractions was analysed directly, and the other was derivatised and then injected in to the GC/MS machine. The derivatization was performed by reacting 200 µL of each samples with 200 µL of mixture of N,O-bis(trimethylsilyl)acetamide and chlorotrimethylsilane 20:1 in the presence of pyridine at 60°C for 1 hr. Authentic compounds (compounds **4.1-4.15**) were analysed before and after silylation under the same conditions using GC/MS. See appendices for spectra. Figure 4.28 shows the structures of detected for derivatised authentic compounds (Compounds **4.19-4.30**).

Nine new product peaks (peaks P1-P4 in non-silylated fraction and P5-P9 in derivatized fraction with N,O-trimethylsilyl acetamide of reaction components, see Figures 4.29 and 4.30) were observed in sample for SpMnSOD1 treated organosolv lignin and were not present in control (except for two small peaks (P5 and P7) at RT of 8.5 and 22.7 min), those peaks gave mass fragmentation patterns and their retention times are shown in Table 4.2. peak P1, P2, P3, P5, P6 P7, P8 and P9 at

11.5, 13.4, 19.0, 8.5, 15.6, 19.2, 20.7 and 22.7 match with authentic compounds guaiacol **4.6**, catechol **4.7**, 4-(1-hydroxyethyl)guaiacol **4.15**, oxalic acid (di-$SiMe_3$ derivative) **4.30**, protocatechuic (tri$SiMe_3$ derivative) **4.22,** acid 2-methoxyhydroquinone (di$SiMe_3$ derivative) **4.26**, p-hydroxybenzoic acid (di$SiMe_3$ derivative) **4.28**, vanillic acid (di$SiMe_3$ derivative) **4.20**. The peak (P4) at 13.5 min gave the mass fragmentation pattern illustrated in Table 4.2 may confirm the generation of 5-hydroxyvanillic acid **4.16** by SOD1.

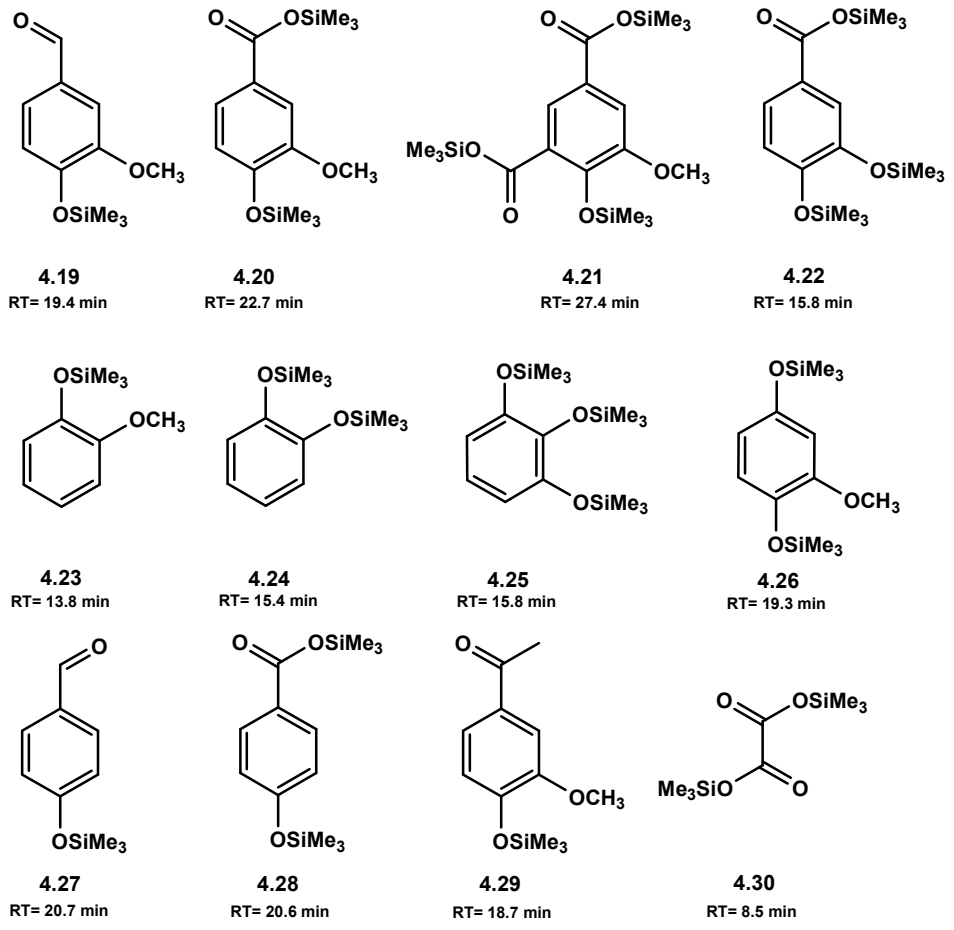

Figure 4.28. The structure of some derivatised lignin model compounds and their retention times on GC/MS.

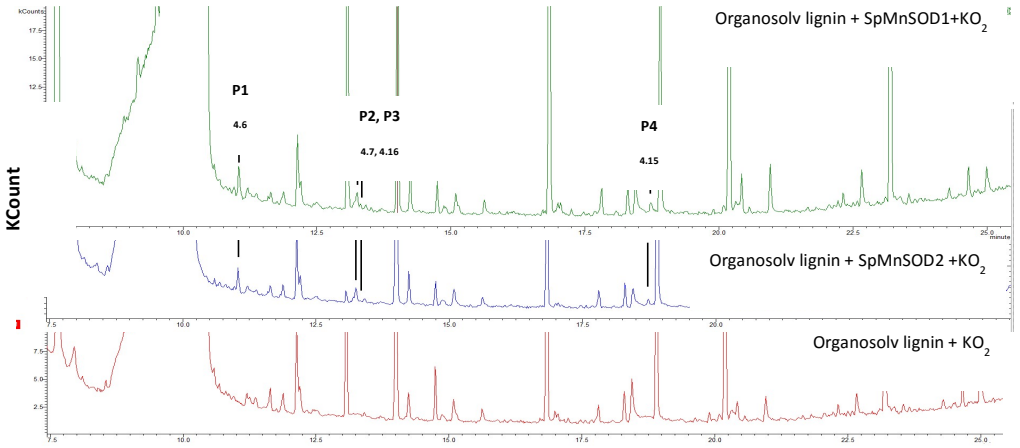

Figure 4.29. GC/MS chromatograms of non-derivatised reaction components of organosolv lignin treated with SpMnSOD1 (green trace) and SpMnSOD2 (blue trace) in presence of KO_2, which compared with control (organosolv lignin and KO_2, red trace) in the same condition. Four new peaks (P1 to P4) were observed in chromatograms for both of treated organosolv lignin with SOD1 and SOD2 not present in control. Peak P1, P2, P3 and P3 correspond to guaiacol **4.6**, catechol **4.7**, 5-hydroxyvanillic acid **4.16** and 4-(1-hydroxyethyl)guaiacol **4.15**, respectively.

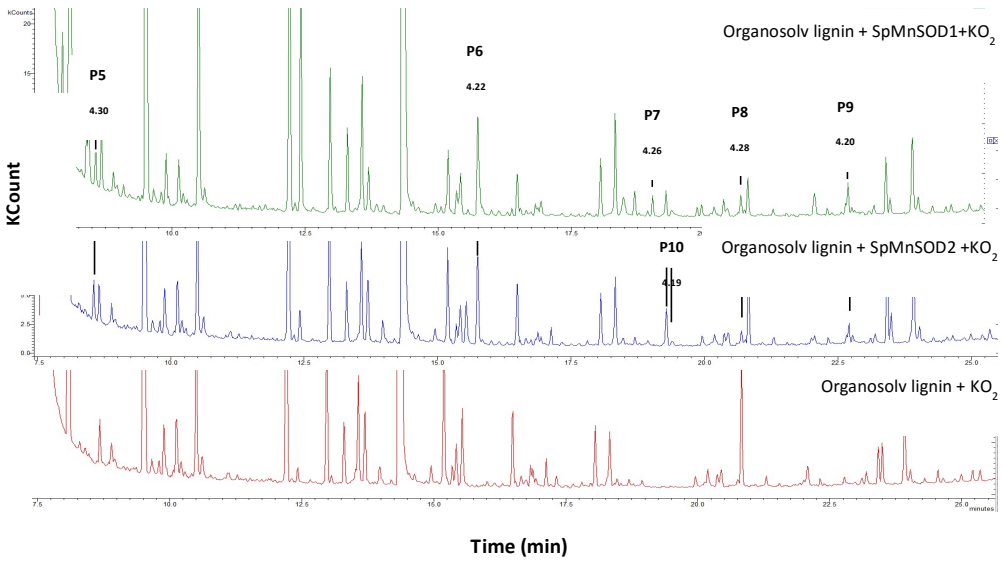

Figure 4.30. GC/MS chromatograms of silylated reaction components of organosolv lignin treated with SpMnSOD1 (green trace) and SpMnSOD2 (blue trace) in presence of KO_2, compared with control (organosolv lignin and KO_2, red trace) under the same conditions. Five new peaks (P1 to P4) were observed in chromatograms for SOD1 and six new peaks forSOD2 treated organosolv lignin only two small peak (P5 and P7) present in control. The retention time and fragmentation pattern of Peak P5, P6, P7, P8, P9 and P10 match with derivatised oxalic acid **4.30**, protocatechuic acid **4.22**, 2-methoxyhydroquinone **4.26**, p-hydroxybenoic acid **4.28**, vanillic acid **4.20**, and vanillin **4.19** with N,O-trimethylsilyl acetamide.

The reaction products from the processing of Organosolv lignin using SpMnSOD2 gave 10 new peaks not present in KO_2 control (except for two small peaks (P5 and P7, at RT of 8.5 and 22.7 min). These peaks gave mass fragmentation pattern and retention times that match to those peaks observed in reaction components for SpMnSOD1 (see Table 4.2), except for a peak at 19.3 min, which was only generated by SpMnSOD2. This peak gave mass fragmentation pattern matching with silylated commercially available vanillin **4.1**. These results match with some of the results observed by both HPLC and LC/MS for SpMnSOD1 (2-methoxyquinone **4.10,** hydroxyvanillic acid **4.16** and compound **4.18**) and SpMnSOD2 (2-methoxyhydroquinone **4.9**, vanillic acid **4.2**, p-hydroxybenzoic acid **4.12**, guaiacol **4.6**, hydroxyvanillic acid **4.16** and compound **4.18**), and confirm that both enzymes are unique lignin oxidizing enzymes generating multiple degradation products of which 9 products identified for SpMnSOD1 and 10 for SpMnSOD2. Differences in product distribution and peak intensities were observed when a different batch of lignin was used, this may be due to heterogeneity of the substrate (lignin), and lack of specificity of the enzymes for certain functional groups in the lignin.

Table 4.2. Compounds observed from organosolv lignin reaction components using GC/MS.

Enzymes	RT	*m/z*	Fragments					Assignments
MnSOD1	11.5	124	109	103	74	61		**4.6**
	13.4	110	81	63	57			**4.7**
	19.0	166	152	151	123			**4.15**
	13.5	184	109	73				**4.16**

	22.7	312	297	282	267	209	181	**4.20**
	15.6	371	357	194				**4.22**
	19.25	284	263	254				**4.26**
	20.7	282	267	224				**4.28**
	8.5	219	191	190	149	147	73	**4.30**
MnSOD2	11.5	124	109	103	74	61		**4.6**
	13.4	110	81	63	57			**4.7**
	19.0	166	152	151	123			**4.15**
	13.5	184	109	73				**4.16**
	19.3	224	209	194				**4.19**
	22.7	312	297	282	267	209	181	**4.20**
	15.6	371	357	194				**4.22**
	19.25	284	263	254				**4.26**
	20.7	282	267	224				**4.28**
	8.5	219	191	190	149	147	73	**4.30**

4.9.1.3. SpMnSOD and function of bacterial extracellular superoxide dismutase

Bacterial superoxide dismutase is usually a cytoplasmic or periplasmic enzyme for protecting cellular components [169], while extracellular SOD is uncommon and its function is not clear. There are several reports in the literature showing the

production of extracellular SOD by bacteria and fungi during the breakdown of recalcitrant compounds such as lignin and rubber. *Phanerochaete chrysosporium* expresses MnSOD during lignin degradation and in a response of exposure to dibenzo-p-dioxin [170]. Rubber degrading bacterial strains *Streptomyces* sp. strain K30, *Xanthomonas* sp. strain Y35, *Gordonia westfalica* Kb1 and *Gordonia polyisoprenivorans* VH2 produce extracellular SOD during rubber decomposition [170]. The *SOD* gene of *Gordonia polyisoprenivorans* VH2 is found in a gene cluster for poly(*cis*-1,4-isoprene) metabolism and is essential for efficient growth on poly(*cis*-1,4-isoprene) as a carbon source. The enzyme is possibly involved in rubber degradation [170]. *Pseudomonas aeruginosa* shows an increase of 50% in the release of extracellular SOD when grown in a medium containing 50 ppm of *p*-nitrophenol [171]. This may suggest that extracellular SOD is involved somehow in the degradation process.

As previously discussed, SpMnSODs are extracellular enzymes, both have been detected from proteomic of extracellular fractions of *Sphingobacterium* sp. T2 [63]. SpMnSOD1 has a leader peptide (analysed by signal peptide prediction program (SignalP 4.0) [161] for extracellular translocation and sequence analysis using web-based software (Phobius [172]) confirms that, in addition, both enzymes are not cytosolic (Figure 4.31). These results suggest that both SpMnSOD enzymes are extracellular enzymes.

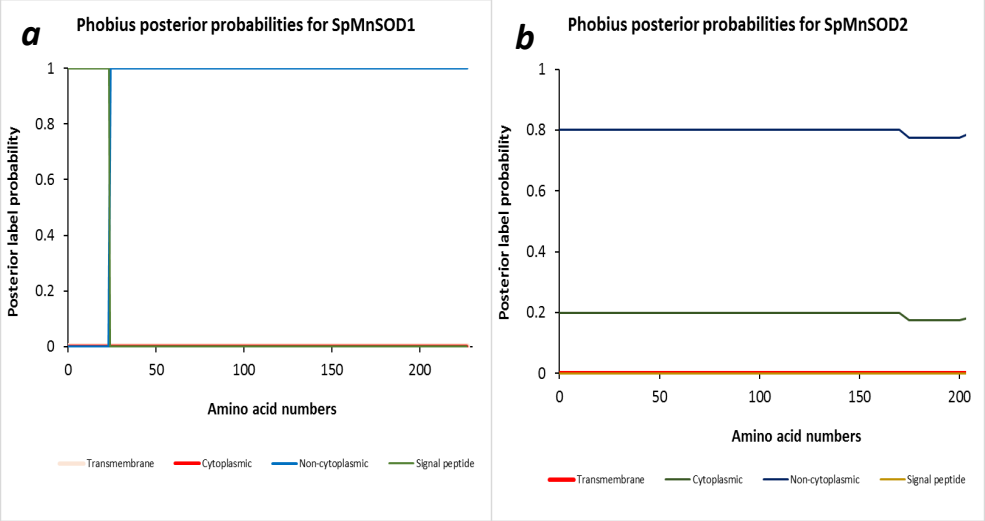

Figure 4.31. Protein sequence analysis using internet based software Phobius [172], a) is the result of prediction of SpMnSOD1 sequence, b) is prediction result of the SpMnSOD2 amino acid sequence.

4.9.1.4. Reactive species involved in degradation of organosolv lignin by SpMnSOD enzymes.

Generation of such a range of products by a single enzyme (SpMnSOD1 or SpMnSOD2) from organosolv lignin, which possibly goes through several steps and a few different types of reactions, indicates that a highly oxidising species is involved. The catalytic cycle of MnSOD consists of two half-reactions, in which the superoxide radical anion converts to dioxygen and peroxide, shown in Section 4.1. In the first half-reaction, Mn(III) oxidises superoxide to dioxygen; in the second half-reaction Mn(II) reduces superoxide to hydrogen peroxide [134].

Oxidation of organosolv lignin by SpMnSOD (SOD1 or SOD2) can be explained through two possible hypotheses. The first hypothesis (Figure 4.32) is that oxidation of lignin is through a diffusible oxidising species, and that the metal cofactor Mn(III) might play this role, analogous to the generation of Mn(III) by fungal manganese peroxidase, versatile peroxidase [173]. In these peroxidase enzymes, there is a manganese binding site consisting of three ligands (two glutamic

acids and one aspartic acid residue, see Figure 1.23), but the manganese is ion not tightly bound. Dye-decolourising enzymes such as DypB from *Rhodococcus josti* RHA1 and Dyp1B from *Pseudomonas fluorescens* Pf-5 might also work in the same manner since they possess manganese oxidizing ability. However, in superoxide dismutase the Mn(III) cofactor is tightly bound to four amino acid residues (three histidines, an aspartate and water/OH^-, see Figure 4.4) and there is no evidence for release of Mn(III) ion from *Sphingobacterium* SOD enzymes.

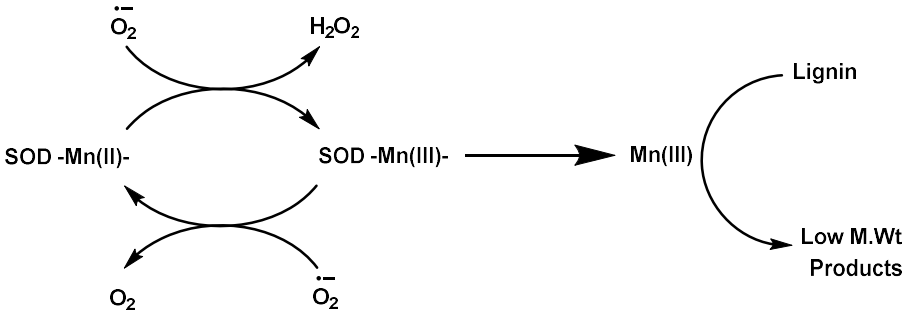

Figure 4.32. Schematic illustration of hypothetical lignin degradation catalysed by SpMnSOD, which metal cofactor Mn^{2+} acts as a diffusible oxidant.

The second hypothesis is that a further reduction of hydrogen peroxide by the SpMnSOD takes place, with the enzymes generating hydroxyl radical from peroxide, similar to the Fenton or Haber-Weiss reactions (Figure 4.33). The hydroxyl radical is a highly reactive oxidant that could then oxidise lignin. It has been proven that Cu/Zn superoxide dismutase from bovine erythrocyte can produce hydroxyl radical from hydrogen peroxide [174] in reaction similar to Haber-Weiss reaction while MnSOD from *E. coli* is not able to generate hydroxyl radical [175]. Both FeSOD and Cu/Zn-SOD are inhibited by hydrogen peroxide, while MnSOD is not. Hydroxyl radical is possibly involved in fungal lignin breakdown; studies suggest that lignin-degrading fungi *Phanerochaete chrysosporium* generate hydroxyl radical from hydrogen

peroxide in ligninolytic culture [176], however, later studies showed that this is not a major contributing strategy for lignin degradation in white-rot fungi [177].

The generation of hydroxyl radical can be demonstrated by oxidative decomposition of ketones such as α-oxo-γ-methylthiobutyric acid, hydroxylation of salicylic acid and p-hydroxybenzoic acid to form protocatechuic acid [167], [178], the OH-radical can also hydroxylate vanillic acid **4.2**, protocatechuic **4.5** and other phenolic compounds with free *ortho*- or *para*- positions to the phenol group (OH group, electron donating groups activate these positions) to produce 5-hydroxyvanillic acid **4.16**, 3,4,5-trihydroxybenzoic acid (gallic acid) and the corresponding hydroxyphenols (Figure 4.34) [179]. Another well-known reaction of •OH is oxidative demethoxylation of methoxylated phenols (Figure 4.35) [180],[179]. It has been reported that hydroxyl radical generated by irradiation of an aqueous solution can convert vanillic acid and iso-vanillic acid to 3,4-dihydroxybenzoic acid [179]. Oxidative demethoxylation proceeds ~4 times faster for methoxyl groups in activated position by electron donor groups than in non-activated positions [180]. Decarboxylation of aromatic carboxylic acids is possibly induced by OH-radical, study of the degradation of polycarboxylic benzoic acids shows that OH-radical generated by UV-irradiated aqueous and/ or positive photo-hole cause hydroxylation and decarboxylation of aromatic carboxylic acids, then ring opening occurs [181].

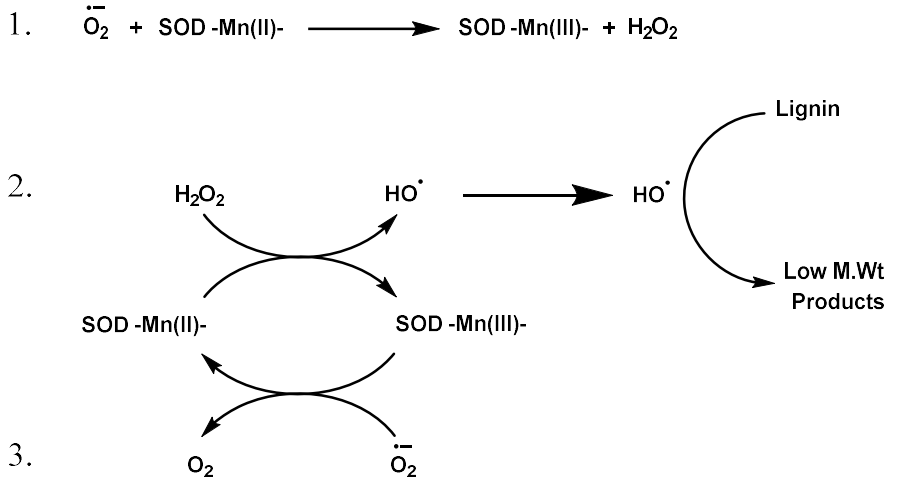

Figure 4.33. Generation of hydroxyl radical by SpMnSOD in a reaction similar to Haber-Weiss reaction which includes three steps, step 1: peroxide generated by SOD using one molecule of superoxide radical anion, step 2: the peroxide reduced by SOD to generate hydroxyl radical and attack lignin; step 3: another molecule of superoxide radical anion reduces Mn(III) back to Mn(II).

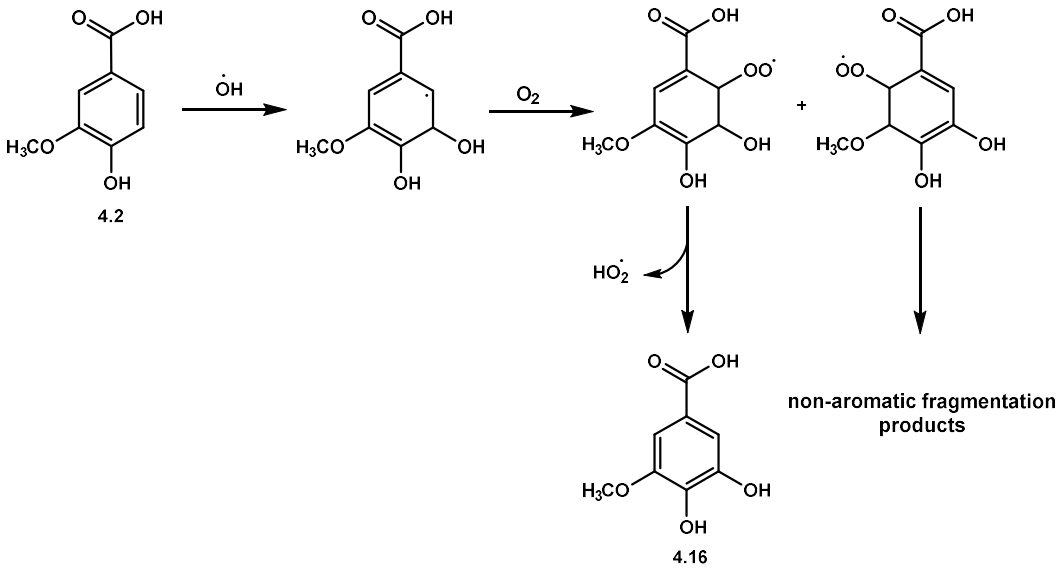

Figure 4.34. Mechanism of vanillic acid hydroxylation[179].

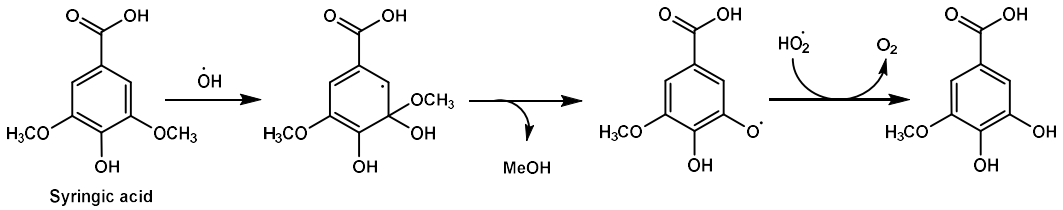

Figure 4.35. Replacement of methoxyl (-OCH_3) group with hydroxyl group (-OH) [180],[179].

Among the enzymatic degradation products identified (Figure 4.29 and 4.30), an additional phenolic hydroxyl group is present in product (**4.16**), while replacement of the methoxy group with a hydroxyl group (products **4.5** and **4.7**) are observed which match with the known ability of ·OH to perform hydroxylation of phenolic compounds [175],[181],[179] and demethoxylation of methoxylated phenols [179],[180]. Also, elimination of a carboxylic group (compound **4.6)** is observed. Therefore, these results suggest that the mechanism for lignin oxidation by these enzymes (SOD1 and SOD2) may involve hydroxyl radical. In a different context, Nature uses the hydroxyl radical to attack lignin, for example, brown rot fungi generate hydroxyl radical via Fenton chemistry which in turn attacks lignin. [173],[182].

4.9.1.5. Types of reactions catalysed by SpMnSOD enzymes.

The multiple reaction products generated from wheat straw organosolv lignin when treated with *Sphingobacterium* sp. T2 SODs (SOD1 and SOD2), of which we have characterised 13 (see Sections 4.9.), imply that a range of different types of reactions have occurred. The reaction types include; aryl-C_α cleavage, C_α-C_β oxidative cleavage, decarboxylation and O-demethylation reactions. Oxidative cleavage of aryl-C_α bond is a less common catalytic activity in fungal lignin-degrading enzymes and not reported in bacterial lignin oxidizing enzymes till now, this oxidative bond cleavage led to the formation of the reaction products **4.6**, **4.7**, **4.9** and **4.30** (Figure 4.36) from lignin. C_α-C_β oxidative cleavage resulted in the production of **4.1**, **4.2**, **4.5** and **4.16** from organosolv lignin. C_α-C_β bond cleavage is the most prevalent type of enzymatic reaction by lignin peroxidases for example

lignin peroxidase from *Phanerochaete chrysosporium* also leads to breakdown C_α-C_β of β-aryl ether lignin model compound [26],[73]. Decarboxylation (e.g. conversion of **4.2** to **4.6**) and O-demethylation (products **4.5** and **4.7**) reactions also appear to be catalysed by SpMnSODs, that further modify reaction products fromed by of lignin breakdown (aryl-C_α and C_α-C_β oxidative cleavage). Decarboxylation reaction was also observed from dye-decolourising enzymes such as DyP2 from *Amycolatopsis sp. 75iv2* [85]. O-demethylation reactions occur in pathways for degradation of aromatic compounds such as biphenyl degradation pathway which is catalysed by LigX enzyme (see Figure 1.31) [26].

4.9.1.6. Mechanism of organosolv degradation

A possible mechanism for generation of metabolites from organosolv lignin treatment with SpMnSOD enzymes can be proposed based on the observed products and considering hydroxyl radical as an oxidising species. Most of the observed metabolites came from cleavage of aryl-C_α or C_α-C_β bonds of aryl ether units. Attack of hydroxyl radical to α-hydroxyl group of aryl-C_3 unit would generate benzylic ketone. Attack of hydroxyl radical on this ketone would cause oxidative cleavage of the benzylic ketone and formation of vanillic acid **4.2** (if the aryl-C_3 unit disubstituted, G units) or p-hydroxybenzoic acid **4.12** (if the aryl-C_3 unit monosubstituted, H units) in case of C_α-C_β cleavage (Figure 4.36, reaction A). Oxidative breakdown of the benzylic ketone can also cause cleavage of aryl-C_α bond and generation of guaiacol **4.6** (Figure 4.36, reaction B). This fragmentation reaction is possible since hydroxyl radical is known to cause oxidative fragmentation of ketones such as α-oxo-γ-methylthiobutyric acid [167], [178]. Hydroxylation of the

vanillic acid **4.2** resulted in the formation of compound **4.16**. Demethoxylation of vanillic acid and guaiacol **4.6** resulted in formation of protocatechuic acid **4.5** and catechol **4.7**, respectively. Hydroxyl radical could also attack an aryl-C_3 unit at aryl C-1, then of 2-methoxyhydroquinone **4.9.** Formation of most of the observed metabolites from organosolv lignin described by the scheme shown in Figure 4.36.

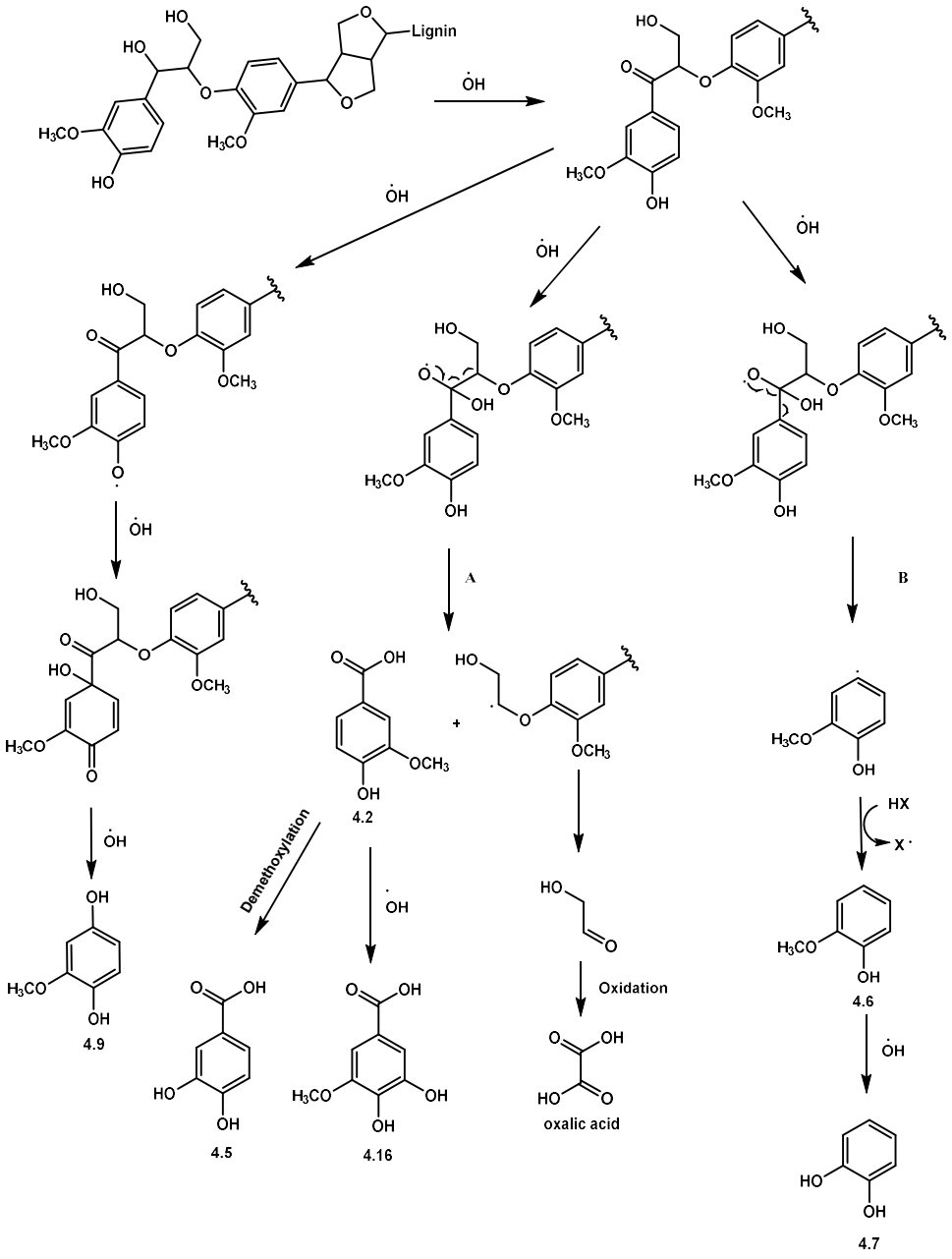

Figure 4.36. Mechanism of transformation of organosolv lignin catalysed by SpMnSODs.

4.9.2. Depolymerization of alkali Kraft lignin.

5 mg of alkali Kraft lignin (Sigma) were added to 3 mL phosphate buffer (50 mM, pH 7.8) containing 8.8 µM of SOD2 and 0.1 mM EDTA, to which 1 mL of KO_2 solution (5 mM) in dry DMSO were added to start the reaction. After 60 min, a visible colour change from yellow to brown was observed. A control experiment was also conducted by adding all components in a test experiment except the enzyme. 500 mL samples were taken after 30, 60, 120, and 300 min, to which 50 µL of trichloroacetic acid (1 g/mL) was added to stop the reaction, then centrifuged at 13,000 rpm for 10 min.

4.9.2.1. Analysis of Kraft lignin treated with SpMnSOD2 by HPLC

Samples from each time point were analysed by HPLC; the separation was monitored at 310 nm. Generating multiple reaction products. The supernatant was analysed by HPLC. The resulting alkali Kraft lignin incubated with SpMnSOD2 was compared with control experiment (reaction Kraft lignin with KO_2) and showed two new peaks (Figure 4.37). There was a slow background reaction in the presence of KO_2 alone, but the background reaction generated only a small envelope of products in the range 12-20 min retention time, with much smaller individual product peaks. These results indicate that SOD2 can also degrade alkali Kraft lignin. Further study needs to identify the new products generated by SpMnSOD2 and to investigate whether SpMnSOD1 can degrade Kraft lignin.

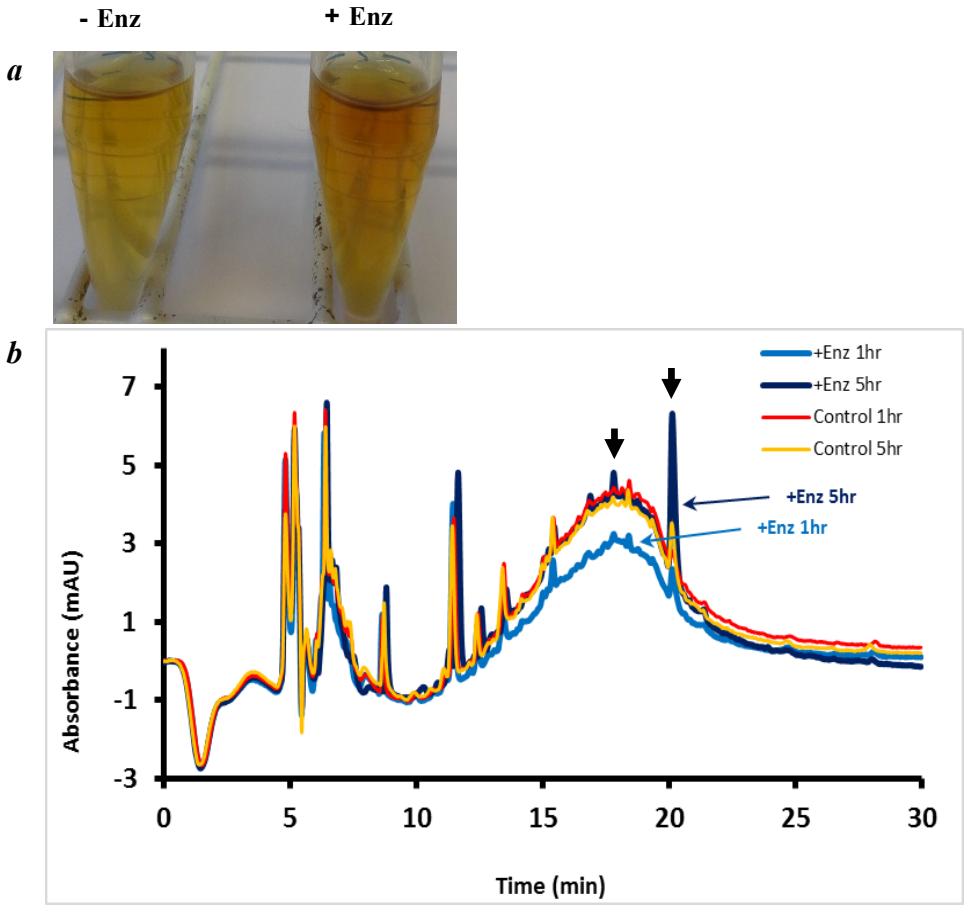

Figure 4.37. Treatment of Kraft lignin with SpMnSOD2, as described in Materials & Methods. ***a.*** Change in visual appearance upon addition of SpMnSOD2 and KO_2 to a solution of alkali Kraft lignin (Sigma) lignin (on right), compared with the control reaction with no enzyme (on left). ***b.*** HPLC analysis of reaction mixtures (control and SpMnSOD2 catalysed) at different time intervals (1hr and 5 hrs). Two new peaks were observed for SpMnSOD2 catalysed reaction at 5 hrs (black arrows).

4.9.3. Modification of lignocellulosic biomass

The ability of SOD2 to modify lignocellulose biomass was also tested. Two types of lignocellulose materials were examined; miscanthus (grass) and pine (softwood). The results of the analysis show that SOD2 from *Sphingobacterium* sp. T2 can modify both lignocellulose materials (grass and softwood). The detail about these experiments is discussed in next sections.

4.9.3.1. Alteration of Miscanthus.

A fine powdered miscanthus in 50 mM phosphate buffer (pH 7.8) was mixed with SOD2, then KO_2 solution in dry DMSO under nitrogen was added to start the reaction. After 60 min a colour change from yellow to brown was visible. A control experiment was conducted containing all reaction components except the enzyme. Aliquots were taken at different time intervals (at 30 min, 1, 2 and 5 hrs) and mixed with trichloroacetic acid and centrifuged for 10 min at 13000 rpm. The reaction components were analysed using HPLC using a reverse-phase column.

HPLC analysis revealed that SpMnSOD2 can modify miscanthus and produce at least two new product peaks (Figure 4.38). The activity of SpMnSOD2 appeared to be time dependent, and highest peak intensity was observed after 5 hrs of incubation. The product peaks have not been identified.

4.9.3.2. Modification of softwood (pine).

Three mL phosphate buffer (50 mM) pH 7.8 containing 10 µM of SpMnSOD2 and 0.1 mM EDTA was added to 5 mg of finely powdered pine. In a separate tube, three mL of the same buffer containing only 0.1 mM EDTA was added to 5 mg of pine. One mL of saturated KO_2 solution in dry DMSO was added to both tubes. A colour change from yellow to brown was visible over 60 min for SOD-treated pine (Figure 4.39). At different time intervals (at 1/2, 1, 2 and 5 hrs), aliquots of 500 µL were taken, to which 50 µL of trichloroacetic acid were added and centrifuged for 10 min at 13,000 rpm.

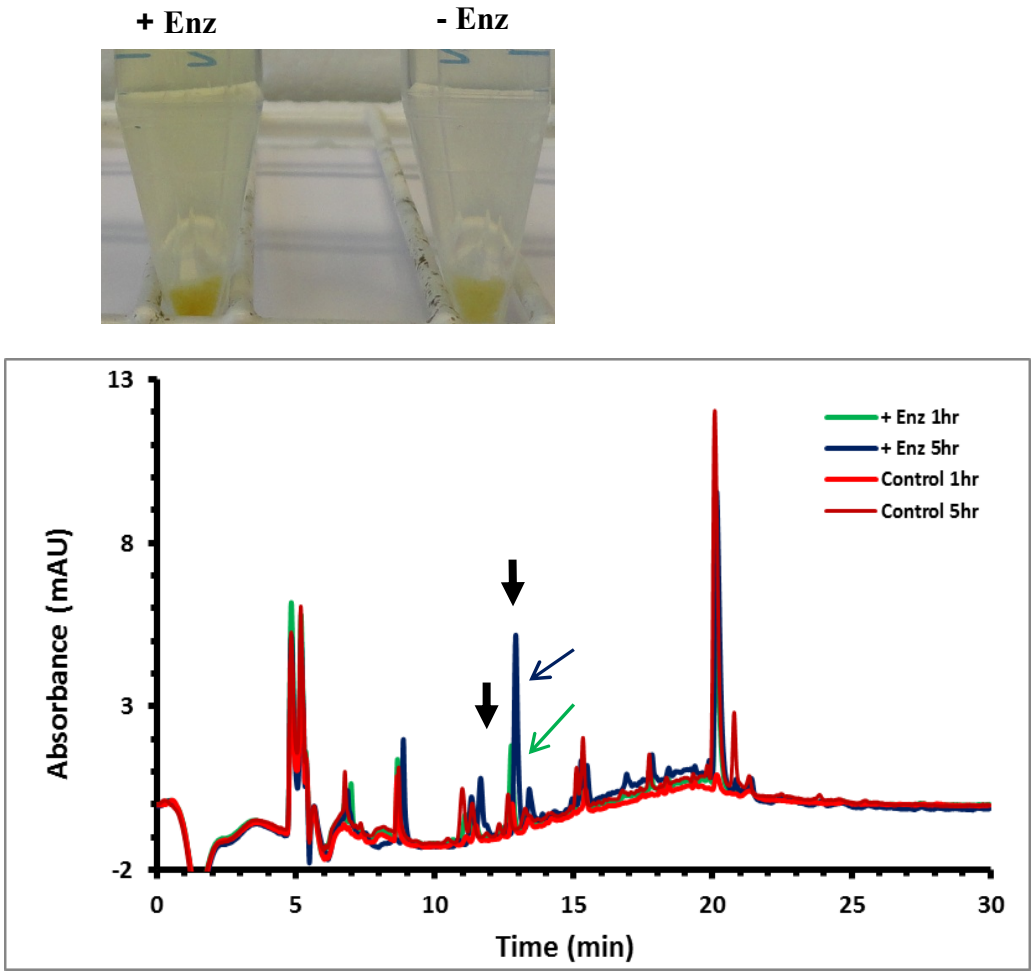

Figure 4.38. Treatment of miscanthus with SOD2 (0.18 mg/mL) in phosphate buffer (50 mM, pH 7.8) in presence of KO_2 (1.25 mg/mL) and EDTA (0.1 mM) analysed by HPLC. New peaks appear after 1 and 5 hrs of incubation at 30ºC (black arows).

Analysis of supernatants with reverse phase HPLC showed new product peaks after 1 and 5 hours of incubation. This result indicates that SpMnSOD2 can modify softwood (pine) and produce new products (Figure 4.39).

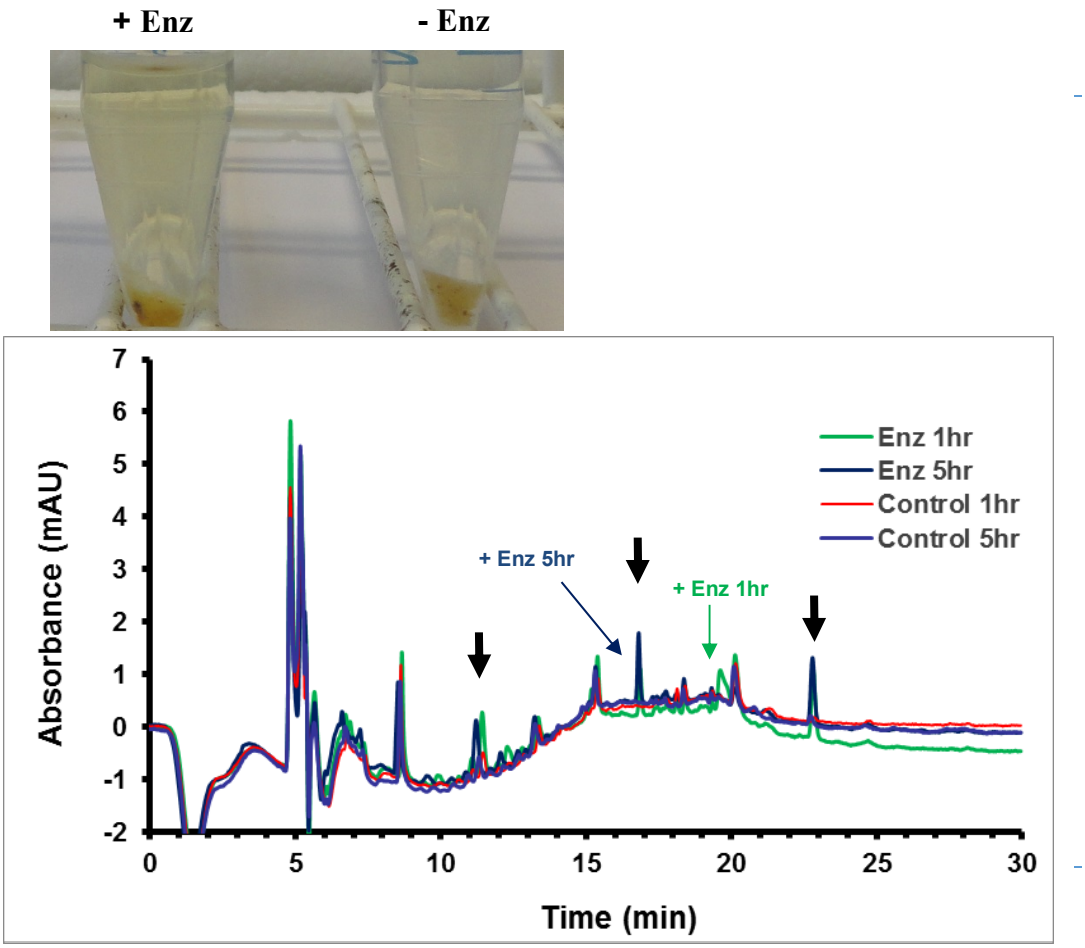

Figure 4.39. Reaction of softwood powder (pine) with SOD2 in 50 mM phosphate buffer (pH 7.8) in presence of KO_2/DMSO (1.25 mM) and EDTA (0.1 mM). Three new peaks appeared when reaction components were analysed by HPLC and compared to control.

4.10. Crystallisation of SpMnSODs

In order to investigate the characteristic features of these superoxide dismutases, screening for protein crystallisation for both SOD1 and SOD2 was performed by Dr. Dean Rea (see experimental Section). Crystals of SOD1 were obtained, as shown in Figure 4.40. The structure of SOD1 was solved by Prof. Vilmos Fülöp, School of Life Science, University of Warwick. Table 4.3 illustrates crystallographic data collection and refinement statistics.

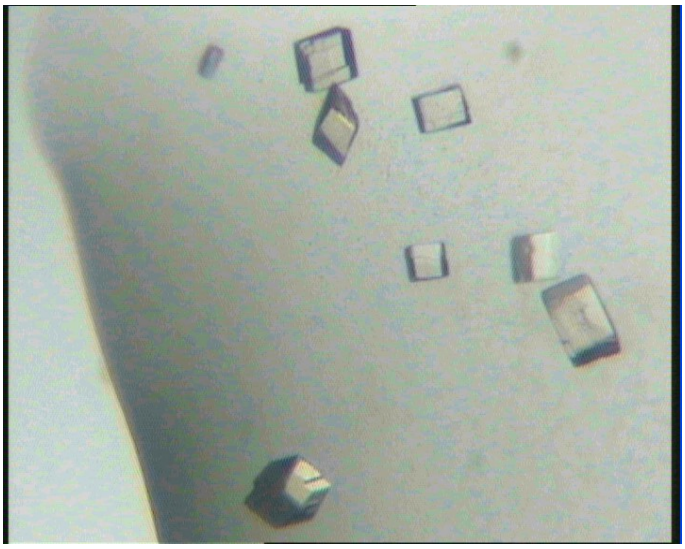

Figure 4.40. SOD1 crystals from *Sphingobacterium* sp. T2.

Table 4.3. Crystallographic data collection and refinement statistics.

Data collection	
Unit cell a,b,c (Å), β (º)	a= 46.70, b= 58.94, c= 75.71, 90.18
Space group	$P2_1$
Resolution (Å)	37-1.35 (1.35-1.385)
Observations	299,716
Unique reflections	87,001
I/σ(I)	18.2 (3.5)
R_{sym}[a]	0.051 (0.413)
Completeness (%)	96.5 (79.0)
Refinement	
Non-hydrogen atoms	3,851 (including 2 Zn^{2+} & 611 waters)
R_{cryst}	0.138 (0.286)
Reflections used	83,589 (4,530)
R_{free}	0.157 (0.292)
Reflections used	3,412 (165)
R_{cryst} (all data)	0.138
Average temperature factor (Å^2)	10.6
Rmsds from ideal values	
Bonds (Å)	0.015
Angles (º)	1.7
DPI coordinate error (Å)	0.045

Numbers in parentheses refer to values in the highest resolution shell.
DPI refers to the diffraction component precision index.

X-ray diffraction data were collected to 1.35 Å. Molecular replacement was used to determine the structure of SpMnSOD1 using the MnSOD structure from *Bacillus subtilis* (PDB: 2RCV) [183]. The SpMnSOD1 crystal structure shows a typical MnSOD homodimer containing two subunits which are characteristic for Fe/MnSOD (Figures 4.41 and 4.42). The SpMnSOD1 monomers superpose with a rmsd of 0.108 Å (165 CA atoms) and are therefore, essentially structurally identical. A high structural similarity was observed for SpMnSOD1 monomer and dimer with other MnSOD enzymes for which crystal structures have been determined. The structure of SpMnSOD1 superposition with homologs from *E. coli* (PDB entry 1D5N), [184] *T. thermophilus* (PDB entry 3MDS), [185] *B. subtilis* (PDB entry 2RCV), [183] and the filamentous cyanobacterium *Anabena* PCC 7120 (PDB entry 1GV3) [186] gave a rmsd of ~0.4-0.7 Å for the monomer, and ~0.5-0.9 Å for the dimer (Figure 4.43).

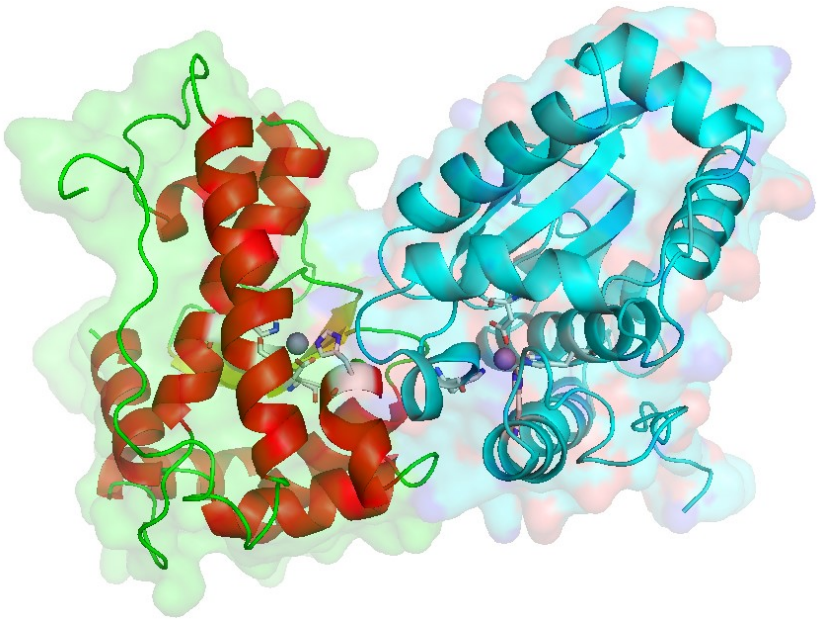

Figure 4.41. A dimeric structure of SpMnSOD1, each subunit has manganese binding site.

In SphMnSOD1, there is a single Mn ion in the active site of each subunit which is coordinated to five ligands, three histidine residues, His26, His76 and His167, an aspartate residue, Asp163, and a non-protein ligand (water/hydroxide) as apical ligands, giving a trigonal bipyramidal shape (Figure 4.44).

In the outer sphere there are some strictly conserved amino acids among FeSOD and MnSOD families, these residues include glutamine 146, tyrosine 34 and histidine 30, along with tyrosine 174 and glutamic acid 171 from the other subunit of the homodimer (numbering for *E. coli* MnSOD) [187]. These amino acids are known as gateway amino acids [171]. In SpMnSOD1, these amino acids include histidine 30, tyrosine 34 and glutamine 144, along with glutamic acid 163 and tyrosine 170 (Figure 4.45). These two amino acids make a network of hydrogen bonds in the active site, Q146 binds to the axial non-protein ligand (water/hydroxide), and Y34 with Q146. Literature studies have shown that Q146 is essential for catalytic activity, since mutation of Q146 in EcMnSOD resulted in disruption of the hydrogen-bond network in the active site and reduction in dismutation activity by 95% [187]. In human MnSOD, Y34 contributes to structure and catalysis, since a substantial decrease in the catalytic rate constant for the reduction of superoxide was observed for mutant Y34V [188]. In another study, it has been reported that W161 in human MnSOD which forms a hydrophobic face of the active site is essential for catalytic activity, W161A and W161F mutants in human MnSOD show 100-fold decrease in the rate constant of reduction of superoxide, and a significant conformational change in the residue near active site was also observed, especially for Y34 and Q143 [189]. E166 is important for both dimerization and activity in the *T. thermophilus* enzyme [190].

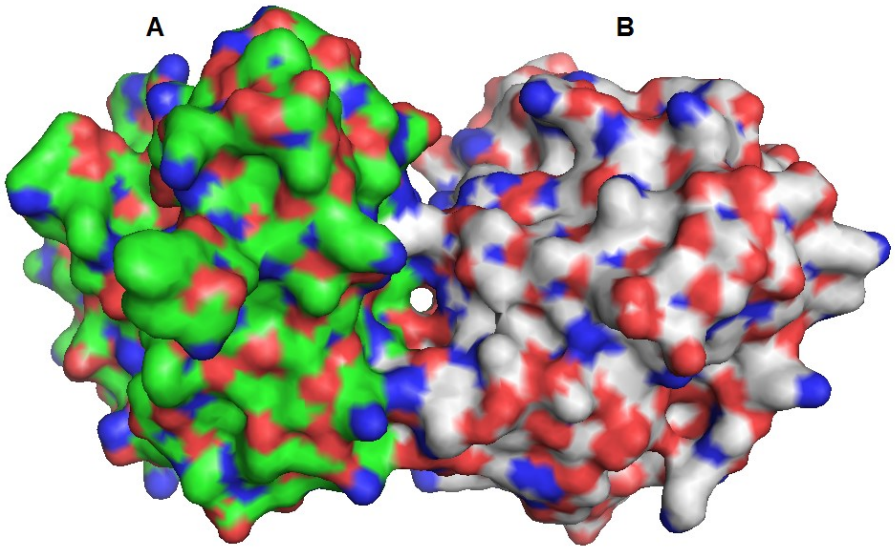

Figure 4.42. The surface of SpMnSOD1 dimer, a tunnel formed in the interface of two subunits (A and B).

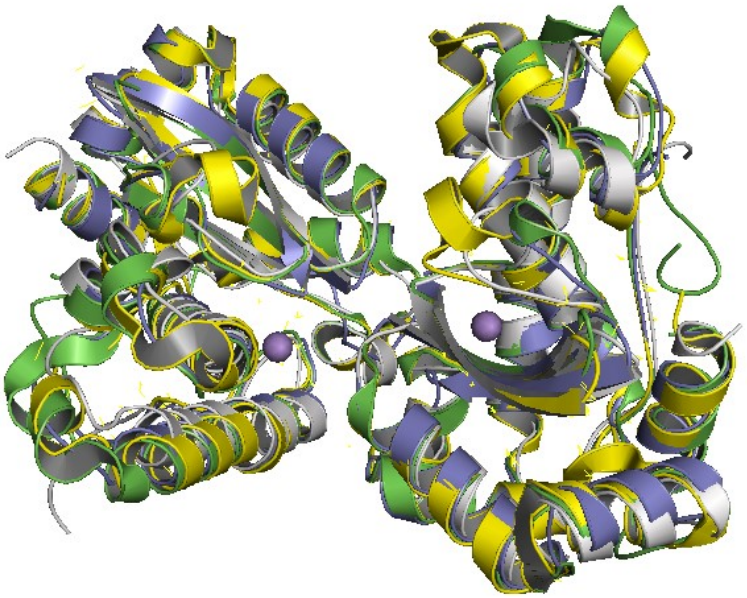

Figure 4.43. Homodimer structure of the SpMnSOD1 (cartoon, gray) aligned with structures of related MnSOD enzymes from *E. coli* (1D5N; yellow cartoon), *T. thermophilus* (3MDS; slate cartoon), and *Anabena* (1GV3; light green cartoon). Purple spheres are Mn(II) ions. PyMOL was used in drawing the figure.

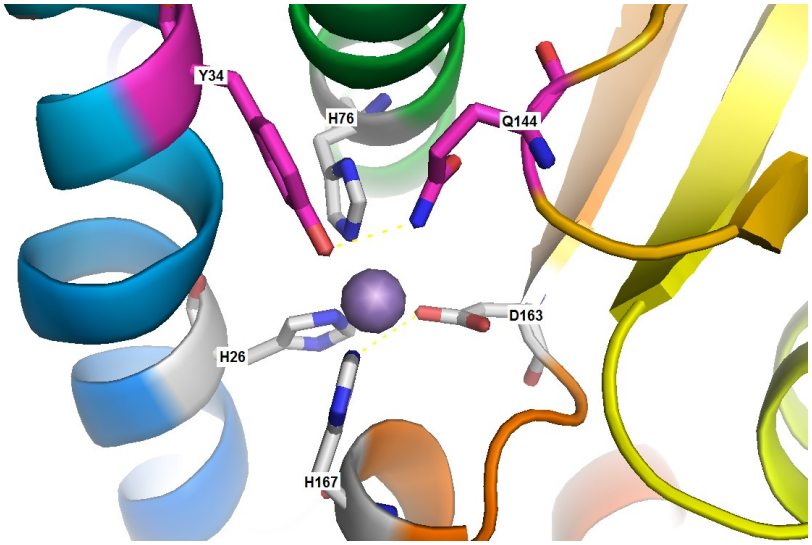

Figure 4.44. The active site of SphMnSOD1, inner-sphere residues include: His26, His76, His167 and Asp163. Tyr34 and Gln144 are two important residues in the outer-sphere, Mn(II) is shown as a purple sphere. The figure was drawn using PyMOL.

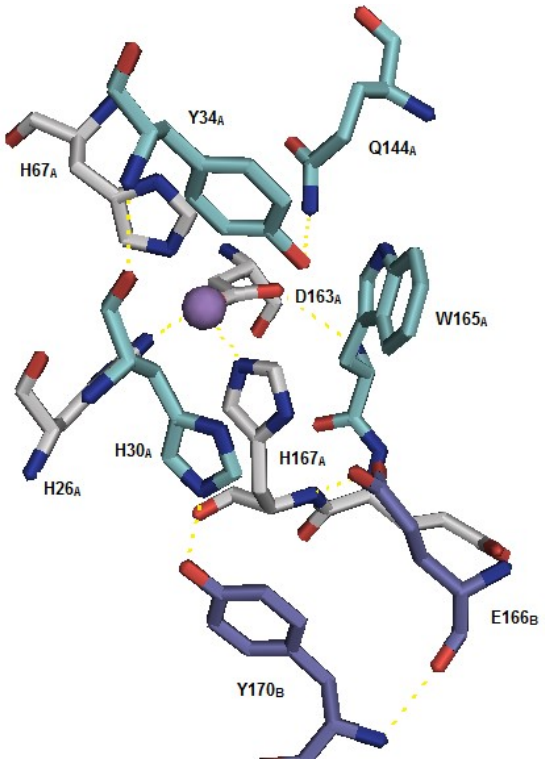

Figure 4.45. The inner-sphere residues (grey sticks) and gateway residues (cyan sticks) include Trp165, Gln144, Tyr34, His30 from subunit A, Glu166 and Tyr170 from subunit B (slate sticks). The purple sphere is Mn(II) ion (numbering for SpMnSOD1).

5. Ability of SpMnSOD enzymes to degrade lignin model compounds

In the previous chapter, the ability of SpMnSOD enzymes in the degradation of organosolv lignin, Kraft and lignocellulose (miscanthus and pine) have been described, and 13 of the lignin metabolites from wheat straw organosolv lignin were identified (MSc. Student Yangqingxue Liu assisted in the structural identification of the reaction products). The results suggest that some of the products undergo several modification reactions. To understand more about the nature, type of the reactions and mechanism of SpMnSOD reaction with lignin, lignin model compounds were examined, three dimeric and 12 monomeric lignin model compounds and their reaction products were identified. These dimers represent common inter-monomeric linkages in lignin. The most predominant one is a β-O-4 linkage, which represents up to ~80% of linkages in lignin [57]. The monomeric lignin model compounds tested with SpMnSOD enzymes are the most common metabolites of lignin degradation.

5.1. Oxidation of Lignin model compounds

The lignin model compounds were incubated separately with SOD1 or SOD2 in buffer (phosphate or ammonium bicarbonate) at pH 7.8. A solution of KO_2 in DMSO was added to start the reaction. After 5 hrs, the reaction was stopped by the inhibition of the enzyme by adding trichloroacetic acid or HCl. The extraction of reaction components was carried out with ethyl acetate. The organic layer was collected and dried under reduced pressure. The residue was dissolved in a suitable solvent prior to analysis by LC/MS and GC/MS.

5.1.1. Degradation of β-aryl ether model compound.

Phenolic lignin model compound (guaiacylglycerol-beta-guaiacyl ether) was incubated with SOD1 and SOD2 separately, to investigate which of the observed products (metabolites from organosolv lignin observed, see Chapter 4) may be derived from the most frequent β-aryl ether (β-O-4) linkage present in polymeric lignin. Two new product peaks (see Figure 5.1) were observed by GC/MS from β-O-4 treated with each of SpMnSOD1 (P1 at RT 11.22 min and P3 at RT 17.12 min) and SpMnSOD2 (P1 at RT 11.20 and P2 at RT 13.28 min). Peak P1, P2 and P3 correspond to guaiacol **4.6**, 2-methoxyquinone **4.10** and 2-methoxyhydroquinone **4.9**) respectively, matching to commercially available authentic compounds (see Table 5.1). LC/MS analysis also shows positively charged ions at *m/z* 125 (RT of 41.3 min) which correspond to MH^+ of **4.6**, *m/z* of 163 at RT of 20 min which corresponds to MNa^+ of **4.6** (in SOD1 reaction component only) and *m/z* of 139 at RT of 26 min which corresponds to MH^+ of 2-methoxyquinone **4.10** (in SOD2 reaction component only), (see Figure 5.2) consistent with aryl-Cα bond cleavage proposed previously in organosolv lignin breakdown.

Table 5.1. Detected β-aryl ether reaction components incubated with SpMnSODs by GC/MS.

Enzymes	RT	*m/z*	Fragments				Assignments
MnSOD1	11.22	124	109	81			**4.6**
	17.12	140	129	125	109		**4.9**
MnSOD2	11.22	124	109	81			**4.6**
	13.28	138	123	119	110	63	**4.10**

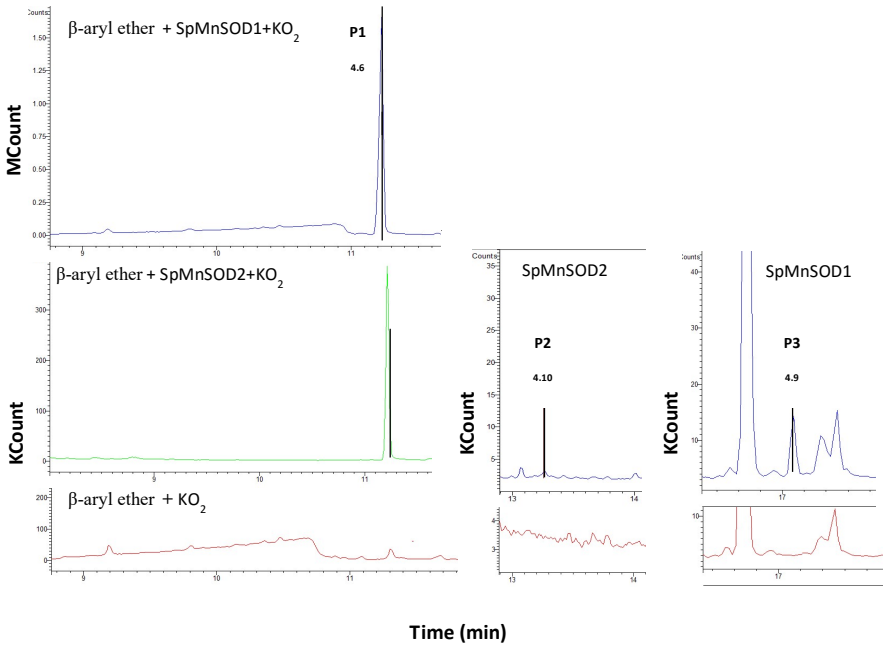

Figure 5.1. GC/MS chromatograms for un-derivatised SpMnSOD treated β-aryl ether lignin model compound reaction components and control (β-aryl ether with KO_2 only at the same condition).

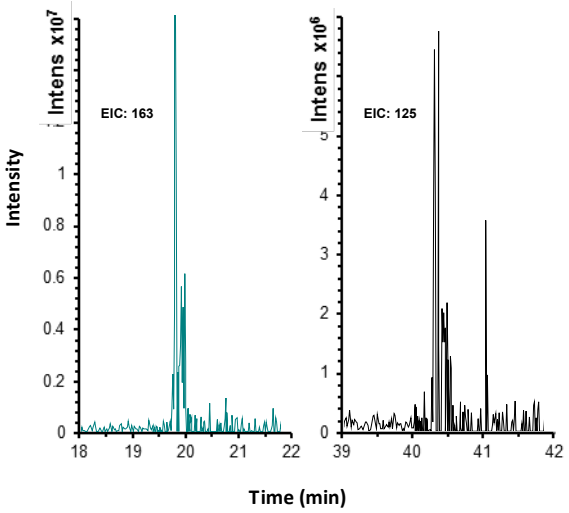

Figure 5.2. Examples of LC/MS chromatograms for β-aryl ether reaction components with SpMnSODs. Extracted ion chromatogram (EIC) for *m/z* 163 (left) and 125 (right)

5.1.1.1. Mechanism of breakdown of guaiacylglycerol-beta-guaiacyl ether

As described in the previous chapter, our hypothesis is that SpMnSODs are most likely to produce hydroxyl radical. Based on that hypothesis and the structures of the metabolites detected from guaiacylglycerol-beta-guaiacyl ether **5.1** treated with SpMnSODs, a mechanism of breakdown of **5.1** can be proposed, see Figure 5.3. The identified metabolites are similar to those observed with organosolv lignin, except for vanillic acid **4.2** formed via C_α-C_β cleavage. Guaiacol **4.6** could perhaps be formed from vanillic acid as shown in Figure 5.3.

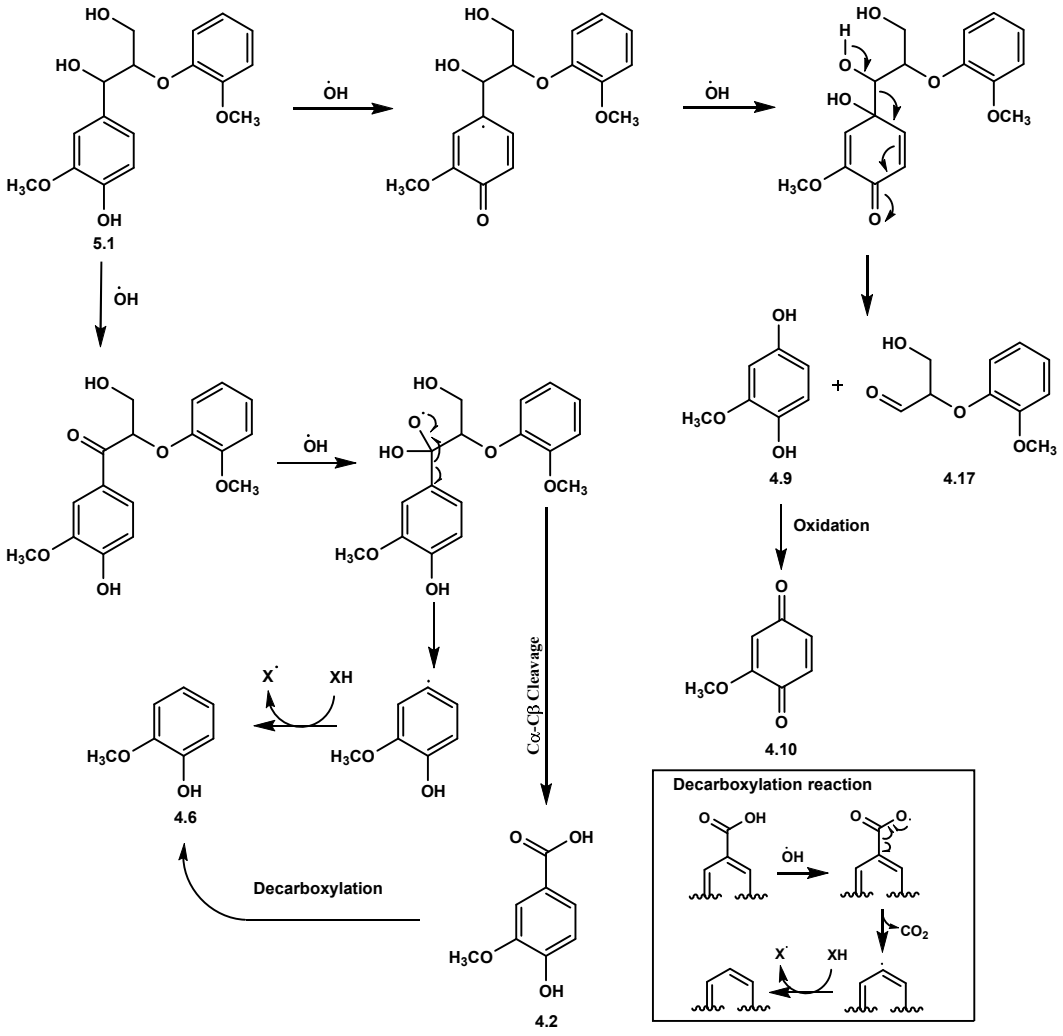

Figure 5.3. Possible mechanism of guaiacylglycerol-β-guaiacyl ether degradation.

5.1.2. Breakdown of biphenyl model compound (5,5`-Dehydrodivanillin)

The biphenyl linkage is one of the main inter-monomeric bonds in lignin. Treatment of 5,5`-dehydrodivanillin (DDVn) with SpMnSODs (SOD1 and SOD2) led to the generation of a range of metabolites which were most likely resulted from ring cleavage of one vanillin unit. Products with *m/z* of 213, 235 at 35.2 min (which corresponds to MH^+ and MNa^+ of 5-carboxyvanillic acid **4.4**), 141, 163 at 20.1 min (MH^+ and MNa^+ of 2-methoxyhydroquinone **4.9**), 155, 177 at 24.9 min (MH^+ and MNa^+ of protocatechuic acid **4.5**), 185 at 27.3 min (which most probably corresponds to MH^+ of 5-hydroxyvanillic acid **4.16**) and 125 at 40 min (MH^+ of guaiacol **4.6**) detected by LC/MS (Figure 5.4). They were eluted at the same retention times as their corresponding commercially available compounds except 5-hydroxyvanillic acid, which is not commercially available.

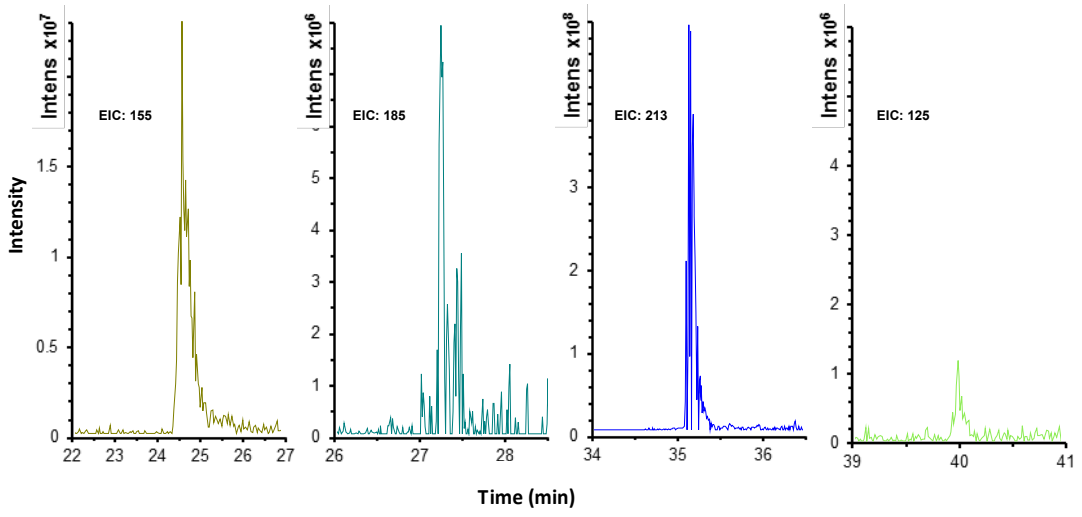

Figure 5.4. Some LC/MS chromatograms of dehydrodivanillin reaction components with SpMnSODs. Extracted ion chromatogram (EIC) for *m/z* of 155, 185, 213 and 125.

The reaction products of SpMnSODs treated DDVn **5.2** were also analysed by GC/MS and the resulting chromatograms (retention times and fragmentation pattern) were compared with those of commercially available standards. The analysis

shows the presence of 5-carboxyvanilllic acid **4.4**, vanillic acid **4.2**, and vanillin **4.1** in the reaction products of SOD2 treated DDVn, while only vanillic acid and vanillin were detected in the SOD1 reaction mixture (Table 5.2).

5.1.2.1. Mechanism of DDVn fragmentation

The structure of the observed products suggest that •OH attacks one of the aromatic rings, oxidation and ring opening occurs, and then 5-carboxyvanillic acid **4.4** is produced as a result of further oxidation of the opened ring (Figure 5.5). 5-carboxyvanillic acid is a known metabolite of 5,5`-dehydrodivanillic acid generated through three enzyme catalysed reactions in *Sphingobium* SYK6 (see Figure 1.31) [26]. Degradation of biphenyl groups through •OH attack and formation of metabolites such as vanillin **4.1,** vanillic acid **4.2** and 5-carboxylic acid **4.4** may answer at least a part of the question of how *Sphingobacterium* sp. T2 metabolises aromatic compounds since the strain has a lack of conventional degradation clusters. This mechanism is possible because studies show that reaction of hydroxyl radical with aromatic compounds results in opening of the aromatic rings [179],[181], and several products (see Chapter 4 and Section 5.1) suggest that SpMnSOD generate hydroxyl radical. Vanillic acid **4.2** can be produced via decarboxylation of 5-carboxyvanillic acid **4.4**.

Table 5.2. Detected masses and their fragmentation pattern for SpMnSODs with 5,5'-Dehydrodivanillin reaction component using GC/MS.

Enzymes	RT	*m/z*	Fragments				Assignments
MnSOD1	22.7	312	297	283	267.7	253.8	**4.20**

	19.3	224	209	194			**4.19**
MnSOD2	19.39	224	209	194			**4.19**
	27.4	414	255	73			**4.21**
	22.7	312	297	283	267.7	253.8	**4.20**

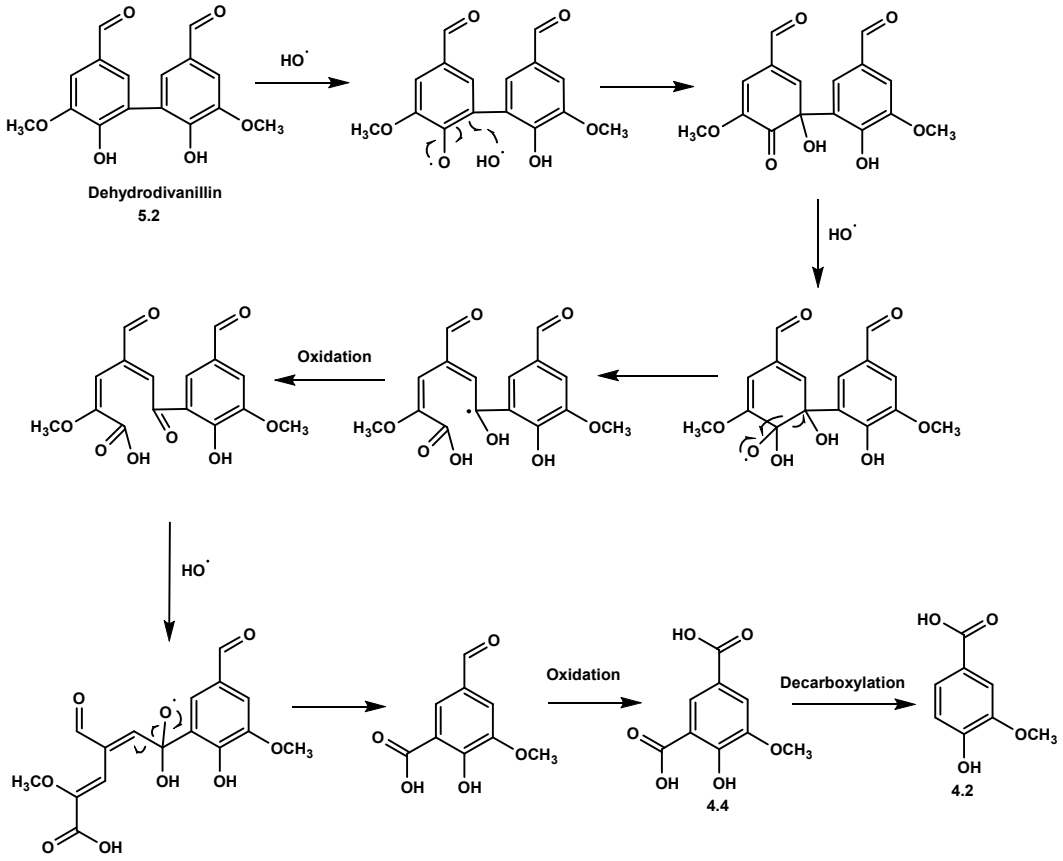

Figure 5.5. Proposed reaction mechanism for 5,5`-dehydrodivanillin with MnSOD enzymes from *Sphingobacterium* sp. T2.

5.1.3. Degradation of pinoresinol.

To obtain more information about the nature of the oxidative ability of SpMnSODs in breaking down of inter-monomeric linkages of lignin, pinoresinol **5.3** was tested, which is one of the primary linkages in polymeric lignin. Incubation of

pinoresinol with both of SOD enzymes gave multiple products. LC/MS analysis show envelopes for extracted ion chromatograms corresponding (Figure 5.6) to protocatechuic acid **4.5** (*m/z* = 155, MH^+ and *m/z* = 177, MNa^+ at 24.4 min) and probably compound **5.4** (proposed, see Figure 5.7) (*m/z* = 283, MH^+ and *m/z* = 305, MNa^+ at 23.5 min) in the reaction mixtures of both enzymes. This compound gave the highest signal in LC/MS with intensity 0.8 $\times 10^9$. On the other hand, in the SOD1 reaction mixture more products were observed. The detected metabolites having *m/z* of 175 (MNa^+ of vanillin **4.1** at 35 min), 191 (MNa^+ of vanillic acid **4.2** at 32.5 min) and 219 with retention time of 35.8 is most likely MH^+ of compound **5.5**, this compound is one of known metabolite of lignocellulose breakdown by *P. putida* and *R. jostii* [62]. Also two additional products were observed at *m/z* of 195, 217, 181 and 203, which most likely are MH^+ and MNa^+ of compound **5.6** and compound **5.7** (proposed, see Figure 5.7) at retention times 43.2 and 38.6 min, respectively.

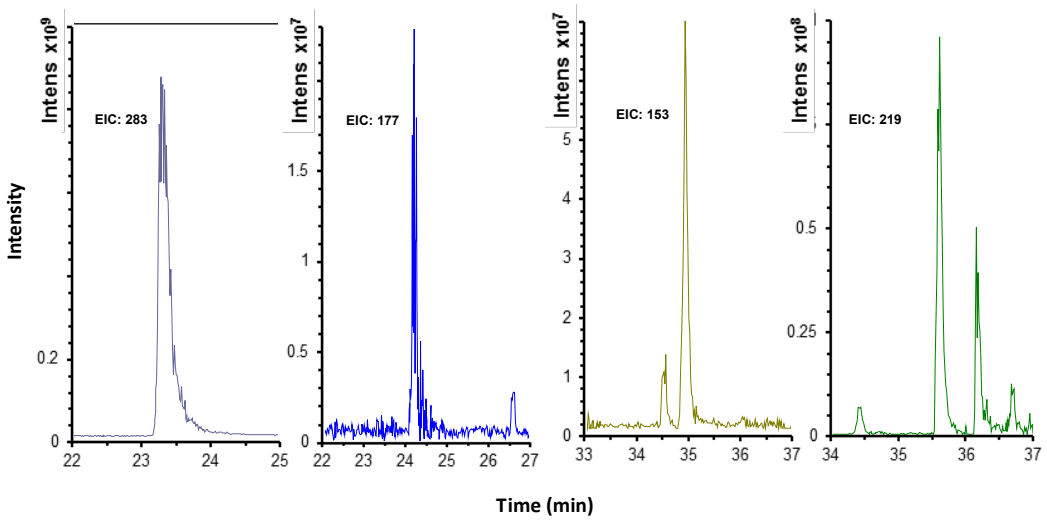

Figure 5.6. Some of extracted ion chromatograms for *m/z* 283, 177, 153 and 219, which were detected from reaction component of pinoresinol with SpMnSODs using LC/MS

Table 5.3. Masses of compounds from SpMnSODs treated pinoresinol reaction detected by GC/MS

Enzymes	RT	*m/z*	Fragments				Assignments
MnSOD1	17.0	140	125	97			**4.9**
	19.25	284.7	255				**4.26**
	22.7	312	297	283	268	254	**4.20**
	19.4	224	209.5	194			**4.19**
MnSOD2	20.9	181	148				**5.7**
	19.29	194	166	149	138	121	**5.6**
	19.27	284.7	255				**4.26**
	19.39	224	209.5	194			**4.19**

The reaction products of SpMnSODs treated pinoresinol were subjected to GC/MS analysis before and after silylation. GC/MS analysis revealed that the reaction constituent of both enzymes contains vanillin **4.1** and 2-methoxyhydroqunone **4.9**. Vanillic acid **4.2** was also observed in SpMnSOD1 reaction. While, two additional products *m/z* of 194 and 181 were observed in SpMnSOD2 reaction, which may confirm the production of compound **5.6** and proposed mechanism of pinoresinol degradation by SpMnSODs. The formation of compound **5.7** via demethylation is also possible, as we detected demethoxylation reactions previously in organosolv and 5,5`-dehydrodivanillin **5.2** treated by SOD1 and SOD2 (see Table 5.3 for GC/MS data).

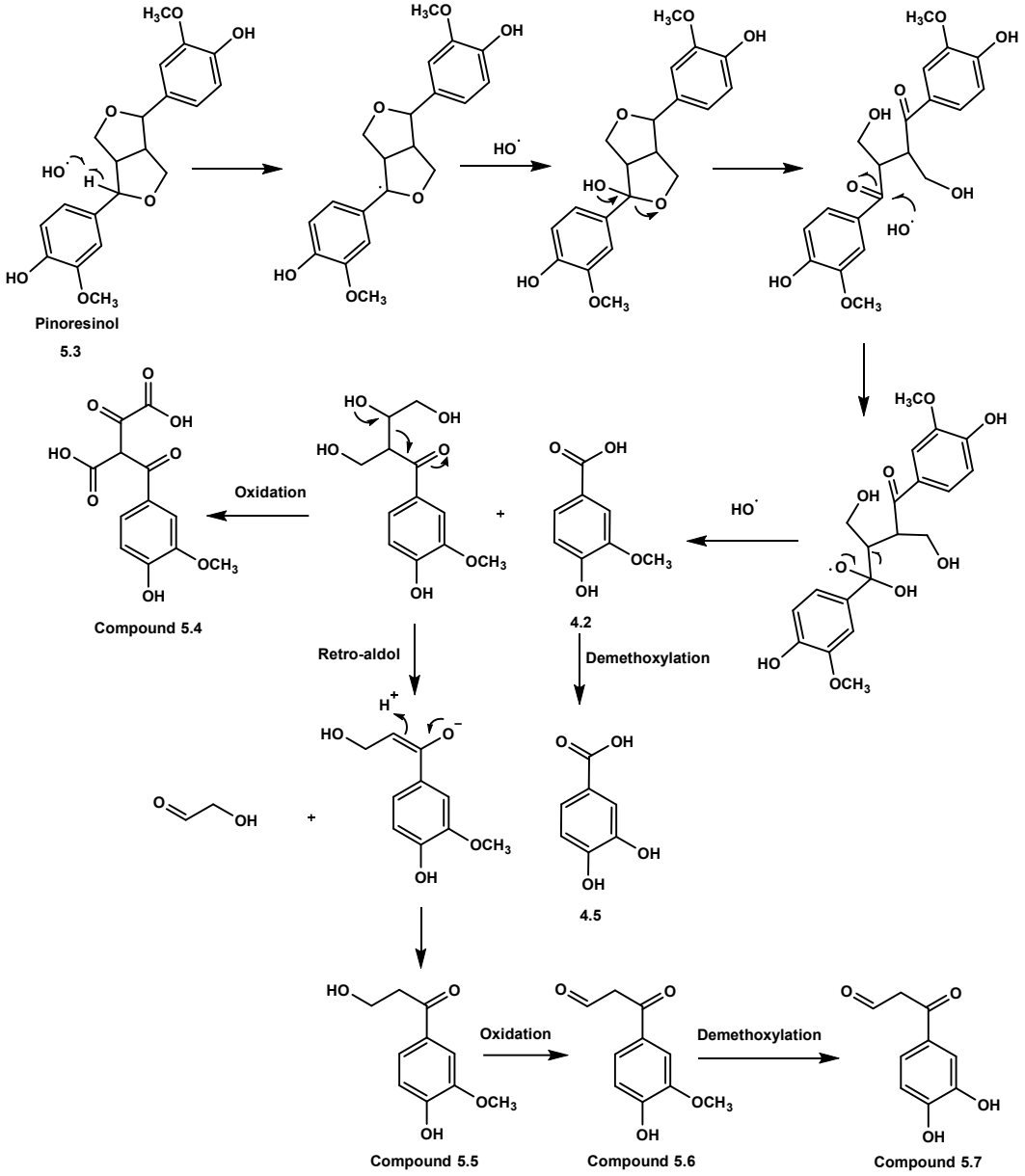

Figure 5.7. Possible mechanism of degradation of pinoresinol catalysed by SpMnSODs

5.2. Degradation of monocyclic aromatic compounds

In order to understand the nature of the reactive species, the mechanisms of the reactions and the reactivity of SpMnSODs toward different monocyclic aromatic compounds, several compounds were tested. The tested monocyclic aromatic compounds include ferulic acid **4.3**, vanillic acid **4.2**, vanillin **4.1**, 5-carboxyvanillic acid **4.4**, veratryl alcohol **5.9**, p-hydroxybenzoic acid **4.12**, p-hydroxybenzaldehyde **4.11**, salicylic acid **4.13**, acetovanillone **4.14**, 4-(1-hydroxyethyl)guaiacol **4.15**, guaiacol **4.6**, and catechol **4.7**. 10 mM of each of these model compounds were incubated with 10 μM of SOD1 and SOD2 in 50 mM potassium phosphate buffer or ammonium bicarbonate buffer pH 7.8 for 5 hrs (since SpMnSODs gave the highest yields after 5 hrs reaction with organosolv lignin, see Section 4.8.1) separately, to which of KO_2 was added. The reactions were quenched by addition of HCl. The control experiments were performed by mixing all the components mentioned and replacing the enzymes with the buffer used. The reaction components were extracted with ethyl acetate then evaporated to dryness. The residues were dissolved in dry chloroform. The samples were divided into three portions for analysis by LC/MS and GC/MS. Samples were analysed by GC/MS before and after derivatization with N,O-bis(trimethylsilyl)acetamide and trimethylsilyl chloride (10:1) in the presence of pyridine at 60ºC for 60 min.

5.2.1. Ferulic acid.

SpMnSODs can react with ferulic acid to produce various products. LC/MS analysis of the reaction components of both SOD1 and SOD2 treated ferulic acid gave ions (*m/z*) corresponding to proton- and/or sodium adducts of each of vanillic

acid **4.2** (*m/z* of 169 and 191 at 32.2 min), vanillin **4.1** (*m/z* of 153 and 175 at 35.0 min), and protocatechuic acid **4.5** (*m/z* of 177 at 23.8 min). These products were eluted at the same retention times as their associated authentic compounds eluted (Figure 5.8). SOD1 most probably generates hydroxyvanillic acid **4.16** (*m/z* of 185 which corresponds to MH^+, at 27 min) and 2,3-dihydroxy-3-guaiacylpropanoic acid **5.8** (*m/z* 229 which corresponds to MH^+, at 29.7 min) as well. Catechol (*m/z* of 111 which corresponds to MH^+, at 25.7 min) was also detected from SOD2 treated ferulic acid.

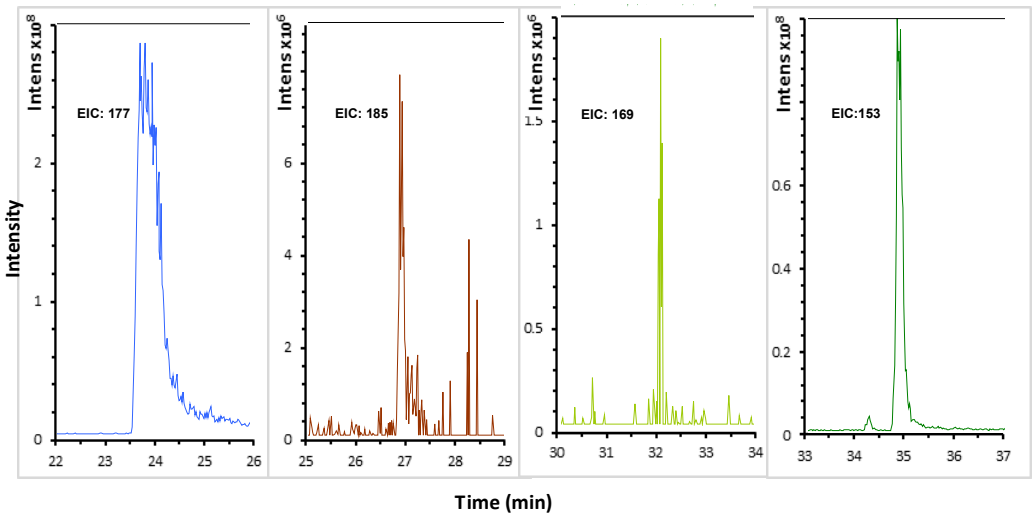

Figure 5.8 Extracted ion chromatograms (EIC) of some products (*m/z* of 177, 185, 169 and 153) from ferulic acid treatmed with *Sphingobacterium* sp. T2 MnSODs analysed by LC/MS.

Table 5.4. Detected metabolites from reaction components of ferulic acid treated with SpMnSODs using GC/MS.

Enzymes	RT	*m/z*	Fragments					Assignments
MnSOD1	13.5	110	81	69	55			**4.7**
	19.7	168	153	138	121	93		**4.2**
	22.7	312	297	28	258			**4.20**

	18.8	224	209	194				**4.19**
MnSOD2	13.2	110	63	55				**4.7**
	11.18	124	109	81	61			**4.6**
	17.2	152	134	81				**4.1**
	19.8	168	153	125	97			**4.2**
	19.3	224	209	194			73	**4.19**
	22.7	312	297	282	257	253		**4.20**

A fraction of reaction mixture was analysed by GC/MS before and after derivatization with bis(trimethylsilyl)acetamide in the presence of pyridine at 60ºC for 60 min. GC/MS results confirm the production of catechol **4.7**, *m/z* 110 at RT 13.5 min, guaiacol **4.6**, *m/z* 124 at RT 11.4 min, vanillin **4.1**, *m/z* of 152 and 224 at RT 17.4 min and 19.3 min respectively, vanillic acid **4.2**, *m/z* of 168 and 312 at RT 20.39 and 22.75 min respectively. The fragmentation pattern and their retention times agree with those of their related authentic compounds shown under the same conditions (Table 5.4).

5.2.1.1. Mechanism of ferulic acid degradation

The mechanism of breakdown of ferulic acid **4.3** by MnSODs can be proposed from LC/MS and GC/MS results. Vanillin **4.1**, vanillic acid **4.2** and catechol **4.7** were observed from both the GC/MS and LC/MS analysis. Guaiacol **4.6** was only observed with GC/MS while both protocatechuic acid **4.5** and hydroxyvanillic acid **4.16** by LC/MS only. Conversion of ferulic acid **4.3** to vanillin **4.1** is one of the well-

known reactions of hydroxyl radical with ferulic acid [179]. Studies show that •OH reacts with propenoic side chains of cinnamic, 4-hydroxycinnamic, ferulic acid and related compounds to produce benzyl-type radicals, which turn to peroxyl radicals in the presence of dioxygen, then fragmentation and rearrangement lead to generation of the corresponding aldehydes (Figure 5.9) [179]. This can be one of the pathways for decay of benzyl-type radicals. Another possibility for degradation of the benzyl-type radical (based on observed products) is that the second hydroxyl radical attacks to generate 2,3-dihydroxy-3-guaiacylpropanoic acid **5.8** (detected by both LC/MS and GC/MS machines) then cleavage of C_α-C_β bond releasing a hydroxy acetic acid radical (Figure 5.10). This radical probably converts to oxalic acid. Oxalic acid is a lignin metabolite, while has been detected from lignocellulose breakdown by *R. jostii* RHA1 [191],[62] and *P. putida* [62] as well as detected in this study from SpMnSOD treated organosolv lignin. Vanillin **4.1** will convert to vanillic acid **4.2** by reaction with hydroxyl radical. Demethoxylation reaction of vanillic acid **4.2**, which was detected previously (reaction of SpMnSODs with organosolv lignin, Section 4.9.1.6) most probably occurs by reaction with hydroxyl radical to generate protocatechuic acid **4.5**. Products such as guaiacol **4.6** and catechol **4.7** are produced as a result of oxidative decarboxylation of vanillic acid **4.2** and protocatechuic acid **4.5** respectively. These two metabolites can also be generated through the breakdown of the aryl-C_α bond of β-aryl ether units of lignin as described in the previous Chapter (see Figure 4.36).

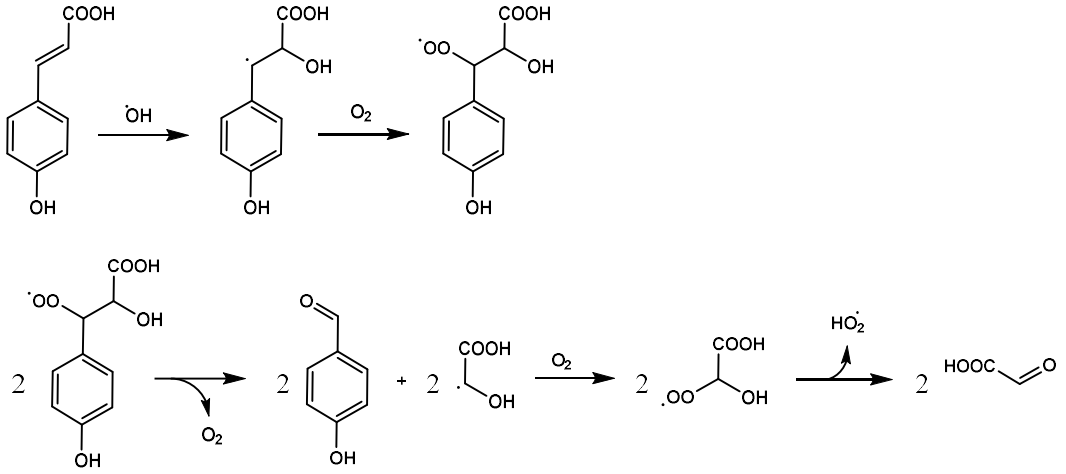

Figure 5.9. Attack of hydroxyl radical to the propenoic side chain of 4-hydroxycinnamic acid [179].

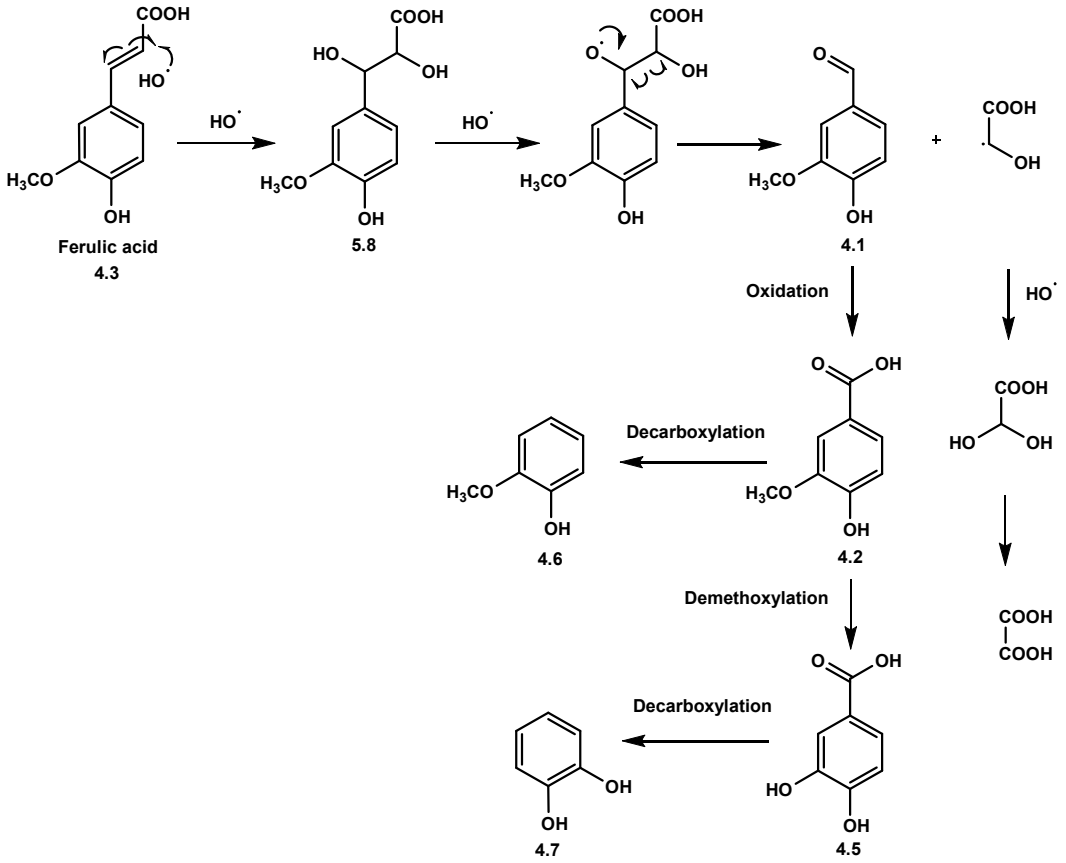

Figure 5.10. Proposed breakdown pathway for ferulic acid catalysed by SpMnSODs.

5.2.2. Veratryl alcohol.

Multiple products were detected upon incubation of veratryl alcohol **5.9** with SpMnSODs. Oxidation of veratryl alcohol **5.9** by SpMnSODs is another evidence for the generation of a potent oxidising agent, since this substrate can only be oxidised by high redox potential enzymes [72]. Proton- and/or sodium adducts of vanillin **4.1** (MH^+, *m/z* = 153 at 35 min), vanillic acid **4.2** (MH^+, *m/z* = 191 at 32 min) and 2-methoxyquinone **4.10** (MH^+, *m/z* = 139 and MNa^+, *m/z* = 161 at 25.7 min) were detected. In the case of SOD2, the sodium adduct of 2-methoxyhydroquinone **4.9** (MNa^+, *m/z* = 163 at 19.8 min) was also detected, its retention time is the same as authentic 2-methoxyhydroquinone (Figure 5.11). The additional products detected are most probably associated with the proton- and sodium adduct of veratryl aldehyde **5.10** (MH^+, *m/z* = 167 and MNa^+, *m/z* = 189 at 43.8 min)

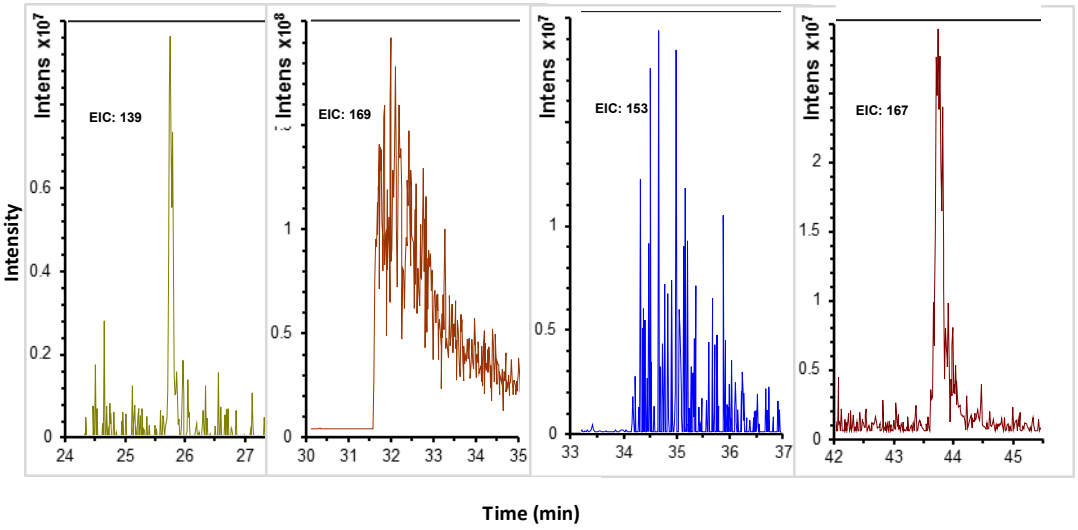

Figure 5.11. Chromatograms of some detected Veratryl alcohol reaction products masses by LC/MS. Extracted ion chromatograms (EIC) for *m/z* of 139, 169, 153 and 167.

The reaction components were also analysed by GC/MS before and after derivatization with bistrimethylsilylacetamide and compared with that of commercially available authentic compounds. The results of GC/MS analysis show

the production of guaiacol **4.6** and vanillin **4.1** from SpMnSOD (SOD1 and SOD2) treated veratryl alcohol (their retention times and fragmentation patterns are similar to authentic compounds, see Table 5.5). It gave also *m/z* of 155 and 298.7 which most likely correspond to vanillyl alcohol and vanillyl alcohol (diSiMe$_3$) and *m/z* of 166 and 282 which most probably correspond to veratryl aldehyde and dihydroxybenzaldehyde (diSiMe$_3$).

Table 5.5. Detected Veratryl alcohol reaction product masses by GC/MS.

Enzymes	RT	*m/z*	Fragments					Assignments
MnSOD1	11.2	124	109	81				**4.6**
	14	152	137	109				**4.1**
	6.3	155	79	78	62	61		**5.11**
	18.5	166	165	95				**5.10**
	19.3	224	209	194	168	139		**4.19**
	8.3	282	281					Dihydroxybenzaldehyde (diSiMe$_3$)
	20.7	298.7	267	240	225	223	151	Vanillyl alcohol (di-SiMe)
MnSOD2	11.15	124	109	81				**4.6**
	13.32	138	110	55				dihydroxybenzaldehyde
	14	152	137	109				**4.1**
	6.3	155	81	61				**5.11**

	18.5	166	165	95				**5.10**
	8.3	282	281					dihydroxybenzaldehyde (diSiMe$_3$)

5.2.2.1. Mechanism of veratryl alcohol breakdown

Generation of multiple products from the veratryl alcohol **5.9** reaction with SpMnSODs suggests that the formation of veratryl aldehyde **5.10**, which was detected by both of GC/MS and LC/MS. Vanillin **4.1** was probably produced from demethoxylation of veratryl aldehyde, this type of reaction was observed with organosolv lignin (Chapter 4) and lignin model compounds (previous Sections). Guaiacol **4.6** and protocatechuic acid **4.5** are most likely generated from vanillic acid **4.2** which may be produced by the oxidation of vanillin **4.1**. Also another type of reaction was spotted which is substitution of a carboxylic acid or benzyl alcohol side chain with hydroxyl group and formation of 2-methoxyquinone **4.10**. This kind of reaction is an ipso-substitution, and can be caused by attack of hydroxyl radical on substituted aromatic rings [180],[179]. 2-Methoxyhydroquinone **4.9** was also observed in reactions with both of SpMnSOD with organosolv and β-aryl ether model compound (Chapter 4 and Section 5.1). The possible mechanism is the reaction of hydroxyl radical with vanillic acid as described in Figure 5.12.

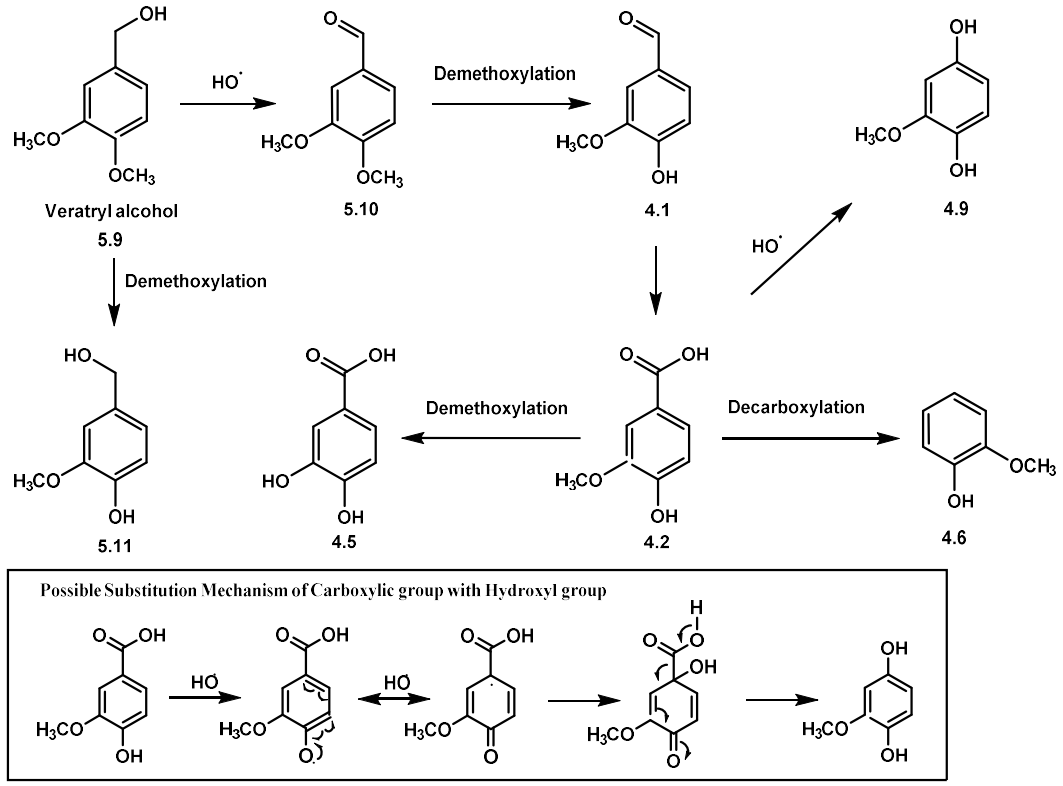

Figure 5.12 Possible degradation path for veratryl alcohol.

5.2.3. p-Hydroxybenzoic acid.

Para-Hydroxybenzoic acid was incubated with SpMnSOD enzymes under conditions described in Section 5.2. LC/MS analysis showed that these enzymes (SOD1 and SOD2) can catalyse the transformation of *p*-hydroxybenzoic acid **4.12** to generate a few products. Extracted ion chromatogram (Figure 5.13) of dihydroxybenzoic acid **4.5** shows *m/z* of 177 (MNa^+ with a retention time of 24.3 min) is the primary product detected from the reaction of both enzymes. SOD2 also generated an ion at *m/z* of 126 eluted at 14.0 min, which matches with MH^+ and retention time of pyrogallol **4.8**. The *m/z* of 94 was observed by GC/MS from non-derivatised reaction mixture of both SOD1 and SOD2 at 35 min, which agree with RT and fragmentation pattern of commercially available phenol. While *m/z* of 370.9

was observed from silylated reaction mixture of both enzymes at 15.7, which matches with protocatechuic acid **4.22** (Table 5.6).

Table 5.6. Observed metabolites of 4-hydroxybenzoic acid reaction with SpMnSOD using GC/MS

Enzymes	RT	*m/z*	Fragments		Assignments
MnSOD1	8.8	94	66	61	**5.12**
	15.7	370.9	356	193	**4.22**
MnSOD2	8.7	94	66	61	**5.12**
	15.7	370.9	356	193	**4.22**

5.2.3.1. Mechanism of p-hydroxybenzoic acid reaction with SpMnSODs

The products observed from the incubation of 4-hydroxybenzoic acid **4.12** with both SOD enzymes include protocatechuic acid **4.22** and phenol **5.12**. Formation of dihydroxybenzoic acid from hydroxybenzoic acid confirms the hypothesis of the involvement of hydroxyl radical in SpMnSODs reactions with lignin and lignin model compounds [167],[178] (Figure 5.14). While the formation of phenol confirms that decarboxylation of benzoic acids is catalysed by SpMnSODs, which may involve hydroxyl radical as described in Section 5.2.1.

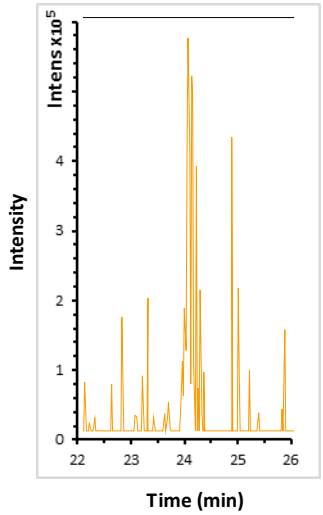

Figure 5.13. Extracted ion chromatogram of mass 177 which correspond to protocatechuic acid observed from reaction of p-hydroxybenzoic acid with SOD1 and SOD2 using LC/MS.

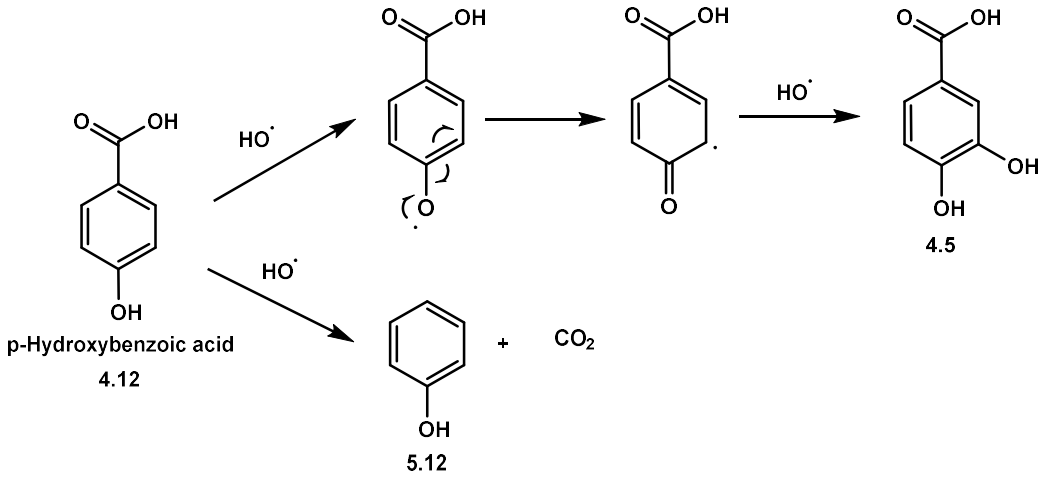

Figure 5.14. Transformation of 4-hydroxybenzoic acid catalysed SOD1 and SOD2.

5.2.4. Salicylic acid

A few products were detected by LC/MS from the reaction of SpMnSOD enzymes with salicylic acid **4.13** (Figure 5.15). The detected *m/z* of 117, 95, 177, 127, 149 and 111 with retention times of 46, 46, 24, 8, 8 and 25.8 min are matches with MH^+ and MNa^+ of phenol, MNa^+ of protocatechuic acid **4.5,** MH^+ and MNa^+ of pyrogallol **4.8** and MH^+ of catechol **4.7**, respectively. In addition, some of these ions

(*m/z* of 117, 95 and 111) were observed at retention times similar to their authentic analogue, which are commercially available, while others (*m/z* of 127 and 149 which eluted earlier than pyrogallol **4.8** and *m/z* of 177 eluted later than protocatechuic acid **4.5** suggesting formation of an isomer of pyrogallol **5.14** and isomer of protocatechuic acid **5.13**). Catechol **4.7** was only observed in SOD1 reaction components.

Analysis of the reaction components by GC/MS shows the production of phenol **5.12** (*m/z* of 94 at 8.9 min) from treatment of salicylic acid **4.13** from each of SOD1 and SOD2. Two additional products were observed at *m/z* of 254 and 369.7 at 16.48 and 15.3 min from derivatized reaction components of SOD1, which correspond to catechol **4.24** and protocatechuic acid **4.22**, respectively. These products were also observed in the SOD2 reaction mixture before (*m/z* of 111 only, which corresponds to catechol **4.7**) and after silylation (*m/z* of 269.7 only, which corresponds to protocatechuic acid **4.22**). Their retention times and fragmentation patterns also match with commercially available catechol and protocatechuic acid (Table 5.7).

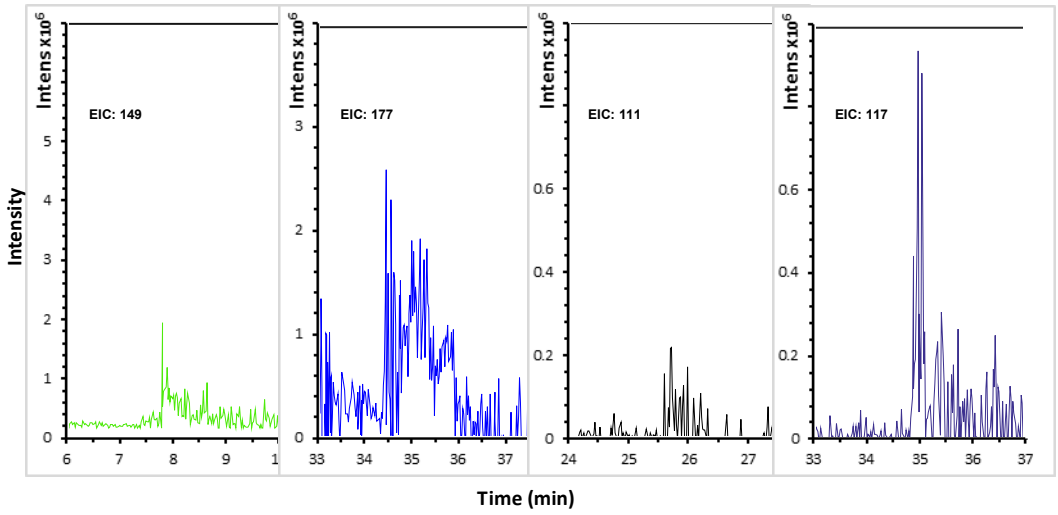

Figure 5.15. Extracted ion chromatograms (EIC) for *m/z* of 149, 177, 111 and 117, which were observed by LC/MS from salicylic acid reaction.

Table 5.7. Salicylic acid products observed by GC/MS

Enzymes	RT	*m/z*	Fragmentations					Assignments
MnSOD1	16.5	369.7	281	221	195	147	73	**4.22**
	15.3	254	195	177	138	120	73	**4.24**
	8.91	94	66					**5.12**
MnSOD2	13.14	110	63					**4.7**
	16.48	369.7	281	221	147	73		**4.22**
	8.91	94	66					**5.12**

5.2.4.1. Mechanism of salicylic acid modification

Hydroxylation of aromatic carboxylic acids leading to the formation of dihydroxybenzoic acid has been used in literature as a test for the presence of hydroxyl radical [167],[178],[179],[180] hence providing further evidence for its involvement in the reaction of MnSODs with lignin and lignin model compounds. This product was eluted at higher retention time in LC/MS (35 min), indicating that the compound is possibly an isomer of protocatechuic acid **5.13**. Products catechol **4.7** and trihydroxybenzene **5.14** were also detected, probably formed via ipso-substitution of the dihydroxybenzoic acid **5.13**. Finally, decarboxylation reaction occurred which resulted in the formation of phenol **5.12**. It also possible that catechol is formed via hydroxylation of phenol (Figure 5.16).

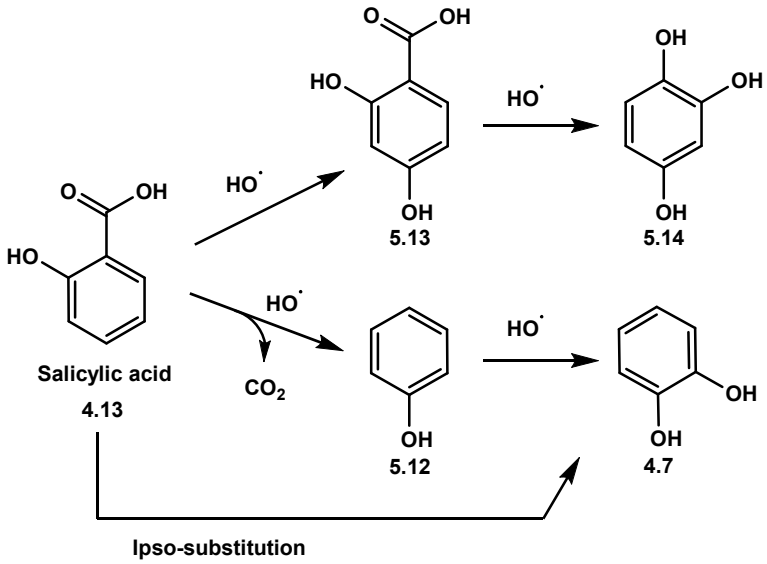

Figure 5.16. The reaction of salicylic acid with SpMnSOD enzymes.

5.2.5. 4-Hydroxybenzaldehyde.

Phenol **5.12** (*m/z* of 94 at 8.9 min) was detected by GC/MS from the reaction of para-hydroxybenzaldehyde **4.11** with both SOD1 and SOD2. A peak at *m/z* 138 was also detected from the reaction of both enzymes, which corresponds to 4-hydroxybenzoic acid **4.12** (its retention time and fragmentation pattern matches with authentic para-hydroxybenzoic acid). From derivatized samples with N,O-bis(trimethylsilyl)acetamide only *m/z* 282 was detected from the SOD2 reaction, which matches with commercially available p-hydroxybenzoic acid (disilylated) **4.28**. See Table 5.8 for GC/MS results.

Few product peaks were detected by LC/MS which gave *m/z* of 139, 127 and 177 with retention times of 29.5, 8 and 23.7 min, and are matches MH^+ of 4-hydroxybenzoic acid **4.12** and pyrogallol **4.8** and MNa^+ protocatechuic acid **4.5**, respectively (Figure 5.17).

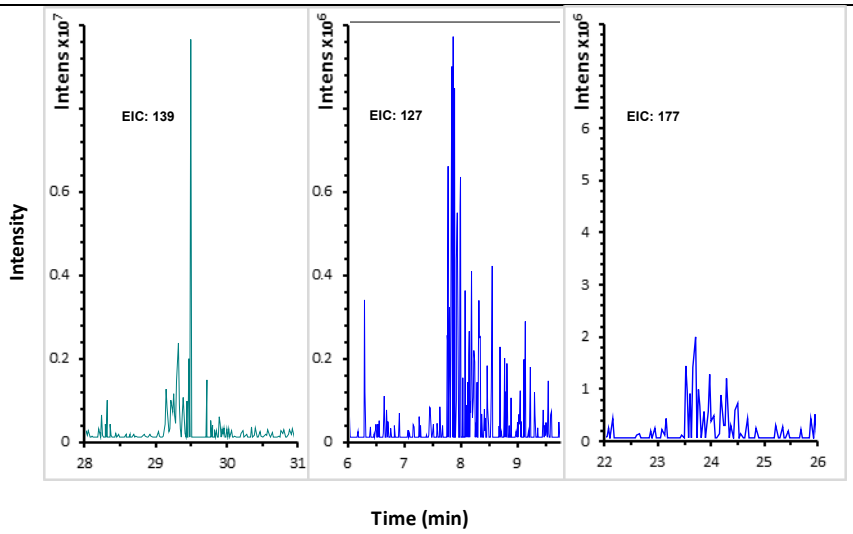

Figure 5.17. Extracted ion chromatograms from reaction of 4-hydroxybenzaldehyde observed by LC/MS.

Table 5.8. Observed metabolites from 4-hydroxybenzaldehyde by GC/MS.

Enzymes	RT	*m/z*	Fragmentations			Assignments
MnSOD1	8.91	94	66			**5.12**
	18.8	138	121			**4.12**
MnSOD2	8.12	94	66			**5.12**
	18.2	138	121			**4.12**
	20.7	282	268	224	194	**4.28**

5.2.5.1. Mechanism of 4-hydroxybenzaldehyde transformation

Para-hydroxybenzaldehyde **4.11** undergoes oxidation to form its corresponding acid. Thus, this product will transform to dihydroxybenzoic acid and phenol (Figure 5.18) as described previously (Sections 5.2.3 and 5.2.4). An additional product trihydroxybenzene **5.14** was also observed. This product was most probably

generated in the same manner as shown in the transformation of p-hydroxybenzoic acid (Figure 5.18).

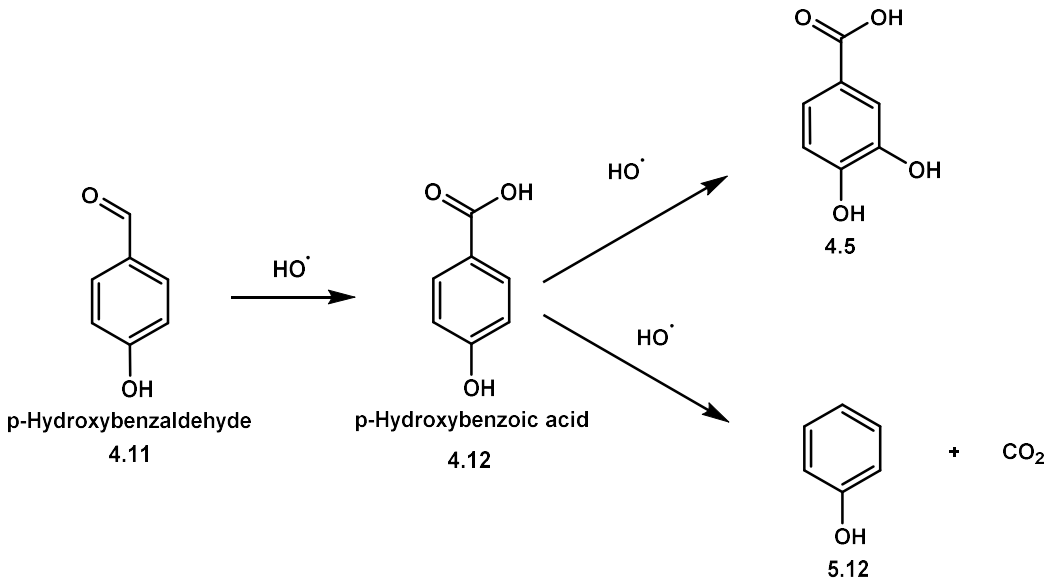

Figure 5.18. Transformation of p-hydroxybenzaldehyde catalysed SpMnSOD enzymes (SOD1 and SOD2).

5.2.6. Acetovanillone.

Analysis of reaction products of acetovanillone **4.14** incubated with SOD1 by LC/MS (Figure 5.19) showed the production of dihydroxybenzoic acid **4.5** (MH^+= 155 at 24 min), while the SOD2 reaction with acetovanillone **4.14** resulted in the production of vanillic acid **4.2** (MH^+= 169 at 31.8 min on LC/MS).

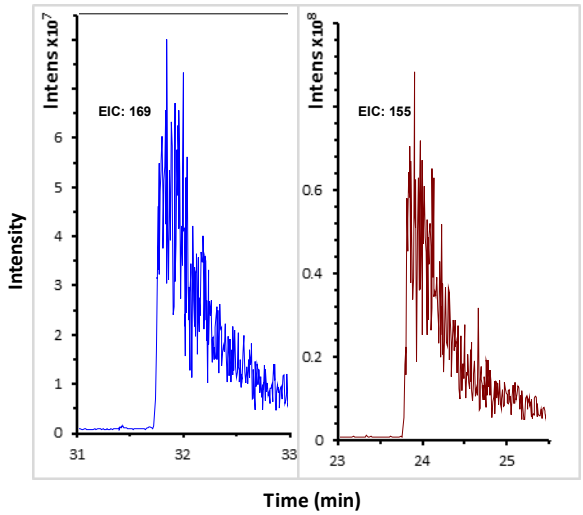

Figure 5.19. Examples of LC/MS chromatogram for acetovanillone reaction components. Extracted ion chromatogram (EIC) for *m/z* of 169 and 155.

Several metabolites were detected with GC/MS from the reaction of both MnSODs. In non-derivatised samples an ion at *m/z* of 140 was observed at retention time of 17.4 which corresponds to 2-methoxyhydroquinone **4.9**, since its retention time and fragmentation pattern matches with authentic compound. In the derivatized reaction components of both enzymes with N,O-bis(trimethylsilyl)acetamide masses of 312 and 284 at 22.8 and 19.3 min were detected, which matches with silylated vanillic acid **4.20** and 2-methoxyhydroquinone **4.26** (Table 5.9).

Table 5.9. Detected reaction metabolites of acetovanillone by GC/MS

Enzymes	RT	*m/z*	Fragmentations			Assignments
MnSOD1	19.3	284	255			**4.26**
	17.4	140	125	109		**4.9**
	22.7	312	298	283	268	**4.20**
MnSOD2	17.3	140	125	97		**4.9**

	19.2	284	255			**4.26**
	22.7	312	298	283	268	**4.20**

5.2.6.1. Mechanism of conversion of acetovanillone

Vanillic acid **4.2**, dihydroxybenzoic acid **4.5** and 2-methoxyhydroquinone **4.9** are the main reaction products of the transformation of acetovanillone with SpMnSODs; this indicates that the side chain has been oxidised. The most likely mechanism for this conversion is the formation of radical with hydroxyl radical then oxidation to give aldehyde and acid intermediates, attack of •OH on ketone group of the intermediate, resulting in the release of vanillic acid **4.2**. Guaiacol **4.6** can be produced either from decarboxylation of vanillic acid or aryl-C_α cleavage of 2-(4-guaiacyl)-2-oxoacetic acid (formed from oxidation of acetovanillone) as intermediate for production of 2-methoxyhydroquinone **4.9**. Protocatechuic acid **4.5** can also be generated from vanillic acid by oxidative demethoxylation reaction, and 2-methoxyhydroquinone **4.9** is a product of ipso-substitution or decarboxylation and then hydroxylation of vanillic acid. The mechanism of acetovanillone fragmentation is described in Figure 5.20.

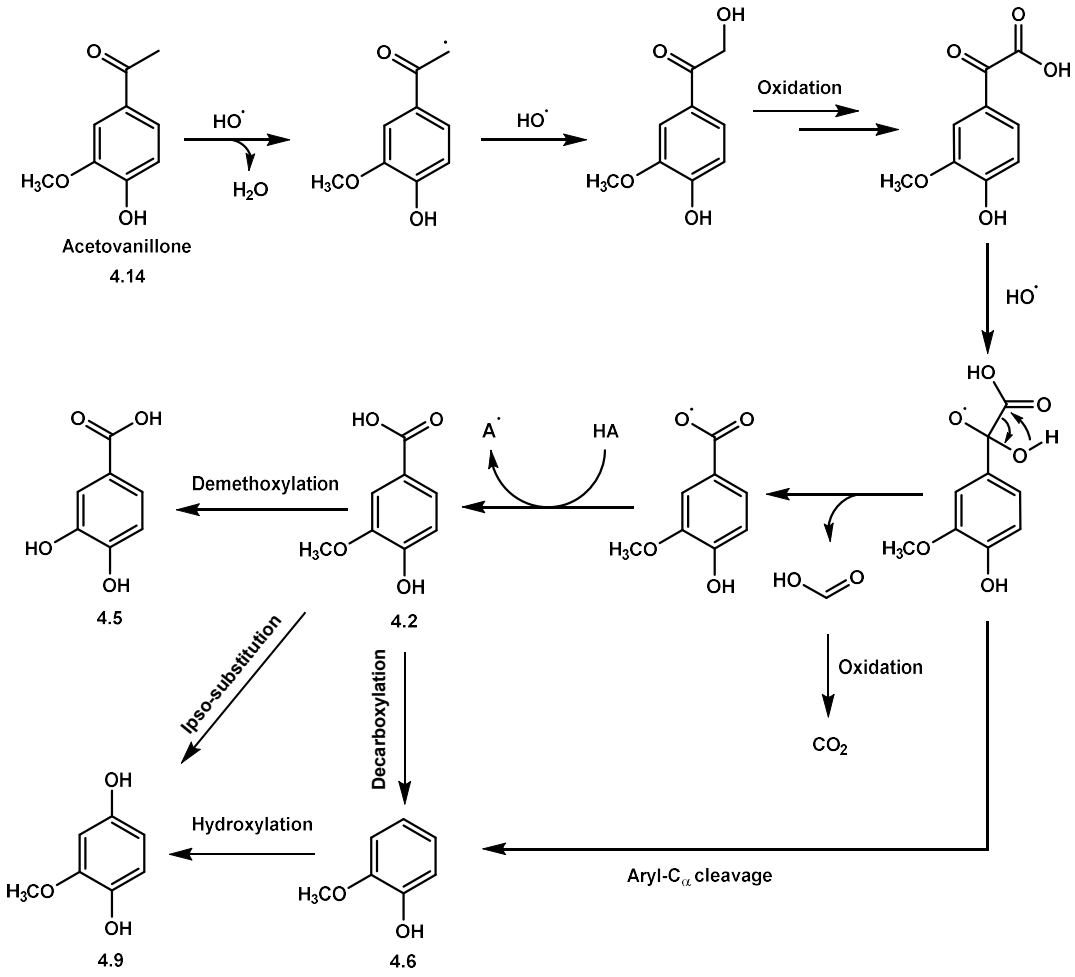

Figure 5.20. Proposed pathway for acetovanillone degradation catalysed by SpMnSODs.

5.2.7. 4-(1-hydroxyethyl)guaiacol.

The reaction of SODs with 4-(1-hydroxyethyl)guaiacol **4.15** resulted in the production of two main products: vanillic acid **4.2** and dihydroxybenzoic acid **4.5**. LC/MS analysis of the reaction components of SOD1 with the substrate showed the generation of MNa^+ and MH^+ for each of vanillic acid **4.2** and dihydroxybenzoic acid **4.5** at retention times of 32.2 and 23.9 respectively. In contrast, only MNa^+ of vanillic acid **4.2** and MH^+ of dihydroxybenzoic acid **4.5** were observed from SOD2 reaction mixture when analysed by LC/MS.

Acetovanillone **4.14** (*m/z* of 166 at 18.7) was observed in the reaction components (non-derivatized) of both enzymes (MnSOD1 and MnSOD2) using GC/MS, this suggests the oxidation of 4-(1-hydroxyethyl)guaiacol **4.15**. Vanillin **4.1** (*m/z* of 152 at 14.4) was also observed in MnSOD2 reaction products. In silylated samples of both enzymes, vanillic acid **4.20** (*m/z* of 312 at 22.7), vanillin **4.19** (*m/z* of 224 at 19.4) and 2-methoxyhydroquinone **4.26** (*m/z* of 284 at 19.2) were detected. Table 5.10 shows RT and mass fragmentation pattern of products observed by GC/MS.

Table 5.10. Observed metabolites by GC/MS from 4-(1-hydroxyethyl)guaiacol reactions with both SpMnSOD enzymes.

Enzymes	RT	*m/z*	Fragmentations			Assignments
MnSOD1	18.7	166	151			**4.14**
	19.2	284	255			**4.26**
	19.4	224	209	194	166	**4.19**
	22.7	312	298	283	268	**4.20**
MnSOD2	18.7	166	151			**4.14**
	14.4	152	137			**4.1**
	19.2	284	255			**4.26**
	19.4	224	209	194	166	**4.19**
	22.7	312	298	283	268	**4.20**

5.2.7.1. Mechanism of oxidation of 4-(1-hydroxyethyl)guaiacol

4-(1-hydroxyethyl) guaiacol **4.15** most likely converted to acetovanillone **4.14**, then oxidised further to produce vanillic acid **4.2**. The produced vanillic acid **4.2** converted to protocatechuic acid **4.5** and 2-methoxyhydroquinone **4.9** or it reduced to vanillin **4.1** (Figure 5.21). So, the reaction of 4-(1-hydroxyethyl)guaiacol **4.15** is similar to that of acetovanillone **4.14** (described in Figure 5.20), since almost the same reaction products were observed.

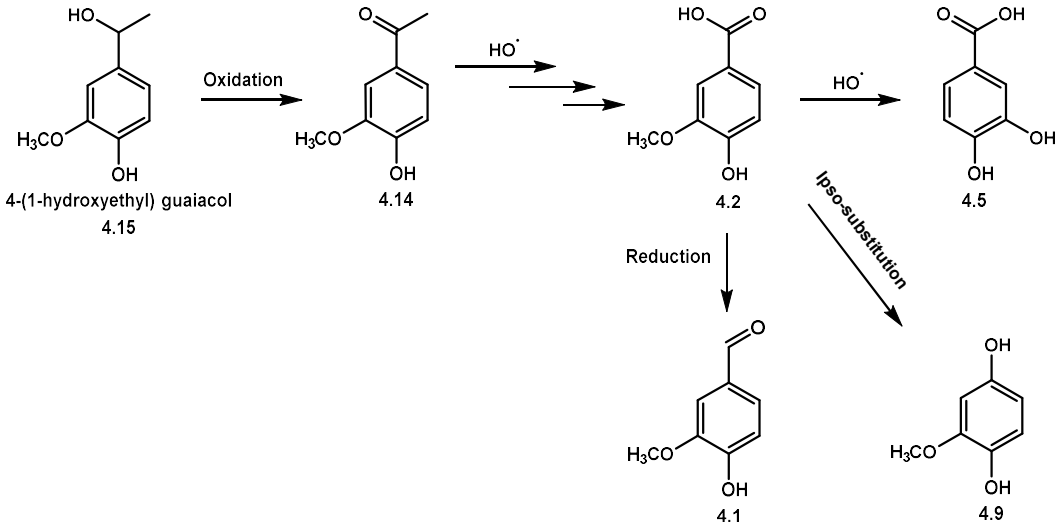

Figure 5.21. Proposed fragmentation pathway for 4-(1-hydroxyethyl)guaiacol.

5.2.8. Vanillic acid.

Treatment of vanillic acid with MnSODs from *Sphingobactium* sp. T2. gave multiple products when analysed by LC/MS. Metabolites observed included: hydroxyvanillic acid **4.16** (*m/z* of 185 at 27.6 min corresponding to MH^+), protocatechuic acid **4.5** (*m/z* of 155 and 177 at 24.3 min corresponding to MH^+ MNa^+), and guaiacol **4.6** (*m/z* of 125 at 40.4 min corresponding to MH^+), see Figure 5.22 for extracted ion chromatograms.

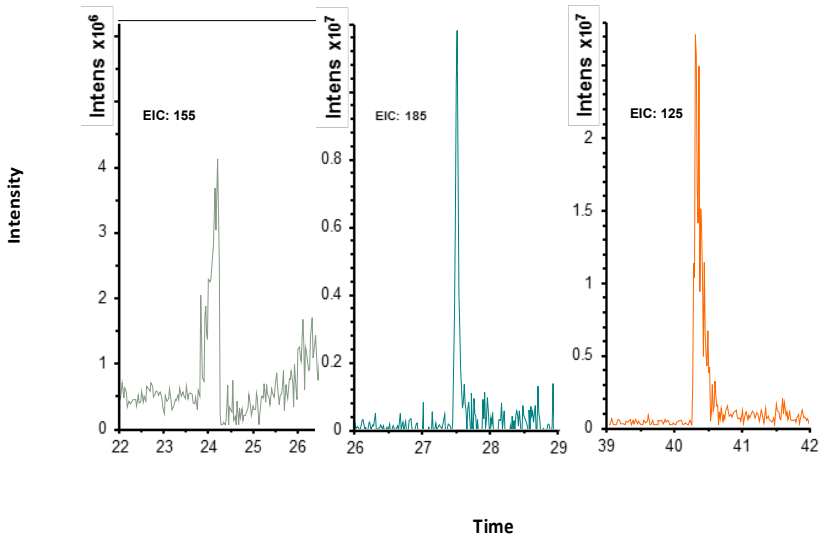

Figure 5.22. Examples of extracted ion chromatograms of vanillic acid metabolites observed by LC/MS.

Guaiacol **4.6** (*m/z* of 124 at 11.3 min), catechol **4.7** (*m/z* of 110 at 13.14 min) and 2-methoxyhydroquinone **4.9** (*m/z* of 140 at 17.11 min) were observed from the reaction mixtures of both SpMnSOD1 and SpMnSOD2. In derivatised samples of both enzymes *m/z* of 284 at 19.2 was observed, which corresponds to 2-methoxyhydroquinone **4.26**. One aditional product (*m/z* of 196 at 13.7 min coresponding to guaiacol **4.23**) was detected by GC/MS from reaction mixture of the SpMnSOD2 treated vanillic acid **4.2** after silylation (Table 5.11).

Table 5.11. Detected reaction components from incubation of vanillic acid with SOD1 and SOD2.

Enzymes	RT	*m/z*	Fragmentations		Assignments
MnSOD1	13.14	110			**4.7**
	11.16	124	109	81	**4.6**
	17.1	140	125	109	**4.9**

	19.2	284	254		**4.26**
MnSOD2	13.2	111	110	64	**4.7**
	11.15	124	109	81	**4.6**
	13.7	196	181	166	**4.23**
	19.2	284	263	254	**4.26**

5.2.8.1. Mechanism of vanillic acid reaction with SpMnSODs

Multiple products observed from the incubation of the vanillic acid **4.2** with both SpMnSOD enzymes may again confirm the involvement of proposed oxidising species (hydroxyl radical) and the anticipated types of reaction. The observed reactions include demethoxylation, hydroxylation of an aromatic ring, decarboxylation and ipso-substitution reactions. The most likely pathway to produce all of the products observed (compound **4.16**, **4.5**, **4.6**, **4.7** and **4.9**) from vanillic acid **4.2** shown in Figure 5.23. Hydroxyl radical can react with vanillic acid to produce hydroxyvanillinic acid **4.16** or cause demethoxylation to generate dihydroxybenzoic acid **4.5**. Decarboxylation of **4.2** and dihydroxybenzoic acid **4.5** will lead to the formation of guaiacol **4.6** and catechol **4.7**. Substitution of carboxylic group of **4.2** with hydroxyl group can result in the formation of 2-methoxyhydroquinone **4.9**. Compound **4.9** can also be formed by hydroxylation of guaiacol **4.6**.

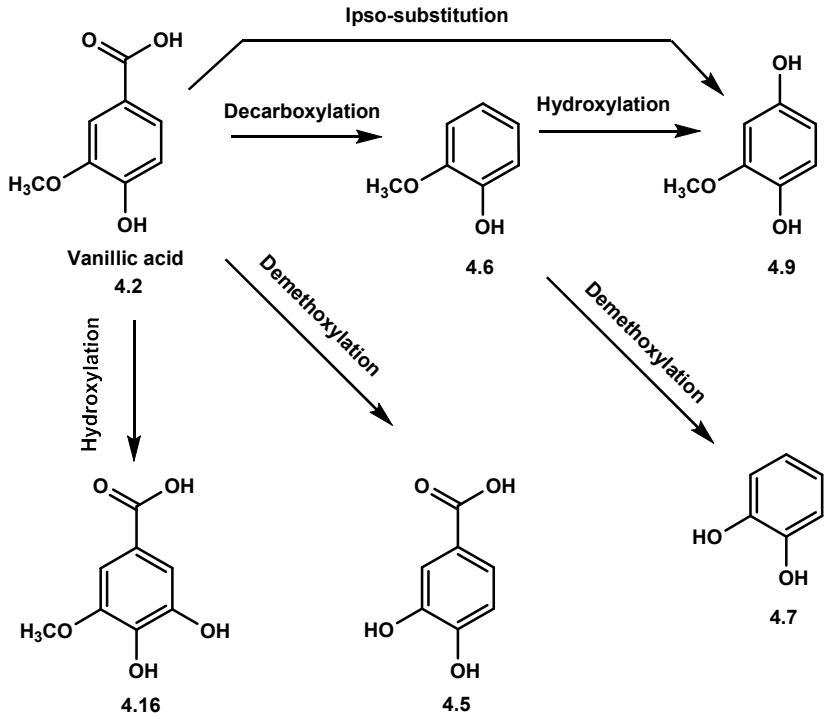

Figure 5.23. The reaction of vanillic acid with SpMnSODs.

5.2.9. Vanillin.

Incubation of vanillin with S*phingobacterium* sp. T2 MnSODs resulted in generation of several products. The observed peak from the reaction components of both enzymes by LC/MS were include *m/z* of 169, 191, 185, 207, 141, 163, 139, and 161, and they are correlated to MH^+ and MNa^+ of vanillic acid **4.2**, hydroxyvanillic acid **4.5**, 2-methoxyquinone **4.10** and 2-methoxyquinone **4.10**, respectively. Two additional products were also observed with *m/z* of 155 and 125, which match with MH^+ of dihydroxybenzene **4.5** and guaiacol **4.6** (Figure 5.24). All these metabolites were eluted at retention times similar to their corresponding authentic compounds, with an exception for 5-hydroxyvanillic acid in which their analogue are not available commercially.

GC/MS analysis of reaction components of the MnSODs treated vanillin **4.1** confirms the generation of multiple products. Compounds observed from non-silylated samples of both enzymes include: guaiacol **4.6** (*m/z* of 124 at 11.5 min), catechole **4.7** (*m/z* of 110 at 13.2 min) and pyrogallol **4.8** (*m/z* of 126 at 12.4 min). In silylated fraction of both enzymes, vanillic acid **4.20** (*m/z* of 312 at 22.7 min), guiacol **4.23** (*m/z* of 196 at 13.7 min) and 2-methoxyhydroquinone **4.26** (*m/z* of 284 at 19.2 min) were observed. See Table 5.12 for RT and mass fragmentation pattern of product peaks detected by GC/MS.

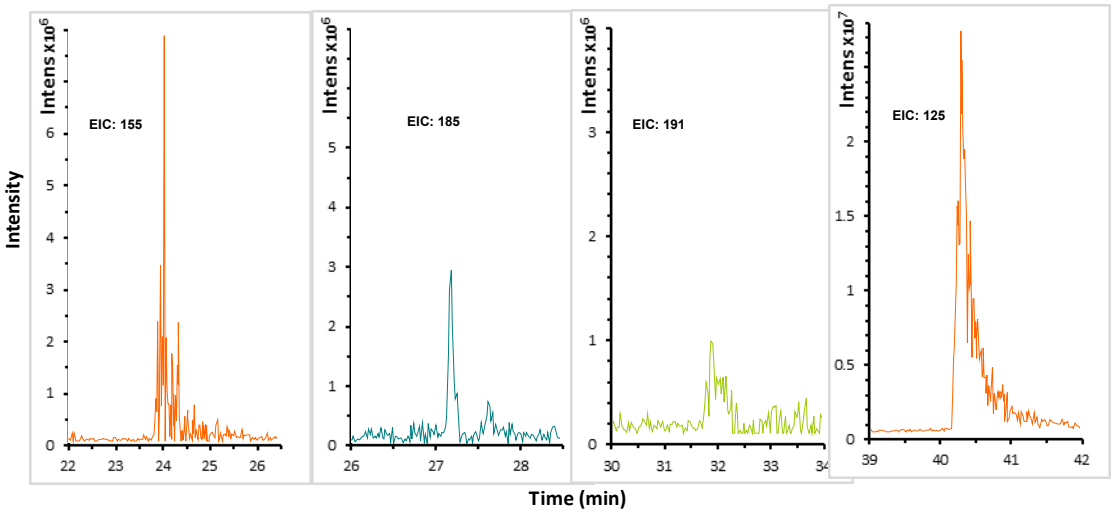

Figure 5.24. Some of chromatograms (EIC) for *m/z* of 155, 185, 191 and 125, which were observed from vanillin reaction mixture using LC/MS

5.2.9.1. Mechanism of vanillin oxidation catalysed by SpMnSODs

Since the same types of products were detected by vanillin incubation with MnSODs as vanillic acid, a possible pathway is oxidation of vanillin to vanillic acid, then vanillic acid is oxidised to form other product (Figure 5.25), in the same manner as vanillic acid transformations (see Figure 5.23 and Section 5.2.8).

Table 5.12. Detected vanillin oxidation products by SpMnDOS using GC/MS.

Enzymes	RT	*m/z*	Fragmentations					Assignment
MnSOD1	13.26	110	63					**4.7**
	11.28	124	109	81				**4.6**
	16.09	126	123	111	69			**4.8**
	13.7	196	181	166				**4.23**
	19.2	284	281	263	254			**4.26**
	22.7	312	297	267	193	178	150	**4.20**
MnSOD2	13.27	110	63					**4.7**
	11.17	124	109	81				**4.6**
	16.09	126	123	111	69			**4.8**
	13.7	196	181	166				**4.23**
	19.25	284	254					**4.26**
	22.7	312	297	283	268			**4.20**

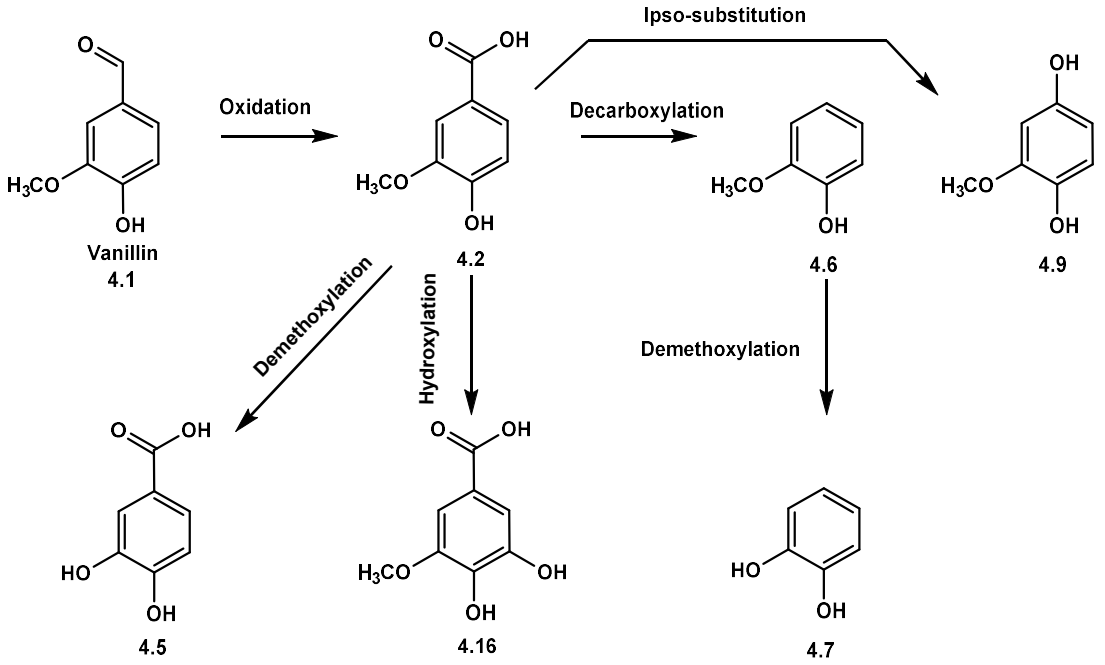

Figure 5.25. Reactions of vanillin with SpMnSOD enzymes.

5.2.10. 5-Carboxyvanillic acid

SOD1 can catalyse the oxidation of 5-carboxyvanillic acid to generate multiple products with *m/z* of 169, 191, 177, 207 and 153, which match with MH^+ and MNa^+ of vanillic acid **4.2**, MNa^+ of dihydroxybenzoic acid **4.5**, MNa^+ of hydroxyvanillic acid **4.16** and MH^+ of vanillin **4.1** (at retention times of 32, 24.3 27.4 and 35 min on LC/MS) produced by authentic compounds. In the case of SOD2, only two products were observed by LC/MS (Figure 5.26). These products were vanillic acid **4.2** (*m/z* = 169, MH^+ with retention time of 32.5 min) and another compound with *m/z* of 201 at 49.7 min.

Guaiacol **4.6** (*m/z* of 124 at 11.5 min) and vanillic acid **4.2** (*m/z* of 168 at 20.3 min) were detected from non-sillylated reaction components of both SOD1 and SOD2 using GC/MS. Analysis of the reaction constituents of both enzymes with

GC/MS after silylation with bis(trimethylsilyl)acetamide shows the existence of vanillic acid **4.20** (*m/z* of 312 at 22.6 min), see Table 5.13.

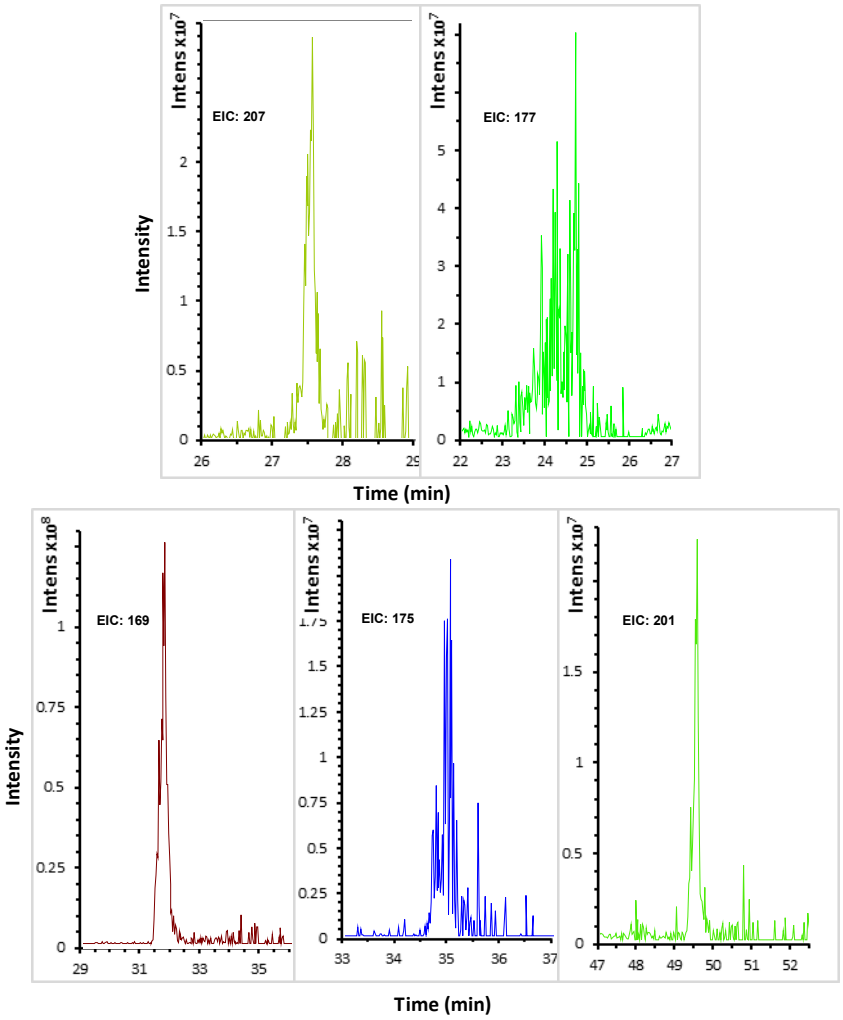

Figure 5.26. Examples of extracted ion chromatograms (EIC) for degradation products of 5-carboxyvanillic acid catalysed by SOD1 and SOD2.

Table 5.13. Observed reaction products of 5-carboxyvanilllic acid using GC/MS.

Enzymes	RT	*m/z*	Fragmentations				Assignment
MnSOD1	19.7	168	153	138	121	93	**4.2**
	11.17	124	109	81			**4.6**

	22.7	312	297	283	268		**4.20**
MnSOD2	19.7	168	153	138	121	93	**4.2**
	11.17	124	109	81			**4.6**
	22.7	312	297	283	268		**4.20**

5.2.10.1. Mechanism of transformation of 5-carboxyvanillic acid by SpMnSODs

The observed reaction products from the oxidation of 5-carboxyvanillic acid **4.4** catalysed by MnSODs from *Sphingobacterium* sp. T2 indicates that this substrate first undergoes decarboxylation to produce vanillic acid, and then other products (such as compound **4.16**, **4.5**, **4.6**, **4.7**, **4.9** and **4.10**) are most likely generated from vanillic acid, as observed with vanillic acid **4.2** and vanillin **4.1** (see Section 5.2.8 and 5.2.9) and other lignin model compounds. There are two possible mechanisms for the formation of 5-hydroxyvanillic acid **4.16**. First, the vanillic acid can be hydroxylated as seen in the case of hydroxybenzoic acid **4.12**. The second possibility is ipso-substitution of one carboxylic acid group of 5-carboxyvanillic acid **4.4** with a hydroxyl group. This type of reaction was also observed with other monomeric lignin model compounds. Vanillin **4.1** was also detected which may come from reduction of vanillic acid **4.2**, although the mechanism for reduction is not clear (Figure 5.27).

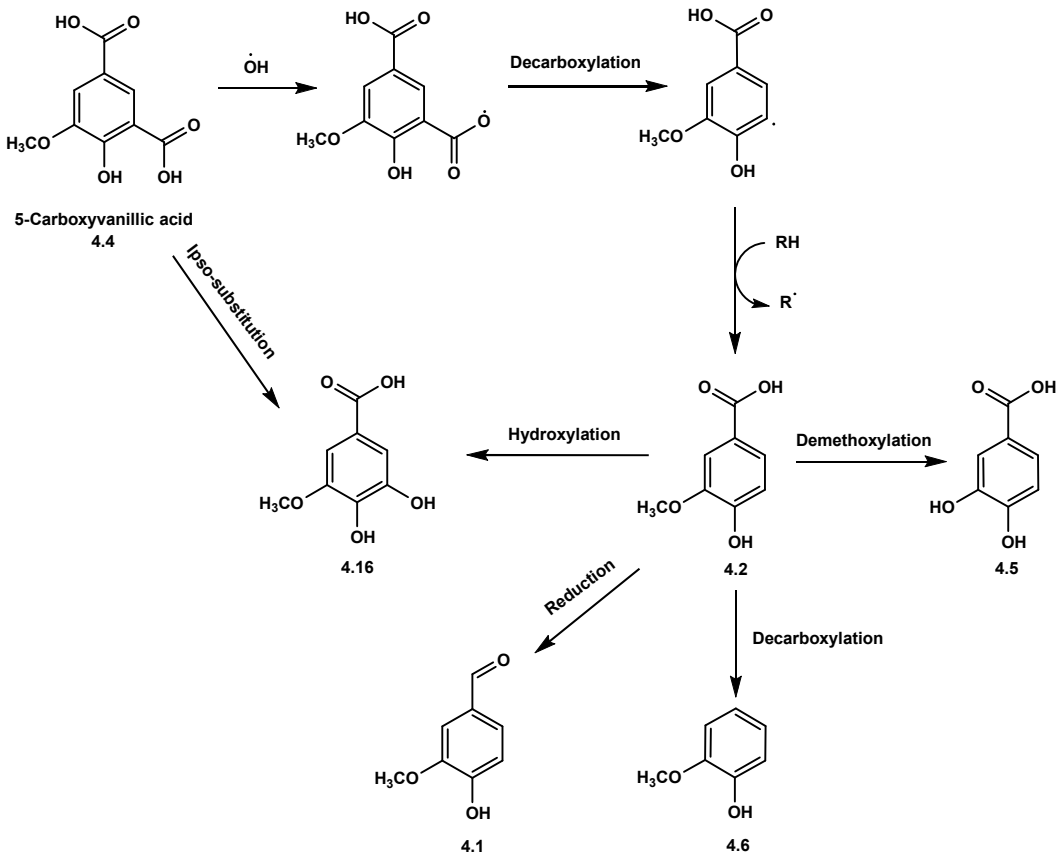

Figure 5.27. Possible mechanism for generation of products from 5-carboxyvanillic acid.

5.2.11. Guaiacol

Two products were observed from the reaction of guaiacol with MnSODs by LC/MS (Figure 5.28). The detected products have *m/z* of 149 and 163 at retention times of 8 and 24.5 min for both enzymes, which match with MNa^+ of pyrogallol **4.8** and 2-methoxyquinone **4.10** respectively. However, the retention time of pyrogallol (14 min) is higher than this product, suggesting that the product is making intermolecular interaction and is a more polar isomer of pyrogallol such as 3,4-dihydroxyphenol **5.14**).

Analysis of underivatized reaction components of both SOD1 and SOD2 with GC/MS shows the presence of catechol **4.7** (*m/z* of 110 at 13.3 min). The derivatized

samples with bis(trimethylsilyl)acetamide confirms that both enzymes can produce catechol (*m/z* of 254 at 15.3 min), see Table 5.14.

Table 5.14. Reaction products detected by GC/MS from reaction components of guaiacol with SOD1 and SOD2.

Enzymes	RT	*m/z*	Fragmentations					Assignments
MnSOD1	13.3	110	63					**4.7**
	15.3	254	195	177	138	120	73	**4.25**
MnSOD2	13.14	110	63					**2.7**
	15.3	254	195	177	138	120	73	**4.25**

5.2.11.1. Mechanism of guaiacol oxidation catalysed by SpMnSODs

Formation of catechol **4.7** confirms the demethoxylation reaction which was observed with several lignin model compounds. Generation of pyrogallol isomer **5.14** from guaiacol **4.6** requires demethoxylation as well as hydroxylation reactions. Production of 2-methoxyhydroquinone **4.9** also confirms hydroxylation of guaiacol. This type of reaction was observed with other lignin monomeric and dimeric model compounds (Figure 5.29).

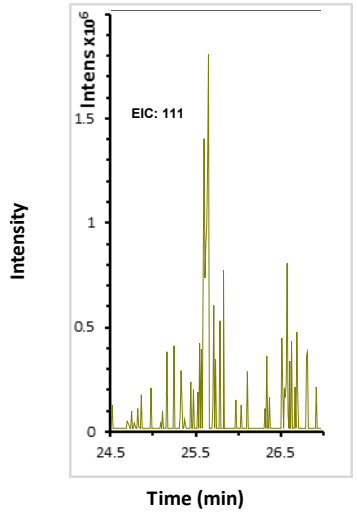

Figure 5.28. Chromatograms for extracted ions for *m/z* of 111, which was detected by LC/MS from reaction components of guaiacol with SpMnSOD1 and SpMnSOD2.

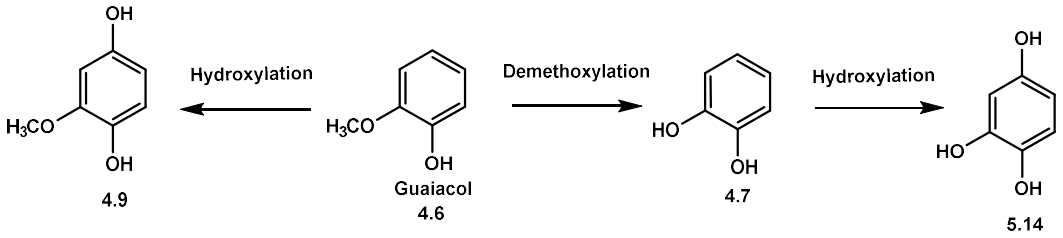

Figure 5.29. SpMnSOD catalysed reactions of Guaiacol.

5.2.12. Catechol

The SpMnSOD enzymes can also react with catechol to produce a few products. The LC/MS analysis of reaction component of both enzymes indicates the presence of *m/z* of 149 which most likely corresponds to MNa^+ of an isomer of pyrogallol **5.14** at 8 min (Figure 5.30).

Trihydroxybenzene **5.14** was detected from the reaction of both SOD1 and SOD2, which may be considered as another evidence of hydroxylation reaction catalysed by these enzymes. GC/MS data (*m/z* of 203, 205 and 317 at 11, 17.3 and 25 min respectively, Table 5.15 and Figure 5.31) may indicate that SpMnSODs catalyse

ring cleavage of catechol. This reaction is possible since attack of hydroxyl radical to aromatic rings can lead to generation of non-aromatic fragmentation products [179] (see Figure 4.36 for more detail), and this has been observed with other lignin model compounds (Section 5.1.2).

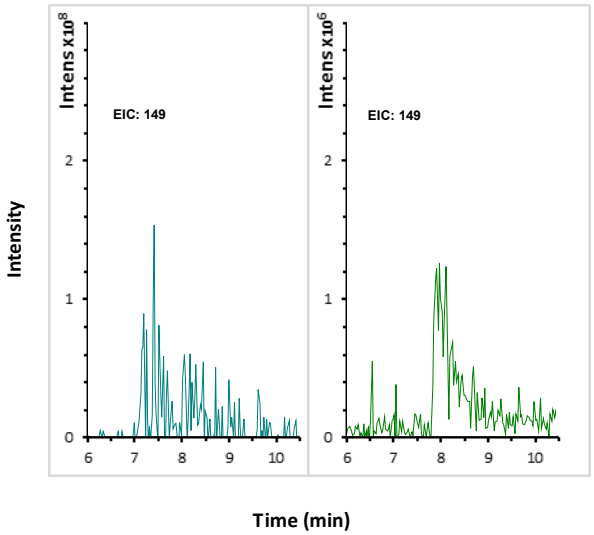

Figure 5.30. Chromatograms (extracted ion chromatogram, EIC for *m/z* 149) of compound detected by LC/MS from reaction of catechol with SpMnSODs.

Table 5.15. Catechol metabolites observed by GC/MS.

Enzymes	RT	*m/z*	Fragmentations			Assignments
MnSOD1	11	203	166	117		**5.16 (monosilylated)**
	17.3	205	147	73		**5.17 (monosilylated)**
MnSOD2	11.2	203	166	117		**5.16 (monosilylated)**
	17.3	205	147	73		**5.17 (monosilylated)**
	25	317	73			**5.15 (disilylated)**

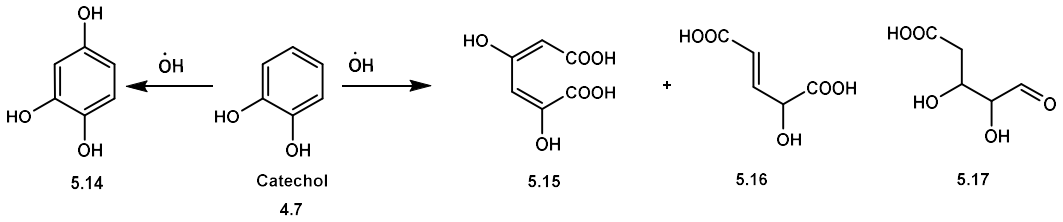

Figure 5.31. The reaction of catechol catalysed by SpMnSOD.

5.2.12.1. Mechanism of catechol transformation by SpMnSODs

Catechol **4.7** undergoes hydroxylation to produce compound **5.14**. The results also indicate that ring cleavage occurred and several products were generated, of which three were observed (compound **5.15**, **5.16** and **5.17**). Several possible mechanisms for fragmentation of catechol ring, either reaction of catechol with hydroxyl radical, or reaction with dioxygen or superoxide, are possible. Reaction of hydroxyl radical with catechol or its derivative can lead to intradiol or extradiol cleavage (see Figure 5.32). Compound **5.15** can be generated from compound **5.14** via intradiol or extradiol ring opening mechanism**.** The extradiol cleavage product of compound **5.14** can undergo decarboxylation and formation of compound **5.16**, but its intradiol cleavage product is less likely to lose one carbon atom to generate compound **5.16**. Whereas Compound **5.17** is most likely formed from extradiol cleavage of catechol after losing one carbon as CO_2 and hydroxylation (see Figure 5.33). In case of reaction of dioxygen with semiquinone generated by •OH, an intermediate known as dioxetane would form and then the ring cleavage will occur (see Figure 5.34). Cleavage of catechol and its derivatives can also be triggered by superoxide radical anion, it has been reported that KO_2 in DMSO can attack catechol to produce extradiol cleavage product (2-hydroxymuconaldyhyde) [192].

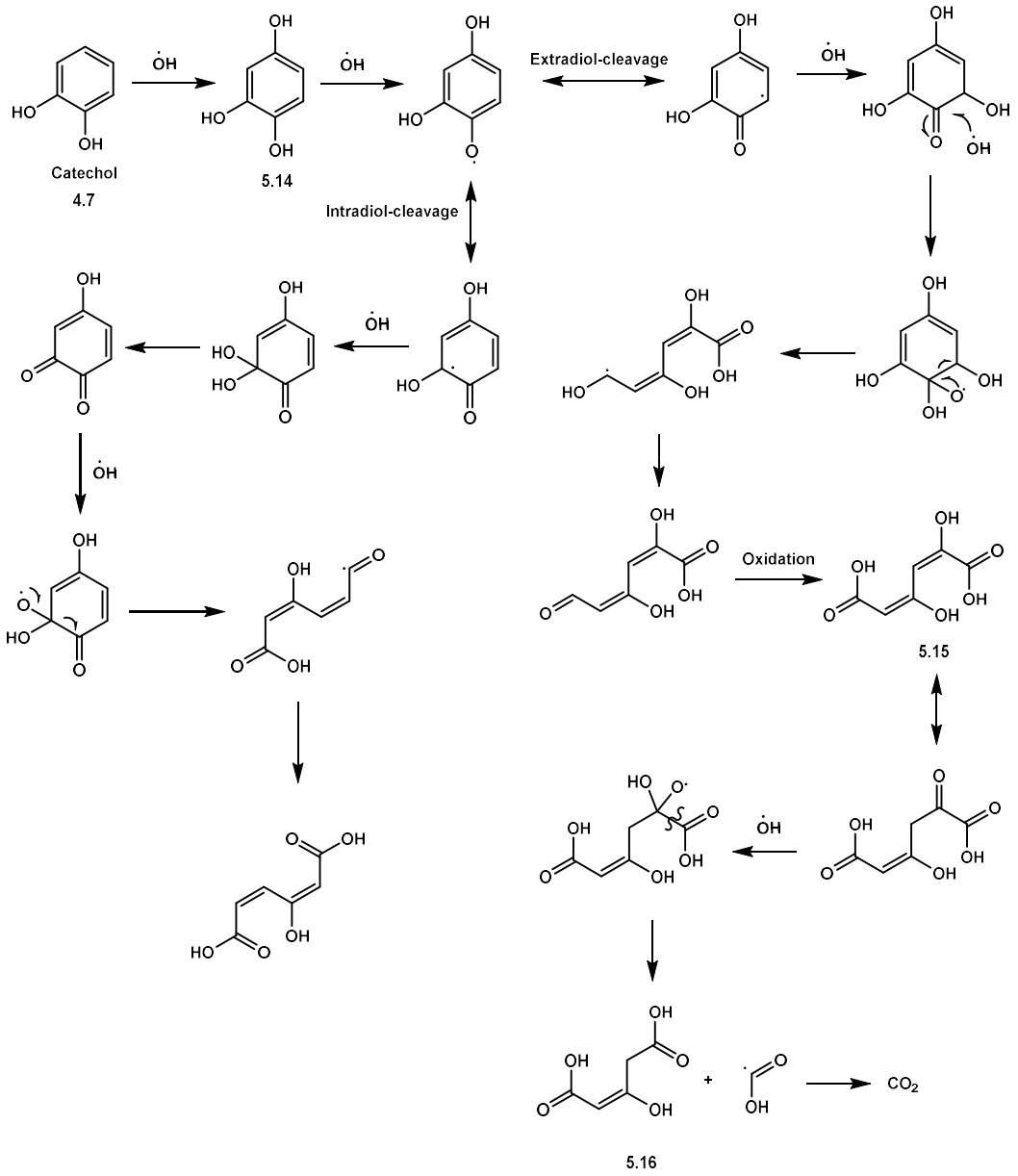

Figure 5.32. Proposed mechanism of catechol conversion by hydroxyl radical.

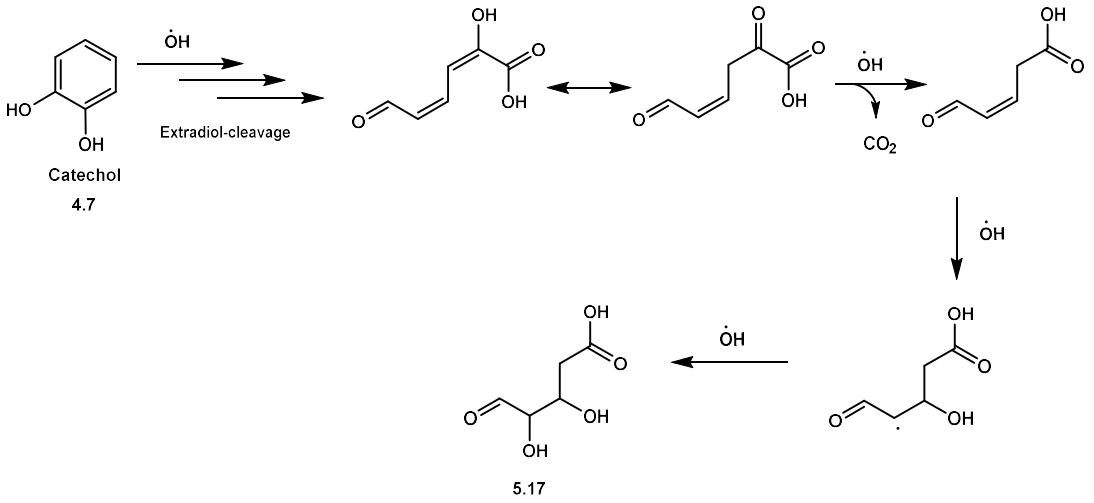

Figure 5.33. Proposed mechanism for formation of compound **5.17**.

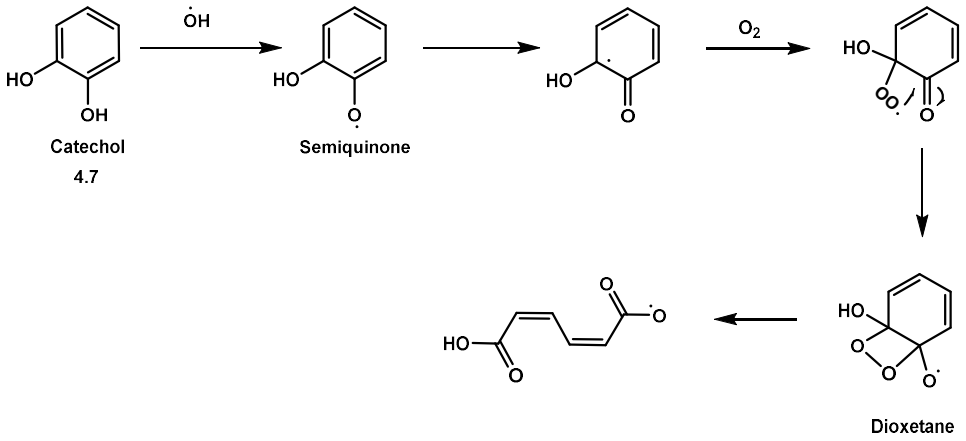

Figure 5.34. Reaction of oxygen with semiquinone.

5.3. Conclusion

The SpMnSOD enzymes can catalyse the breakdown of three lignin model compounds and a range of the monocyclic aromatic compounds examined. Multiple reaction products and several type of reactions were observed with all most all substrates. The SpMnSOD enzymes have not shown specificity toward certain type of linkage or functional group in lignin. The type of reactions catalysed by these

enzymes (listed in Table 5.16 with some examples) and products identified confirms the involvement of hydroxyl radical.

Table 5.16. Type of reactions catalysed by SpMnSOD enzymes.

Reaction types	Example of substrates involved
C_α-C_β oxidative cleavage	β-aryl ether, Pinoresinol and Ferulic acid
Aryl-C_α oxidative cleavage	β-aryl ether and Acetovanillone
Decarboxylation	β-aryl ether, 5,5`-DDVn, Ferulic acid, , Veratryl alcohol, 4-Hydroxybenzoic acid, Salicylic acid, 4-Hydroxybenzaldehyde, Acetovanillone, vanillic acid, Vanillin and 5-carboxyvanillic acid
Demethoxylation	Pinoresinol, Ferulic acid, Veratryl alcohol, Acetovanillone, 4-(1-hydroxyethyl) guaiacol, vanillic acid, Vanillin, 5-carboxyvanillic acid and Guaiacol
Hydroxylation of phenol	4-Hydroxybenzoic acid, Salicylic acid, 4-Hydroxybenzaldehyde, Acetovanillone, 4-(1-hydroxyethyl) guaiacol, vanillic acid, Vanillin, , 5-carboxyvanillic acid, Catechol and Guaiacol
Dihydroxylation of alkene	Ferulic acid and Catechol
Ipso-substitution by –OH group	β-aryl ether, Veratryl alcohol, Salicylic acid, Acetovanillone, 4-(1-hydroxyethyl) guaiacol, vanillic acid, Vanillin and 5-carboxyvanillic acid
Oxidative aromatic ring cleavage	5,5`-DDVn and Catechol
Benzylic oxidation	Pinoresinol

6. Conclusions

It has been demonstrated that functional screening of genomic DNA libraries for lignin-degrading enzymes can be performed in liquid medium for inducible gene constructs in *E. coli* after lysing cells using ABTS as a substrate. It has also been proved that conducting functional screening for ligninases is difficult to perform on solid agar plates, since the screening process includes addition of several reagents. In addition, the cells needed to be lysed as the substrates cannot be taken by *E. coli*. Thus, on the basis of these findings, a functional screening method has been adopted.

The results of screening of genomic DNA libraries of *Sphingobacterium* sp. T2 using the adopted screening method suggest that there are no lignin peroxidase or laccase enzymes in the genomic DNA libraries of the strain, which may indicate that *Sphingobacterium* sp. T2 lacks these enzymes and that a different type of enzyme may be responsible for its high lignin degradation ability. Two enzyme candidates have been identified based on bioinformatics and proteomic analysis; catalase peroxidase (KatG) and superoxide dismutase (SOD1 and SOD2).

It was shown that *Sphingobacterium* sp. T2 KatG displayed weak oxidation ability toward some common lignin peroxidase substrates (guaiacol, DCP, and ABTS) and it cannot degrade β-aryl ether lignin model compounds as homologous enzyme from *Amycolatopsis* sp. 72vi2.

On the other hand, SOD enzymes displayed high activity for oxidation of Organosolv lignin producing multiple reaction products. It has also been illustrated that these enzymes (SOD1 and SOD2) can degrade Kraft lignin, lignocellulose (pine), 3 lignin model compounds and 12 monocyclic aromatic compounds.

It has been presented that both SpMnSOD enzymes are manganese containing enzymes. It was also shown that SpMnSODs do not possess any specificity toward certain lignin model compounds or monocyclic aromatic compounds. Through structure of the reaction products, the oxidizing species responsible for high reactivity of these enzymes (SpMnSOD1 and SpMnSOD2) has been proposed and several types of reactions catalysed by SpMnSODs have been recognised which include: C_α-C_β oxidative cleavage, aryl-C_α oxidative cleavage, decarboxylation, demethoxylation, hydroxylation of phenolic compounds, Ipso-substitution by –OH group, dihydroxylation of alkene, oxidative aromatic ring cleavage and benzylic oxidation.

This is the first demonstration that shows the direct involvement of superoxide dismutase in the depolymerisation of lignin. The discovery of novel enzymes such as SpMnSODs could in principle enable synthetic biology to be used in the production of valuable chemicals from Organosolv lignin or Kraft lignin, and even from raw material such as untreated lignocellulose (pine powder).

7. Experimental

7.1. General information

All chemical reagents and solvents were purchased from Sigma-Aldrich UK, VWR, Fischer Scientific or Invitrogen unless otherwise stated and were used as received. All experiments were performed at room temperature (about 23°C). All biological procedures were conducted under sterile conditions.

Organosolv Lignin (from CIMV company, France) provided by C. Taylor. Alkali lignin purchased from Sigma-Aldrich. The source of lignocellulose in experiments were miscanthus and pine milled in a Retsch grinding mill (model RM 200) sieved through a 0.5 mm mesh.

Genomic DNA libraries of *Sphingobacterium* sp.T2 and *M. phyllosphaerae* were provided by prof. E. Willington, Life Science, University of Warwick. Table 7.1 is a summary of the DNA libraries.

Table 7.1. Summary of libraries provided

Type of libraries	Strains	Type of vector	Average insert size	estimated the size of the genome
Plasmid	*Sphingobacterium* sp.	pCF430 (Figure 7.1)	4.75 Kbp	3.4 Mbp
Plasmid	*M. phyllosphaerae*	pCF430	N/A	N/A

Fosmid	*Sphingobacterium sp.*	CopyControl™pCC2FOS™ (Figure 7.2)	35 kbp	3.4 Mbp

The plasmid libraries of both of *Sphingobacterium* sp. T2 and *M. phyllosphaerae* were transformed into Transformax EC100 electrocompetent *E. coli* cells (Epicentre). Twelve colonies of each of *Sphingobacterium* sp. T2 and *M. phyllosphaerae* plasmid libraries were picked for estimation of total genome coverage. For *Sphingobacterium* sp. T2 library, 33.3% of clones has an insert of average size 4.75 Kb while *M. phyllosphaerae* library contains no insert in 12 clones tested. The estimated size of *Sphingobacterium* sp. T2 genome was 3.45 MB. The Fosmid libraries were prepared using CopyControl™ Fosmid Library Production Kit. The average size of fragments is 35 kb. They were transformed into TransforMax™ EPI300™ *E. coli*.

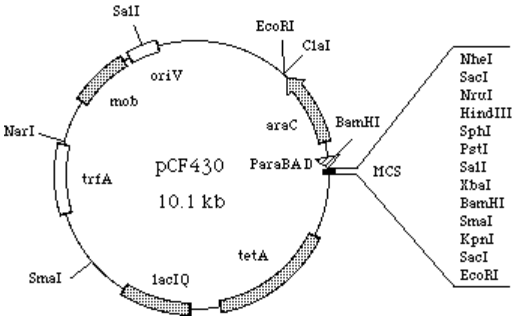

Figure 7.1. pCF430 vector map.

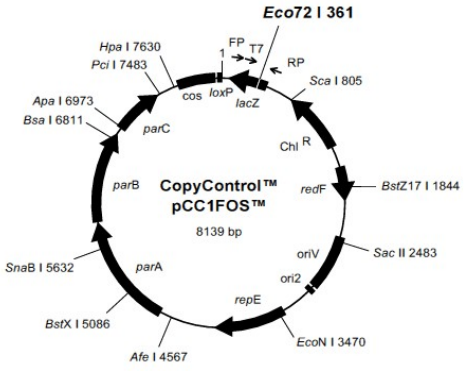

Figure 7.2. pCC1FOS™ vector map.

The *mco* and *DypB* constructs (from *Rhodococcus jostii* RHA1) were kindly provided by Dr. E. Hardimam. Dimeric lignin model compound (2-(2, 6-dimethoxyphenol)-1-(4-hydroxy-3,5-dimethoxyphenyl)-1, 3-propanediol)

synthesised by M. Ahmed. 5,5'-Dehydrodivanillin and 2-methoxyhydroqunone were synthesised by Y. Liu.

7.1.1. Laboratory instruments and equipment

The tools and equipment used are listed below:-

Balances	Oxford A1204.
	SartΦrius laboratory L2200P
Autoclave	Prioclave autoclave
Shakers	Innova 44 shaker
	Innova 4300 shaker
Centrifuges	Fisher Scientific AccuSpin Microcentrifuges
	Eppendorf Centrifuge5415R
	Eppendorf models 5810R or 5804R.
	Sorval Rc 6 Plus centrifuge with an SLA-3000.
Spectrophotometers	Thermo BioMate3 spectrophotometer
	Varian Cary 1 UV/ Visible
	Varian Cary 50 Bio UV/ Visible
	GENios Microplate Reader (Tecan, Switzerland)
	NANODROP LITE Spectrophotometer (Thermo Scientific)
Thermocycler	Eppendorf Mastercycler Personal.

Electrophoresis system	BioRad Mini-protein BioRad Mini-Sub Cell GT system (Agarose gel electrophoresis)
Transilluminator	UVP Ultraviolet (UV) transilluminator
Cell disrupter	pneumatic cell disrupter (ConstantSystems, UK)
Fast Protein Liquid Chromatography (FPLC)	ÄKTAFPLC system consisting of a P-920 system pump connected to a UPC-900 monitor (GE Healthcare, UK).
High-performance liquid chromatography (HPLC)	Agilent 1100 Series, Agilent Technologies, Cheshire, UK equipped with:- quaternary pump (G1311A) and photodiode array detector (G1315A). Agilent 1200 Series, Agilent Technologies, Cheshire, UK equipped with:- quaternary pump (G1311A) and variable wavelength UV detector (G1314B)
Gas chromatography-mass spectrometry (GC-MS)	ion trap mass spectrometer Varian 4000 GC-MS system with silica capillary column (30 m x 0.25 mm)
Liquid chromatography-mass spectrometry (LC-MS)	Agilent 1200 Series system equipped with a DAD photodiode detector (G1315B) connected to a Bruker HTC-Ultra ESI mass spectrometer (Coventry, UK)

Low-resolution ESI mass spectra	Bruker Esquire 2000

7.1.2. Buffers and solutions

Buffers and solutions prepared according standard procedures unless otherwise specified. All solution and buffers were made with deionized water. Buffers were filtered through 0.2 μm filter or autoclaved then stored at 4°C [193].

5x M9 salts	64 g Na_2HPO_4-$7H_2O$
	15 g KH_2PO_4
	2.5 g NaCl
	5.0 g NH_4Cl
	H_2O added to 1000 mL
	Sterilize by autoclaving
M9 media	200 mL of M9 salts
(minimal medium)	2 mL of 1 M $MgSO_4$ (sterile)
	20 mL of 20% glucose (or another carbon source)
	100 μL of 1 M $CaCl_2$ (sterile)
	H_2O added to 1000 mL

Trace element solution	5 g of Citric Acid, 5 g of $ZnSO_4 \cdot 7H_2O$, 1 g of $Fe(NH_4)_2(SO_4)_2.6H_2O$ 0.25 g of $CuSO_4 . 5H_2O$ 0.05 g of H_3BO_3 0.05 g of $Na_2MoO_4.2H_2O$ H_2O added to 1000 mL Sterilize by autoclaving
Luria-Bertani (LB) medium	1 g Bacto-tryptone 0.5 g Bacto-yeast extract 1 g NaCl H_2O added to 100 mL pH adjusted to 7.2; autoclaved
LB agar	1.5 g Bacto agar 100 mL LB medium added to autoclaved
Potassium phosphate buffer	100 mM pH 7.5 16 mL of solution A (200 mM KH_2PO_4 (27.2 g/L))

	84 mL of solution B (200 mM K_2HPO_4 (34.8 g/ L))
	H_2O added to 200 mL
Tris-HCl buffer	100 mM pH 8
	12.1 g Tris base in 800 mL H_2O
	pH adjusted to 8.0 with HCl
	H_2O added to 1 liter
Glycine-HCl buffer	200 mM pH 3.0
	50 mL of solution A (200 mM Glydine (1.5 g/L))
	11.4 mL of solution B (200 mM HCl (17.18 g/L))
	H_2O added to 200 mL
Glycine-NaOH buffer	200 mM pH 10.0
	50 mL of solution A (200 mM Glycine (15 g/L))
	32 mL of solution B (200 mM NaOH (8 g/L))
	H_2O added to 200 mL
Acetate buffer	200 mM pH 5.0
	50 mL of solution A (200 mM Acetic acid (11.55 g/L))
	32 mL of solution B (200 mM sodium acetate (16.4 g of $C_2H_3O_2Na$/

	L))
	H_2O added to 200 mL
Antibiotics	100 mg/mL Ampicillin;
	40 mg/mL Kanamycin
	30 mg/mL Chloramphenicol in ethanol
	24 mg/mL Tetracycline in ethanol
4x SDS-PAGE	2.5 mL of 500 mM Tris-HCl pH 6.8
Sample buffer	2 g of Glycerol
	0.4 g of SDS
	20 mg of Bromophenol Blue
	400 µL of 2-Mercaptoethanol
	H_2O added to 5 mL
SDS-PAGE	3 g of Tris base
running buffer	14.4 g of Glycine
	1 g of SDS
	pH adjusted to 8.3
	H_2O added to 1000 mL

6x DNA loading dye	200 mg of Bromophenol Blue
	60 mL of Glycerol
	40 mL of 60 mM EDTA
Coomassie	0.1 g Coomassie R250
staining solution	10 mL glacial acetic acid
	40 mL methanol
	50 mL water
De-stain for Coomassie	100 mL methanol
	50 mL glacial acetic acid
	350 mL water
Dithiothreitol (DTT)	1 M
	1.55 g of DDT
	H_2O added to 10 mL

7.1.3. Bacterial Strains

Unless otherwise stated all bacterial strains were the property of the chemical biology department, University of Warwick.

The following wild-type strains were used:

- *Rhodococcus erythropolis*
- *Microbacterium phyllosphaerae*
- *Microbacterium Luteus*
- *Sphingobacterium* sp. T2
- *Bacillus subtilis* DSMZ 10

The following *Escherichia coli* were used:

- *E. coli* DH5α
- *E. coli* BL21 (DE3)

7.2. Methods

7.2.1 Culture condition

The bacterial strains (Section 7.1.3.) were grown in Luria-Bertani (LB) medium (1% w/v tryptone 0.5% w/v yeast extract 0.5% NaCl in distilled water), from a single colony. Stocks of bacteria were stored at -80° C in cryovials of 10% glycerol (v/v). LB agar plates were produced by the addition of 1.5% Bacto-Agar in LB broth. Overnight cultures were grown in 50 mL glass tubes in a shaking incubator (180 rpm) at 37°C unless otherwise stated. LB-agar plate cultures were incubated statically at 37°C. When required media was supplemented with antibiotics at the concentrations and solvents shown in Section 7.2. All antibiotics were filter sterilised.

7.2.2. Nitrated substrates

All nitrated substrates (nitrated-milled wood lignin, nitrated-Alkaline lignin and nitrated-β-aryl ether) have been provided kindly by C. Taylor except nitrated organosolv lignin which was prepared as follows.

7.2.3. Nitration of organosolv lignin

The nitration of lignin (organosolv) was performed as demonstrated previously [62]. To 25 mg of lignin 5 mL of glacial acetic acid was added, shaken and stirred, then filtered. Concentrated nitric acid (5 drops) was added to the supernatant, and the reaction mixture was stirred under foil at for one hr. After one hour at room temperature water (2 mL) was added and the mixture was neutralised to pH 7 using

NaOH (1.0 M). The resulting yellow solution was diluted 25-fold with Tris-HCl buffer pH 7.4 and used as stock solution UV-vis assay.

7.2.4. Nitrated spray test on Luria Broth agar plates

Five LB agar plates for each of bacterial strains were streaked and grown overnight at 37ºC or 45ºC (for *Sphingobacterium* sp. T2). One of these plates for each bacterial strain was sprayed with nitrated- MWL, Alkaline lignin, Organosolv Lignin or nitrated β-aryl ether (4 mg/ 100 mL) and the others were sprayed with sterilised distilled water. After 1 and two days, the plates were checked for colour development.

7.2.5. Nitrated spray test on minimal media agar plates

The above protocol was used, but instead of LB agar media M9 media agar plates (for 100 mL, 1,128 g of 5 x M9 salts, 1.5 g of agar, 2 mL glucose (1 M), 200 µL $MgSO_4$ (1 M), 10 µL and $CaCl_2$ (1 M)) were used.

7.2.6. Nitrated lignin UV-vis assay

A total of 10 mL of LB media was inoculated with a single colony of each of *M. Phyllosphaerae*, *Sphimgobacterium sp*., *M. Luteus* and *R. erythropolis* under sterile conditions. All strains were incubated overnight at 37 ºC (except for S*phingobacterium sp.* T2, which was grown at 45ºC). When the OD_{600} of cultured solutions reached 0.7 to 0.9, the solutions were centrifuged at 10,000 rpm for 5 min and supernatants were used in the assay.

The assay was carried out as previously described [62]. Nitrated lignin substrates (160 µL), bacterial supernatants (30 µL), and Tris buffer pH 7.4 (10 µL) or 2 mM final concentration of H_2O_2 in the same buffer (10 µL) were added to each well of a 96 well plate. For experimental controls, the cultural supernatant was replaced with Tris buffer pH 7.4. The concentration of nitrated lignin substrates were 4 mg/ 100 mL and the absorbance was measured at 430 nm over 20 min at 1 min intervals using a TECAN GENios plate reader.

7.2.7. Testing different substrates with *E. coli* containing *dypB* and *mco* constructs on agar plates.

The recombined *dypB* and *mco* were prepared previously in the Bugg group. In addition, the empty vector which was used for the recombination process and the recombined *dypB* were transformed into *E. coli* BL21. Therefore, recombined *mco* was transformed into *E. coli* BL21 using protocol described bellow:-

Transformation of recombined mco into E. coli BL21star (DE3) one shot®

One vial of BL21 cells was thawed on ice then 2 µL of plasmid DNA containing mco construct (5-10 ng) was added and mixed gently with the pipette tip. The mixture was incubated for 30 min on ice. Heat shock was performed by transferring the mixture into a water bath for 30 seconds at 42ºC without shaking, and then the mixture was returned to the ice immediately. At room temperature, 250 µL of S.O.C medium was added to the transformation mixture and vial capped tightly. For better aeration, the vial was taped on its sides then incubated at 37ºC for 30 min with shaking (200 rpm). Finally, 100 µL of the transformation reaction plated on LB agar plates containing 30 µg / mL Kanamycin.

For developing a screening method *E. coli* strains containing *dypB*, *mco* and control (empty vector) were used to imitate DNA examine known lignin degrading enzyme substrates. Several substrates have been reviewed in four different ways as following:-

1. The addition of the substrates into media before plating.
2. Spraying of the substrates after growth.
3. The addition of the substrates to wells on agar plates (produced by cutting agar).
4. The addition of the secondary agar layer containing substrates on to grown *E. coli* plates.

All of these approaches minimal medium ((for 100 mL, 1,128 g of 5 x M9 salts, 2 g of agar, 2 g glucose, 200 µL $MgSO_4$ (1M), 10 µL, $CaCl_2$ (1M) and Kanamycin (30 µg /mL)) were used as basal medium, but in some of theses methods additional materials were added (see bellow for details).

7.2.7.1. The addition of the substrates into the medium before plating.

The concentration for each of the substrates, IPTG and H_2O_2, are listed in Table 7.2. The substrates to be tested were filter sterilised and added to the basal medium with IPTG. For each experiment, three plates were streaked with the *E. coli* strains containing *dypB*, *mco* constructs and control, separately. The plates were incubated at 37ºC for 24 hrs. When the bacterial colonies were visible (after 24 hrs), H_2O_2 or veratryl alcohol were sprayed. Subsequently, all plates were compared with their corresponding control daily up to 10 days.

Table 7.2. Concentration of substrates, IPTG and H_2O_2 used in the method described above (Section 7.2.7.1).

Substrates	Final concentration		
	Substrate	IPTG	H_2O_2
ABTS	1, 4, 8 & 16 mM	0, 0.5 &1 mM	0, 2, 5 & 10 mM
DCP *	0.1 mM	0.5 mM	0 & 10 mM
Guaiacol	4 & 8 mM	0, 0.5 &1 mM	0, 2, 5 & 10 mM
Remozal B B R	0.04 % (w/v)	0 & 0.5 mM	0 & 2, mM
Azure B	0.01 % (w/v)	0 mM	0 mM
Phenol Red	0.01 % (w/v)	0 mM	0 mM
Tannin	0.1 % (w/v)	0 mM	0 mM
Bromophenol Blue	0.1 mM	0 & 0.5 mM	2 mM Veratryl alcohol
Methylene Blue	0.1 mM	0 & 0.5 mM	2 mM Veratryl alcohol

*4-Aminoantipyrine was also added to DCP in the ratio of 1:5.6.

7.2.7.2. Spraying of the substrates after growth.

Strains were plated on basal medium containing $CuSO_4$ at 1 mM final concentration and incubated overnight at 37ºC then plates were sprayed with IPTG (20 mM) for inducing protein expression or with sterilised distilled water. The plates were incubated at room temperature overnight then sprayed with substrates (ABTS at 20 and 40 mM; Guaiacol at 50 mM; DCP at 10, 20, & 50 mM (4-Aminoanitpyrine was also added to DCP in ratio of 1:5.6); nitrated alkaline Lignin at 4 mg/mL) then

they were checked after 30 min, 1 hr, then daily until 10 days after any change in colour against their associated control. The experiments were repeated, but H_2O_2 (5, 10 & 50 mM), or sterilised water was sprayed after spraying of the substrates. When the sprayed H_2O_2 or water has been dried under sterile conditions, cell lysis reagent (CelLytic™ B 10×) was diluted 10 fold and sprayed onto the plates as well. The plates were checked for colour change after 30 min, 1 hour, 1 day and then daily up to 10 days at room temperature.

7.2.7.3. The addition of the substrates to wells on agar plates (well test).

Prior to streaking the recombinant *E coli* strains onto agar plates (basal medium with 0.2 % (w/v) urea, 0.01% (w/v) yeast extract, 0.001% (w/v) $FeSO_4$, 0.001% (w/v) $CuSO_4$, and 0.001% (w/v) $MnSO_4$) 5 equally distanced wells were cut on agar plates. The strains were induced after growth overnight at 37ºC by adding IPTG (1 mM; assuming the volume of agar medium in each plate as 20 mL) to wells and plates were incubated at 30ºC overnight. Subsequently, the substrates (few drops) were added to wells in agar plates. Each well in agar plates was used for testing the effect of H_2O_2 (0 or 1 mM) and/or cell lytic reagents, then plates were monitored for any change in colour after 30 min, 1 hour, 1 day and then daily up to 10 days at room temperature. The concentration and types each of substrates and cell lytic reagent is listed in Table 7.3.

Table 7.3. The concentration and types each of substrates and cell lytic reagents used in the well in agar plates test.

Substrates	concentrations	
	Substrate	Cell lytic reagents (50 µl)
ABTS	40 mM	C1 *R1,R2 & R3* and C2 *R1,R2 & R3*
DCP*	5 mM	C1 *R1* and C2 *R1*
Guaiacol	10 mM	C1 *R1,R2 & R3* and C2 *R1,R2 & R3*
Remozal B B R**	0.04 %	C1 *R1& R2* and C2 *R1& R2*

*4-Aminoanitpyrine was also added to DCP in the ratio of 1:5.6. ** added to the medium before pouring the agar. C1: concentrated reagent and C2: diluted reagent 1:2 with sterile water. R1: CelLytic ™ B 10X (Sigma-Aldrich), R2: BugBuster Protein Extraction Reagent (Novagen) and R3: B-PER Protein Extraction Reagents (Thermo).

7.2.7.4. The addition of the secondary agar layer containing substrates onto grown *E. coli* plates.

The *E. coli* strains containing recombined *dypB* and *mco* were cultured on primary agar (the same medium used in well test) at 37ºC overnight. The secondary agar layer (1% (w/v) agar and 30 µg/mL Kanamycin) were poured on it containing substrate (ABTS at 40 mM; Guaiacol 50 mM; Phenol red at 0.001% (w/v); Azure B at 0.001 and 0.002% (w/v) , separately) to be examined and IPTG (0.5 mM). After overnight incubation, the plates were checked for colour change daily up to 10 days.

7.2.8. Testing ABTS with *E. coli* containing *dypB* and mco constructs in liquid culture after lysing the cells.

7.2.8.1. Testing lysis ability of CelLyticTM B 10×.

Single colony of *E coli* strain containing recombined *dyp*B, or empty vector (pET200) was grown overnight in 10 mL of LB containing 30 µg/mL Kanamycin. Then 100 µL of the culture was transferred into fresh 10 mL of LB containing 30 µg /mL Kanamycin and incubated at 37ºC. When the OD600 of the culture medium was between 0.6-0.8 IPTG (0.5 mM final) was added and incubated overnight at 15ºC. After induction, the cells were harvested by centrifugation at (10000 rpm for 5min) the culture medium. The cells were lysed by adding 500 µL of CelLyticTM B (diluted 10 fold with 100 mM K-phosphate buffer pH 6) only, with sonication or lysozyme (1 mg/mL) added to buffer and incubated for 1 hr at 37ºC. The lysed culture solutions were centrifuged at 1600 rpm for 15 min. Finally, ABTS assay was used for detection (visually) of enzyme activity (100 µL ABTS in K-phosphate buffer (pH 6) with to 30 µL cell lysate and 70 µL of the same buffer with H_2O_2 (1 mM final concentration)).

7.2.8.2. Testing *E. coli* containing *dypB* and *mco* constructs in liquid culture after lysing the cells with lysozyme and Tween-20.

The above approach was repeated (Section 7.2.8.1.) for testing of *E coli* strain containing recombined *dypB*, mco or empty vector (pET200), but instead of using CelLytic^{TM} B a cell lysis reagent (100 mM K-phosphate buffer (pH 6) containing 1 mg/mL lysozyme and 0.25% (v/v) Tween 20) with incubated at 37ºC for 1 hr was used. Moreover enzymes activity was detected spectrophotometrically rather than

visually using the plate reader (TECAN GENios at 430 nm) with ABTS (100 µL ABTS in K-phosphate buffer (pH 6) with to 30 µL cell lysate and 70 µL of the same buffer with or without H_2O_2 (2 mM final concentration)).

7.2.9. Screening method for genomic libraries for LiP and laccases

The method included growing single bacterial colonies in 150 µL LB with antibiotic in sterile 96-well plates (300 µL capacity) overnight. Then diluting the culture medium 1:20 with fresh medium (800 µL) and transferring it into the 96-deep well (2 mL capacity). After 4 hrs (when, the OD_{600} is between 0.6-0.7) the cells will be induced by adding 0.5 mM IPTG (or another inducer) with 1 mM of each of $CuSO_4$, $FeSO_4$ and $MnSO_4$ and incubation overnight at 15ºC. The cells were harvested by centrifugation (1600 xg for 10 min). Then they were lysed with 500 µL of the lysis reagent (described in Section 7.2.8.2.), and the cell debris was removed by centrifugation (1600 xg for 15 min). Finally, the extracted enzymes were detected spectrophotometrically with the ABTS assay.

7.2.9.1. Pilot screening experiment

A single colony of each *E. coli* strain containing *dypB* construct and *E. coli* control (containing pET200 vector) were inoculated in 10 mL LB medium with Kanamycin (30 µg/mL) separately then incubated at 37ºC for 4 hrs. A total of 100 µL of *E. coli* containing *dypB* construct was mixed with 900 µL of *E. coli* control. 10 µL of the mixture was plated on LB agar containing Kanamycin (30 µg/mL). After overnight incubation at 37ºC, the colonies (about 100 colonies were chosen arbitrary) were used for screening using the method demonstrated in Section 7.2.9.

7.2.9.2. Preliminary screening experiment

For screening of *Sphingobacterium* sp.T2 plasmid libraries a screening method described in Section 7.2.9. was used.

7.2.9.3. Trial screening experiment

In this experiment the screening method in Section 7.2.9. was modified as follows:-

The whole plasmid libraries of *Sphingobacterium sp*. were divided between 190 well of sterile 96-well plates and one well per each plate was left as a control. They were grown overnight at 37ºC in 150 µL LB medium with tetracycline (12 µg /mL). A volume of 30 µL of overnight culture medium was transferred into new wells of 96-deep well plates which contain fresh LB (800 µL) with antibiotic (tetracycline 12 µg /mL) and grown at 37ºC until OD_{600} reached to 0.6. Subsequently the libraries were induced overnight at 15ºC by arabinose (50 mM) and 1mM (final concentration) of each of $FeSO_4$, $CuSO_4$, and $MnSO_4$ were also added. After induction the 96-well plate was centrifuged at 1600 rpm for 10 min then the cells were lysed by 500 µL of 100 mM K-phosphate buffer (pH 6) containing 1 mg/mL lysozyme and 0.25% Tween 20. The cell lysates were centrifuged (1600 rpm 15 min) and supernatants were checked for enzyme activity using the ABTS assay as described in previous section 7.2.8.

7.2.10. Bacterial genomic DNA extraction

Genomic DNA was isolated using Wizard SV Genomic DNA (Promega) kit according to the manufacturer's instructions. From 5 mL overnight cultures of

Sphingobacterium sp. T2 cells were harvested, the supernatant removed and the cells re-suspended in 600 µL of nuclei lysis solution and incubated at 80°C for 5 min. RNA was then digested using 3 µL of RNAse at 37°C for 15 min and the sample cooled to room temperature. Proteins were then precipitated with 200 µL of protein precipitation solution and vortexed vigorously for 20 sec before incubating on ice for 5 min. Precipitated proteins were then pelleted by 3 min 60 centrifugation at 13,000 xg and the DNA containing supernatant transferred to a clean tube containing 600 µL of isopropanol to precipitate the DNA. The DNA was then harvested by centrifugation (13,000 xg for 2 min) and the supernatant discarded. The pellet was washed with 70% ethanol (ice-cold) and harvested. The supernatant was discarded and the pellet allowed to dry before being re-suspended in nuclease-free water to the desired volume.

7.2.11. Plasmid DNA extraction

Plasmid DNA was isolated using GeneJET™ Plasmid MiniPerp Kit according to the manufacturer's instructions. Briefly, from 5 mL of overnight culture the bacterial cells are harvested and lysed by high alkaline conditions. The plasmid DNA is then neutralised and adsorbed on a QIAprep membrane, washed then eluted with nuclease free water.

7.2.12. Purification of PCR products

PCR amplicons required for further applications were purified to remove excess primer and nucleotides using a Wizard® SV Gel and PCR Cleanup Kit according to the manufacturer's instructions. Products excised from agarose gels

were purified using a GeneJET™ Gel Extraction Kit according to the manufacturer's protocol. Briefly, the agarose gel was dissolved and the DNA bound to a membrane. This was then washed and eluted with nuclease-free water.

7.2.13. Agarose gel electrophoresis

DNA preparations were routinely separated by agarose gel electrophoresis. Agarose concentration was 0.8%, and TAE buffer (40 mM tris-HCl acetate, 1 mM EDTA) was used. Gel Red was added to the gel as DNA staining agent. DNA samples were mixed with DNA loading buffer (0.25% (w/v) bromophenol blue, 30% (v/v) glycerol) to a ratio of 4:1 and loaded into the wells of the solid agarose gel submerged in TAE buffer and run at 80-100 V. All samples were compared to one Kilobase DNA ladder (Invitrogen™). The DNA was visualised on a UV transilluminator. Photographic records were taken using UV-Transilluminator.

7.2.14. Quantification of DNA by spectroscopy

The concentration of the DNA was measured by NANODROP 2000 spectrophotometer and 2 µL of elution buffer or water was used as blank. 2 µL of the plasmid was used for measurement. The NanoDrop method determines absorbance at 260 nm. A conversion factor of 50 for DNA for every unit of absorbance represents an estimated 50 µg/µL.

7.2.15. Cloning of SOD2

7.2.15.1. DNA restriction

DNA sequence encoding the second *SOD* gene (SODA2) was amplified by PCR and cloned into pET 28a^{+} using to restriction enzyme (Thermo Scientific^{TM} FastDigest BamHI and FastDigest NedI). PCR product was purified using purification kit. Digestion of plasmid and PCR product were performed according to the manufacturer's instructions. 20 units of enzymes (FastDigest BamHI and FastDigest NedI) were used in a reaction mixture containing a green buffer (Thermo), 10 µL of DNA and incubated at 37°C for 10 min in a water bath.

7.2.15.2. Ligation

The digested vector (pET28a^{+}) and PCR product separated on agarose gel and purified using method described in Section 7.2.13. The ligation reaction was set at 1: 3 vector to insert ratio and final reaction volume 20 µL. The vector (100 ng, 1 µL), 12 µL insert, 2 µL of 10x ligation buffer, 2 µL of T4-DNA-ligase (Thermo Scientific^{TM}) and 3 µL H_2O. The reaction mixture was incubated at room temperature overnight. The ligated mixture (3 to 5 µL) was used for transformation into competent bacteria.

7.2.15.3. Oligonucleotides

KatG primers were synthesised by Invitrogen™ while both SODA1 and SODA2 primers were synthesised by Sigma-Aldrich (Table 7.4). The oligonucleotides were centrifuged briefly and re-suspended in nuclease-free water to

a concentration of 100 mM. These solutions were diluted further to make 10 mM working solutions.

Table 7.4. Primers used in this study.

Primer name	Sequence (5'→3')	application
Sphingo_katG_F	CACC ATG AAC AAA GGA ATT GCA GGT GC	Amplification of *KatG* gene
Sphingo_katG_R	TTA ATT TTG ACG GGC AAT GAC ATC A	
SOD87-F	CAC CATG ATG AAG ATG AAT ATT TTT AAG ACT G	Amplification of *SOD1* gene
SOD87-R	TTA TTT TTT CAA GGC TTT CTC ATA TCG	
SOD2FW	GAT CTA CAT ATG ATG GAA ATC CAT CAC G	Amplification of *SOD2* gene
SOD2Re	ACT ATC GGA TCC TTA TTT TTT AGC AGC TGC	
MSOD2-F	CAC CATG GAA ATC CAT CAC GAT CGT C	Amplification of *SOD2* gene without sequence for leader peptide
MSOD2-Re	TTA TTT TTT AGC AGC TGC ATA GTT AG	

7.2.15.4. TOPO Cloning

The PCR products were purified as described prior cloning. The cloning of PCR products was performed using the Champion™ pET Directional TOPO

Cloning kit according to the manufacturer's instructions. The PCR product (2 µL), 1 µL of salt solution and 1 µL of vector mix in a final volume of 6 µL were incubated at room temperature for five minutes. Finally, the DNA was transformed.

7.2.15.5. Polymerase chain reaction (PCR)

The DNA fragments were amplified from the *Sphingobacterium* sp. T2 genome using primers listed in (Table 7.4). A master mix sufficient for all reactions was prepared, allowing for a 1 X reaction mix once the DNA template was added (45 µL of mix and 5 µL of the template). The standard reaction mix contained 5 µL of 10x Buffer, 1 µL of 50 mM MgSO4, 1.5 µL of 10 mM dNTPs, 1.5 µL of 10 mM of each primer and 0.4 µL of Platinum® Taq DNA Polymerase (Fermentas). PCR were carried out using thermocycler (Eppendorf) and the following cycling profile:

1. Initial denaturation 95°C 5 min.

2. Denaturation 95°C 30 s

3. Annealing 55, 58 and 53ºC for *KatG*, SOD1 and SOD2, respectively 30 s

4. Extension 72°C 2 min for *KatG* gene and 1 min for both *SOD* genes.

5. Cycle from step 2 to step 4 35x

6. Final extension 72°C 10 min

7. Storage 4°C hold

The PCR products were agarose gel extracted.

7.2.15.6. Screening for recombinant DNA

Three methods were employed for the screening of positive clones. The first method was fast screening using method in which colonies were grown on agar plates with appropriate antibiotic then digested with lysis solution (10% sucrose, 100 mM NaOH, 60 mM KCl, 5 mM EDTA, 0.25% SDS and 0.01% bromophenol blue). The cell lysates were analysed on an agarose gel. In the second method, colonies were grown up individually in 10 mL of LB and plasmid DNA isolated. The extracted plasmid was screened with restriction endonuclease profiles on agarose gel electrophoresis. The third procedure which used for finding recombinant DNA was PCR screening, in which isolated plasmid was used as a template. The primers used for producing initial PCR product (Table 7.4) was employed in this method for detection positive clone. The positive clones identified by these methods were sent for to GATC-biotechnology company for sequencing.

7.2.15.7. Chemical transformation into *E. coli* cells

After ligation plasmids had been first transformed to Dh5α - *E coli* strain and then the positive clones were transformed into BL21 *E coli* strain for overexpression. Frozen cells were thawed on wet ice and 5 µL of plasmid DNA added to one aliquot of cells for 30 minutes. Cells were then placed in a water bath at 42°C for 45 s and returned to the ice for 2 minutes before the addition of 250 µL of recovery media

SOC (10 mM $MgCl_2$, 10 mM $MgSO_4$ and 20 mM glucose in LB). Cells were incubated at 37°C for 1-2 hours. 50 µL, 100 µL and 150 µL aliquots were plated onto selective agar plates and incubated overnight at 37°C. An aliquot of cells without addition of the DNA was used as a negative control.

7.2.16. Overexpression of proteins

Single colonies of *E. coli* BL21 strain containing the recombinant gene were inoculated in 10 mL LB with suitable antibiotic, and the cultures were grown overnight. The overnight culture (10 mL) was used for inoculation of 500 mL LB with the same antibiotic and grown for 4 hrs approximately or until the culture reached mid-log phase. At an optical density at 600 nm between 0.6-0.80. the cells were induced with 0.5 mM IPTG unless otherwise stated. The culture was then incubated overnight at 18ºC with shaking at 220 rpm. The cells were harvested by centrifugation (5000 rpm, 15 min) and pellets frozen at -80ºC prior to use. The overexpression fusion protein was confirmed by SDS-PAGE analysis.

7.2.17. Purification of His-tagged protein using Immobilised ion affinity chromatography (IMAC) under native conditions

The induced cells were resuspended in lysis buffer (10 mM imidazole, 20 mM Tris in HCl, 0.5 M NaCl pH 8) at 1 mL to 1 g wet weight ratio and PMFS were added to a final concentration of 1 mM. Cells were disrupted with cell disruptor with one shot at 20 Kpsi. The disrupted cells were centrifuged at 11,000 rpm for 35 min. The supernatant was filtered with Whatman® 0.2 syringe filter. The soluble protein fraction was loaded onto a 5 mL equilibrated Ni-NTA column (Qiagen) with

washing buffer (20 mM imidazole, 20 mM Tris in HCl, 0.5 M NaCl pH 8) and washed with 20 mL of the same buffer. The retained protein was recovered using His elution buffer (300 mM imidazole, 20 mM Tris in HCl, 0.5 M NaCl pH 7.8). Protein fractions (unbound, washed and eluted) were analysed by SDS-polyacrylamide gel chromatography.

7.2.18. Sodium dodecyl sulphate SDS-polyacrylamide gel (SDS-PAGE)

Discontinuous SDS-PAGE was routinely used to separate protein preparation. The gel were prepared according to the method of Laemmli (1970). Resolving gels (12 %) were prepared by mixing 5.5 mL of 30% (w/v) acrylamide / bis-acrylamide , 2.82 mL of 1.5 mM Tris-HCl, pH 8.8, 3.77 mL dH_2O, 150 µL of 20% (w/v) SDS, 150 µL of 10 % (w/v) ammonium persulphate and 10 µL TEMED (Tetramethylethylenediamine). The stacking gel (4 %) was polymerised by mixing 0.5 mL of 30% (w/v) acrylamide / bis-acrylamide , 1.25 mL of 0.5 mM Tris-HCl, pH 6.8, 3.0 mL dH_2O, 25 µL of 20% (w/v) SDS, 25 µL of 10 % (w/v) ammonium persulphate and 7.5 µL TEMED. Protein samples were diluted with an equal volume of 2x loading buffer (0.1 M Tris-HCl, pH 6.8, 20 % (v/v) glycerol, 200 mM DTT, 4% (w/v) SDS, 0.2 % (w/v) bromophenol blue) and incubated at 95°C for 10 min. The samples were loaded into wells and the gel was run in SDS-PAGE running buffer (25 mM Tris, 192 mM glycine, 0.1 % SDS, pH 8.3) at 200 V until the dye front reached the bottom of the gel.

Protein visualisation

To visualise proteins resolved by SDS-PAGE, proteins were stained with Coomassie Blue reagent. Proteins were fixed for 1 hour in 40% methanol, 10% acetic acid then stained for 1 hour with Brilliant Blue G and prepared in (0.01 % in ethanol: water 95:5 (v/v)). The gel was soaked for 1 min in 25% methanol, 5% acetic acid then de-stained in 25% methanol until the bands were visible. The protein sizes were determined by comparing the migration of the protein band to a molecular mass standard (PageRuler Prestained Marker, Fermentas).

7.2.19. Gel filtration chromatography using Superdex 200

A superdex gel filtration column (10 X 300 mm) was equilibrated with 25 mL of 50 mM phosphate buffer, pH 7.8, 0.15 M NaCl at a flow rate of 0.5 mL/min. Then the enzyme fraction (1.5 mL) derived from IMAC column was applied in the same buffer for further purification. 1 mL fractions were collected and then analysed by SDS-PAGE. the absorbance monitored for at 280 nm.

7.2.20. PD10 column

Enzyme preparations were desalted, and/or their buffer exchanged using PD10 Sephadex G25 columns. The columns were prewashed with 25 mL of appropriate buffer, and then a 2.5 mL of sample was loaded onto the column. The protein was then eluted with 3.5 mL of buffer. Finally, the column was washed to remove any remaining salt from the column with approximately 25 mL of buffer prior to re-use.

7.2.21. Protein assays of Bradford [194]

The total protein content of enzyme preparations were determined using Bradford protein dye-binding reagent according to manufacturer's instructions. Bovine serum albumin at concentrations of 1.400, 1.00, 0.500, 0.250, 0.125 mg/mL were used as standards.

7.2.22. Enzyme assays

7.2.22.1. ABTS assay [84]

ABTS assay was carried out in 1 mL of 50 mM sodium acetate (pH 5) containing 0.5 mM ABTS, 4.0 mM H_2O_2, and the appropriate amount of KatG. Reactions were monitored at 414 nm(ε_{414} = 36.6 mM^{-1} cm^{-1}) which started with the addition of H_2O_2.

7.2.22.2. Guaiacol oxidation [84]

Guaiacol (100 μM) oxidation was monitored at 465 nm (ε=26.6 mM^{-1} cm^{-1}) in 1 mL of 50 mM sodium acetate (pH 5) with 4.0 mM H_2O_2 and a suitable amount of enzyme.

7.2.22.3. Mn oxidation [84]

In 50 mM sodium malonate (pH 4.5) reactions with 1-20 mM $MnSO_4$ and 4 mM H_2O_2 were performed. The formation of Mn^{3+}-malonate was monitored at 458 nm (ε_{458}, 1.93 mM^{-1} cm^{-1}). The reaction was started by the addition of H_2O_2.

7.2.22.4. Dye decolourising activity of KatG

The dye decolourising activities were assayed spectrophotometrically in 50 mM sodium acetate (pH 5). The reaction mixtures contained 20-250 µM of dyes and 5 µL of purified enzyme (100 µg/mL). The reactions were initiated by adding 4 mM H_2O_2 and the decrease in absorbance at appropriate wavelength (Table 7.5).

Table 7.5. List of dyes used in for measuring of dye decolourising activity of catalase-peroxidase KatG.

No	Dyes	λ max	Concentration
1	Azure B	651	50 µM
2	RBBR	595	80 µM
3	Bromophenol blue	590	20 µM
4	malachite green	616	20 µM
5	congo red	519	250 µM
6	orange G	510	250 µM
7	BBR250	555	100 µM
8	Bromothymol Blue	430	250 µM
9	Methyl orange	459	250 µM
10	Methylene blue	662	250 µM
11	Phenol red	460	250 µM

12	Reactive Black 5	579	20 µM

7.2.22.5. Veratryl alcohol [106]

Oxidation of veratryl alcohol was assayed by mixing 100 µM Veratryl alcohol appropriate amount of enzyme and 4 mM H_2O_2 in 50 mM sodium acetate (pH 5). The absorbance was measured at 340 nm (ε=93 $mM^{-1}cm^{-1}$).

7.2.22.6. Incubation of KatG with Lignocellulose

Powdered wheat straw lignocellulose (5 mg) was added to succinate buffer (3 mL, 50 mM, pH 5.5), and then KatG (100 µL, 1 mg/mL) added, followed by H_2O_2 (400 µL, 40 M). The resulting solution was incubated at 30 C for 4 hrs. Aliquots (1 mL) were taken at 1, 3, 5, 24, and 48 hrs. These fractions were analyzed by HPLC. Aliquots for HPLC (400 µL) were mixed with CCl_3COOH (100%, w/v, 40 µL), and the solution was then centrifuged for 4 min at 10000 rpm. The experiment was also repeated with hydrogen peroxide replaced with glucose (final concentration of 0.3 mM) and glucose oxidase (final concentration of 0.5 mg/mL). Both experiments were conducted with and without $MnCl_2$ (1 mM). HPLC analysis was carried out using a Phenomenex Luna 5 µm C18 reverse phase column (100 Å, 50 mm, 4.6 mm) on a Hewlett-Packard Series 1100 analyzer, at a flow rate of 0.5 mL/min, with monitoring at 310 nm. The gradient was as follows: 20 to 30% MeOH/H_2O over 5 min, 30 to 50% MeOH/H_2O from 5 to 12 min, and 50 to 80% MeOH/H_2O from 12 to 25 min.

7.2.22.7. Reaction of KatG with Lignin Model Compounds

In glass vials lignin model compounds (5 mM) were prepared in a 2 mL solution of acetone/water mixture (9:1). To this 3 mL succinate buffer (50 mM, pH 5.5), KatG (25 µL, 1 mg/mL) $MnCl_2$ (100 µL, 50 mM) and H_2O_2 (100 µL, 40 mM) were added. The resulting solution was incubated at 30 C for 48 hrs. Aliquots (1 mL) were taken at 1, 3, 5, 24, and 48 hrs and analyzed by HPLC. Samples were prepared for HPLC by adding CCl_3COOH to a final concentration of 10% w/v to each aliquot and centrifuged at 13000 rpm for 5 min prior to analysis. The solution was left for 1 hr and then diluted 100 fold with methanol/water (1:4) prior to injection. For each model compound, control in which KatG had been omitted was also run.

The experiments were repeated once more in which the H_2O_2 was not directly added to the reaction but generated by glucose oxidase (final concentration of 0.5 mg/mL) in the presence of glucose (final concentration of 0.3 mM).

The assay was repeated a further time without $MnCl_2$. The HPLC method was the same as those used in 7.2.22.6.

7.2.22.8. SOD activity

Two methods have been used for determination of SOD activity.

A: Pyrogallol assay performed with a slight modification of procedure reported [162]. Pyrogallol undergoes autoxidation at high pH, which can be inhibited by SOD enzyme. Inhibition of pyrogallol autoxidation was monitored at 325 to measure the formation of oxidized pyrogallol. In an assay, the enzyme (4 µL, 1 mg/mL) was

mixed with 986 µL of 50 mM Tris-HCl and 0.1 mM EDTA at pH 8.2. After pre-incubation for 5 min at 25°C, the reaction was initiated by adding of 10 µL of 10 mM pyrogallol solution in 10 mM HCl. The control experiment was carried out by replacing enzyme solution with buffer. The change of absorbance at 325 was measured every 30 s for 4 min at 23°C. A unit of an enzyme is defined as the amount of enzyme that inhibit the autoxidation rate of pyrogallol by 50%.

B: Ferricytochrome c assay [152]. In this assay, superoxide radicals have been generated enzymatically using xanthine/ xanthine oxidase system and cytochrome c as the indicator for superoxide radical anion. The assay mixture (1.0 mL) contained 50 µM xanthine, 20 µM cytochrome c, and 10 µL of purified SOD sample (3.5 mg/mL) 50 mM phosphate buffer (pH 7.8), 0.1 mM EDTA,. The absorbance at 550 nm was monitored with a spectrophotometer after the addition of 50 µL of a solution containing 0.2 units/mL xanthine oxidase. The rate of cytochrome c reduction was measured by replacing SOD with water. One unit of SOD was defined as the amount of enzyme, which inhibits the rate of cytochrome reduction by 50% at pH 7.8 and 23°C, calculated from the initial rate reaction.

7.2.23. Measuring metal content with ICP-OES

To determine the metal contents of SOD1 and SOD2, both enzyme purified and the 6His fusion tag was removed from a fraction of each enzyme. Samples were prepared by adding 3% nitric acid to 300 µL of 1 mg/mL purified SOD enzymes to make 5.0 mL using balance. Two series of the standard were used for calibration the ICP-OES spectrophotometer. The first set was containing a mixture of Cu^{2+}, Zn^{2+}, Fe^{2+} and Mn^{2+} in 3% nitric acid, with concentrations of 0.2, 0.4, 0.6, 0.8 and 2 mg/L.

The second series contain 0.2, 0.4, 0.6, 0.8, 2, 4, 6, 8, and 10 mg/L sulphur ($(NH_4)_2SO_4$) in 3% nitric acid.

7.2.24. Metal reconstitution

Removal and Reconstitution of the metal ions from SOD enzymes were performed following reported procedure [158]. To prepare Apoenzymes, purified SOD1 and SOD2 were treated first with 10 mM EDTA in 8 M urea/50 mM acetate buffer (pH 3.8) for 16 hrs at room temperature, then dialyzed sequentially against 8 M urea/50 mM acetate buffer (pH 3.8), 50 mM phosphate buffer (pH 7.0) containing 8 M urea and 50 mM phosphate buffer pH (7.0).

The reconstituted SOD1 and SOD2 with Fe^{2+} and Mn^{2+} were prepare by dialysing their apo-protein was dialyzed for 4 hrs by turns the following buffers at room temperature, 8M urea 50 mM acetate buffer 10 mM $FeSO_4$ or $MnSO_4$, pH 3.8; 8M urea 50 mM phosphate buffer 10 mM $FeSO_4$ or $MnSO_4$, pH 7.0; 4M urea 50 mM phosphate buffer 10 mM $FeSO_4$ or $MnSO_4$, pH 7; 2 M urea 50 mM phosphate buffer 10 mM $FeSO_4$ or $MnSO_4$, pH 7; 50 mM phosphate buffer 10 mM $FeSO_4$ or $MnSO_4$, pH 7; 50 mM phosphate buffer 0.5 mM EDTA, pH 7.0 [162].

7.2.25. Titration of SOD2 with different metal ions

Purified and fusion tag removed apo-SOD2 enzyme was incubated overnight at room temperature with various metal ions, Cu^{2+}, Zn^{2+}, Mn^{2+} and Fe^{2+}. The metal ions and enzyme were mixed in 20 mM MOPS buffer pH 7.4 to make 1 mL of 20 µM SOD2 solutions containing five different concentrations, 0, 5, 10, 20 and 40 µM for each metal ion. The superoxide dismutation activity was measured using pyrogallol

autoxidation assay. The activity of 20 µM SOD2 without metal ion was also measured.

7.2.26. Incubation of SpMnSODs with organosolv, Kraft lignin and lignocellulose and lignin model compounds

In 15 mL Falcon tube 5 mg wheat straw organosolv or Kraft lignin or lignocellulose (fine powdered miscanthus or pine) was added 2.9 mL phosphate buffer (50 mM, pH 7.8) containing 0.13 mM EDTA, to which 100 µL of SOD1 or SOD2 (8 µM, final concentration) was added. Dimethylsulphoxide (DMSO) was dried with molecular sieve A3.A saturated solution of superoxide was prepared by adding 150 mg of KO_2 with 10 mL of dried DMSO under nitrogen. 1 mL of a saturated solution of KO_2 to start the reaction. A control was also prepared in which SOD enzyme was replaced with the buffer. A liquates of 500 µL were taken at 30, 60 min and 5 hrs, to which 200 µL of 1 M HCl was used to stop the reaction.

7.2.27. Incubation of lignin model compounds with SOD1 and SOD2

In 7 mL glass vial, 2.5 mL of 50 mM NH_4HCO_3 buffer pH 7.8 containing 1.6 mM EDTA was added, to which 100 µL SOD1 or SOD2 (final concentration of 8-10 µM) and 400 µL of lignin model compound (10 mM of dimeric lignin model compounds or 100 mM monomeric lignin model compounds) were added. The reaction was started by addition of 1 mL of saturated KO_2. After 5 hrs, 1 mL of 1 M HCl was added to stop the reaction.

7.2.28. Analysis of degradation products

7.2.28.1. HPLC analysis

The reaction components was filtered using cotton wools and centrifuged at 13 rpm for 10 min, then 50 µL of filtrate was injected to Phenomenex Luna 5 µm C18 reverse phase column (100 Å, 50 mm, 4.6 mm) on a Hewlett-Packard Series 1100 analyzer, at a flow rate of 0.5 mL/min, with monitoring at 310 and 270 nm. The gradient was as follows: - 20 to 30% MeOH/H_2O over 5 min, 30 to 50% MeOH/H_2O from 5 to 12 min, and 50 to 80% MeOH/H_2O from 12 to 25 min

7.2.28.2. LC/MS analysis

Samples for LC/MS analysis were extracted with ethyl acetate (twice of the volume of the samples) then dried using rotary vacuum evaporator. The organic residues were redissolved in 50% of MeOH. The analysis of samples were started by injection of 30 µL to reverse phase column Phenomenex Luna 5 µm C18 (100 Å, 50 mm, 4.6 mm) on Agilent 1200 and Bruker HCT Ultra mass spectrometer, at a flow rate of 0.5 mL/min, with monitoring at 310 and 270 nm. The solvent system was water (A) and MeOH (B) containing 1% formic acid (for positive ionisation mode), starting with 5% of buffer B, 0-20 min %B increased to 30%, held 10 min, then %B risen to 100% from 30-45 min. 100% of buffer B held 8 min and in the following 8 min 5% B.

7.2.28.3. GC/MS analysis

The degradation products from SOD enzymes incubation were extracted with ethyl acetate; the organic layer evaporated to dryness. The residues were

reconstituted with dry chloroform (1 mL) and dried through glass pipettes filled with 50 mg of magnesium sulphate, then analysed by GC-MS directly or silylated with N,O-bis(trimethylsilyl)acetamide. Silylation reaction for GC-MS was carried out by mixing 200 µL of samples in dry solvent with 100 µL silylation mixture of chlorotrimethylsilane (TMCS), N,O-bis(trimethylsilyl)acetamide (BSA) (1:20) and 200 µL of pyridine at 60 for 1 hr and diluted by a factor of 10. The analysis was performed using a gas chromatograph-mass spectrometer (GC/MS/MS, Varian 4000) on a Varian Factor Four column (length= 30 m, i.d= 0.25 mm, thickness= 0.25 um). Electron impact mass spectra (EI-MS) were recorded at ionization energy of 70 eV. The temperature gradient was as follows: hold at 50°C for 1 min, oven temperature raised to 300°C at the rate of 7.5°C and then maintained for 5.67 minutes.

References

[1] R. C. Kuhad and A. Singh, *Biotechnology for Environmental Management and Resource Recovery*. New delhi: Springer India, pp. 3, 9, 161-189, 2013, DOI 10.1007/978-81-322-0876-1

[2] R. L. Howard, E. Abotsi, J. V. R. E. L, and S. Howard, "Lignocellulose biotechnology : issues of bioconversion and enzyme production," *African J. Biotechnol.*, vol. 2, no. December, pp. 602–619, 2003.

[3] J. Pérez, J. Muñoz-Dorado, T. de la Rubia, and J. Martínez, "Biodegradation and biological treatments of cellulose, hemicellulose and lignin: an overview.," *Int. Microbiol.*, vol. 5, no. 2, pp. 53–63, Jun. 2002.

[4] T. Jeffries, "Biodegradation of lignin-carbohydrate complexes," *Physiol. Biodegrad. Microorg.*, pp. 163–176, 1991.

[5] T. Q. Yuan, S. N. Sun, F. Xu, and R. C. Sun, "Characterization of lignin structures and lignin-carbohydrate complex (LCC) linkages by quantitative 13C and 2D HSQC NMR spectroscopy," *J. Agric. Food Chem.*, vol. 59, no. Lcc, pp. 10604–10614, 2011.

[6] G. Wallace, a. Chesson, J. a. Lomax, and M. C. Jarvis, "Lignin-carbohydrate complexes in graminaceous cell walls in relation to digestibility," *Anim. Feed Sci. Technol.*, vol. 32, pp. 193–199, 1991.

[7] P. D. Sainsbury, E. M. Hardiman, M. Ahmad, H. Otani, N. Seghezzi, L. D. Eltis, and T. D. H. Bugg, "Breaking down lignin to high-value chemicals: The

conversion of lignocellulose to vanillin in a gene deletion mutant of rhodococcus jostii RHA1," *ACS Chem. Biol.*, vol. 8, no. 10, pp. 2151–2156, 2013.

[8] V. Faraco, Ed., *Lignocellulose Conversion*. Berlin, Heidelberg: Springer Berlin Heidelberg, pp.1, 48 , 2013, DOI 10.1007/978-3-642-37861-4.

[9] A. Abe, K. Dusek, and S. Kobayashi, "*Biopolymers,*" Berlin, Heidelberg: Springer-Verlag, vol. 232, p. 5, 2010, DOI 10.1007/978-3-642-13630-6.

[10] P. M. Visakh, A. P. Mathew, and S. Thomas, "*Advances in Natural Polymers,*" Berlin Heidelberg: Springer-Verlag, vol 18, pp. 1–20, 2013, DOI 10.1007/978-3-642-20940-6

[11] R. Vanholme, B. Demedts, K. Morreel, J. Ralph, and W. Boerjan, "Lignin biosynthesis and structure.," *Plant Physiol.*, vol. 153, no. 3, pp. 895–905, Jul. 2010.

[12] N. P. Kutscha and J. R. Gray, *The potential of lignin research*, vol. 40, pp. 1-3, 1970.

[13] C. a. Gasser, G. Hommes, A. Schäffer, and P. F. X. Corvini, "Multi-catalysis reactions: New prospects and challenges of biotechnology to valorize lignin," *Appl. Microbiol. Biotechnol.*, vol. 95, pp. 1115–1134, 2012.

[14] P. M. Visakh, A. P. Mathew, and S. Thomas, "*Advances in Natural Polymers,*" Berlin Heidelberg: Springer-Verlag, vol 18, p. 255, 2013, DOI 10.1007/978-3-642-20940-6

[15] T. K. Kirk and R. L. Farrell, “Enzymatic ‘combustion’: the microbial degradation of lignin.,” *Annu. Rev. Microbiol.*, vol. 41, pp. 465–505, Jan. 1987.

[16] I. Brodin, “Chemical Properties and Thermal Behaviour of Kraft Lignins,” *M.Sc. Thesis,* KTH Royal Institute of Technology, 2009.

[17] M. Leisola, O. Pastinen, and D. Axe, “Lignin-Designed Randomness,” *BIOcomplexity.*, vol. 2012, no. 3, pp. 1–11, 2012.

[18] M. P. Pandey and C. S. Kim, “Lignin Depolymerization and Conversion: A Review of Thermochemical Methods,” *Chem. Eng. Technol.*, vol. 34, no. 1, pp. 29–41, 2011.

[19] J. Li, “Isolation of lignin from wood,” p. 57, 2011.

[20] M. Kosa, “Multistep and Direct Conversion of Lignin to Biofuels,” *Ph.D. Thesis*, Georgia Institute of Technology, pp.11-29, 2012.

[21] D. T. D’Souza-Ticlo, “The Lignin - Degrading Enzyme , Laccase from Marine Fungi ; Biochemical and Molecular Approaches,” *Ph.D. Thesis*, Institute of Oceanography, pp. 14-17, 2008.

[22] H. P. Blaschek and T. C. Ezeji, “Chapter 7 Science of Alternative Feedstocks Introduction,” *Sci. Altern. Feed.*, pp. 112–128, 2010.

[23] E. Genomes, “*Biotechnology for Environmental Management and Resource Recovery,*” New delhi, Springer India, pp. 161–189, 2013, DOI: 10.1007/978-81-322-0876-1.

[24] E. Sjostom, *wood chemistry: fundamentals and applications.* San Diego, California: Acadimic Press, Inc., p. 54 1993.

[25] R. Pettersen, "The chemical composition of wood," *Chem. solid wood,* pp. 1–9, 1984.

[26] T. Bugg, M. Ahmad, E. M. Hardiman, and R. Rahmanpour, "Pathways for degradation of lignin in bacteria and fungi," *Nat. Prod. Rep,* vol. 28, no. 12, pp. 1871-1960, 2011.

[27] W. Thompson and S. Meyer, "Second generation biofuels and food crops: Co-products or competitors?," *Glob. Food Sec.*, vol. 2, no. 2, pp. 89–96, Jul. 2013.

[28] A. Sakakibara, "A structural model of softwood lignin," *Wood Sci. Technol.*, vol. 14, no. 2, pp. 89–100, 1980.

[29] G. A. Smook, *Handbook for pulp & paper technologists*, 3rd editio., vol. 11, no. 2. Angus Wilde Publications, Inc, pp. 163-183, 2003.

[30] X. Zhao, K. Cheng, and D. Liu, "Organosolv pretreatment of lignocellulosic biomass for enzymatic hydrolysis," *Appl. Microbiol. Biotechnol.*, vol. 82, no. 5, pp. 815–827, 2009.

[31] F. Xu, J. X. Sun, R. Sun, P. Fowler, and M. S. Baird, "Comparative study of organosolv lignins from wheat straw," *Ind. Crops Prod.*, vol. 23, no. 2, pp. 180–193, 2006.

[32] Y. Sun, J. Wen, F. Xu, and R. Sun, "Fractional and structural characterization of organosolv and alkaline lignins from Tamarix austromogoliac," *Sci. Res. Essays*, vol. 5, no. 24, pp. 3850–3864, 2010.

[33] A. L. Macfarlane, R. Prestidge, M. M. Farid, and J. J. J. Chen, “Dissolved air flotation: A novel approach to recovery of organosolv lignin,” *Chem. Eng. J.*, vol. 148, no. 1, pp. 15–19, 2009.

[34] L. Mesa, E. González, C. Cara, M. González, E. Castro, and S. I. Mussatto, “The effect of organosolv pretreatment variables on enzymatic hydrolysis of sugarcane bagasse,” *Chem. Eng. J.*, vol. 168, no. 3, pp. 1157–1162, 2011.

[35] R. El Hage, N. Brosse, L. Chrusciel, C. Sanchez, P. Sannigrahi, and A. Ragauskas, “Characterization of milled wood lignin and ethanol organosolv lignin from miscanthus,” *Polym. Degrad. Stab.*, vol. 94, no. 10, pp. 1632–1638, 2009.

[36] L. P. Novo, L. V. A. Gurgel, K. Marabezi, and A. A. da S. Curvelo, “Delignification of sugarcane bagasse using glycerol-water mixtures to produce pulps for saccharification,” *Bioresour. Technol.*, vol. 102, no. 21, pp. 10040–10046, 2011.

[37] L. Jiménez, M. J. De La Torre, J. L. Ferrer, and J. C. García, “Influence of process variables on the properties of pulp obtained by ethanol pulping of wheat straw,” *Process Biochem.*, vol. 35, no. 1–2, pp. 143–148, 1999.

[38] X. Pan, C. Arato, N. Gilkes, D. Gregg, W. Mabee, K. Pye, Z. Xiao, X. Zhang, and J. Saddler, “Biorefining of softwoods using ethanol organosolv pulping: Preliminary evaluation of process streams for manufacture of fuel-grade ethanol and co-products,” *Biotechnol. Bioeng.*, vol. 90, no. 4, pp. 473–481, 2005.

[39] F. Solar, R., Gajdos, E., Kacikova, D., & Kacik, “A preliminary study on medium temperature uncatalyzed an acid catalyzed organosolv pulping of poplar wood.,” *Cell. Chem. Technol,* vol. 34, pp. 571–580.

[40] J. J. Bozell, C. J. O'Lenick, and S. Warwick, “Biomass fractionation for the biorefinery: Heteronuclear multiple quantum coherence-nuclear magnetic resonance investigation of lignin isolated from solvent fractionation of switchgrass,” *J. Agric. Food Chem.*, vol. 59, no. 17, pp. 9232–9242, 2011.

[41] M. Li, S. Sun, F. Xu, and R. Sun, “Successive Solvent Fractionation of Bamboo Formic Acid Lignin for Value-Added Application,” *Proceedings of the 55th International Convention of Society of Wood Science and Technology*, pp. 1–9, 2012.

[42] S. Bauer, H. Sorek, V. D. Mitchell, A. B. Ibáñez, and D. E. Wemmer, “Characterization of Miscanthus giganteus lignin isolated by ethanol organosolv process under reflux condition,” *J. Agric. Food Chem.*, vol. 60, no. 33, pp. 8203–8212, 2012.

[43] S. Zhu, Y. Wu, Q. Chen, Z. Yu, C. Wang, S. Jin, Y. Ding, and G. Wu, “Dissolution of cellulose with ionic liquids and its application: a mini-review,” *Green Chem.*, vol. 8, no. 4, p. 325, 2006.

[44] Y. Pu, N. Jiang, and A. J. Ragauskas, “Ionic Liquid as a Green Solvent for Lignin,” *J. Wood Chem. Technol.*, vol. 27, no. 1, pp. 23–33, 2007.

[45] J. Y. Kim, E. J. Shin, I. Y. Eom, K. Won, Y. H. Kim, D. Choi, I. G. Choi, and J. W. Choi, “Structural features of lignin macromolecules extracted with ionic

liquid from poplar wood," *Bioresour. Technol.*, vol. 102, no. 19, pp. 9020–9025, 2011.

[46] D. Fu, G. Mazza, and Y. Tamaki, "Lignin extraction from straw by ionic liquids and enzymatic hydrolysis of the cellulosic residues," *J. Agric. Food Chem.*, vol. 58, no. 5, pp. 2915–2922, 2010.

[47] L. Crowhurst, N. L. Lancaster, J. M. Pérez Arlandis, and T. Welton, "Manipulating solute nucleophilicity with room temperature ionic liquids," *J. Am. Chem. Soc.*, vol. 126, no. 37, pp. 11549–11555, 2004.

[48] L. Crowhurst, P. R. Mawdsley, J. M. Perez-Arlandis, P. A. Salter, and T. Welton, "Solvent-solute interactions in ionic liquids," *Phys. Chem. Chem. Phys.*, vol. 5, no. 13, p. 2790, 2003.

[49] S. S. Y. Tan, D. R. MacFarlane, J. Upfal, L. A. Edye, W. O. S. Doherty, A. F. Patti, J. M. Pringle, and J. L. Scott, "Extraction of lignin from lignocellulose at atmospheric pressure using alkylbenzenesulfonate ionic liquid," *Green Chem.*, vol. 11, no. 3, p. 339, 2009.

[50] J. B. Binder, M. J. Gray, J. F. White, Z. C. Zhang, and J. E. Holladay, "Reactions of lignin model compounds in ionic liquids," *Biomass and Bioenergy*, vol. 33, no. 9, pp. 1122–1130, 2009.

[51] C. Li, B. Knierim, C. Manisseri, R. Arora, H. V. Scheller, M. Auer, K. P. Vogel, B. a. Simmons, and S. Singh, "Comparison of dilute acid and ionic liquid pretreatment of switchgrass: Biomass recalcitrance, delignification and enzymatic saccharification," *Bioresour. Technol.*, vol. 101, no. 13, pp. 4900–4906, 2010.

[52] K. M. Holtman, H. M. Chang, and J. F. Kadla, “Solution-State Nuclear Magnetic Resonance Study of the Similarities between Milled Wood Lignin and Cellulolytic Enzyme Lignin,” *J. Agric. Food Chem.*, vol. 52, no. 4, pp. 720–726, 2004.

[53] J. J. Villaverde, J. Li, M. Ek, P. Ligero, and A. De Vega, “Native lignin structure of Miscanthus x giganteus and its changes during acetic and formic acid fractionation,” *J. Agric. Food Chem.*, vol. 57, no. 14, pp. 6262–6270, 2009.

[54] J. R. Obst and T. K. Kirk, “Isolation of lignin,” *Methods Enzymol.*, vol. 161, no. C, pp. 3–12, 1988.

[55] S. M. Geib, T. R. Filley, P. G. Hatcher, K. Hoover, J. E. Carlson, M. D. M. Jimenez-Gasco, A. Nakagawa-Izumi, R. L. Sleighter, and M. Tien, “Lignin degradation in wood-feeding insects.,” *Proc. Natl. Acad. Sci. U. S. A.*, vol. 105, pp. 12932–12937, 2008.

[56] S. A. Chambers, “The production, purification and catalytic utility of lignin peroxidase from "*Sporotrichum pulverulentum,*” *Ph.D. Thesis*, University of Warwick, pp. 1-26, 1989.

[57] M. E. Brown and M. C. Y. Chang, “Exploring bacterial lignin degradation,” *Curr. Opin. Chem. Biol.*, vol. 19, pp. 1–7, 2014.

[58] A. R. Hainal, A. M. Capraru, I. Volf, V. I. Popa, and A. Roxana, “LigninCarbon Source for the Cultivation of Some Rhodotorula Species,” *Cellulose Chem. Technol.*, vol. 46, pp. 87–96, 2012.

[59] V. S. K. Haider, J. Trojanowski, “Screening for Lignin Degrading Bacteria by Means of 14C-Labelled Lignins,” *Arch. Microbiol.*, vol. 6, pp. 103–106, 1978.

[60] L. E. and H. Sahm, “Degradation of Coniferyl Alcohol and Other Lignin-Related Aromatic Compounds by Nocardia sp. DSM 1069,” *Microbiol, Arch*, vol. 148, pp. 216– 220, 1981.

[61] M. Ahmad, J. N. Roberts, E. M. Hardiman, R. Singh, L. D. Eltis, and T. D. H. Bugg, “Identification of DypB from Rhodococcus jostii RHA1 as a Lignin Peroxidase,” *Biochemistry*, vol. 50, no. 23, pp. 5096–5107, 2011.

[62] M. Ahmad, “Development of novel assays for lignin breakdown and identification of a new bacterial lignin degrading enzyme,” *Ph.D. Thesis,* pp. 109-111, 2010.

[63] C. R. Taylor, E. M. Hardiman, M. Ahmad, P. D. Sainsbury, P. R. Norris, and T. D. H. Bugg, “Isolation of bacterial strains able to metabolize lignin from screening of environmental samples.,” *J. Appl. Microbiol.*, pp. 1–10, May 2012.

[64] K. M. DeAngelis, M. Allgaier, Y. Chavarria, J. L. Fortney, P. Hugenholtz, B. Simmons, K. Sublette, W. L. Silver, and T. C. Hazen, “Characterization of trapped lignin-degrading microbes in tropical forest soil,” *PLoS One*, vol. 6, no. 4, 2011.

[65] R. Chandra, A. Raj, H. J. Purohit, and A. Kapley, “Characterisation and optimisation of three potential aerobic bacterial strains for kraft lignin degradation from pulp paper waste,” *Chemosphere*, vol. 67, no. 4, pp. 839–846, 2007.

[66] S. Nishikawa, T. Sonoki, T. Kasahara, T. Obi, S. Kubota, S. Kawai, N. Morohoshi, and Y. Katayama, "Cloning and sequencing of the Sphingomonas (Pseudomonas) paucimobilis gene essential for the O demethylation of vanillate and syringate," *Appl. Environ. Microbiol.*, vol. 64, no. 3, pp. 836–842, 1998.

[67] K. M. DeAngelis, P. D'Haeseleer, D. Chivian, J. L. Fortney, J. Khudyakov, B. Simmons, H. Woo, A. P. Arkin, K. W. Davenport, L. Goodwin, A. Chen, N. Ivanova, N. C. Kyrpides, K. Mavromatis, T. Woyke, and T. C. Hazen, "Complete genome sequence of '*Enterobacter lignolyticus'* SCF1," *Stand. Genomic Sci.*, vol. 5, pp. 69–85, 2011.

[68] N. H. Rahman, N. a Rahman, S. Aziz, and M. a Hassan, "Production of Lignolytic enzymes by newly isolated bavteria from palm oil plantation soils," *BioResources*, vol. 8, no. 4, pp. 6136–6150, 2013.

[69] R. Chandra, A. Raj, H. J. Purohit, and A. Kapley, "Characterisation and optimisation of three potential aerobic bacterial strains for kraft lignin degradation from pulp paper waste.," *Chemosphere*, vol. 67, no. 4, pp. 839–846, 2007.

[70] X. F. Huang, N. Santhanam, D. V. Badri, W. J. Hunter, D. K. Manter, S. R. Decker, J. M. Vivanco, and K. F. Reardon, "Isolation and characterization of lignin-degrading bacteria from rainforest soils," *Biotechnol. Bioeng.*, vol. 110, no. 6, pp. 1616–1626, 2013.

[71] Y. C. Chang, D. Choi, K. Takamizawa, and S. Kikuchi, "Isolation of Bacillus sp. strains capable of decomposing alkali lignin and their application in

combination with lactic acid bacteria for enhancing cellulase performance," *Bioresour. Technol.*, vol. 152, pp. 429–436, 2014.

[72] D. W. S. Wong, "Structure and action mechanism of ligninolytic enzymes," *Applied Biochemistry and Biotechnology*, vol. 157, no. 2. pp. 174–209, 2009.

[73] T. D. H. Bugg, M. Ahmad, E. M. Hardiman, and R. Singh, "The emerging role for bacteria in lignin degradation and bio-product formation.," *Curr. Opin. Biotechnol.*, vol. 22, no. 3, pp. 394–400, 2011.

[74] M. Sundaramoorthy, K. Kishi, M. H. Gold, and T. L. Poulos, "Preliminary crystallographic analysis of manganese peroxidase from Phanerochaete chrysosporium.," *J. Mol. Biol.*, vol. 238, no. 5, pp. 845–848, 1994.

[75] M. Pérez-Boada, F. J. Ruiz-Dueñas, R. Pogni, R. Basosi, T. Choinowski, M. J. Martínez, K. Piontek, and A. T. Martínez, "Versatile peroxidase oxidation of high redox potential aromatic compounds: Site-directed mutagenesis, spectroscopic and crystallographic investigation of three long-range electron transfer pathways," *J. Mol. Biol.*, vol. 354, no. 2, pp. 385–402, 2005.

[76] W. Bao, Y. Fukushima, K. A. Jensen, M. A. Moen, and K. E. Hammel, "Oxidative degradation of non-phenolic lignin during lipid peroxidation by fungal manganese peroxidase.," *FEBS Lett.*, vol. 354, no. 3, pp. 297–300, 1994.

[77] F. J. Ruiz-Dueñas, M. Morales, E. García, Y. Miki, M. J. Martínez, and A. T. Martínez, "Substrate oxidation sites in versatile peroxidase and other basidiomycete peroxidases," *Journal of Experimental Botany*, vol. 60, no. 2. pp. 441–452, 2009.

[78] D. I. Colpa, M. W. Fraaije, and E. Van Bloois, “DyP-type peroxidases: A promising and versatile class of enzymes,” *J. Ind. Microbiol. Biotechnol.*, vol. 41, no. 1, pp. 1–7, 2014.

[79] D. Salvachúa, A. Prieto, Á. T. Martínez, and M. J. Martínez, “Characterization of a novel dye-decolorizing peroxidase (DyP)-type enzyme from Irpex lacteus and its application in enzymatic hydrolysis of wheat straw,” *Appl. Environ. Microbiol.*, vol. 79, no. 14, pp. 4316–4324, 2013.

[80] S. J. U. N. Kim and M. Shoda, “Purification and Characterization of a Novel Peroxidase from Geotrichum candidum Dec 1 Involved in Decolorization of Dyes,” *Appl. Environ. Microbiol.*, vol. 65, no. 3, pp. 1029–1035, 1999.

[81] M. Scheibner, B. Hülsdau, K. Zelena, M. Nimtz, L. De Boer, R. G. Berger, and H. Zorn, “Novel peroxidases of Marasmius scorodonius degrade β-carotene,” *Appl. Microbiol. Biotechnol.*, vol. 77, no. 6, pp. 1241–1250, 2008.

[82] E. Van Bloois, D. E. Torres Pazmiño, R. T. Winter, and M. W. Fraaije, “A robust and extracellular heme-containing peroxidase from Thermobifida fusca as prototype of a bacterial peroxidase superfamily,” *Appl. Microbiol. Biotechnol.*, vol. 86, no. 5, pp. 1419–1430, 2010.

[83] J. N. Roberts, R. Singh, J. C. Grigg, M. E. P. Murphy, T. D. H. Bugg, and L. D. Eltis, “Characterization of dye-decolorizing peroxidases from rhodococcus jostii RHA1,” *Biochemistry*, vol. 50, no. 23, pp. 5108–5119, 2011.

[84] R. Rahmanpour and T. D. H. Bugg, “Characterisation of Dyp-type peroxidases from Pseudomonas fluorescens Pf-5: Oxidation of Mn(II) and polymeric lignin by Dyp1B,” *Arch. Biochem. Biophys.*, vol. 574, pp. 93–98, 2015.

[85] M. E. Brown, T. Barros, and M. C. Y. Chang, “Identification and Characterization of a Multifunctional Dye Peroxidase from a Lignin-Reactive Bacterium,” *ACS Chem. Biol.*, vol. 7, no. 12, pp. 2074–2081, 2012.

[86] R. Singh, J. C. Grigg, W. Qin, J. F. Kadla, M. E. P. Murphy, and L. D. Eltis, “Improved Manganese-Oxidizing Activity of DypB, a Peroxidase from a Lignolytic Bacterium,” *ACS Chem. Biol.*, vol. 8, no. 4, pp. 700–706, Apr. 2013.

[87] P. Dwivedi, V. Vivekanand, N. Pareek, A. Sharma, and R. P. Singh, “Co-cultivation of mutant Penicillium oxalicum SAU E-3.510 and Pleurotus ostreatus for simultaneous biosynthesis of xylanase and laccase under solid-state fermentation,” *N. Biotechnol.*, vol. 28, no. 6, pp. 616–626, 2011.

[88] U. N. Dwivedi, P. Singh, V. P. Pandey, and A. Kumar, “Structure-function relationship among bacterial, fungal and plant laccases,” *J. Mol. Catal. B Enzym.*, vol. 68, no. 2, pp. 117–128, 2011.

[89] G. Alexandre and I. B. Zhulin, “Laccases are widespread in bacteria,” *Trends Biotechnol.*, vol. 18, no. 2, pp. 41–42, 2000.

[90] L. Ausec, M. Zakrzewski, A. Goesmann, A. Schlüter, and I. Mandic-Mulec, “Bioinformatic analysis reveals high diversity of bacterial genes for laccase-like enzymes,” *PLoS One*, vol. 6, no. 10, 2011, e25724. doi: 10.1371/journal.pone.0025724.

[91] A. Raj, S. Kumar, I. Haq, and S. K. Singh, “Bioremediation and toxicity reduction in pulp and paper mill effluent by newly isolated ligninolytic Paenibacillus sp.,” *Ecol. Eng.*, vol. 71, pp. 355–362, 2014.

[92] Z. M. Fang, T. L. Li, F. Chang, P. Zhou, W. Fang, Y. Z. Hong, X. C. Zhang, H. Peng, and Y. Z. Xiao, "A new marine bacterial laccase with chloride-enhancing, alkaline-dependent activity and dye decolorization ability," *Bioresour. Technol.*, vol. 111, pp. 36–41, 2012.

[93] S. Majumdar, T. Lukk, J. O. Solbiati, S. Bauer, S. K. Nair, J. E. Cronan, and J. a. Gerlt, "Roles of small laccases from streptomyces in lignin degradation," *Biochemistry*, vol. 53, pp. 4047–4058, 2014.

[94] D. Tropel and J. R. Van Der Meer, "Bacterial Transcriptional Regulators for Degradation Pathways of Aromatic Compounds Bacterial Transcriptional Regulators for Degradation Pathways of Aromatic Compounds," *Society*, vol. 68, no. 3, pp. 474–500, 2004.

[95] E. Masai, N. Kamimura, D. Kasai, A. Oguchi, A. Ankai, S. Fukui, M. Takahashi, I. Yashiro, H. Sasaki, T. Harada, S. Nakamura, Y. Katano, S. Narita-Yamada, H. Nakazawa, H. Hara, Y. Katayama, M. Fukuda, S. Yamazaki, and N. Fujita, "Complete genome sequence of Sphingobium sp. strain SYK-6, a degrader of lignin-derived biaryls and monoaryls," *J. Bacteriol.*, vol. 194, no. 2, pp. 534–535, 2012.

[96] E. Masai, Y. Katayama, S. Kubota, S. Kawai, M. Yamasaki, and N. Morohoshi, "A bacterial enzyme degrading the model lignin compound beta-etherase is a member of the glutathione-S-transferase superfamily.," *FEBS Lett.*, vol. 323, no. 1–2, pp. 135–40, May 1993.

[97] M. a. Abril, C. Michan, K. N. Timmis, and J. L. Ramos, "Regulator and enzyme specificities of the TOL plasmid-encoded upper pathway for

degradation of aromatic hydrocarbons and expansion of the substrate range of the pathway," *J. Bacteriol.*, vol. 171, no. 12, pp. 6782–6790, 1989.

[98] G. Fuchs, M. Boll, and J. Heider, "Microbial degradation of aromatic compounds — from one strategy to four," *Nat. Rev. Microbiol.*, vol. 9, no. 11, pp. 803–816, 2011.

[99] L. Tomás-Gallardo, I. Canosa, E. Santero, E. Camafeita, E. Calvo, J. a López, and B. Floriano, "Proteomic and transcriptional characterization of aromatic degradation pathways in Rhodoccocus sp. strain TFB.," *Proteomics*, vol. 6 Suppl 1, pp. S119–S132, 2006.

[100] C. R. Taylor, "Isolation of environmental lignin-degrading bacteria and identification of extracellular enzymes," University of Warwick, pp. 152-180, 2012.

[101] A. Heinfling, F. J. Ruiz-Dueñas, M. J. Martínez, M. Bergbauer, U. Szewzyk, and A. T. Martínez, "A study on reducing substrates of manganese-oxidizing peroxidases from Pleurotus eryngii and Bjerkandera adusta," *FEBS Lett.*, vol. 428, no. 3, pp. 141–146, 1998.

[102] C. Grassin and D. Dubourdieu, "Quantitative determination of Botrytis Laccase in musts and wines by syringaldazine test," *J. Sci. Food Agric.*, vol. 48, no. 1978, pp. 369–376, 1989.

[103] G. Palmieri, G. Cennamo, and G. Sannia, "Remazol Brilliant Blue R decolourisation by the fungus Pleurotus ostreatus and its oxidative enzymatic system," *Enzyme Microb. Technol.*, vol. 36, no. 1, pp. 17–24, 2005.

[104] S. Pointing, “Qualitative methods for the determination of lignocellulolytic enzyme production by tropical fungi,” Fungal Divers 2, pp. 17-33, 1999. http://www.researchgate.net/profile/Stephen_Pointing/publication/228686372_Qualitative_methods_for_the_determination_of_lignocellulolytic_enzyme_production_by_tropical_fungi/links/02bfe50d2bf0036a55000000.pdf

[105] E. Rodríguez, M. A. Pickard, and R. Vazquez-Duhalt, “Industrial dye decolorization by laccases from ligninolytic fungi,” *Curr. Microbiol.*, vol. 38, no. 1, pp. 27–32, 1999.

[106] D. S. Arora and P. K. Gill, “Comparison of two assay procedures for lignin peroxidase.,” *Enzyme Microb. Technol.*, vol. 28, no. 7–8, pp. 602–605, May 2001.

[107] K. Kato, S. Kozaki, and M. Sakuranaga, “Degradation of lignin compounds by bacteria from termite guts,” *Biotechnol. Lett.*, vol. 20, pp. 459–462, 1998.

[108] M. E. Brown, M. C. Walker, T. G. Nakashige, A. T. Iavarone, and M. C. Y. Chang, “Discovery and characterization of heme enzymes from unsequenced bacteria: application to microbial lignin degradation.,” *J. Am. Chem. Soc.*, vol. 133, no. 45, pp. 18006–9, Nov. 2011.

[109] S. Thomas, A. P. Mathew, and P. M. Visakh, *Advances in Natural Polymers*, vol. 18. Berlin, Heidelberg: Springer Berlin Heidelberg, pp. 1-9, 2013.

[110] E. T. Farinas, T. Bulter, and F. H. Arnold, “Directed enzyme evolution.,” *Curr. Opin. Biotechnol.*, vol. 12, no. 6, pp. 545–51, Dec. 2001.

[111] T. K. Kirk and J. M. Lynch, “Lignin-Degrading Enzymes [and Discussion],” *Philos. Trans. R. Soc. A Math. Phys. Eng. Sci.*, vol. 321, no. 1561, pp. 461–474, 1987.

[112] F. S. Archibald, “A New Assay for Lignin-Type Peroxidases Employing the Dye Azure B,” *Appl. Environ. Microbiol. Sept. 1992, p.3110-3116*, vol. 58, no. 9, 1992.

[113] R. Vicuña, “Bacterial degradation of lignin,” *Enzyme Microb. Technol.*, vol. 10, no. 11, pp. 646–655, Nov. 1988.

[114] M. Tien and T. K. Kirk, “Lignin-Degrading Enzyme from the Hymenomycete Phanerochaete chrysosporium Burds.,” *Science*, vol. 221, no. 4611, pp. 661–3, Aug. 1983.

[115] L. Bandounas, N. J. Wierckx, J. H. de Winde, and H. J. Ruijssenaars, “Isolation and characterization of novel bacterial strains exhibiting ligninolytic potential.,” *BMC Biotechnol.*, vol. 11, no. 1, p. 94, Jan. 2011.

[116] S. Camarero, D. Ibarra, M. J. Martínez, and Á. T. Martínez, “Lignin-Derived Compounds as Efficient Laccase Mediators for Decolorization of Different Types of Recalcitrant Dyes Lignin-Derived Compounds as Efficient Laccase Mediators for Decolorization of Different Types of Recalcitrant Dyes,” *Appl. Environ. Microbiol. , Apr. 2005, p. 1775–1784*, 2005.

[117] C. Johannes and a Majcherczyk, “Laccase activity tests and laccase inhibitors.,” *J. Biotechnol.*, vol. 78, no. 2, pp. 193–9, Mar. 2000.

[118] M. Ye, G. Li, W. Q. Liang, and Y. H. Liu, “Molecular cloning and characterization of a novel metagenome-derived multicopper oxidase with alkaline laccase activity and highly soluble expression.,” *Appl. Microbiol. Biotechnol.*, vol. 87, no. 3, pp. 1023–31, Jul. 2010.

[119] a. Leonowicz and K. Grzywnowicz, “Quantitative estimation of laccase forms in some white-rot fungi using syringaldazine as a substrate,” *Enzyme Microb. Technol.*, vol. 3, no. 1, pp. 55–58, Jan. 1981.

[120] C. Eggert, U. Temp, J. F. Dean, and K. E. Eriksson, “A fungal metabolite mediates degradation of non-phenolic lignin structures and synthetic lignin by laccase.,” *FEBS Lett.*, vol. 391, no. 1–2, pp. 144–8, Aug. 1996.

[121] M. Ahmad, C. R. Taylor, D. Pink, K. S. Burton, D. C. Eastwood, G. D. Bending, and T. D. H. Bugg, “Development of novel assays for lignin degradation: comparative analysis of bacterial and fungal lignin degraders,” *Mol. Biosyst.*, vol. 6, no. 5, pp. 815–821, 2010.

[122] T. Gobble, “A Genome-Wide, Phenotypic Screen for Genes Regulating Quorum Sensing in Pseudomonas aeruginosa,” *B.Sc. Project*, Oregon State University, pp.19, 2008.

[123] T. Bertrand, N. a J. Eady, J. N. Jones, Jesmin, J. M. Nagy, B. Jamart-Grégoire, E. L. Raven, and K. a Brown, “Crystal structure of Mycobacterium tuberculosis catalase-peroxidase.,” *J. Biol. Chem.*, vol. 279, no. 37, pp. 38991–9, Sep. 2004.

[124] S. Chouchane, “Analysis of Heme Structural Heterogeneity in Mycobacterium tuberculosis Catalase-Peroxidase (KatG),” *J. Biol. Chem.*, vol. 278, no. 10, pp. 8154–8162, Dec. 2002.

[125] R. a Ghiladi, G. M. Knudsen, K. F. Medzihradszky, and P. R. Ortiz de Montellano, “The Met-Tyr-Trp cross-link in Mycobacterium tuberculosis catalase-peroxidase (KatG): autocatalytic formation and effect on enzyme catalysis and spectroscopic properties.,” *J. Biol. Chem.*, vol. 280, no. 24, pp. 22651–63, Jun. 2005.

[126] R. Singh, B. Wiseman, T. Deemagarn, L. J. Donald, H. W. Duckworth, X. Carpena, I. Fita, and P. C. Loewen, “Catalase-peroxidases (KatG) exhibit NADH oxidase activity.,” *J. Biol. Chem.*, vol. 279, no. 41, pp. 43098–106, Oct. 2004.

[127] S. Chouchane, I. Lippai, and R. S. Magliozzo, “Catalase-peroxidase (Mycobacterium tuberculosis KatG) catalysis and isoniazid activation.,” *Biochemistry*, vol. 39, no. 32, pp. 9975–83, Aug. 2000.

[128] X. Zhao, H. Yu, S. Yu, F. Wang, J. C. Sacchettini, and R. S. Magliozzo, “Hydrogen peroxide-mediated isoniazid activation catalyzed by Mycobacterium tuberculosis catalase-peroxidase (KatG) and its S315T mutant.,” *Biochemistry*, vol. 45, no. 13, pp. 4131–40, Apr. 2006.

[129] R. Singh, B. Wiseman, T. Deemagarn, V. Jha, J. Switala, and P. C. Loewen, “Comparative study of catalase-peroxidases (KatGs).,” *Arch. Biochem. Biophys.*, vol. 471, no. 2, pp. 207–14, Mar. 2008.

[130] U. Hinz, “From protein sequences to 3D-structures and beyond: the example of the UniProt Knowledgebase,” *Cell. Mol. Life Sci.*, vol. 67, no. 7, pp. 1049–1064, Apr. 2010.

[131] W. Adam, U. Hoch, C. R. Sahamoller, and P. Schreier, “Enzyme-catalyzed asymmetric-synthesis - kinetic resolution of chiral hydroperoxides by enantioselective reduction to alcohols with horseradish-peroxidase,” *Angew. Chem., Int. Ed. Engl.*, vol. 32, no. 12, pp. 1737–1739, 1993.

[132] K. Ryu, J. H. Kang, L. Wang, and E. K. Lee, “Expression in yeast of secreted lignin peroxidase with improved 2,4-dichlorophenol degradability by DNA shuffling,” *J. Biotechnol.*, vol. 135, pp. 241–246, 2008.

[133] C. Liers, C. Bobeth, M. Pecyna, R. Ullrich, and M. Hofrichter, “DyP-like peroxidases of the jelly fungus Auricularia auricula-judae oxidize nonphenolic lignin model compounds and high-redox potential dyes,” *Appl. Microbiol. Biotechnol.*, vol. 85, pp. 1869–1879, 2010.

[134] I. Fridovich, “Superoxide Dismutases,” *Annu. Rev. Biochem.*, vol. 44, no. 1, pp. 147–159, 1973.

[135] J. M. McCord and I. Fridovich, “Superoxide Dismutase. An enzymatic function for erythrocuprein (Hemocuprein),” *J. Biol. Chem.*, vol. 244, no. 22, pp. 6049–6055, 1969.

[136] J. L. Hsu, Y. Hsieh, C. Tu, D. O’Connor, H. S. Nick, and D. N. Silverman, “Catalytic properties of human manganese superoxide dismutase.,” *J. Biol. Chem.*, vol. 271, no. 30, pp. 17687–17691, 1996.

[137] C. a Kerfeld, S. Yoshida, K. T. Tran, T. O. Yeates, D. Cascio, H. Bottin, C. Berthomieu, M. Sugiura, and A. Boussac, "The 1.6 A resolution structure of Fe-superoxide dismutase from the thermophilic cyanobacterium Thermosynechococcus elongatus.," *J. Biol. Inorg. Chem.*, vol. 8, no. 7, pp. 707–14, Sep. 2003.

[138] A.-F. Miller, "Superoxide dismutases: active sites that save, but a protein that kills.," *Curr. Opin. Chem. Biol.*, vol. 8, no. 2, pp. 162–8, Apr. 2004.

[139] I. Bertini, H. B. Gray, A. Edward I. Stiefel, and J. S. Valentine., Eds., *Biological Inorganic Chemistry: Structure and Reactivity*, First edit. Sausalito, California: University Science Books, pp. 331-340, 2007.

[140] V. C. Culotta, M. Yang, and T. V O'Halloran, "Activation of superoxide dismutases: putting the metal to the pedal.," *Biochim. Biophys. Acta*, vol. 1763, no. 7, pp. 747–58, 2006.

[141] L. T. Benov, W. F. Beyer, Jr., R. D. Stevens, and I. Fridovich, "Purification and Characterization of the Cu,Zn SOD from Escherichia," *Free Radic. Biol. Med.*, vol. 21, no. I, pp. 117–121, 1996.

[142] W. R. Rypniewski, S. Mangani, B. Bruni, P. L. Orioli, M. Casati, and K. S. Wilson, "Crystal structure of reduced bovine erythrocyte superoxide dismutase at 1.9 A resolution.," *J. Mol. Biol.*, vol. 251, no. 2, pp. 282–296, 1995.

[143] J. Pierre, "One electron at a time oxidations and enzymatic paradigms: from metallic to non-metallic redox centers," *Chem. Soc. Rev.*, vol. 29, no. 4, pp. 251–257, 2000.

[144] G. E. D. Tainer JA Richardson JS, Richardson DC, "Structure and mechanism of copper, zinc superoxide dismutase," *Nature*, vol. 306 , no. 5940, p. 284–7, 1983.

[145] S. Pcc, T. Li, X. Huang, R. Zhou, Y. Liu, B. Li, C. Nomura, and J. Zhao, "Differential Expression and Localization of Mn and Fe Superoxide Dismutases in the Heterocystous Cyanobacterium Anabaena Differential Expression and Localization of Mn and Fe Superoxide Dismutases in the Heterocystous Cyanobacterium Anabaena sp . Strain P," *J. Bacteriol.*, vol. 184, no. 18, pp. 5096–5103, 2002.

[146] A. Bajw, "Superoxide dismutase and their role in plants and in some human diseases." *Slideshare.net*, 2012, Accessed: Jun 2015, [Online]. Available: http://www.slideshare.net/azfarali2/seminar-on-sods.

[147] W. B. Jr and I. Fridovich, "Effect of hydrogen peroxide on the iron-containing superoxide dismutase of Escherichia coli," *Biochemistry*, no. 1974, pp. 1251–1257, 1987.

[148] P. A. Belinky, N. Flikshtein, S. Lechenko, S. Gepstein, and C. G. Dosoretz, "Reactive Oxygen Species and Induction of Lignin Peroxidase in Phanerochaete chrysosporium," *Appl. Environ.Microbiol.*, vol. 69, no. 11, pp. 6500–6506, Nov. 2003.

[149] P. A. Belinky, N. Flikshtein, and C. G. Dosoretz, "Induction of lignin peroxidase via reactive oxygen species in manganese-deficient cultures of Phanerochaete chrysosporium," *Enzyme Microb. Technol.*, vol. 39, no. 2, pp. 222–228, 2006.

[150] D. P. B. and S. D. Aust, “Effect of Superoxide and Superoxide Dismutase on Lignin Peroxidase-Catalyzed Veratryl Alcohol Oxidation,” *Arch. Biochem. Biophys.*, vol. 311, no. 2, pp. 378–384, 1994.

[151] C. Schulte, M. Arenskötter, M. M. Berekaa, Q. Arenskötter, H. Priefert, and A. Steinbüchel, “Possible involvement of an extracellular superoxide dismutase (SodA) as a radical scavenger in poly(cis-1,4-isoprene) degradation.,” *Appl. Environ. Microbiol.*, vol. 74, no. 24, pp. 7643–53, Dec. 2008.

[152] J. M. McCord and I. Fridovich, “Superoxide Dismutase. An enzymatic function for erythrocuprein (hemocuprein),” *J. Biol. Chem.*, vol. 244, no. 22, pp. 6049–6055, Nov. 1969.

[153] L. Flohé and F. Otting, “Superoxide dismutase assays.,” *Methods Enzymol.*, vol. 105, pp. 93–104, 1984.

[154] L. Flohe, R. Becker, R. Brigelius, E. Lengfelder, and F. Otting, Eds., *CRC handbook of free radicals and antioxidants in biomedicine.*, vol. III, no. 1. Boca Raton, Florida: CRC Press, Inc., pp. 287-292, 1990.

[155] C. J. Weydert and J. J. Cullen, “Measurement of superoxide dismutase, catalase and glutathione peroxidase in cultured cells and tissue.,” *Nat. Protoc.*, vol. 5, no. 1, pp. 51–66, 2010.

[156] S. Marklund and G. Marklund, “Involvement of the superoxide anion radical in the autoxidation of pyrogallol and a convenient assay for superoxide dismutase.,” *Eur. J. Biochem.*, vol. 47, no. 3, pp. 469–74, Sep. 1974.

[157] M. Lombard, D. Touati, M. Fontecave, and V. Nivière, “Superoxide reductase as a unique defense system against superoxide stress in the microaerophile Treponema pallidum,” *J. Biol. Chem.*, vol. 275, no. 35, pp. 27021–27026, 2000.

[158] Y. Z. He, K. Q. Fan, C. J. Jia, Z. J. Wang, W. Bin Pan, L. Huang, K. Q. Yang, and Z. Y. Dong, “Characterization of a hyperthermostable Fe-superoxide dismutase from hot spring,” *Appl. Microbiol. Biotechnol.*, vol. 75, no. 2, pp. 367–376, 2007.

[159] K. Arnold, L. Bordoli, J. K. And, and T. Schwede, “The SWISS-MODEL workspace: a web-based environment for protein structure homology modelling,” *Bioinformatics, 22,195-201*, vol. 22, no. 2, pp. 195–201, 2006.

[160] M. C. Peitsch, “Protein modeling by E-mail,” *Nat. Biotechnol.*, vol. 13, pp. 658–660, 1995.

[161] G. von H. & H. N. Thomas Nordahl Petersen, Søren Brunak, “SignalP 4.0: discriminating signal peptides from transmembrane regions,” *Nat. Methods*, vol. 8, pp. 785–786, 2011.

[162] Y.-Z. He, K.-Q. Fan, C.-J. Jia, Z.-J. Wang, W.-B. Pan, L. Huang, K.-Q. Yang, and Z.-Y. Dong, “Characterization of a hperthermostable Fe-superoxide dismutase from hot spring,” *Appl. Microbiol. Biotechnol.*, vol. 75, no. d, pp. 367–376, May 2007.

[163] Y. Hsieh, “Catalytic Properties of Human Manganese Superoxide Dismutase,” *J. Biol. Chem.*, vol. 271, no. 30, pp. 17687–17691, 1996.

[164] R. El Hage, N. Brosse, L. Chrusciel, C. Sanchez, P. Sannigrahi, and A. Ragauskas, “Characterization of milled wood lignin and ethanol organosolv lignin from miscanthus,” *Polym. Degrad. Stab.*, vol. 94, no. 10, pp. 1632–1638, Oct. 2009.

[165] F. S. Chakar and A. J. Ragauskas, “Review of current and future softwood kraft lignin process chemistry,” *Ind. Crops Prod.*, vol. 20, no. 2, pp. 131–141, 2004.

[166] M. D. Engelmann, R. T. Bobier, T. Hiatt, and I. F. Cheng, “Variability of the Fenton reaction characteristics of the EDTA, DTPA, and citrate complexes of iron,” *BioMetals*, vol. 16, no. 4, pp. 519–527, 2003.

[167] M. Tienfl and S. D. Austfl, “The involvment of hydroxyl radical derived from hydrogen peroxide in lignin degradation by the white rot fungus *phanerochaete chrysosporium*,” *J. Biol. Chem.*, vol. 257, no. 19, pp. 11455–11462, 1982.

[168] S. GOLDSTEIN, C. MICHEL, W. BORS, M. SARAN, and G. CZAPSKI, “A critical reevaluation of some assay methods for superoxide dismutase activity,” *Free Radic. Biol. Med.*, vol. 4, no. 5, pp.

[169] J. a Imlay, “Cellular defenses against superoxide and hydrogen peroxide,” *Annu. Rev. Biochm.*, no. 217, pp. 755–776, 2011.

[170] C. Schulte, M. Arenskötter, M. M. Berekaa, Q. Arenskötter, H. Priefert, and A. Steinbüchel, “Possible involvement of an extracellular superoxide dismutase (SodA) as a radical scavenger in poly(cis-1,4-isoprene) degradation,” *Appl. Environ. Microbiol.*, vol. 74, no. 24, pp. 7643–7653, 2008.

[171] M. E. Stroupe, M. Didonato, J. Tainer, A. Messerschmidt, R. Huber, T. Poulos, and K. Wieghardt, “Manganese superoxide dismutase,” *Handbook of Metalloproteins*, Chichester: John Wiley & Sons, Ltd, p. 940. 2001.

[172] L. Käll, A. Krogh, and E. L. . Sonnhammer, “A Combined Transmembrane Topology and Signal Peptide Prediction Method,” *J. Mol. Biol.*, vol. 338, no. 5, pp. 1027–1036, May 2004.

[173] R. Ten Have and P. J. M. Teunissen, “Oxidative mechanisms involved in lignin degradation by white-rot fungi,” *Chem. Rev.*, vol. 101, no. 11, pp. 3397–3413, 2001.

[174] M. B. Yim, P. B. Chock, and E. R. Stadtman, “Copper, zinc superoxide dismutase catalyzes hydroxyl radical production from hydrogen peroxide.,” *Proc. Natl. Acad. Sci. U. S. A.*, vol. 87, no. 13, pp. 5006–5010, 1990.

[175] A. Brune and B. Schink, “Nicrobielogy fermentation of trihydroxybenzenes to acetate via triacetic acid,” *Arch. Microbiol.,* vol. 157, no. 5, pp. 417–424, 1992.

[176] H. Kutsuki and M. H. Gold, “Generation of hydroxyl radical and its involvement in lignin degradation by Phanerochaete chrysosporium.,” *Biochem. Biophys. Res. Commun.*, vol. 109, no. 2, pp. 320–327, 1982.

[177] T. K. Kirk, M. D. Mozuch, and M. Tien, “Free hydroxyl radical is not involved in an important reaction of lignin degradation by Phanerochaete chrysosporium Burds.,” *Biochem. J.*, vol. 226, no. 2, pp. 455–460, 1985.

[178] R. L. Kelley and C. a Reddy, “Ethylene production from alpha-oxo-gamma-methylthiobutyric acid is a sensitive measure of ligninolytic activity by Phanerochaete chrysosporium.,” *Biochem. J.*, vol. 206, no. 2, pp. 423–425, 1982.

[179] B. Krimmel, F. Swoboda, S. Solar, and G. Reznicek, “OH-radical induced degradation of hydroxybenzoic- and hydroxycinnamic acids and formation of aromatic products-A gamma radiolysis study,” *Radiat. Phys. Chem.*, vol. 79, no. 12, pp. 1247–1254, 2010.

[180] S. Steenken and P. O. Neill, “Oxidative demethoxylation of methoxylated phenols and hydroxybenzoic acids by the hydroxyl radical. An in situ electron spin resonance, conductometric pulse radiolysis and product analysis study,” *J. Phys. Chem.*, pp. 505–508, 1976.

[181] A. Assabane, Y. Ait Ichou, H. Tahiri, C. Guillard, and J.-M. Herrmann, “Photocatalytic degradation of polycarboxylic benzoic acids in UV-irradiated aqueous suspensions of titania.,” *Appl. Catal. B Environ.*, vol. 24, no. 2, pp. 71–87, 2000.

[182] C. G. Tsai, D. M. Gates, W. M. Ingledew, and G. a Jones, “Products of anaerobic phloroglucinol degradation by Coprococcus sp. Pe15.,” *Can. J. Microbiol.*, vol. 22, no. 2, pp. 159–164, 1976.

[183] P. Liu, H. E. Ewis, Y. J. Huang, C. D. Lu, P. C. Tai, and I. T. Weber, “Structure of Bacillus subtilis superoxide dismutase,” *Acta Crystallogr.*, vol. 63, no. 12, pp. 1003–1007, 2007.

[184] G. E. Borgstahl, M. Pokross, R. Chehab, A. Sekher, and E. H. Snell, “Cryo-trapping the six-coordinate, distorted-octahedral active site of manganese superoxide dismutase.,” *J. Mol. Biol.*, vol. 296, no. 4, pp. 951–959, 2000.

[185] M. L. Ludwig, A. L. Metzger, K. A. Pattridge, and W. C. Stallings, “Manganese superoxide dismutase from Thermus thermophilus,” *Journal of Molecular Biology*, vol. 219, no. 2. pp. 335–358, 1991.

[186] W. Atzenhofer, G. Regelsberger, U. Jacob, G. A. Peschek, P. G. Furtmüller, R. Huber, and C. Obinger, “The 2.0 Å resolution structure of the catalytic portion of a cyanobacterial membrane-bound manganese superoxide dismutase,” *J. Mol. Biol.*, vol. 321, no. 3, pp. 479–489, 2002.

[187] R. a. Edwards, M. M. Whittaker, J. W. Whittaker, E. N. Baker, and G. B. Jameson, “Outer sphere mutations perturb metal reactivity in manganese superoxide dismutase,” *Biochemistry*, vol. 40, no. 1, pp. 15–27, 2001.

[188] J. J. P. Perry, A. S. Hearn, D. E. Cabelli, H. S. Nick, J. A, and D. N. Silverman, “Human Manganese Superoxide Dismutase Tyrosine 34 Contribution to Structure and Catalysis,” *Structure*, vol. 48, no. 15, pp. 3417–3424, 2010.

[189] a. S. Hearn, M. E. Stroupe, D. E. Cabelli, J. R. Lepock, J. a. Tainer, H. S. Nick, and D. N. Silverman, “Kinetic analysis of product inhibition in human manganese superoxide dismutase,” *Biochemistry*, vol. 40, no. 40, pp. 12051–12058, 2001.

[190] M. M. Whittaker and J. W. Whittaker, “A glutamate bridge is essential for dimer stability and metal selectivity in manganese superoxide dismutase,” *J. Biol. Chem.*, vol. 273, no. 35, pp. 22188–22193, 1998.

[191] P. D. Sainsbury, “Biocatalytic valorisation of lignin via genetic or chemical intervention of bacterial aromatic degradation pathways,” *Ph.D. thesis,* pp.51-44, University of Warwick, 2014.

[192] T. D. H. Bugg, “Dioxygenase enzymes: catalytic mechanisms and chemical models,” *Tetrahedron*, vol. 59, no. 36, pp. 7075–7101, 2003.

[193] D. D. Moore, “Commonly Used Reagents and Equipment,” in *Current Protocols in Molecular Biology*, Hoboken, NJ, USA: John Wiley & Sons, Inc., pp. A.2A.1-A.2A.10, 2001

[194] T. Zor and Z. Selinger, ‘Linearization of the Bradford protein assay increases its sensitivity: theoretical and experimental studies.,’ Anal. Biochem., vol. 236, no. 2, pp. 302–8, May 1996.”

Appendices

A.1. Alignment of KatG amino acid sequence (C-terminal domain) from 32 different species with *Sphingobacterium sp.* T2. The species are bacteria (gram-positive and gram-negative), fungi and archaea. The C-terminal sequence of all of these organisms not contain heme binding site and show high similarity.

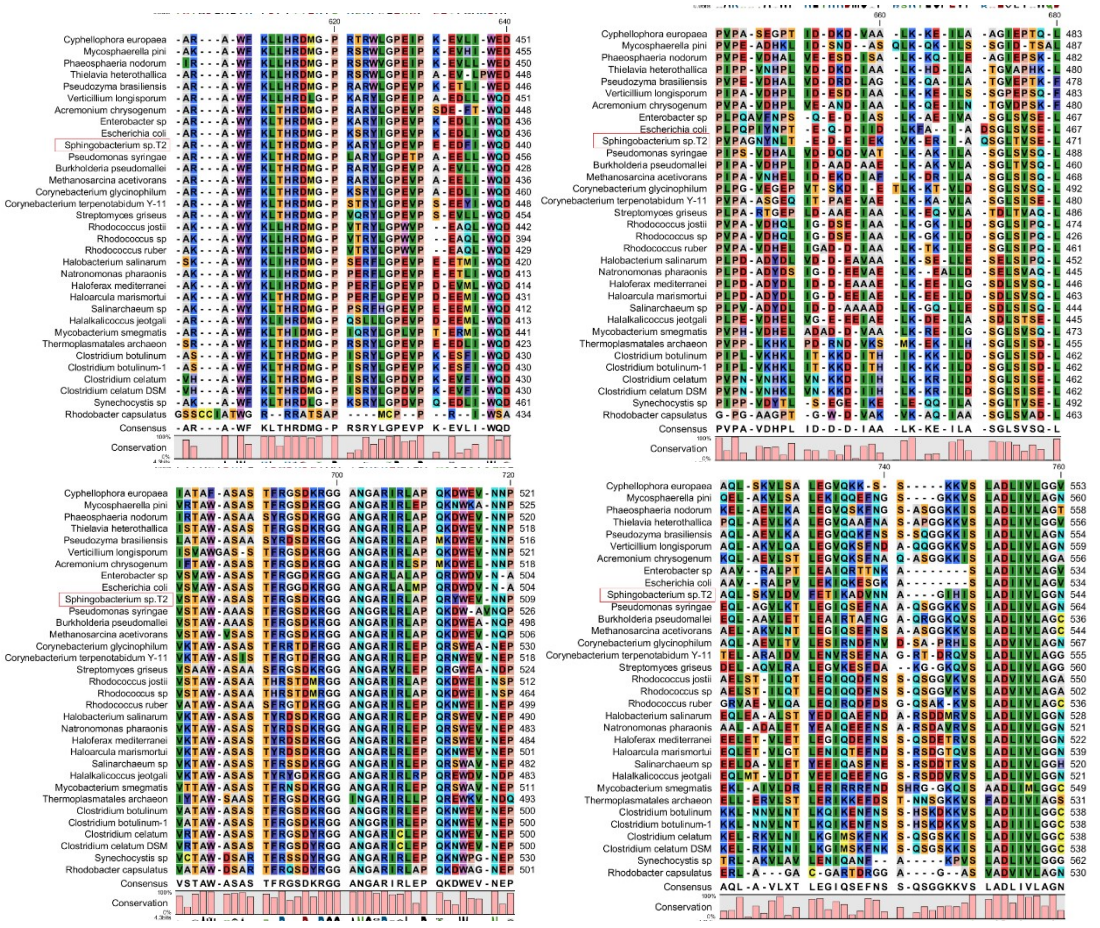

A.2. Genomic context of *Sphingobacterium* sp. T2 Mn superoxide dismutase genes (*sod1* and *sod2*, highlighted in yellow). The *sod1* is located adjacent to an ECF sigma factor and anti-sigma factor regulatory genes, while *sod2* is located within a cluster of 14 genes containing two *araC* transcriptional regulatory genes (regulatory genes highlighted in blue), and three ABC transporter component genes.

SOD1

Direction	Gene annotation
-	Haloacid dehalogenase-like hydrolase
+	tRNA-Met-CAT
-	hypothetical protein
+	hypothetical protein
+	Manganese superoxide dismutase 1
-	putative anti-sigma factor
-	RNA polymerase ECF-type sigma factor
-	hypothetical protein
-	3-carboxymuconate cyclase
+	Survival protein SurA precursor (Peptidyl-prolyl cis-trans isomerase SurA)
-	cysteinyl-tRNA synthetase

SOD2

Direction	Gene annotation
-	hypothetical protein
+	hypothetical protein
+	Protein secretion chaperonin CsaA
+	tRNA-specific adenosine-34 deaminase
+	Manganese superoxide dismutase 2
-	hypothetical protein
+	Peptide methionine sulfoxide reductase MsrA
+	hypothetical protein
+	Transcriptional regulator, AraC family
+	Delta-1-pyrroline-5-carboxylate dehydrogenase
+	Delta-1-pyrroline-5-carboxylate dehydrogenase
+	hypothetical protein
+	putative ATP-binding component of ABC transporter
+	ATP-binding protein
-	Na+/H+-dicarboxylate symporter
-	Na+/H+-dicarboxylate symporter

A.3. DNA sequences of *SOD1* and *SOD2*.

A.3.1. DNA sequence of *SOD1* (684 bp).

ATGATGAAGATGAATATTTTTAAGACTGCACTGGTAGCTACAGCTTTATTTGCTACTC
AGACGACATTTGCACAATTTAAACAGACCCCACTTCCATATGCGTATGACGCCTTGGA
AGGAGCTATCGACGCCAAGACCATGGAGATCCACTACAGCAAGCATGCTGCAGGATA
TACGGCCAACCTGAACAAAGCTATTGCAGGAACGCCGGCAGAGAAAGAATCTATAGA
AAATATTTTAGCTAAGGTGTCACAATATTCAGATGCCGTGCGTAATAATGCGGGAGG
CCACTACAACCACGAGCTGTTTTGGTCTATCCTAACCCCTAACAAGGGTACTAAACCT
TCGGCAGCCTTACAGAAGGCTATAGACGAAACGTTCGGTTCCTTGGATGCCTTGAAA
GAAAAAATCAATGCTGCAGGTGCGGCACGCTTCGGTTCGGGATGGGCATGGCTTATC
GTGGACAATGGAGGCAAGCTGCAGGTAACCTCCACCCCTAATCAGGACAATCCGCTC
ATGGATTTTACTAAAGAAAAGGGAACGCCAATCTTGGGTATAGATGTGTGGGAACAT
GCCTACTATCTAAGATATCAAAATAAGAGAGCGGACTATCTCACCACGATCTGGGAT
GTTATCAACTGGGAGGAAGTATCGGCACGATATGAGAAAGCCTTGAAAAAATAA

A.3.2. DNA sequence of *SOD2* (543 bp).

ATGGAAATCCATCACGATCGTCACCACCAAGCTTATGTGGATAACTTAAACAAAGCTA
TTGCTGGTACGGATGCAGAGAATGCTTCTTTAGAAGATATTCTTAAAAATGTGAGCAA
ATATTCGGCTGCTGTTCGCAACAATGGTGGCGGTCACTATAACCACAAATTGTTCTGG
TCAATCCTGAGTCCTAACGGTGGCGGTGAACCTAAAGGGGAGTTGGCAGAAGCCATC
AATGCTGCTTTCGGTTCTTTCGCTGAACTGAAGACACAGTTGCAAAATGCAGGTGCTA
CCCGCTTCGGATCGGGCTGGGCTTGGCTGATTGTGGATGAGTCAGGTAAGTTGGCAG
TTACCTCTACACCAAACCAAGACAACCCATTAATGGACGTAGCAGAGGTAAAAGGTA
CACCTATCTTGGGTATTGACGTGTGGGAGCATGCTTATTATTTGAAATATCAAAACAA
ACGTCCGGCTTATTTGGAAGCCATCTTCAATGTAATTGACTGGGATGCTGTAGCCGCT
AACTATGCAGCTGCTAAAAAATAA

A.4. Sequencing results for *SOD1* and *SOD2*.

A.4.1. Sequencing result of *SOD1* on pET 151 vector**.**

ATGCATCATCACCATCACCATGGTAAGCCTATCCCTAACCCTCTCCTC
GGTCTCGATTCTACGGAAAACCTGTATTTTCAGGGAATTGATCCCTT
CACCCAATTTAAACAGACCCCACTTCCATATGCGTATGACGCCTTGG
AAGGAGCTATCGACGCCAAGACCATGGAGATCCACTACAGCAAGCAT
GCTGCAGGATATACGGCCAACCTGAACAAAGCTATTGCAGGAACGCC
GGCAGAGAAAGAATCTATAGAAAATATTTTAGCTAAGGTGTCACAAT
ATTCAGATGCCGTGCGTAATAATGCGGGAGGCCACTACAACCACGAG
CTGTTTTGGTCTATCCTAACCCCTAACAAGGGTACTAAACCTTCGGC
AGCCTTACAGAAGGCTATAGACGAAACGTTCGGTTCCTTGGATGCCT
TGAAAGAAAAAATCAATGCTGCGGGTGCGGCACGCTTCGGTTCGGG
ATGGGCATGGCTTATCGTGGACAATGGAGGCAAGCTGCAGGTAACC
TCCACCCCTAATCAGGACAATCCGCTCATGGATTTTACTAAAGAAAA
GGGAACGCCAATCTTGGGTATAGATGTGTGGGAACATGCCTACTATC
TAAGATATCAAAATAAGAGAGCGGACTATCTCACCACGATCTGGGAT
GTTATCAACTGGGAGGAAGTATCGGCACGATATGAGAAAGCCTTGAA
AAAATAA

A.4.2. Sequencing result of *SOD2* on pET 151 vector.

ATGCATCATCACCATCACCATGGTAAGCCTATCCCTAACCCTCTCCTC

GGTCTCGATTCTACGGAAAACCTGTATTTTCAGGGAATTGATCCCTT

CACCATGGAAATCCATCACGATCGTCACCACCAAGCTTATGTGGATA

ACTTAAACAAAGCTATTGCTGGTACGGATGCAGAGAATGCTTCTTTA

GAAGATATTCTTAAAAATGTGAGCAAATATTCGGCTGCTGTTCGCAA

CAATGGTGGCGGTCACTATAACCACAAATTGTTCTGGTCAATCCTGA

GTCCTAACGGTGGCGGTGAACCTAAAGGGGAGTTGGCAGAAGCCAT

CAATGCTGCTTTCGGTTCTTTCGCTGAACTGAAGACACAGTTGCAAA

ATGCAGGTGCTACCCGCTTCGGATCGGGCTGGGCTTGGCTGATTGTG

GATGAGTCAGGTAAGTTGGCAGTTACCTCTACACCAAACCAAGACAA

CCCATTAATGGACGTAGCAGAGGTAAAAGGTACACCTATCTTGGGTA

TTGACGTGTGGGAGCATGCTTATTATTTGAAATATCAAAACAAACGT

CCGGCTTATTTGGAAGCCATCTTCAATGTAATTGACTGGGATGCTGT

AGCCGCTAACTATGCAGCTGCTAAAAAATAA

A.5. GC/MS spectrums of vanillin (**4.1**), vanillic acid (**4.2**), ferulic acid (**4.3**), 5-carboxyvanillic acid (**4.4**), protocatechuic acid (**4.5**) guaiacol (**4.6**), catechol (**4.7**), pyrogallol (**4.8**), 2-methoxyhydroquinone (**4.9**), 2-methoxyquinone (**4.10**), p-hydroxybenzaldehyde (**4.11**), p-hydroxybenzoic acid (**4.12**), salicylic acid (**4.13**), acetovanillone (**4.14**) and 4-(2-hydroxyethyl) guaiacol (**4.15**) before and after derivatization Bis(trimethylsilyl)acetamide (compound **4.19**-**4.30**).

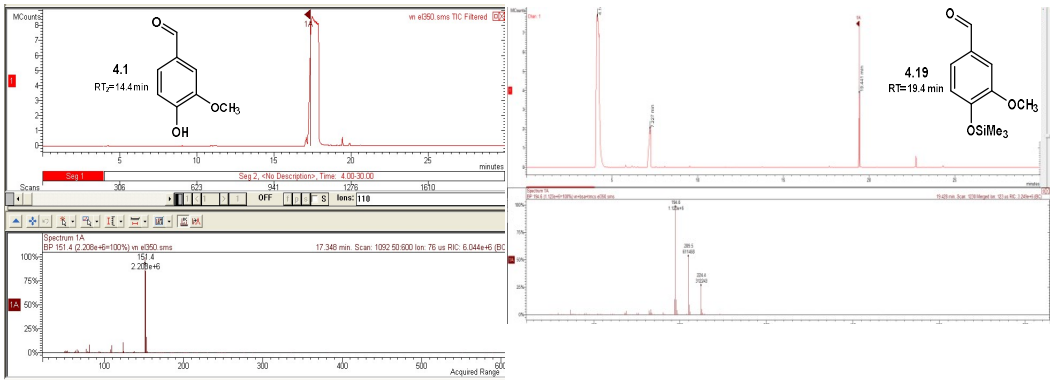

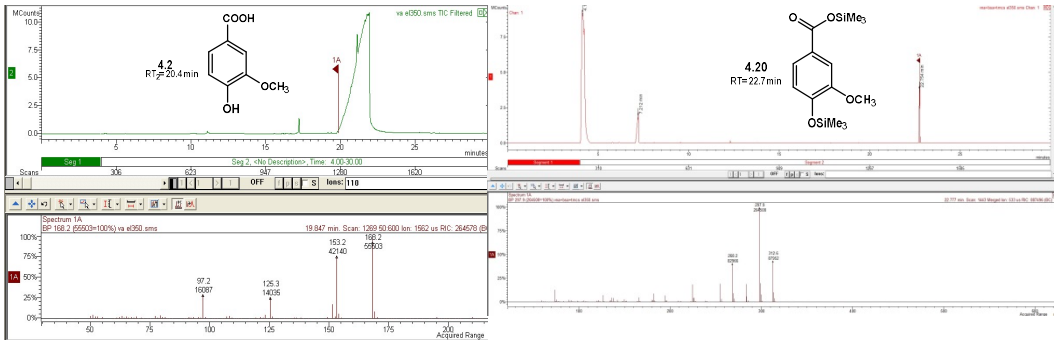

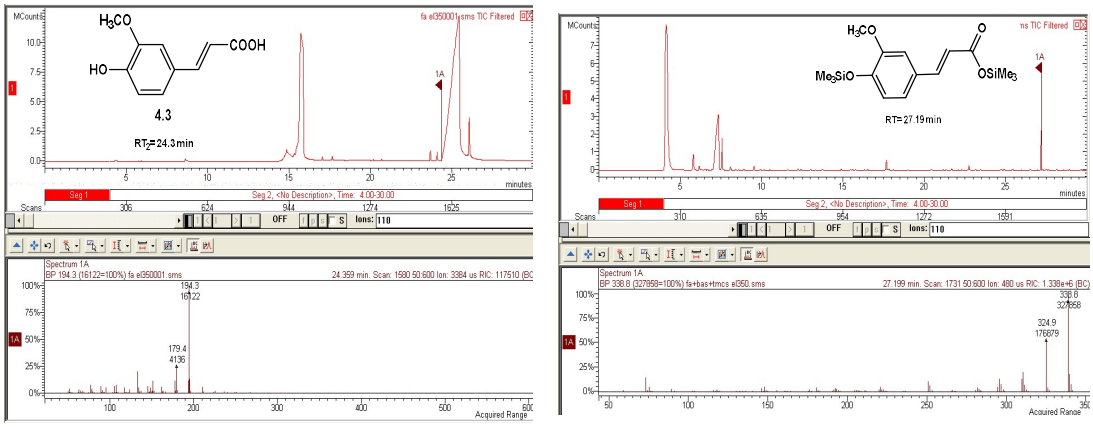

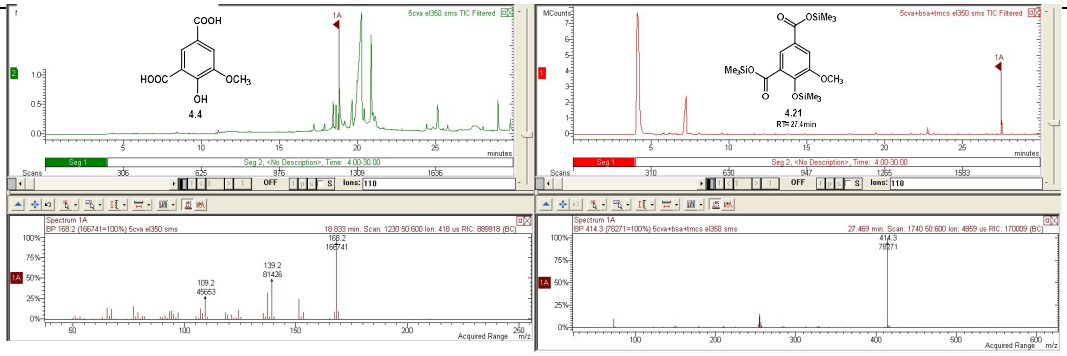
COOH
HOOC
OCH3
OH
4.4
OSiMe3
Me3SiO
OCH3
OSiMe3
4.21
RT=27.4min

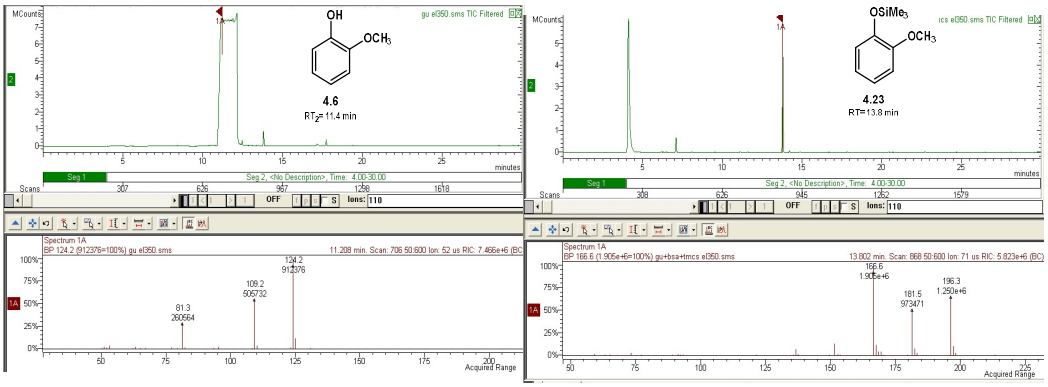
OH
OCH3
4.6
RT=11.4 min
OSiMe3
OCH3
4.23
RT=13.8 min

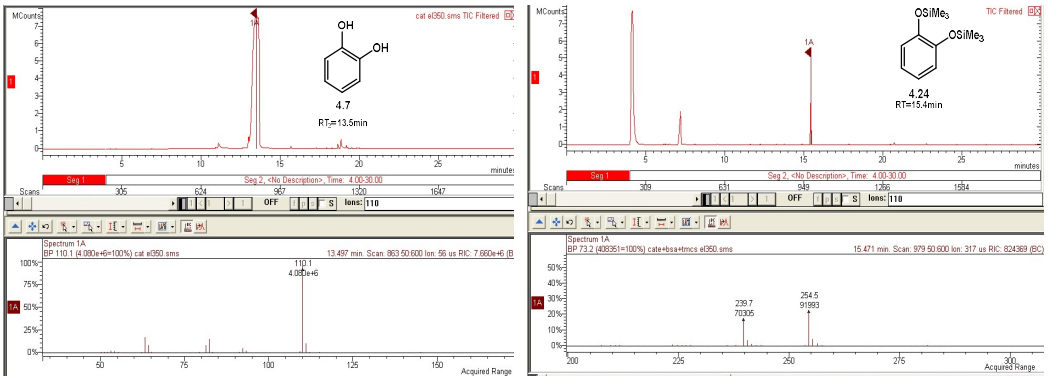
OH
OH
4.7
RT=13.5min
OSiMe3
OSiMe3
4.24
RT=15.4min

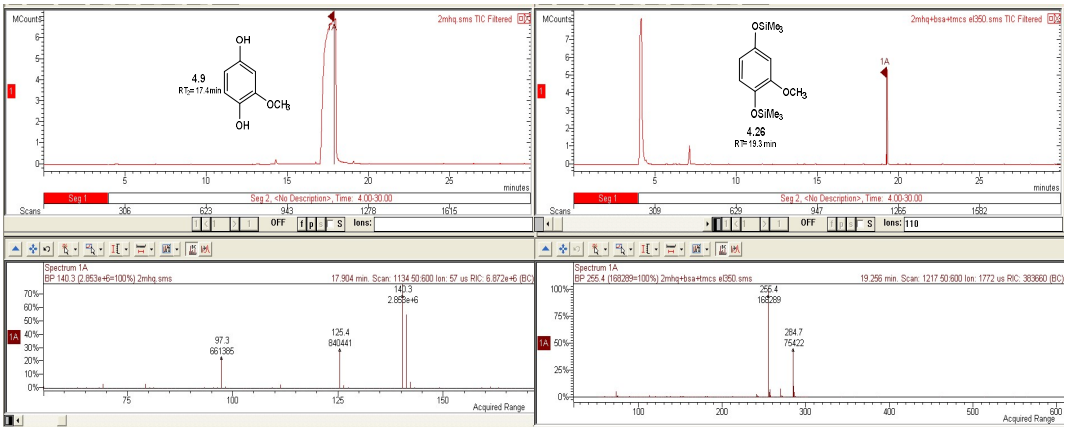
OH
OCH3
OH
4.9
RT=17.4min
OSiMe3
OCH3
OSiMe3
4.26
RT=19.5min

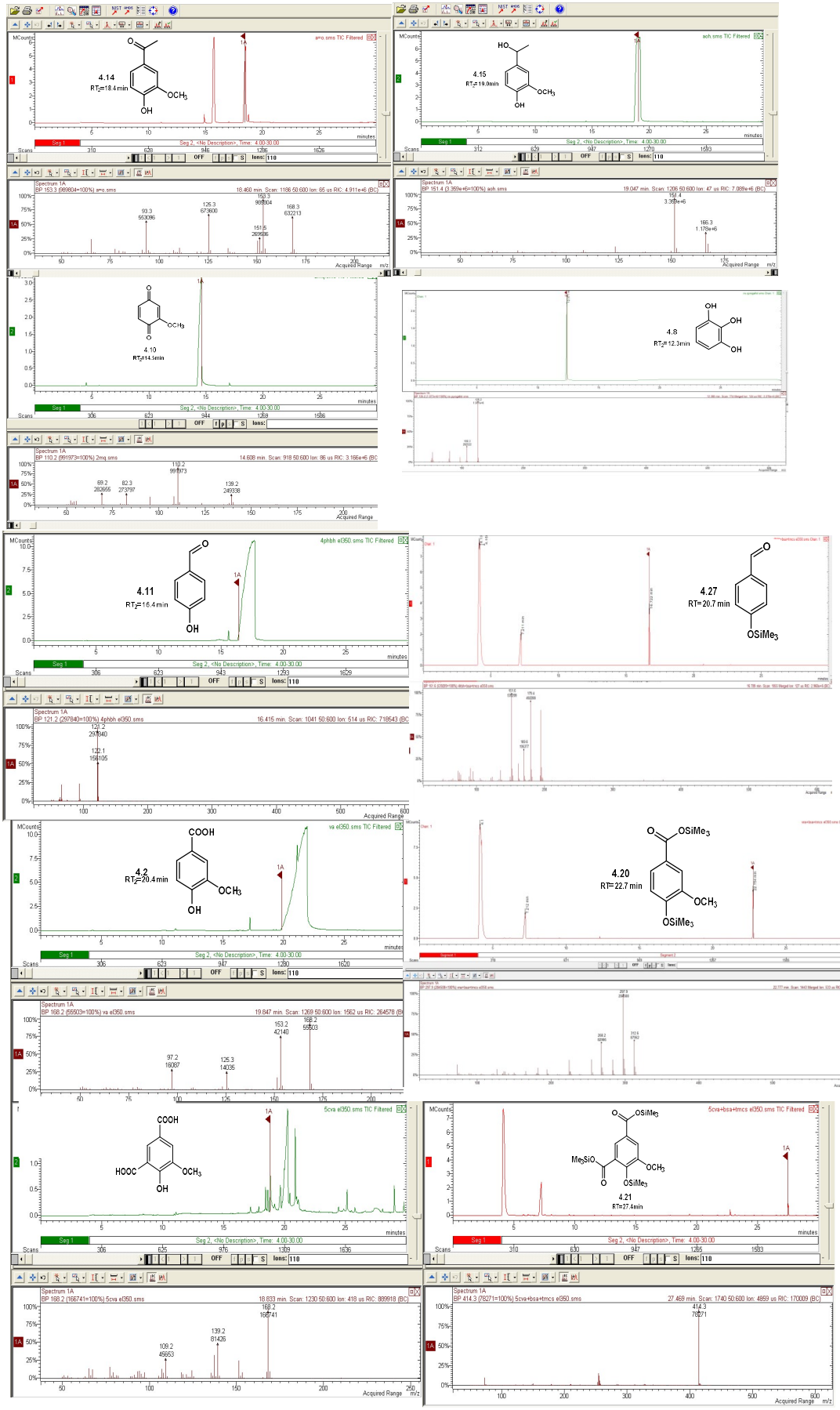
4.14
RT=18.4 min
4.15
RT=19.0min
4.10
RT=14.5min
4.8
RT=12.3mm
4.11
RT=16.4 min
4.27
RT=20.7 min
4.2
RT=20.4 min
4.20
RT=22.7 min
4.21
RT=27.4min

A.6. GC/MS spectrums of the reaction products of SpMnSODs treated ferulic acid (**4.3**), veratryl alcohol (**5.9**), *p*-hydroxybenzoic acid (**4.12**), salicylic acid (**4.13**), *p*-hydroxybenzaldehyde (**4.11**), acetovanillone (**4.14**), 4-(2-hydroxyethyl) guaiacol (**4.15**), vanillic acid (**4.2**), vanillin (**4.1**), 5-carboxyvanillic acid (**4.4**), guaiacol (**4.6**) and catechol (**4.7**).

GC/MS spectra of products from SOD1 treated Ferulic acid

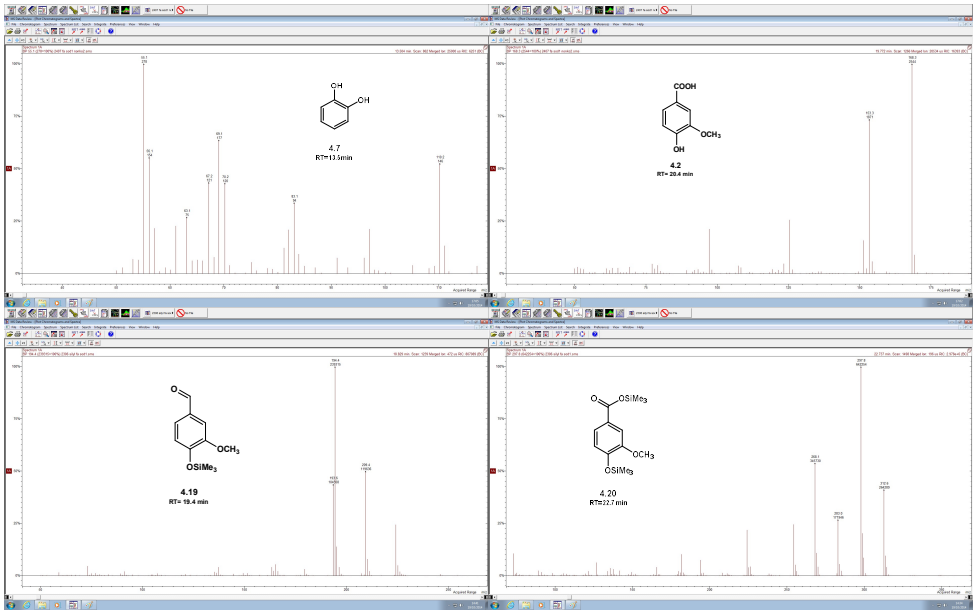

GC/MS spectra of products from SOD2 treated Ferulic acid

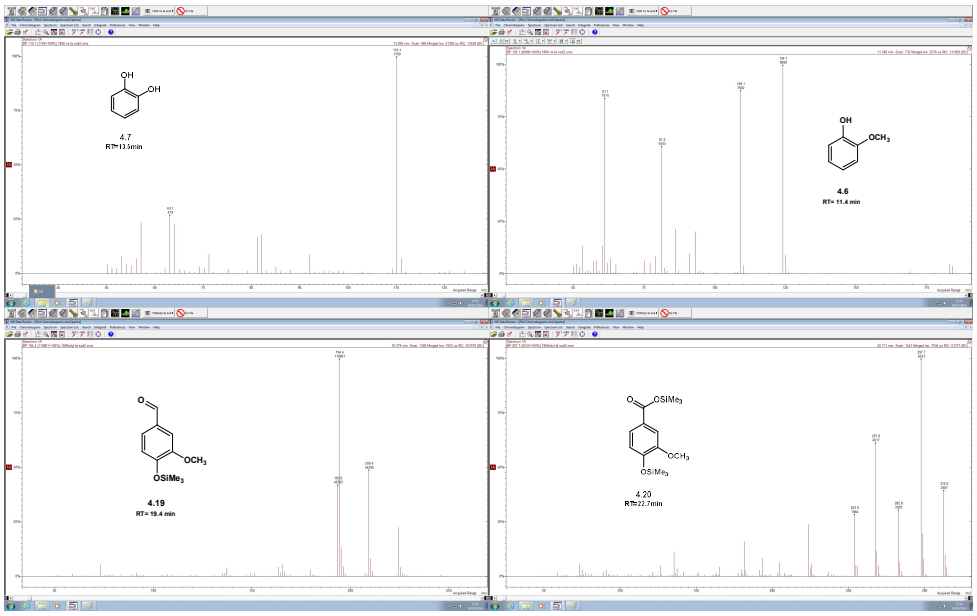

GC/MS spectra of products from SOD1 treated Veratryl alcohol

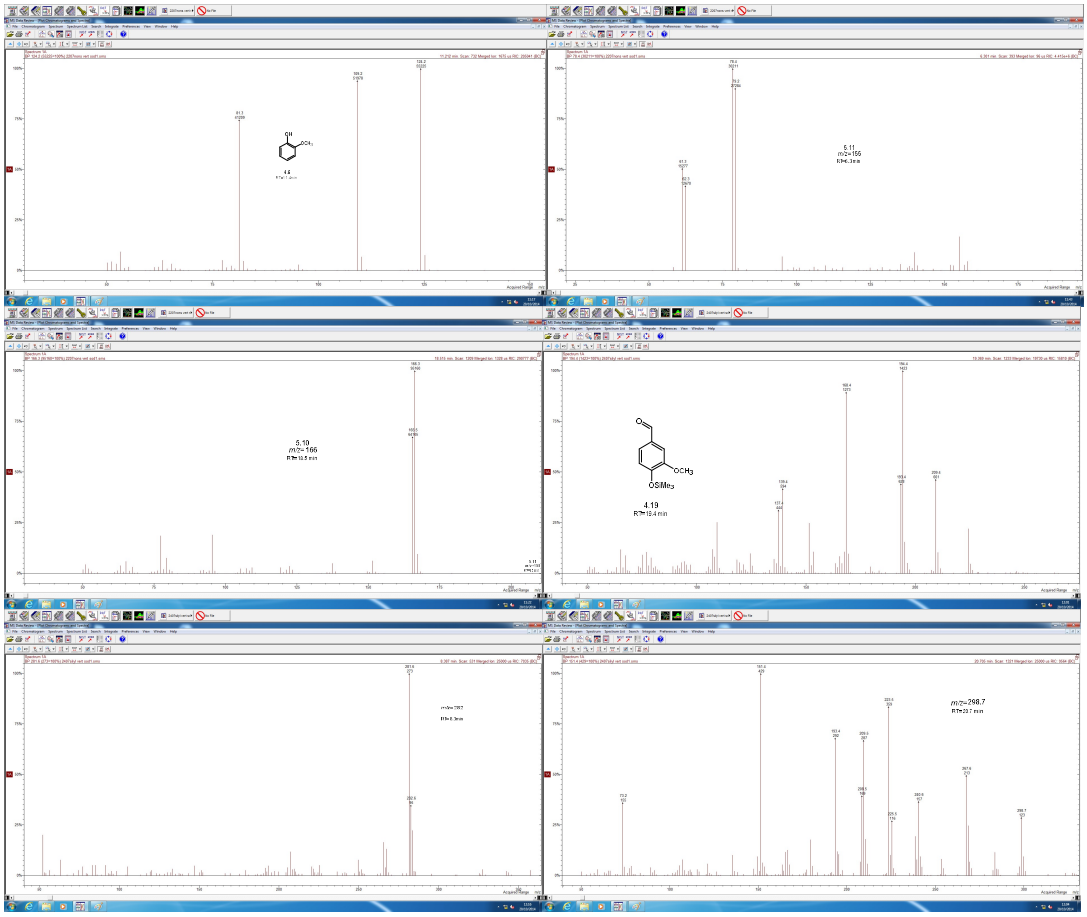

GC/MS spectra of products from SOD2 treated Veratryl alcohol

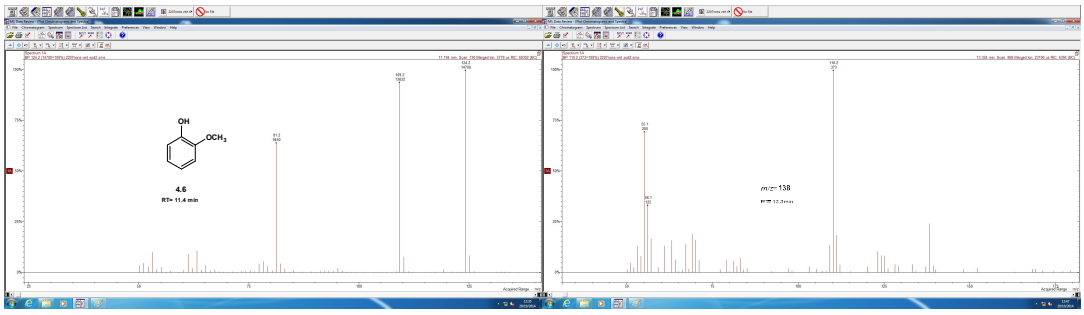

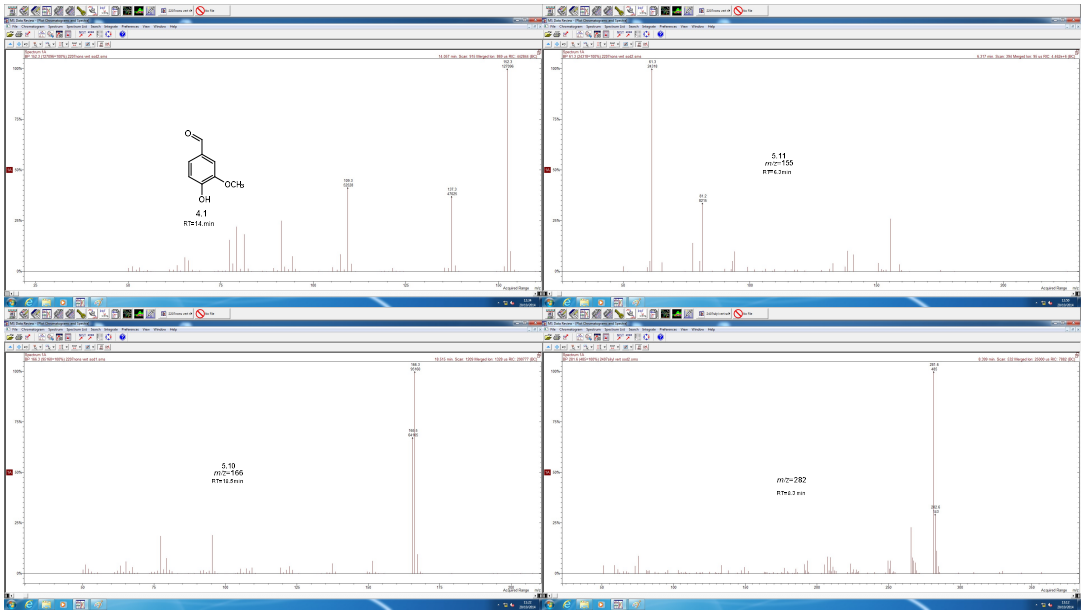

GC/MS spectra of products from SOD1 treated *p*-Hydroxybenzoic acid

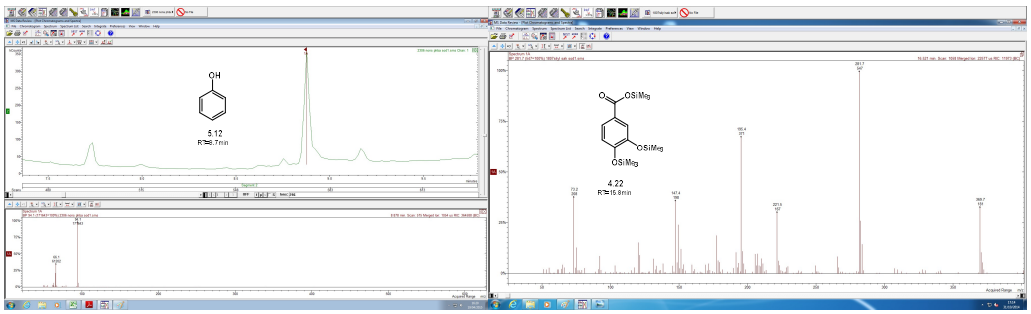

GC/MS spectra of products from SOD2 treated *p*-Hydroxybenzoic acid

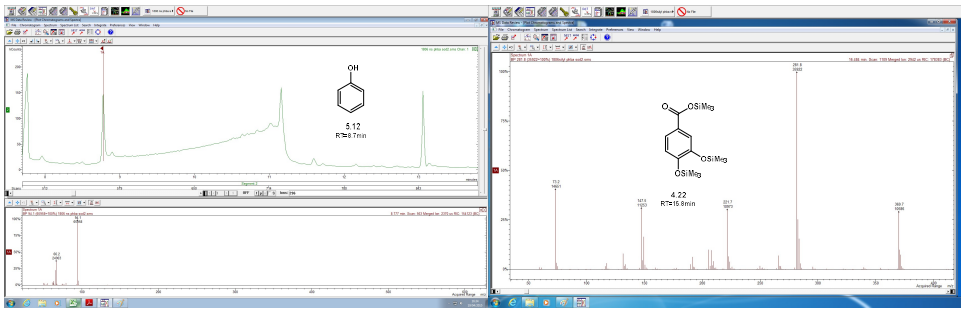

GC/MS spectra of products from SOD1 treated Salicylic acid

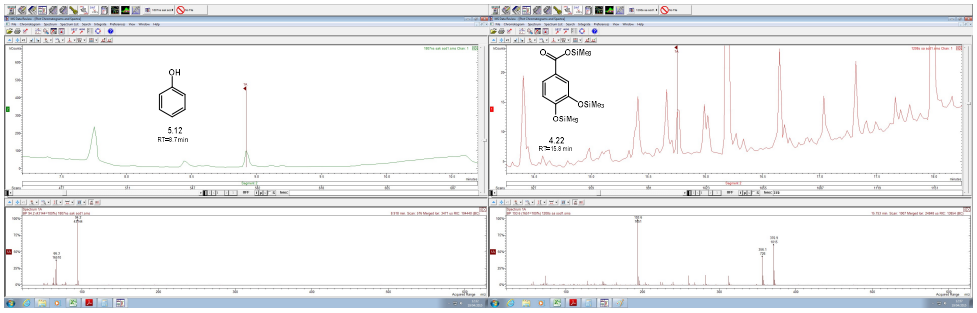

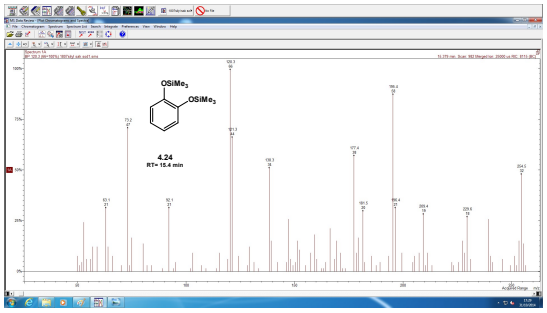

GC/MS spectra of products from SOD2 treated Salicylic acid

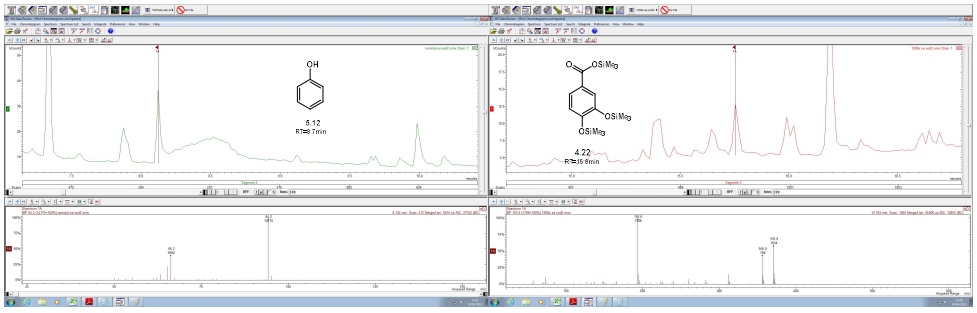

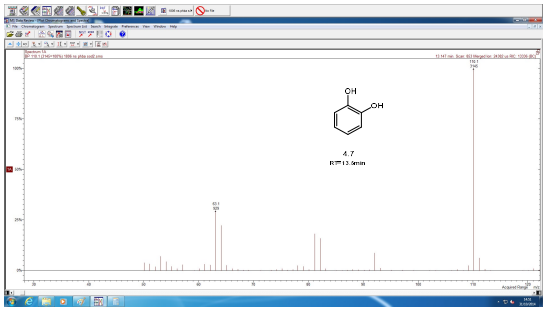

GC/MS spectra of products from SOD1 treated 4-Hydroxybenzaldehyde

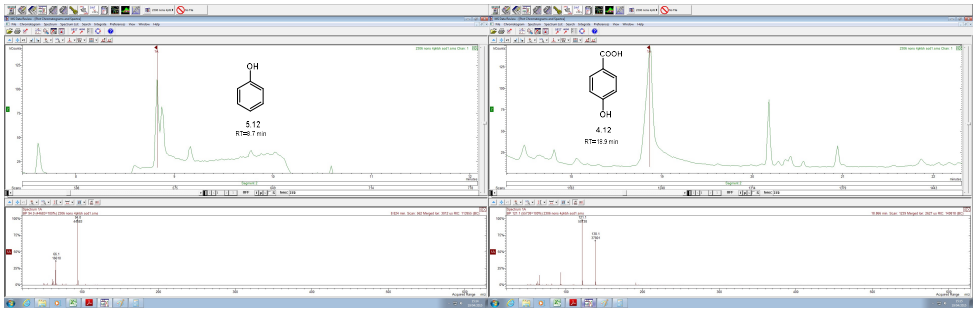

GC/MS spectra of products from SOD2 treated 4-Hydroxybenzaldehyde

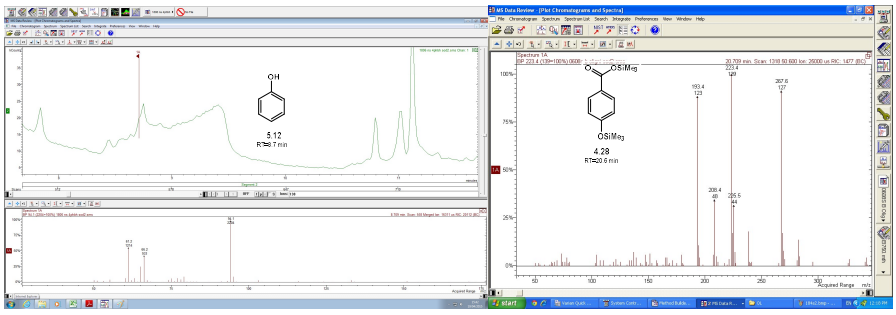

GC/MS spectra of products from SOD1 treated Acetovanillone

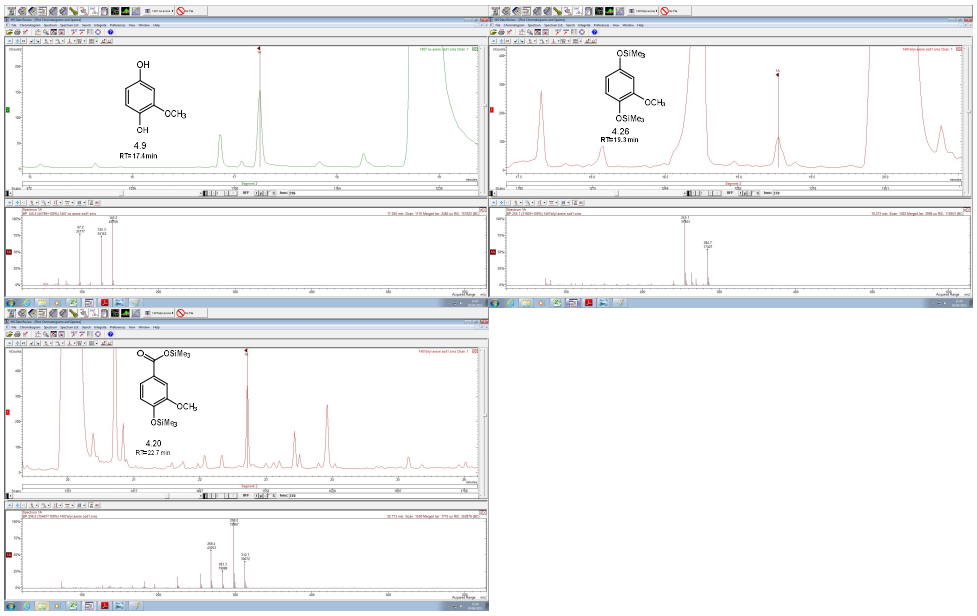

GC/MS spectra of products from SOD2 treated Acetovanillone

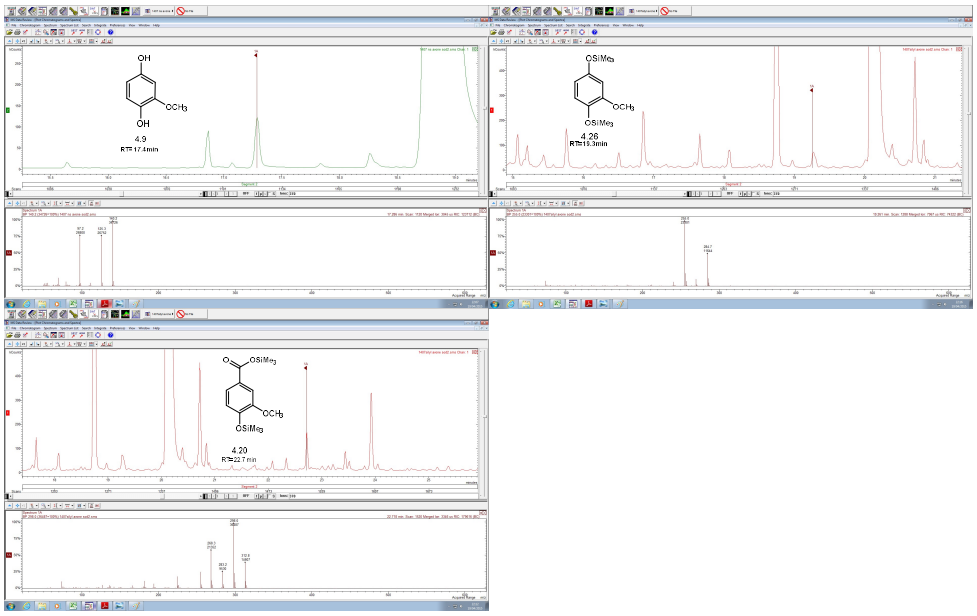

GC/MS spectra of products from SOD1 treated 4-(1-Hydroxyethyl)guaiacol

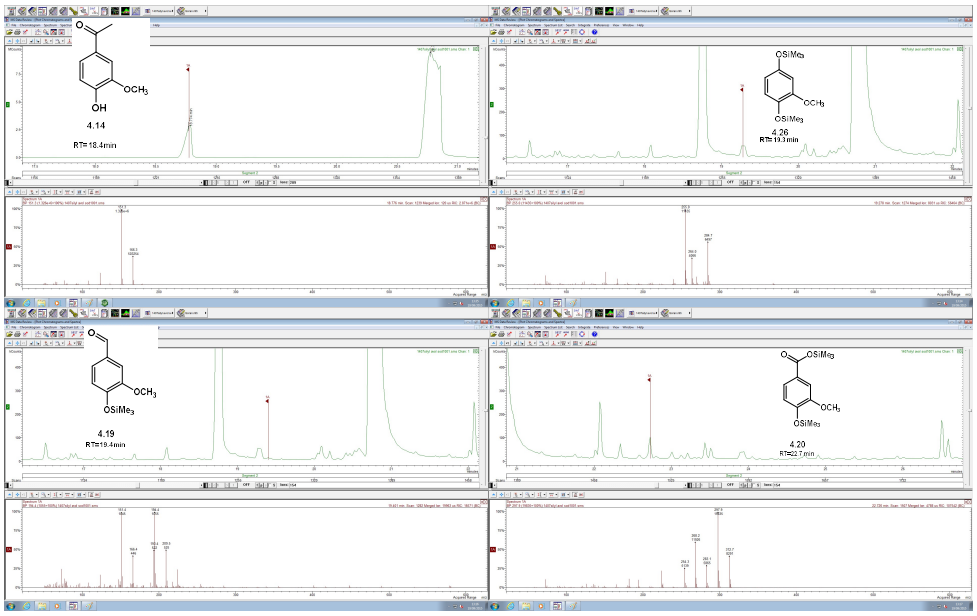

GC/MS spectra of products from SOD2 treated 4-(1-Hydroxyethyl)guaiacol

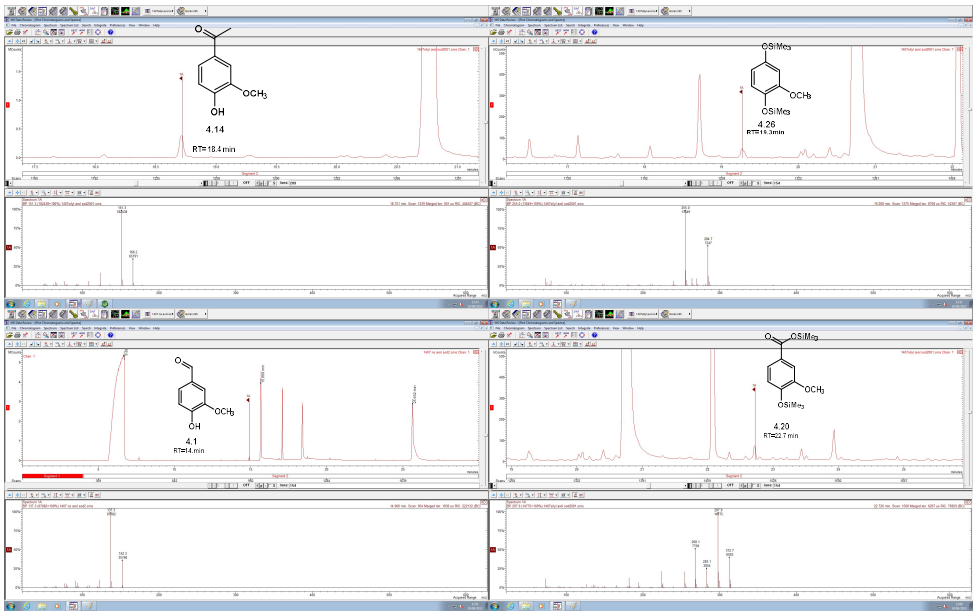

GC/MS spectra of products from SOD1 treated Vanillic acid

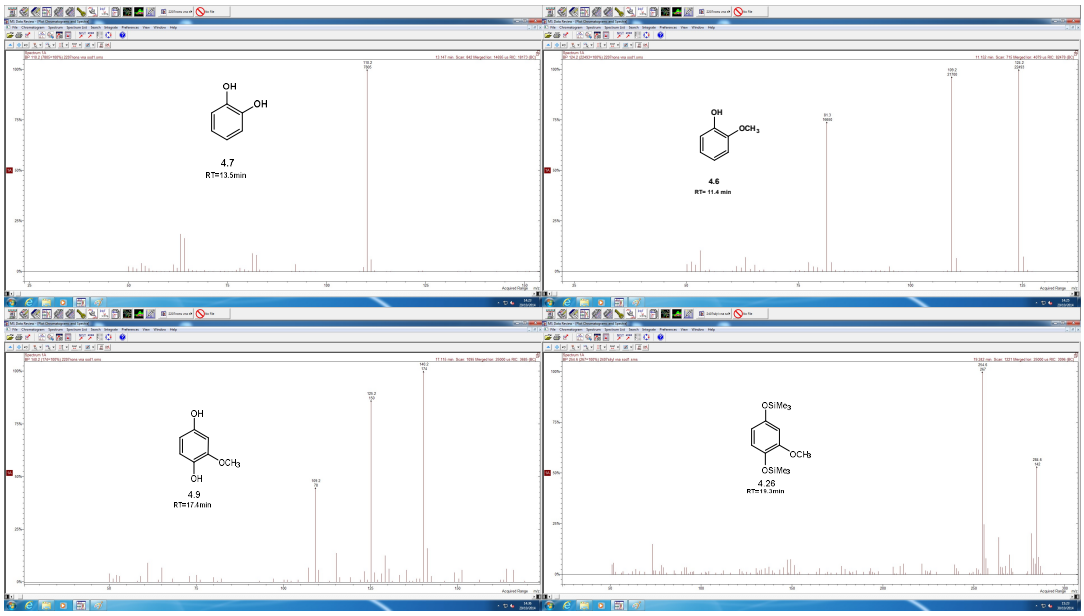

GC/MS spectra of products from SOD2 treated Vanillic acid

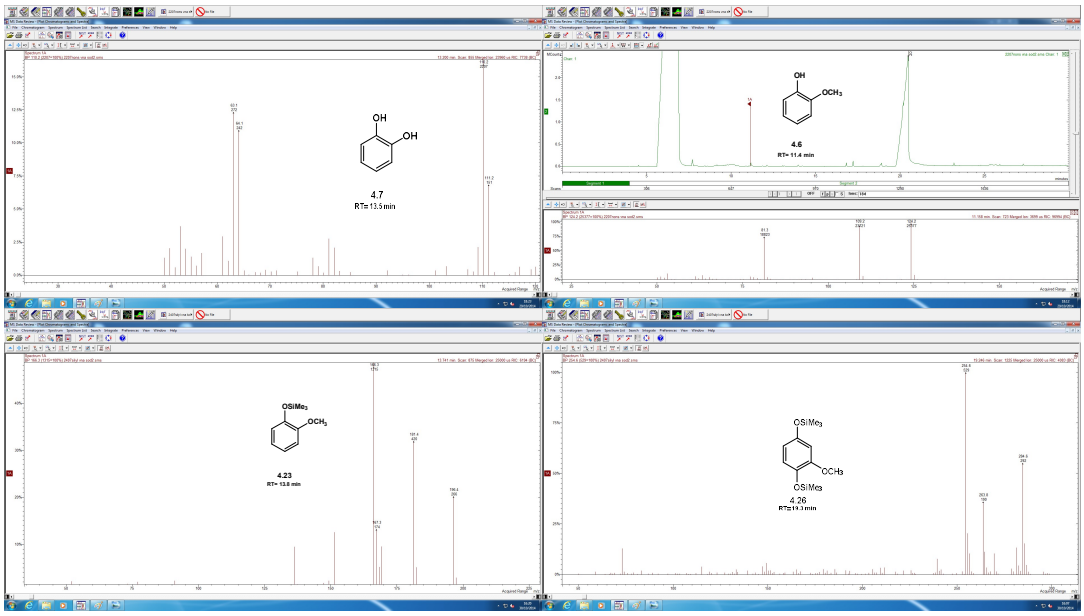

GC/MS spectra of products from SOD1 treated Vanillin

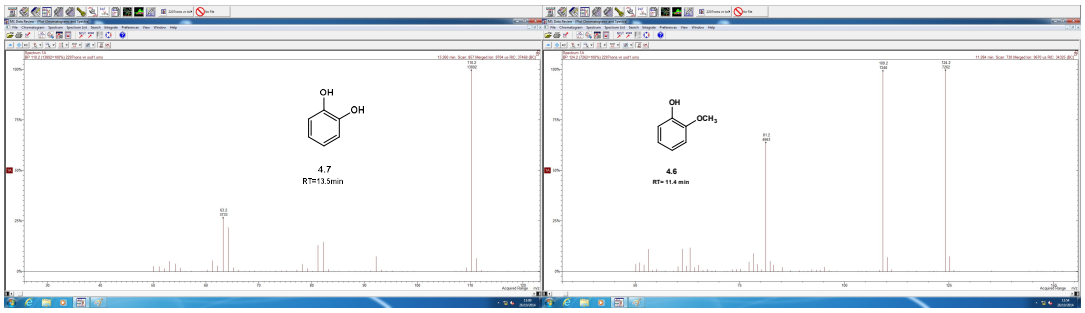

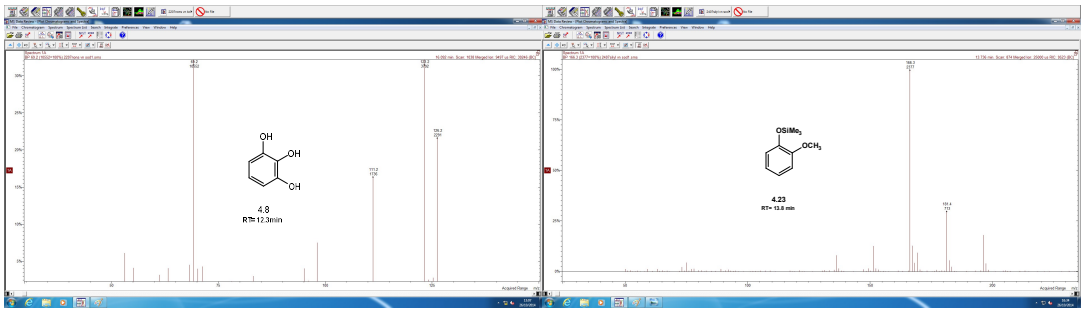

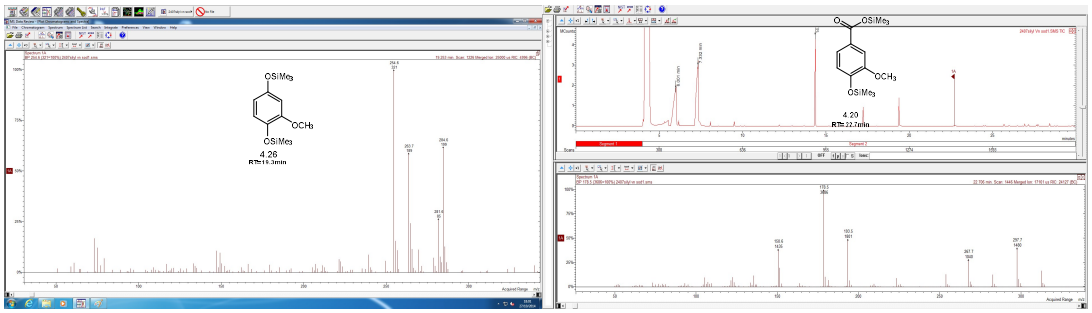

GC/MS spectra of products from SOD2 treated Vanillin

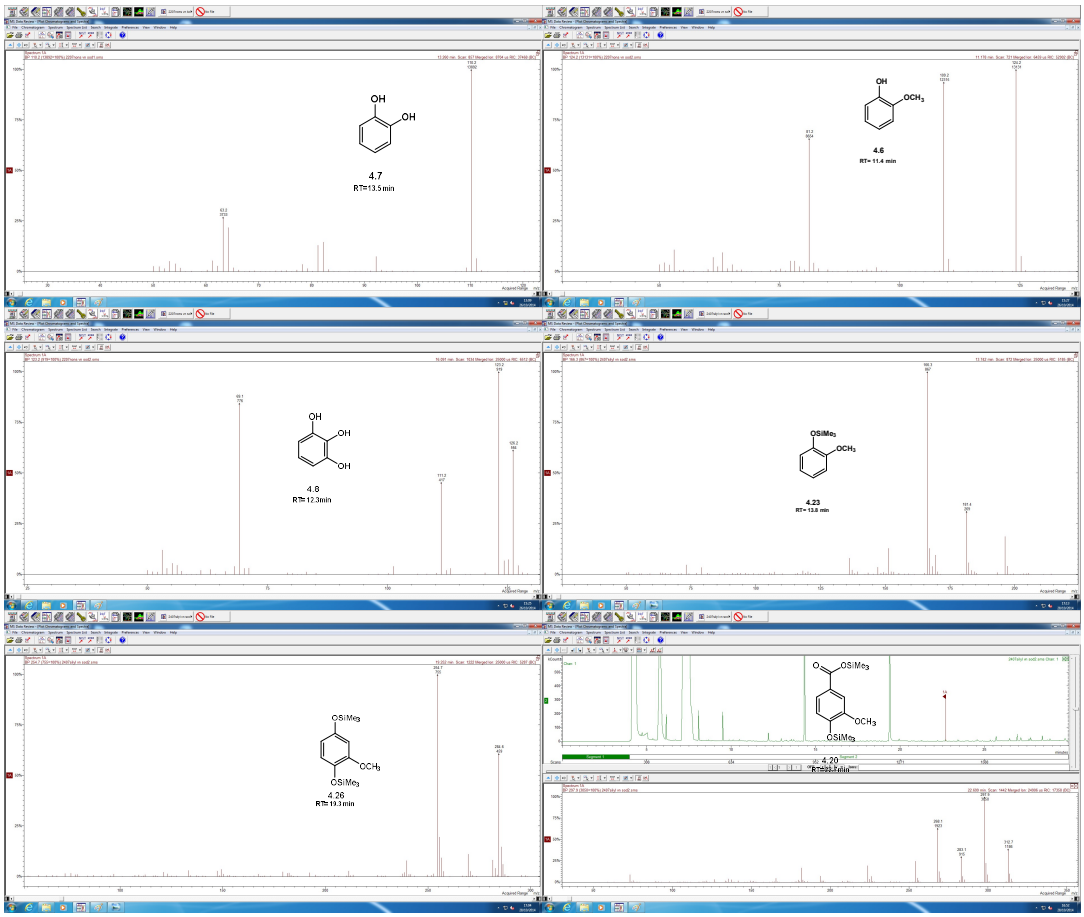

GC/MS spectra of products from SOD1 treated 5-Vanillic acid

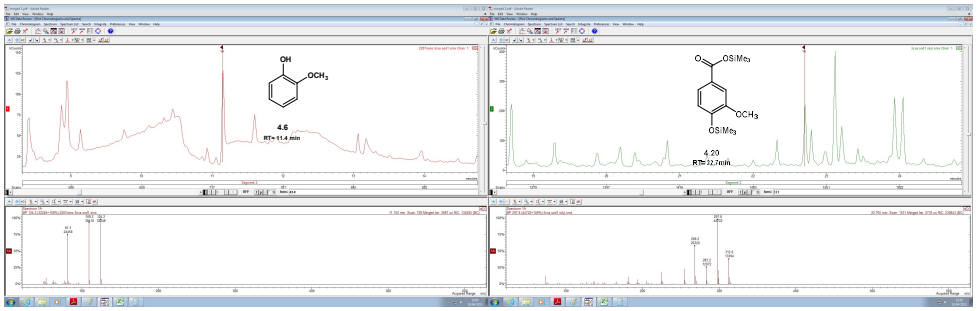

GC/MS spectra of products from SOD2 treated 5-Vanillic acid

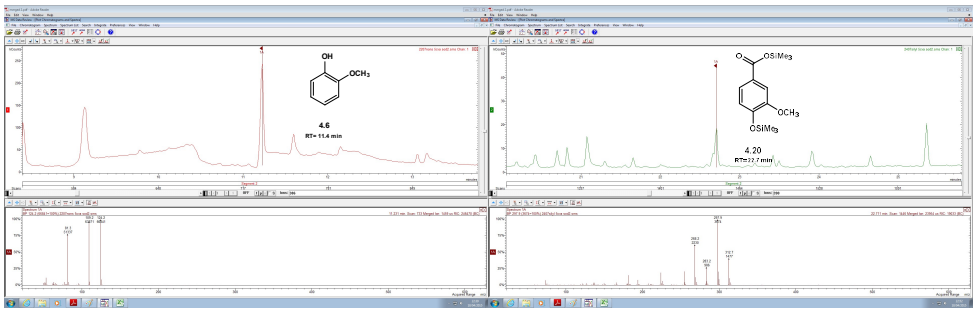

GC/MS spectra of products from SOD1 treated Guaiacol

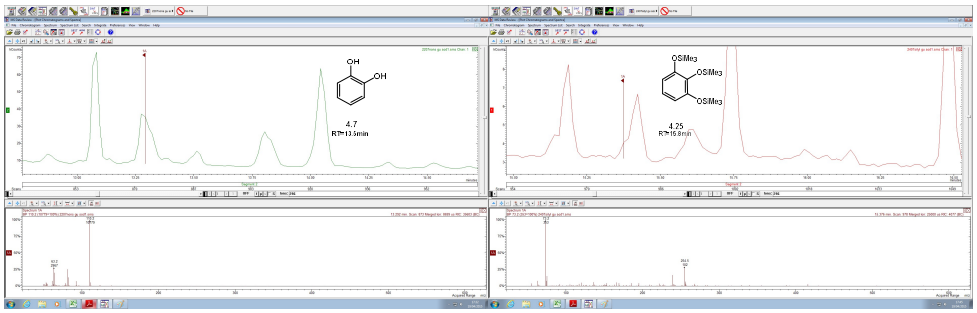

GC/MS spectra of products from SOD2 treated Guaiacol

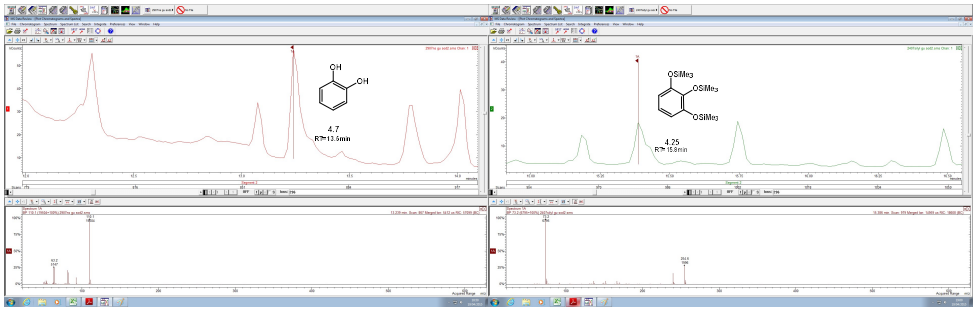

GC/MS spectra of products from SOD1 treated Catechol

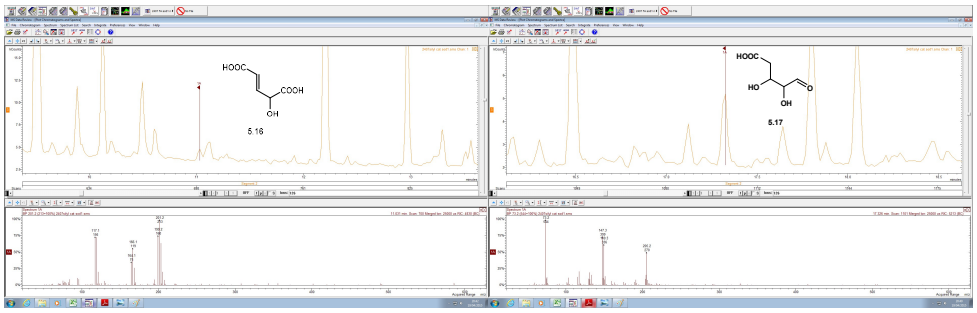

GC/MS spectra of products from SOD2 treated Catechol